Cronfa - Swansea University Open Access Repository

_____

This is an author produced version of a paper published in:
Chemical Society Reviews

_____

Cronfa URL for this paper:
http://cronfa.swan.ac.uk/Record/cronfa39516

_____

Paper:

Foster, E., Moon, R., Agarwal, U., Bortner, M., Bras, J., Camarero-Espinosa, S., Chan, K., Clift, M., Cranston, E., et. al. (2018). Current characterization methods for cellulose nanomaterials. *Chemical Society Reviews, 47*(8), 2609-2679.

http://dx.doi.org/10.1039/C6CS00895J

_____

http://www.swansea.ac.uk/library/researchsupport/ris-support/

Current characterization methods for cellulose nanomaterials

E. Johan Foster (VT),*
Robert J. Moon (FPL),*
Umesh Agarwal (FPL)
Michael J Bortner (VT)
Julien Bras (Grenoble INP)
Sandra Camarero-Espinosa (U Maastricht)
Kathleen J. Chan (VT)
Martin J.D. Clift (Swansea)
Emily D. Cranston (McMaster)
Steve Eichhorn (Bristol)
Doug Fox (American U)
Wadood Hamad (FPInnovations)
Laurent Heux (CERMAV)

Bruno Jean (CERMAV)
Matthew Korey (Purdue)
World Nieh (USFS HQ)
Kimberly J. Ong (Vireo Advisors)
Michael S. Reid (McMaster)
Scott Renneckar (UBC)
Rose Roberts (VT)
Jo Anne Shatkin (Vireo Advisors)
John Simonsen (OSU)
Kelly Stinson-Bagby (VT)
Nandula Wanasekara (Exeter)
Jeff Youngblood (Purdue)

Corresponding Author Address:
For JF: 445 Old Turner St, 203 Holden Hall, 24060, Blacksburg, VA. Email: johanf@vt.edu
For RM: U. S. Forest Service, Forest Products Laboratory, Madison, WI. Email: robertmoon@fs.fed.us

<u>Sections:</u>
1 Introduction: –Robert J Moon (FPL), World Nieh (USFS), E. Johan Foster (VT)
2 Know your Starting Material: Handling, drying and redispersing CNM and suspension properties: – Emily D. Cranston (McMaster), Michael S. Reid (McMaster), Scott Renneckar (UBC)
3 Determination of CNM surface charge: - Julien Bras(Grenoble INP), Sandra Camarero-Espinosa (Maastricht), Emily D. Cranston (McMaster), Michael S. Reid (McMaster)
4 Elemental analysis: – Jeff Youngblood (Purdue), Matthew Korey (Purdue)
5 Solid-State Properties of CNM: – Wadood Hamad (FPInnovations), Laurent Heux (CERMAV), Umesh Agarwal (FPL)
6 Surface Modification Determination: – John Simonsen (OSU), Bruno Jean (CERMAV), Laurent Heux (CERMAV)
7 Electron microscopy imaging: prep / staining / techniques: – Rose Roberts (VT), Kelly Stinson-Bagby (VT), E. Johan Foster (VT)
8 Rheology: – Michael J Bortner (VT), Jeff Youngblood (Purdue), Kathleen J. Chan (VT)
9 Preparation of thin CNM films for particle size analysis and optical, surface forces and adsorption studies: - Michael S. Reid (McMaster), Emily D. Cranston (McMaster)
10 Tagging for characterization: – Doug Fox (American), Julien Bras (Grenoble INP)
11 Mechanical properties: – Steve Eichhorn (Bristol), Nandula Wanasekara (Exeter)
12 Health/safety methods, in vitro, in vivo: – Jo Anne Shatkin (Vireo Advisors), Martin J.D. Clift (Swansea), Kimberly J. Ong (Vireo Advisors)
13 Ramifications/Implications: – World Nieh (USFS), Robert J Moon (FPL), E. Johan Foster (VT)

SECTION 1: Introduction
Robert J. Moon, World Nieh, E. Johan Foster

1.1 Relevance of Cellulose Nanomaterials
A new class of cellulose particles, cellulose nanomaterials (CNMs), having properties and functionalities distinct from molecular cellulose and wood pulp, are being developed for applications that were once thought impossible for cellulosic materials.[1] Commercialization, paralleled by research in this field, is fueled by the unique combination of characteristics, such as high on-axis stiffness, sustainability, scalability, and mechanical reinforcement of a wide variety of materials, leading to their utility across a broad spectrum of performance material applications. However, with this exponential growth in interest/activity, the development of measurement protocols necessary for consistent, reliable and accurate materials characterization have been outpaced. These protocols, developed in the broader research community, are critical for the advancement in understanding, process optimization, and utilization of CNMs in materials development. This review establishes detailed best practices, methods and techniques for characterizing CNM particle morphology, surface chemistry, surface charge, purity, crystallinity, rheological properties, mechanical properties, and toxicity for two distinct forms of CNMs: cellulose nanocrystals, and cellulose nanofibrils. Key to this will be the development of measurement protocols necessary for consistent, reliable and accurate characterization of CNMs that are critical for advancing the mechanistic understanding of the various processes needed for optimizing CNM utilization.

Cellulose is a highly functionalizable polymer with many existing industrial applications. Cellulose in the nano-scale exhibits unique characteristics due to its size, morphology and large surface area. Research and development of CNMs spans across various application areas including: adhesives, cements, inks, drilling fluids, polymer reinforcement, nanocomposites, transparent films, layer-by-layer films, paper products, cosmetics, barrier/separation membranes, transparent-flexible electronics, batteries, supercapacitors, catalytic supports, templates for electronic components, electroactive polymers, continuous fibers and textiles, food coatings, health care, antimicrobial films, biomedical, tissue engineering scaffolds, pH-responsive CNMs, drug delivery, *etc.*.[2-6] Recently, several companies have started marketing CNMs, and from their experience, thixotropic additive/agent has emerged as one the major markets. For example, addition of CNM can increase the yield stress of drilling mud slurry, keep liquid and gas from seeping into the borehole, allow drilling debris to rise to the surface and keeps the drill bit cool and clean during drilling.[7] Other emerging markets include as strength enhancers for paper, for increased mineral loads on paper surface, as flavor carriers for foods, for food packaging to improve shelf life and as a better medium for growing human cells. However, despite the great potential of CNMs, industrial scale application will require reduced financial risks associated with CNM manufacturing, thus continued research and development will be needed to address various cost related issues associated with CNM manufacturing.[8]

1.2 Introduction to Cellulose Nanomaterials
Cellulose nanomaterials encompass a wide spectrum of nano-scale cellulose based particles having various, shapes, sizes, surface chemistries and properties, and we use the term CNM to embody the entirety of different nano-scaled celluloses. CNMs can be grouped into five broad categories: cellulose nanocrystals (CNCs), cellulose nanofibrils (CNFs), tunicate CNCs (t-CNCs), algal cellulose (AC), and bacterial cellulose (BC). Representative micrographs for each CNM type are shown in **Figure 1.1**. Variations in CNM generally arise from three factors: i) cellulose source, ii) the extraction/production method, and iii) surface chemistry. Detailed summaries of these processes are given in various review papers.[1, 9-13] CNMs can be isolated from various sources: trees/plants, tunicates (*e.g.*, sea squirt) and algae, or are generated by bacteria. These raw material sources have large differences in the cellulose biosynthesis processes, which affect cellulose chain stacking, and thus the resulting CNMs extracted from them have different degree of crystallinity, cellulose I polymorph (*e.g.*, I_α/I_β ratio), particle aspect ratios, lengths, widths, and cross-section morphologies. It should be noted that throughout the years the CNMs nomenclature has been inconsistent, where CNCs have been also referred to as whiskers, needles, nanocrystalline cellulose (NCC), *etc.*, while CNFs have also referred to as nanofibrillated cellulose (NFC) cellulose microfibrills (CMF), *etc.*. This article uses International Organization for Standardization (ISO) standard terms for CNM whenever possible.[14] If an ISO term is not available, the object will be identified by a commonly used term.[15]
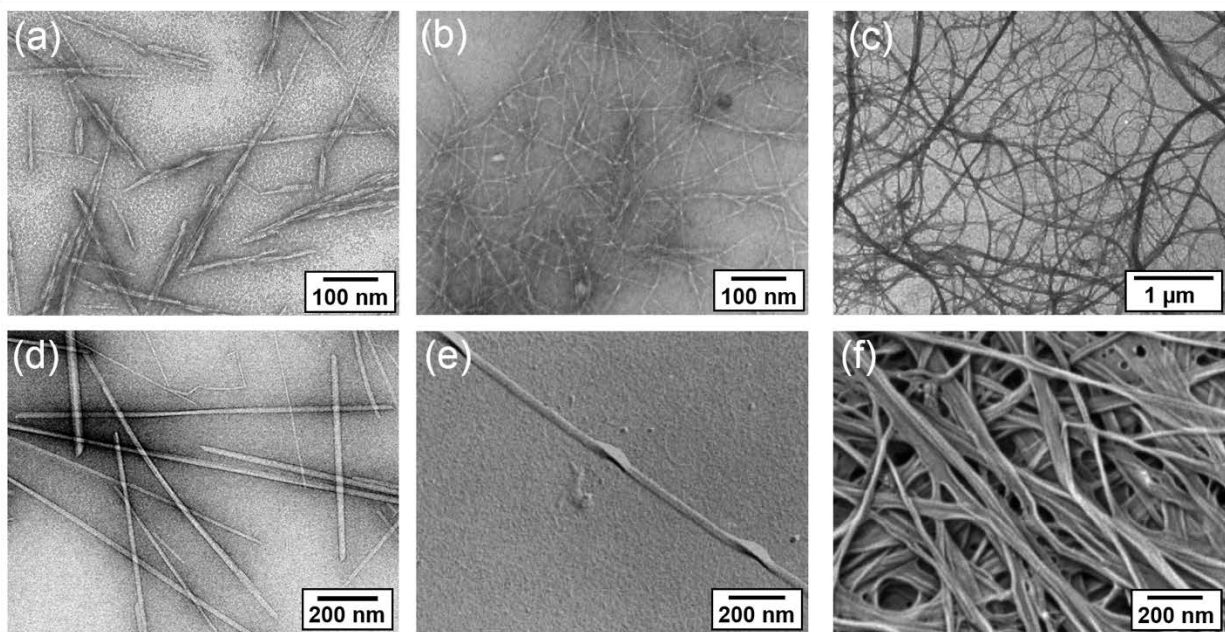
Figure 1.1. Electron micrographs of several CNM types, (a) transmission electron microscopy (TEM) image of CNCs,[16] (b) TEM image of CNF with fibrillation pretreatment to impart surface charge,[17] (c) TEM image of CNF without fibrillation pretreatments,[18] (d) TEM image of t-CNCs (image courtesy of Yu Ogawa, CERMAV), (e) TEM of AC,[19] (f) scanning electron microscopy (SEM) image of BC.[20] Reprinted with permission, (a) from ref. 15 TAPPI Press, (b) from ref. 16 TAPPI Press, (c) from ref. 17 © 1997 John Wiley & Sons, (e) from ref. 18 © 1997 Springer Science+Business Media B.V., (h) from ref.19 © 2007 American Chemical Society.

For brevity, this review focuses primarily on CNMs extracted from plants, *e.g.,* CNCs and CNFs. CNM extraction from plants generally consists of pretreatment step(s) followed by refinement step(s).[10, 21] Pretreatments typically purify and homogenize the starting material so that it reacts more consistently in subsequent treatments. Following this, additional chemical or enzymatic treatments are performed to facilitate the controlled fragmentation of the cellulose source material during the refinement step(s). There are two main refinement approaches to fragment cellulose source materials into nano-scale particles: acid hydrolysis and mechanical shear. Refinement by acid hydrolysis (typically sulfuric acid, hydrochloric or phosphoric) preferentially cleaves the chains at the disordered regions of the cellulose source material, and the resulting particles are called CNCs.[10, 22, 23] CNCs are stiff, with spindle-like morphology of typical length: 50-350 nm, width 5-20 nm, and aspect ratios of 5-30, where the surface chemistry, charge, and particle aspect ratio are determined by the hydrolysis conditions.[24] In contrast, refinement by mechanical treatments uses high shear to comminute the cellulose source material and the resulting particles are called CNFs. CNFs are flexible, with a fiber/fibril morphology of typically length: >1 µm, width 20-100 nm, and aspect ratios of 10-100, where the surface chemistry, charge, and the particle width and degree of branching are determined by the pretreatments and mechanical shear process.[21] When specific fibrillation pretreatments are used, *e.g.*, 2,2,6,6-tetramethylpiperidine-1-oxyl radical (TEMPO) oxidation, prior to mechanical shear, finer fibrils (*e.g.*, width: 4-10 nm), can be obtained.[9, 21] With the vastly different particle morphologies, CNCs and CNFs will interact/respond to a given environment or application in very different ways. This also follows through to their characterization, and because of this, within each section of this review differences in characterization protocols needed between CNC vs CNF are highlighted and discussed.

CNM surface chemistry is critically important in how the particles interact with their environment, dictating CNM dispersion in solvents or polymers, self-assembly and agglomeration, and CNM–CNM and CNM-polymer interfacial bond strength, and thus affecting all ensuing uses of these materials. In their many forms, CNMs generally consist of surface primary and secondary alcohols, but may have other chemistries as a byproduct of the process used to extract them (*e.g.*, sulfate half ester, carboxylic acid, *etc.*). In addition,
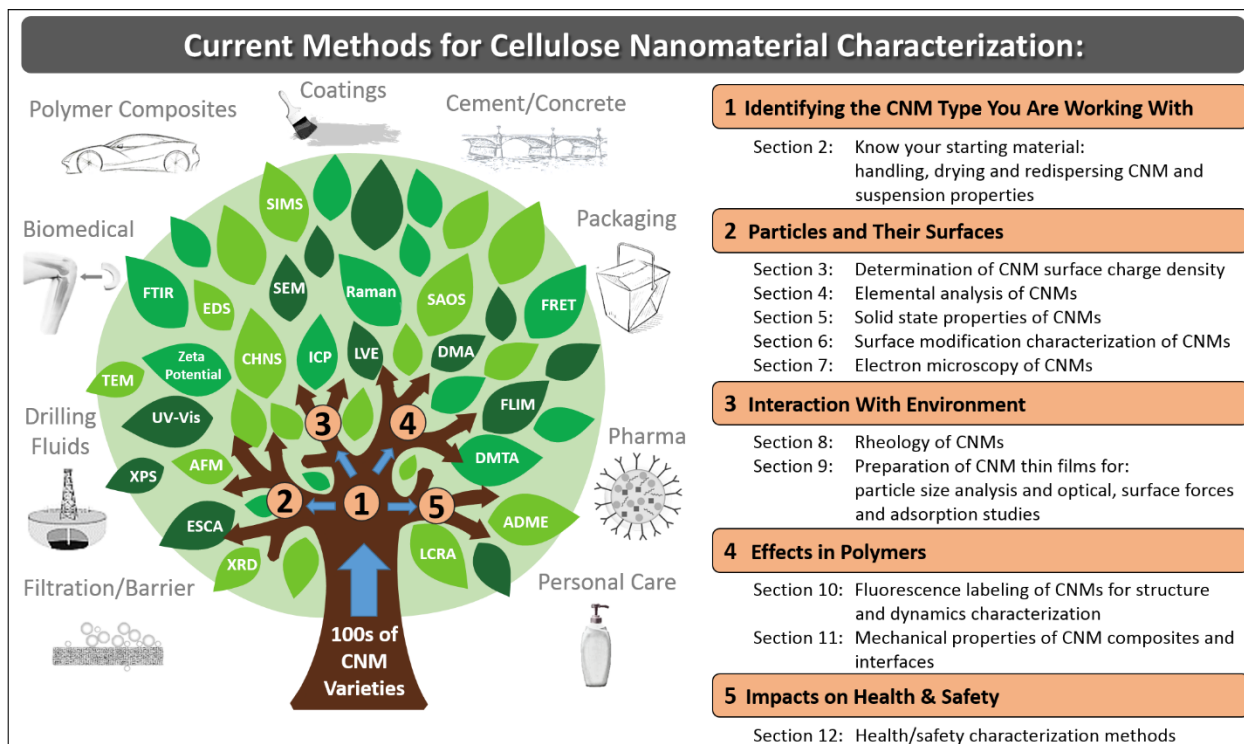
initial modification of the CNM surface chemistry can be relatively straightforward by grafting molecules, polymers, or supramolecular units, or by adding florescent tags, nanoparticles, *etc.* These modifications have been summarized in several review papers.[12, 13] Given the wide varieties of chemistries, a generalized approach toward characterization is as outlined, with detailed protocols for the expressed purpose of characterizing the nature of the bonding to cellulose.

1.3 How to use this Review

The goal of this review is to provide sufficient background to help with the determination of which techniques/methods are applicable to characterize various aspects of CNMs. However, researchers will need to assess the level of characterization required for their particular needs, a blind application of all possible characterization techniques can lead one to "over-characterize", which runs counter to the intent of this review. This review provides detailed best practices and limitations for several key techniques/methods typically used for the characterization of CNMs, in particular, surface charge, purity, crystallinity, surface chemistry, particle morphology, rheology, mechanical properties, and toxicity. Each section is written by experts in the field for the given technique, with the purpose to inform the reader why one should consider using a given technique (*e.g.*, use "this" technique for "that" reason"), then provides a detailed best practice for the technique (*e.g.*, "here is the proper way to do "this" technique). Where possible examples have been given to highlight how "this" technique shows "these" data on "these" CNMs.

Each section describes the relevance of the property to be measured, options for techniques that can be used to measure the property, and explanations and citations of important papers on the technique(s). Some techniques have been standardized for CNM characterization or are described in more general "test method" Standards; when this is the case, reference to the appropriate Standard is given. A "decision tree" flow diagram is given for each section to help guide the reader through the decision process of which technique to use and why one would use a given technique verses a complimentary technique(s). The advantages and limitations of each method and common pitfalls are described. Suggested lab protocols are given, and where appropriate, aspects unique to CNMs are highlighted. In some cases representative data are given, and tricks for interpretation of data are discussed. Throughout the review, specific comments are made regarding any differentiation in the characterization of CNC versus CNF.

The outline of this review follows the characterization tree shown in **Figure 1.2**. The review starts by addressing an extremely important point: "Know your starting material." Thus **Section 2** outlines an approach to capture the baseline characteristics of CNMs, which are critical in identifying/confirming which CNM type you are working with. This section also gives information on how to work/handle these materials. Subsequent sections are more targeted for specific characterization techniques of CNM particles and surfaces (**sections 3-7**), and how CNMs interact with their surroundings (**sections 8-11**). With one of the foremost uses of CNMs being as an additive for rheology modification, specific characterization approaches for measuring rheology of CNM suspensions is covered in **section 8**. A second notable application of CNMs is as a reinforcement phase in polymers, and **section 10** covers tagging CNMs as a way to characterize the location of CNMs within the polymer composite (or other surrounding media), while **section 11** covers mechanical property measurement and modeling to assess the effects of CNM on composite properties. With many applications of CNMs nearing commercialization, the importance of understanding the biological effects of CNM exposure cannot be understated. Potential end-users of CNMs need to know how these materials will impact health and the environment and potentially be impacted by governmental regulations. Accordingly, **Section 12** provides a generalized approach toward characterization of CNMs to address many issues regarding human and environmental health and safety.

Current Methods for Cellulose Nanomaterial Characterization:

Polymer Composites
Coatings
Cement/Concrete
Biomedical
Packaging
Drilling Fluids
Pharma
Filtration/Barrier
Personal Care

SIMS, SEM, Raman, SAOS, FRET, FTIR, EDS, Zeta Potential, CHNS, ICP, LVE, DMA, TEM, FLIM, UV-Vis, DMTA, XPS, AFM, ESCA, ADME, XRD, LCRA

100s of CNM Varieties

1 Identifying the CNM Type You Are Working With

Section 2:	Know your starting material: handling, drying and redispersing CNM and suspension properties

2 Particles and Their Surfaces

Section 3:	Determination of CNM surface charge density
Section 4:	Elemental analysis of CNMs
Section 5:	Solid state properties of CNMs
Section 6:	Surface modification characterization of CNMs
Section 7:	Electron microscopy of CNMs

3 Interaction With Environment

Section 8:	Rheology of CNMs
Section 9:	Preparation of CNM thin films for: particle size analysis and optical, surface forces and adsorption studies

4 Effects in Polymers

Section 10:	Fluorescence labeling of CNMs for structure and dynamics characterization
Section 11:	Mechanical properties of CNM composites and interfaces

5 Impacts on Health & Safety

| Section 12:	Health/safety characterization methods

Figure 1.2 There are hundreds of CNM varieties, and their characterization is critical for their utilization across various industry segments. To facilitate CNMs in utilization development it is necessary to have accurate, consistent and reliable characterization of CNM particles, and their interaction with local environment. This review addresses a few of these key measurement protocols for CNMs to improve/facilitate the characterization of CNM particles, their surfaces, their effects in rheology and composites and their impact on health and safety.

SECTION 2: Know your Starting Material: Handling, Drying and Redispersing CNM and Suspension Properties

Emily D. Cranston, Michael S. Reid, Scott Renneckar

2.1. Cellulose Nanomaterial Basics

The shift from "academic curiosity" to industrial production and application of CNMs implies that new researchers, companies and industrial sectors are now coming into contact with CNMs in many forms. Getting started with new materials can be challenging, despite the vast quantity of literature reports describing a range of detailed fundamental investigations and performance testing. This section helps the "newcomer" to cellulose nanomaterials understand the basics of what the materials should look like, how the nanoparticles/fibrils should behave and what the key properties are to measure and report. There are many different types of CNMs, as outlined briefly in the introduction, and as such, having a known starting material is of upmost importance to ensure reliable and comparable results. We provide a sample checklist (**Section 2.1.4**) for the critical information you should know before working with CNM samples, and we describe the dominant physical and chemical properties that dictate material performance (*i.e.,* dispersibility, colloidal stability, rheology, self-assembly behavior, reinforcement potential, *etc.*). Straightforward suggestions and tips for handling, storing, drying and redispersing CNMs are described along with basic protocols to measure CNM suspension properties. A decision tree is given in **Figure 2.1** to guide the reader how to begin characterizing their starting CNMs.
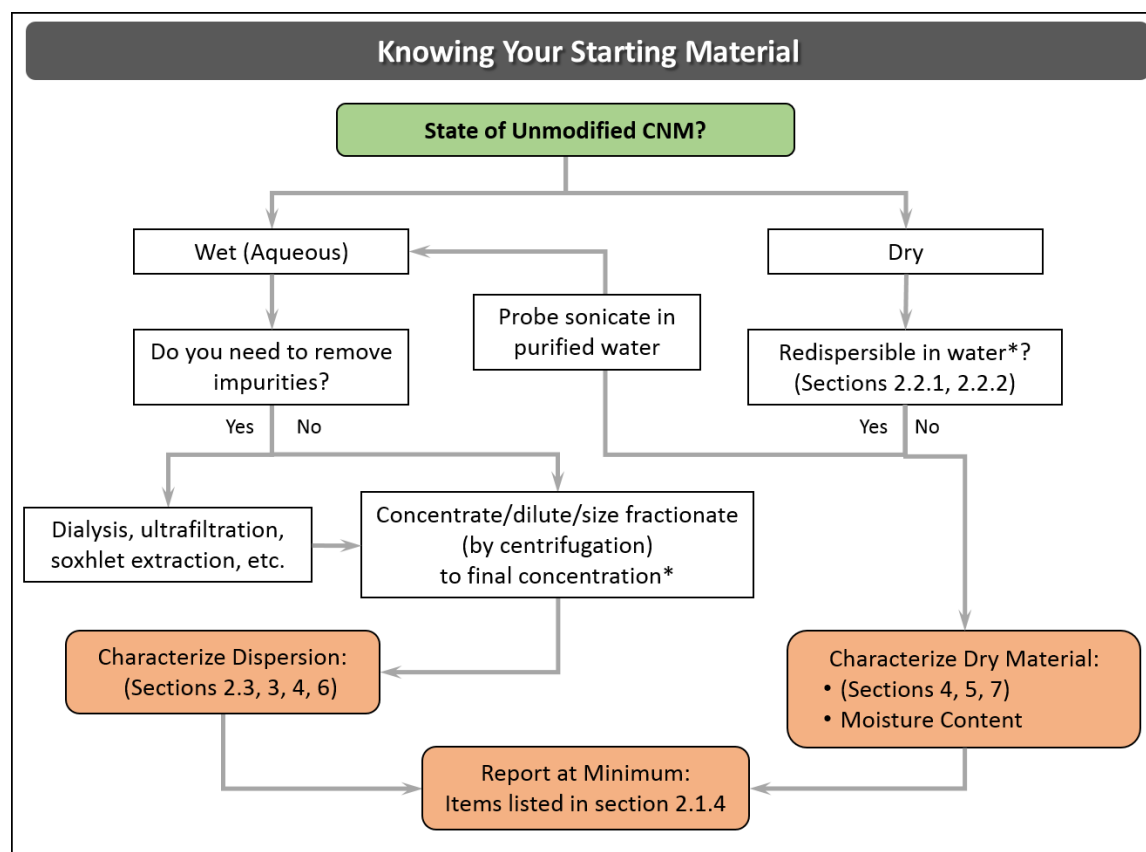

Figure 2.1: A decision tree for how to start characterizing your starting CNMs. *Upper limit to suspension concentration dependent upon type of CNM- (*e.g.*, CNC, CNF, charge density, counterion and additives).

2.1.1. Forms and Appearance of CNMs

When CNMs are produced, their final form is generally an aqueous suspension (which is used synonymously here with the terms dispersion and slurry). After acid hydrolysis or oxidation to produce CNCs, they are diluted with water and purified, normally giving a suspension with a concentration of 1-2 wt.%.[25] CNFs are mechanically produced, also in water (with or without chemical/enzymatic pretreatment) and common concentrations after production range from 0.5-3 wt.%.[26-29] Charged CNMs can form stable colloidal suspensions at low concentrations, which are transparent with a translucent blueish hue passing to semi-opaque with increasing concentration. The suspensions remain thermodynamically or kinetically stable over a large concentration range; while CNCs typically do not gel on their own until approximately 10-14 wt.%,[30, 31] oxidized CNFs form a gel at very low concentrations, such as 1-2 wt.%, and are a thick paste by 10 wt.%.

The general appearance of CNMs is shown in **Figure 2.2**. While lab-made and industrially produced sulfuric acid hydrolyzed CNCs are known to be very similar in appearance and properties,[32] CNFs can show a much larger range of dimensions, surface charge densities and fraction of micro and nanofibrils in the mixture, depending on the production method and the producer.
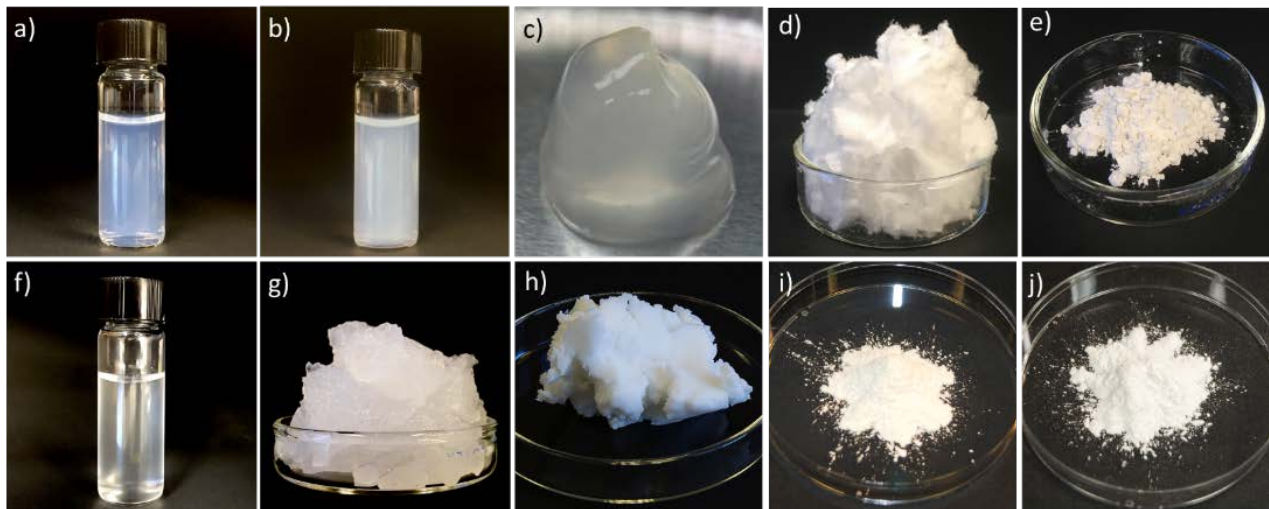
Figure 2.2. Photographs of CNMs from various producers, showing sulfuric acid hydrolyzed CNCs (produced from cotton or wood pulp) in the top row and CNFs (from wood pulp) in the bottom row. (a) lab-made CNCs fully dispersed in water at 1 wt.%, (b) lab-made CNCs at 5 wt.%, (c) CNCs at 15 wt.% from FPInnovations, (d) 0.5 g of freeze dried lab-made CNCs, (e) 2 g of spray dried CNCs from CelluForce, (f) nano-fraction of carboxymethylated CNFs produced by Innventia at 0.1 wt.%, (g) 2 wt.% CNF gel from Innventia, (h) 10 wt.% Exilva paste produced by Borregaard, (i) 1 g of freeze dried and ground mechanically produced CNFs from the University of Maine and (j) 1 g of spray dried CNFs from University of Maine. (Photo credits: M. Reid – McMaster; FPInnovations; M. Hjørnevik – Borregaard; M. Bilodeau and D. Johnson – University of Maine).

2.1.2. Commercially Available Forms of CNMs

With the intensification of industrial production of CNMs has come the necessity to dry or concentrate both CNCs and CNFs primarily to save costs on shipping and storage, and to increase the shelf-life of the materials. There are many potential applications where adding an easily dispersible dried material has advantages (*e.g.*, most liquid based formulations), and even some cases where water could be detrimental to the processing and product performance (*e.g.*, melt compounding for nanocomposites). As such, CNM producers have turned to concentrating suspensions or producing dried powders, prior to shipping to customers.

CNCs can be purchased as concentrated suspensions (6-12 wt.%), or as redispersible freeze/spray dried powders. All commercially available sulfuric acid hydrolyzed CNCs are sold in the neutralized sodium-salt form. CNFs can be purchased in water with concentrations ranging from 1-25 wt.% which are either gels or pastes. At the current time there are no drying technologies for CNFs which give redispersible materials although freeze dried or spray dried forms are sold. These dried materials are not intended to be redispersed back to individual nanofibrils.

We note that despite appearing dry in their powder form, CNMs hold residual moisture contents of approximately 2-5 wt.%[33] which can greatly increase the difficulty of analyzing results for certain characterization techniques (such as specific surface area measurements), processing conditions and applications. With heavy heating (i.e., ca. 100 ^{o}C), often under vacuum, most moisture can be removed; however, CNMs will re-adsorb water immediately upon contact with the atmosphere.[34, 35]

2.1.3. CNM Storage and Handling
All CNMs in wet formats should be stored in the refrigerator whereas dried powders should be stored under low temperature and humidity conditions. This is to reduce microbial growth, which can also be avoided by adding small amounts of sodium azide or toluene to suspensions. However, if the CNMs are intended to be used in toxicity testing or biomedical applications then antimicrobial agents should not be added and microbiological stability must be ensured by low water activity, low temperature, or a combination of both. For sulfuric acid hydrolyzed CNCs, storage in the refrigerator is further needed to slow down self-catalyzed desulfation of the nanoparticles.[36] It has been shown that CNCs will lose their sulfate half ester groups over time leading to CNCs with reduced surface charge and colloidal stability as well as a suspension with a lower pH.[36]

Cellulose nanomaterials should always be handled wearing lab-grade gloves and when handling dried powders it is recommended to wear a disposable dust mask to avoid inhalation of the powder. While inhalation toxicity studies of spray dried micron-sized CNC aggregates has been found harmless,[37] further studies of CNCs in various formats have shown mixed biological responses.[38, 39] Occupational, consumer and environmental exposure to CNMs throughout the product life cycle is presented elsewhere [40] and in **Section 12**.

2.1.4.   Sample checklist
When purchasing or obtaining CNM samples, the following is a checklist of information to request from the manufacturer (or determine experimentally), as most of these parameters will impact redispersion alongside other properties. Additionally, this checklist can be considered the minimum information that should be reported to describe CNMs in scientific publications. Many of these parameters and ways to measure them are discussed further in this review, and detailed protocols are described in a Canadian Standard, *Cellulosic Nanomaterials - Test Methods for Characterization* (CSA Z5100-14),[15] and in ISO Standards currently in preparation.[41]
1. **Type of CNM:** Determining whether the CNM is CNCs or CNFs should be fairly obvious based on the production method and standard definitions,[15, 31] however, some "other" nanocellulose materials have recently become available on the market and new users are encouraged to understand how these materials differ from the traditional sulfuric acid hydrolyzed CNCs and mechanically fibrillated CNFs.[32] The ISO Standard terms "cellulose nanocrystal" and "cellulose nanofibril" are highly recommended to avoid propagating the confusion that has arisen due to the multitude of terms and acronyms present in the literature over the last 30 years.[14]
2. **Suspension concentration or drying method:** Rarely will CNMs be used as received without at least one processing step (i.e., redispersing, diluting, purifying, *etc.*) and to do so reproducibly requires general knowledge of the sample concentration. There are small differences in redispersing spray dried vs. freeze dried CNCs, as mentioned below. If unknown, the concentration can be measured by thermogravimetric analysis whereby 100-200 µL of a well mixed CNM suspension is dried in a pre-weighed aluminum weighing dish by heating until constant mass at 105 ^{o}C (the mass of suspension is determined before and after drying, without significant exposure to environmental humidity, to calculate the concentration).
3. **Surface charge group type/density:** The surface chemistry of CNMs dictates their colloidal stability, rheological and interfacial properties, and their interactions with other chemical species. It is important

to recognize whether CNCs are produced by acid hydrolysis or oxidation and by which reagents, or whether CNFs are TEMPO oxidized, carboxymethylated or have residual charge groups from hemicelluloses, *etc.*[9] Performing experiments using CNMs with different surface charge groups or charge densities may lead to unpredictable results.

4. **Counterion/pH:** The pH is an indication of whether CNMs are in the acid or neutral form (discussed more in the next subsection) and mono and divalent salts as CNM counterions are known to change suspension properties significantly.[42-44]

5. **Additives:** Polymers, glycerol, alcohols and salts are sometimes added to commercial CNMs to aid with drying, redispersion, rheological performance, film flexibility, and as mentioned, antimicrobial agents may also be added. For example, polyethylene glycol (PEG) has been demonstrated to aid in CNC redispersion from freeze dried powder.[45] Most additives can be removed by dialysis, centrifugation or ultrafiltration and in some cases, Soxhlet extraction is recommended.[32, 46]

6. **Cellulose source material:** As widely reported,[47, 48] the starting material used to produce CNMs can have a large influence on nanoparticle dimensions, size distribution, aspect ratio and surface chemistry, even though most plant sources give similar CNCs.[49, 50] CNF width, length and span also varies considerably with the cellulose source, number of homogenization cycles, and, moreover, degree of modification prior to fibrillation (i.e., enzymatic pretreatment, carboxymethylation, and TEMPO oxidation).[51] It is best to measure CNM size and size distribution as described below on all new samples.

7. **Batch number/date of production:** Because industrial production of CNMs is relatively new, producers are potentially changing starting materials and reaction sizes, i.e., scaling up, which can lead to variability in the final products.[32] It is recommended to work with consistently produced CNMs whenever possible.

2.2. Drying CNMs to be Redispersible

CNMs can be freeze dried, spray dried, supercritically dried, oven dried or freeze-spray dried into powders and films.[33, 44, 52-55] As discussed, for CNCs these forms are redispersible in water at low concentrations with sonication. These drying methods lead to different drying mechanisms and morphologies; freeze and supercritical drying gives a highly networked multi-scalar structure whereas spray drying may be more suited to industrial applications as the aggregates are more particulate and range from hundreds of nanometers to tens of microns in size.[44, 52]

For CNCs it has been shown that residual moisture in the material and the counterion of the surface charge groups play a significant role in redispersibility and stability.[33, 44] Some moisture must remain (ca. 4%) and only neutralized CNC suspensions in the sodium-salt form can be fully redispersed after drying.[44] Similarly, CNF suspensions in the sodium-salt form with a slight excess of salt have been demonstrated to be partially redispersible.[56] Drying acid-form CNCs (i.e., with H^+ counterions) leads to significant hydrogen bonding and van der Waals attraction[52, 57] resulting in a material that will not redisperse even with intense sonication. Strong cellulose-cellulose interactions for acid-form celluloses are also evidenced by the inability to fibrillate acid-form oxidized pulp.[58] While hydrogen bonding plays a significant role in cellulosic material behavior, we highlight that in the presence of water, hydrogen bonding is primarily between water and CNMs, and that strong cellulose-cellulose hydrogen bonds only form after complete dehydration.[44, 59]

For CNCs it is common to freeze dry them for storage or incorporation into other materials and it is recommended to freeze dry from well-dispersed sodium-salt form suspensions at low concentrations (0.5 – 3 wt.%).[60] The resulting product should be a loosely packed aerogel however, depending on CNC concentration and freezing method/rate, freeze dried CNCs can be denser, flake-like structures. Freeze dried CNCs can also have an iridescent appearance which implies that liquid crystal phases formed before the final drying – these dried CNCs may be harder to redisperse. Also, after surface functionalization, it is common to freeze dry the products but the ease of dispersion of dried, modified CNCs in water or solvents is highly dependent on the degree of surface functionalization and the surface chemistry itself. Spray drying,[61] spray freeze drying[62] and other supercritical/gas expanded drying methods[63] have many advantages and a range of input parameters that can be adjusted to optimize powder properties and yield, however this has not been fully undertaken with CNMs from a research perspective (as it has been, for example, for processing pharmaceuticals[64]). Industrial producers have optimized various drying processes

but this information remains proprietary. Nonetheless, it is important to recognize that all dried CNC material from industrial producers is in the sodium-salt form.

CNFs are less commonly dried due to their inherently entangled nature which leads to difficulty in redispersing them. However, new drying processes and additive dispersants have been investigated. For carboxymethylated CNFs, redispersion of dried samples has been achieved by solvent exchanging aqueous suspensions with mixed alcohols and drying CNFs under stirring at 60°C.[65] To avoid the use of organic solvents, the addition of 2-3 wt.% carboxymethyl cellulose to CNFs prior to oven drying has also been reported to create water redispersible CNFs (as measured by sedimentation tests).[66] For TEMPO-oxidized celluloses, redispersibility can be improved by removing excess aldehyde groups through additional oxidation. This treatment prevents the formation of hemiacetal bonds and allows for oven drying of a CNF material with enhanced redispersibility.[67]

2.2.1. Redispersing CNCs in Water

The advantage of using nanomaterials stems from their high surface area to volume ratio and that a "little goes a long way", provided the nanoparticles are fully dispersed. Many examples in the literature discuss the importance of dispersion and uniformity on nanocomposite performance,[68] and reliable dispersion is a prerequisite for reproducible research results and for all envisioned CNM products to meet quality control specifications. In fact, two of the major challenges in developing commercial CNMs are the need to improve their dispersibility in aqueous and non-aqueous media and the development of better methods to assess dispersion, as outlined by FPInnovations, Natural Resources Canada/Canadian Standards Association, the USA's Nanotechnology Initiative and the TAPPI Roadmap towards the Development of International Standards for Cellulose Nanomaterials.[69]

Dried CNC powders contain micro and macro-sized particles, which must be separated down to individual nanoparticle to achieve the full benefits of a nanomaterial. In water, this can be achieved by adding a known weight of a dried material at as low a concentration as possible, followed by mechanical mixing to loosen the aggregated gel that forms and then probe sonication. Note that a bath sonicator does not provide high enough energy to be efficient with this redispersion process. Probe sonication, such as with a Sonifier 450 from Branson Ultrasonics (regularly mentioned in the literature) is recommended and the procedure is described briefly below following the CSA Standard.[15] Spray dried CNCs have been reported as easier to redisperse than freeze dried CNCs[44] but this depends on the density of the freeze dried material and most likely the spray drying processing conditions.

We do not recommend trying to redisperse dried CNCs in water at concentrations over 2-3 wt.%. This comes from suggestions in the literature[44] and furthermore it has been described that even in a uniform CNC suspension the nanoparticles have slight side-by-side aggregation at concentrations below 1 wt.% and this effect is exacerbated through the addition of small amounts of salt.[70] One strategy is to redisperse CNCs in 1 wt.% increments which can allow for good dispersion, achieved in steps, up to 6 wt.%. To redisperse CNCs, slowly add CNC powder to water with strong stirring until no visible aggregates remain and let it sit for at least 1 h. Sonicate the sample using 10-20 kJ of sonication energy per gram of CNC as described by Beck *et al.*[44] noting that the amount of sonication energy can also influence the bound oligosaccharide layer on CNCs changing their colloidal stability, rheological and self-assembly properties.[71, 72] With the Sonifier 450 we sonicate 1 wt.% suspensions continuously in an ice bath for 30 s, two times (with cooling to room temperature in between) at 60% maximum amplitude. Ice is used to control the temperature and ensure that the suspension does not exceed 60°C. The exact procedure may vary depending on the sonicator type, probe size used, amount of CNC suspension, *etc.* but this is a crucial step to "unhinge" the loose aggregates both when producing CNCs and when redispersing them from a dried powder. The obtained suspension can be filtered or gently centrifuged to remove remaining aggregates or metallic probe contamination from the sonicator. Glass microfiber filter paper is recommended to avoid material loss, which happens when cellulose-based filter papers are used. The CNC concentration should be confirmed by gravimetric analysis again (as described in the checklist in **Section 2.1.4**).

If higher concentrations of CNC suspensions are required, they can be carefully concentrated. Most commonly, evaporation in a large open evaporation dish in a well-ventilated area is used. An air blower/heat gun can be used to speed up the process by blowing horizontally a few centimeters above the dish to

increase the speed of air turnover. Gentle heating from a hot plate can be used but the suspension should never exceed 60°C and should be carefully monitored. This will take a few days and it should be noted that evaporation rates are not linear – as suspensions get more concentrated they evaporate faster.

Another method to concentrate CNC suspensions is ultrafiltration (for example using a Millipore stirred cell with membranes; Ultracel® 30kDa) wherein pressurized filtration will both remove impurities and create a loose CNC gel on top of the membrane. Some material may be lost when using ultrafiltration but it is the fastest method. Dilute CNCs can be dialysed against PEG (instead of water) to concentrate, however, this can result in a CNC suspension with some low molecular weight PEG contaminants. Finally, a rotary-evaporator can be used with very gentle (or no) heating, however, this leads to the formation of a gel that coats the inside of the round bottom flask and is difficult to remove quantitatively and as such, this method is not recommended.

2.2.2. Redispersing and Size Fractionation of CNFs in Water

Uniform CNF suspensions are required for the preparation of common CNF materials, for example, films and nanopapers are normally made from dilute 0.2 wt.% suspensions,[73] fiber wet spinning is performed from 1 wt.%,[74] and fiber dry spinning is performed from 8-12 wt.%.[75] Certain treatments prior to fibrillation enhance the charges on the fibril surface, such as carboxymethylation and TEMPO oxidation; this facilitates CNF fractions with a small diameter, < 5 nm, and leads to well-dispersed transparent suspensions apparent to the naked eye. Other fibrillation methods create fractions of fibrils with the range of 50 nm in diameter that can have a milky appearance when dispersed. Hence, there is a wide range of CNF sizes after fibrillation, dependent upon pretreatment and fibrillation procedures. Drying causes aggregation of individualized cellulose fibrils and/or aggregation of bundled cellulose fibrils, particularly with freeze drying.[76] While highly oxidized and fully fibrillated CNFs should not have any components that can be removed from typical centrifugation procedures, other CNFs do have naturally occurring aggregates that make judging the redispersion difficult using comparative methods like turbidity and sedimentation speed. Handheld homogenizers or blending can be used to facilitate dispersion of partially dried CNF suspensions and this is generally followed by sonication to create a suspension. Aggregates from drying are difficult to redisperse without significant mechanical treatment, which often results in losing a portion of the higher aspect ratio component.

For CNF materials that are a combination of nano and microfibrillated cellulose (i.e., most commercially available materials) the nano-fraction can be easily separated as follows: dilute the suspension to 1-2 g/L and mix thoroughly using an ultra turrax, homogenizer or similar equipment. Probe sonicate the suspension at ~70% output for 10 min total (dividing the sonication treatments into 2-5 minute intervals to control the temperature below 60°C). Finally, centrifuge the dispersion for one hour at, at least, 5000 g. The nanofibrils will remain in the clear supernatant phase. Note that the concentration of the nano-fraction of the CNF is now significantly reduced and should be measured by gravimetric analysis.

2.2.3. Redispersing CNMs in Non-Aqueous Solvents

For many envisioned CNM applications it will be necessary to uniformly distribute CNCs and CNFs in solvents and polymers, however, complete dispersion has only been achieved with minor success to date.[9, 77, 78] The two main (oversimplified) methods to incorporate CNMs into non-aqueous media are to extensively mix/sonicate dried CNM powder into the surrounding material or through solvent exchange processes. Dispersing CNMs in polymer melts is not described here and the reader is referred to the review and book by A. Dufresne for further insight into this challenging aspect of CNM processing.[79, 80]

One straightforward option for CNCs is to disperse dried powders in polar organic solvents as described by Viet *et a*l.[81] Good suspensions of CNCs in DMSO and DMF were achieved through sonication, although it is speculated that the dispersibility may be partially attributed to trace amounts of water in the solvent. Fundamental studies have further looked at predicting "dispersibility parameters" of aggregated CNCs and found that no solvents are suitable to overcome the van der Waals forces that hold dried aggregates together (without significant energy input).[54, 55, 57] Nonetheless, and despite minor agglomeration that persists even in polar organic solvents, many publications have described successful compounding or surface functionalization of CNCs in organic solvents.

Never-dried CNMs can be solvent exchanged into organic solvents. This procedure typically is performed through multiple centrifugation steps, initiated by the addition of a miscible solvent such as an alcohol or acetone to an aqueous CNM suspension. This addition will cause the dispersion to collapse, allowingthe samples to be centrifuged and the supernatant to be decanted. Multiple steps are required to remove the majority of the water. Another procedure involves the addition of a high boiling solvent such as DMF to the suspension; water can then be removed using a rotary-evaporator. These procedures are usually done in order to surface modify CNMs with reactants that will not work in aqueous systems.

Due to the polar and hydrophilic nature of cellulose, surface modification of CNMs or addition of compatibilizers, are inevitably required to achieve good dispersion in non-polar media or matrices. A huge body of literature has focused on the functionalization of CNMs, as reviewed by Habibi,[12] but a detailed description is outside the scope of the current review. A selection of interesting surface modification routes that lead to easily dispersible CNMs is briefly discussed below.

Both non-covalent (i.e., adsorption) and covalent modification routes, such as esterification (mostly acetylation, butyration, and palmitoylation), urethanization, amidation, silylation and polymer grafting have been reported for CNMs. For CNCs, surfactant adsorption[82-84] has allowed for redispersion in toluene, cyclohexane, chloroform, THF and ethanol due to improved surface hydrophobicity, and PEG grafting has imparted steric stabilization for CNCs in high salt concentrations and chloroform.[85, 86] A few "greener" approaches have modified CNCs with fatty acids,[87] castor oil[88] and tannic acid,[89] and a gas phase hydrophobization of CNC aerogels led to highly solvent-redispersible materials.[90] For oxidized CNFs, aqueous reactants such as carbodiimides combined with N-hydroxysuccinimide can be used for amidization of CNFs with fatty amines.[91]

2.3.   Characterization of CNM Suspension Properties

Since CNMs are produced in suspension format, or redispersed from dry into suspension, it is important to have basic quantitative measurements to assess the state of dispersion. While specific instrument requirements vary, a set of standard characterization protocols for CNM suspensions is recommended below:

2.3.1. Dynamic Light Scattering

Hydrodynamic "apparent particle size" of CNMs in suspension can be determined by dynamic light scattering (DLS) which measures the time-dependent fluctuations in scattered light intensity of particles undergoing Brownian motion.[92] Under the assumption that the particles have a single, constant rate of diffusion (i.e., spherical particles) the intensity fluctuations are related to the particle size (radius) via the Stokes-Einstein equation. However, since CNMs are high aspect ratio, rod or fibrillar-like materials with differing translational diffusion constants parallel and perpendicular to the particle axis, the values obtained from DLS cannot be directly linked to the particle length or cross-section. Moreover, because translational diffusion of rod shaped particles is a function of orientation, distributions cannot be directly correlated to particle size distributions. (Even monodispersed rods would appear to have a large particle size distribution by DLS!) Instead, DLS gives a hydrodynamic "apparent particle size" that can be used as an internally consistent method to assess dispersion quality/state of aggregation, if the same equipment, sample preparation and protocol are employed. In some cases, Nanosight particle tracking (another light scattering method) is recommended for CNMs to assess dispersion and nanoparticle size.[93] Static light scattering can also be used but is fairly arduous.[94] While more sophisticated analysis of light scattering data can provide deeper insight,[94, 95] for particle size and size distribution measurements, a combination of light scattering and microscopy,[95] or microscopy alone are recommended,[96, 97] as discussed in **Sections 7 and 9**.

For CNCs in water, the "apparent particle size by DLS" for well-dispersed suspensions ranges significantly due to cellulose source, extraction procedure, and the specific instrument used. As a result, researchers are encouraged to use DLS as a relative measurement only (values within ±10 nm can generally be taken as statistically identical). Nonetheless, particle sizes typically range from 10s to 100s of nanometers with average values from 55 to 200 nm reported in the literature. While standard DLS measurements do not specifically provide information regarding particle length or cross-section it is useful when assessing CNC aggregation/colloidal stability in aqueous media of varying pH and ionic strength.[32, 98, 99] Generally, reliable DLS values can easily be obtained from fully dispersed CNC suspensions (0.025-0.05 wt.%)[15, 32] however,

CNF suspensions can be more difficult to measure by DLS due to the flexibility and very high aspect ratio of the particle. DLS has also been used to assess colloidal stability and gelation of CNFs in water.[100] For CNMs dispersed in non-aqueous solvents, DLS can still be used, provided there is sufficient refractive index contrast between CNM and the solvent and that the solvent does not absorb at the measurement wavelength (instrument parameters should be adjusted according to the solvent type.)

In addition to the inability to directly measure the length and cross section of CNMs, further limitations to DLS are as follows. If DLS measurements are taken on less concentrated samples, multiple peaks and inaccurate data may appear due to the low scattering count. On the other hand, too high of a concentration can potentially promote aggregation and particle-particle interactions,[70] or lead to multiple scattering events, reducing the apparent particle size. Salt can also affect the apparent particle size by altering the double layer and mobility of particles in dispersion (i.e., the diffusion coefficient changes with salt), again emphasizing the need for consistent sample preparation and purity. For charged spherical particles, salt also affects the hydrodynamic radius and thus the apparent size but it is important to recognize that this is not a change in the actual physical dimensions of the particle. Because DLS output describes a weight average and light scattering scales with the particle diameter to the sixth power (d^6), small particles may be a very small fraction of the total intensity and be entirely obscured by larger particles or impurities. Due to the high aspect ratio of CNMs, DLS size should never be reported as hydrodynamic radius, as is done for polymers and spherical particles, but as an "apparent particle size".

2.3.2. Zeta Potential

The colloidal stability of CNMs is often the result of electrostatic repulsion due to the presence of charged groups at the particle surface (see **Table 3.1**). As a result, understanding the surface potential and/or surface charge density is critical when investigating CNM behavior. While conductometric titrations can be used to determine surface charge density (see **Section 3**) they do not provide significant insight into particle aggregation and/or colloidal stability, particularly in media of varying pH and/or ionic strength. As a result, the zeta potential, which is related to surface potential and surface charge density, is used to rapidly assess CNM colloidal stability in a variety of media. Zeta potential can be measured using an electrophoretic mobility analyzer whereby the mobility of a particle in an applied electric field is determined by electrophoretic light scattering or laser Doppler velocimetry. Subsequently, electrophoretic mobility is converted to zeta potential using the Henry equation with Smoluchowski or Huckel approximations.[101] Although the electrophoretic mobility is a more accurate measure of particle behavior, as it requires fewer assumptions, the zeta potential is commonly reported within literature and is conventionally used to assess relative changes in colloidal stability. Generally, suspensions with absolute zeta potential values above 20 mV are considered colloidally stable.[92] Common values for CNCs are -20 to -50 mV (not including CNCs produced by HCl, which are uncharged) and CNFs can have values near to -60 mV, dependent upon the degree of oxidation. Reliable zeta potential values can easily be measured on fully dispersed 0.25 wt.% CNC suspensions or 0.05 wt.% CNF suspensions (although specific concentrations depend on the instrument), with 5-10 mM added NaCl, and should be done in triplicate.[15, 32] Note that some salt addition is necessary to obtain an accurate zeta potential measurement such that the double layer thickness around the CNM is not infinite. Suspensions that are unstable by eye (such as hydrophobically modified CNMs in water) will not give meaningful zeta potential readings. Moreover, due to the high aspect ratio of CNMs and the sometimes high surface charge density, the assumptions inherent to Henry's equation are often not met and thus zeta potential should not be considered as a quantitative measure of surface potential or surface charge density, but only as a relative assessment of colloidal stability. A more in-depth look at zeta potential, its theories and assumptions, is described comprehensively in a recent article.[92] Finally, zeta potential is affected by the pH, temperature, and the presence of salt and impurities in the suspension, all of which should be controlled to obtain meaningful data.

2.3.3. Turbidity

Turbidity is the reduction in transparency of a sample due to the presence of light-scattering matter whereby larger particles scatter more light. As such, turbidity can assess the dispersion of CNMs, lower turbidity means less aggregated nanoparticles or more fibrillated CNFs.[15] More recently, turbidity has been proposed as a method to quickly estimate the width of various CNMs.[102] Although turbidity of a suspension is a complicated function of the number of scatterers per unit volume, size distribution, and optical properties of the light-scattering bodies[15] it is again a robust and internally consistent method if the same equipment,

sample preparation and protocol are employed. Turbidity can be measured as the amount of light scattered, transmitted, or absorbed (and furthermore measured as a function of time, to assess colloidal stability or sedimentation rate) using for example, a UV-Vis spectrometer or Turbiscan[TM] equipment. If a spectrometer is to be used, a wavelength where the sample does not absorb should be chosen. Generally, the transmittance of CNC samples at 0.25-3.0 wt.% can be measured at 500 nm. A normal transmittance value for a well dispersed 0.25 wt.% suspension is about 85%. Samples should be uniform, degassed, stable and repeated three times for reliable measurements. For CNMs dispersed in non-aqueous solvents, turbidity can be measured provided the instrument is solvent compatible, parameters are adjusted accordingly and a non-absorbing wavelength is chosen. One limitation to turbidity characterization is that changes in turbidity can be linked to multiple physical phenomena and kinetic effects that are not solely related to nanoparticle aggregation. As such, turbidity should be combined with the other characterization methods described in this review.

2.3.4. Self-Assembly and Shear Birefringence

CNCs are optically anisotropic (i.e., birefringent) and observation with polarized light gives significant insight into their dispersion and organization in suspension (which furthermore relates to their aspect ratio and surface charge density). Well-dispersed CNCs phase separate into a lower chiral nematic liquid crystalline phase and an upper isotropic phase above a critical concentration of ca. 4.5 wt.%.[25] Differences in the onset of phase separation, the ratio of isotropic to anisotropic phase, and the pitch of the chiral nematic texture can all be measured visually or by polarized optical microscopy/electron microscopy and related back to suspension properties.[103-105] Uncharged CNCs (which aggregate extensively) and CNMs containing only a fraction of CNCs combined with other cellulose fibrils/fibres do not show liquid crystalline ordering. To compare liquid crystal properties of different CNC samples side by side, it is important to compare identical concentrations and samples that have had the same time to reach equilibrium. For highly concentrated CNCs (ca. 8 wt.%) it can take up to 10 days for clear chiral nematic phases to form.[32] Flat capillary tubes (inner dimensions 10 × 1 mm) are useful for equilibrating CNC suspensions in and taking polarized optical microscopy images.

In addition, shear birefringence implies that when a well-dispersed CNC suspension around 2 wt.% is shaken/stirred gently between crossed polarizers, bright light diffraction patterns appear. This has been demonstrated in the literature for CNCs and CNFs in water and organic solvents.[48, 81, 83, 91, 106] The light diffraction is due to parallel alignment of the individual nanocrystals in response to the shear forces. If the CNCs are aggregated, parallel alignment is hindered. When more small particles that are well dispersed are present, small bright polychromatic domains are visible; when fewer particles with poorer dispersion are present, larger, monochromatic domains are visible. Above a threshold aggregate size, no shear birefringence is observed. Both of these phenomena (liquid crystal phase separation and shear birefringence) can thus be used as qualitative measurements of dispersion quality.

SECTION 3: Determination of CNM Surface Charge Density

Julien Bras, Sandra Camarero-Espinosa, Emily D. Cranston, Michael S. Reid

3.1. Importance of Surface Charge Density and Common Charge Groups

Generally, CNMs possess at least a small surface charge density that imparts sufficient electrostatic repulsion to render them colloidally stable in aqueous suspension, this is particularly relevant for CNCs. In the case of CNFs, the surface charge density is most often controlled to reduce the energy consumption required to delaminate the fibers.[31] Other material properties that are affected by the surface charge density include self-assembly behavior,[104] rheological properties in suspension,[107] surface activity,[108] metallic interactions in sol-gel precipitation,[109] physical/chemical interactions[110] and thermal stability.[111] These properties are crucial in the fabrication of hybrid and composite CNM materials because they dictate the ability of the nanoparticles to disperse and form a predictable, robust and homogeneous final product. Thus, the determination of the surface charge density is essential to the characterization of CNMs. A comprehensive decision tree, **Figure 3.1**, can help guide the reader in determining the protocol to be followed depending on the CNM type and surface functionalization.
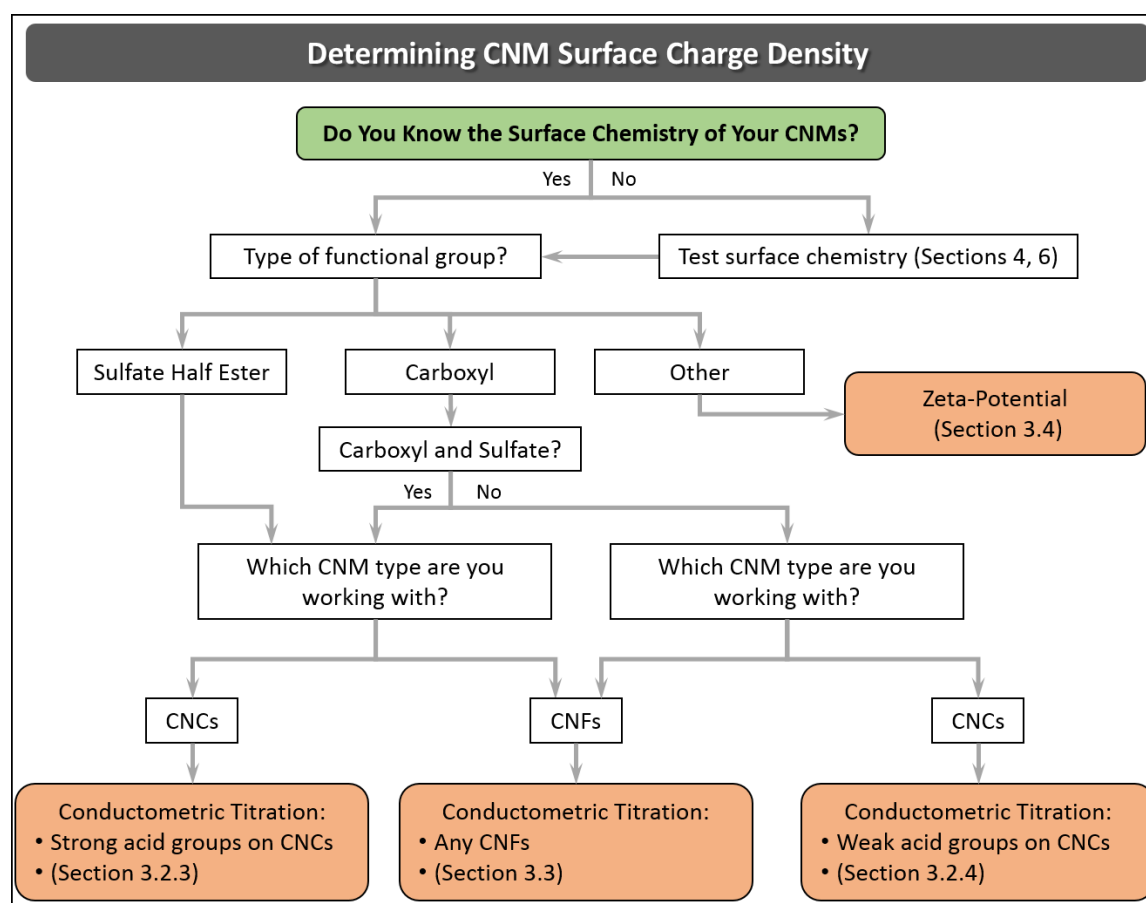
Figure 3.1. Decision tree for the determination of surface charge density for different CNMs and functionalizations.

As discussed, CNCs have traditionally been isolated by hydrolysis with mineral acids, resulting in the grafting of small functional groups such as sulfate or phosphate half esters on the hydroxyl groups of the cellulose surface, or by oxidation to impart aldehyde and carboxyl groups.[48, 49, 112, 113] (Below we refer to sulfuric acid and phosphoric acid hydrolysed CNCs as S-CNCs and P-CNCs, respectively, and CNCs with carboxyl groups are denoted COOH-CNCs.) Moreover, these nanoparticles can be further post-functionalized, giving rise to CNCs that bear small surface functional groups.[12, 49] On the other hand, CNFs possess surface charge from residual hemicelluloses or from chemical pretreatment; most commonly carboxyl[27] or carboxymethyl [114] groups are introduced in high content to the CNF surface but also cationic charge can be added with similar approaches[115, 116] or with post treatment of aldehydes with Girard's reagent.[117] TEMPO oxidation to impart carboxyl groups is one of the most common methods used to increase surface charge density in both CNFs and CNCs.[27, 48] Regardless of the isolation method or post-functionalization treatment, CNM surface charge is the result of grafting charged species to the particle surface. Hydroxyl groups alone are not responsible for surface charge, as these species are protonated under typical solution conditions (pK_a > 12).[118] Evidence of this is clearly seen in suspensions of CNCs produced through HCl hydrolysis, which exhibit poor colloidal stability due to the lack of charged surface groups.

The surface charge density of CNMs is dependent on the type and character of the introduced surface functional groups (including whether the group is a strong or weak acid/base [119]), the process and yield of the production/functionalization,[50, 120, 121] the cellulose starting material,[31, 50] and the physical properties of the nanoparticles (such as their dimensions, size distribution and total surface area).[107] CNMs are generally anionic but cationic examples exist in the literature as well. [31, 122, 123] **Table 3.1** shows common charge groups and density values for different CNMs based on their isolation method. Surface charge densities range greatly from about 10 to 3500 mmol of charged groups per kg of cellulose. More specifically, S-CNC surface charge densities range from 100 - 350 mmol/kg which for CNCs with dimensions of 122 nm long × 8 nm in cross section (assuming square prism geometry and a density of 1.55 g/cm^3) corresponds to 0.18 - 0.63 charges/nm^2 or about 0.3 - 1.0 charges per surface anhydroglucose unit.

In terms of industrial production, on the largest scale, CNCs are made by sulfuric acid hydrolysis and CNFs are made by mechanical processing with minimal chemical treatments; hence CNCs with sulfate half ester surface groups and CNFs with residual COOH groups are the most common commercially. Note that while a number of publications, patents and websites use the terminology "sulfonated CNCs", this is an error; the groups on CNCs produced by sulfuric acid hydrolysis are sulfate half esters, attached to the cellulose carbon through an oxygen, sulfonate would imply sulfur bound directly to carbon, which has not been demonstrated to date.

Table 3.1. Common CNM surface charge groups and charge densities obtained during the isolation process. Other groups and charges can be imparted post production.[12]

CNM type	Cellulose surface group	Isolation process	Common range of surface charge density (mmol/kg)
S-CNCs	Sulfate half ester	Hydrolysis with H_2SO_4[32, 50, 70, 124, 125]	80-350
Uncharged CNCs	None	Hydrolysis with HCl[85]	0
P-CNCs	Phosphate half ester	Hydrolysis with H_3PO_4 [22, 126]	10-30
COOH-CNCs	Carboxylic acid	• Hydrolysis with HCl and TEMPO oxidation,[127] • Hydrolysis with dicarboxylic acids,[128] • Oxidation with ammonium persulfate[112, 119] • Oxidation with $NaIO_4$ [113, 129, 130]	100-3500
CNFs	Residual carboxylic acid	Mechanical isolation (with or without enzymatic treatment and/or additives)[26, 51]	40-80
COOH-CNFs	Carboxylic acid	TEMPO mediated oxidation and mechanical treatment[27]	200-1800
Carboxy-methylated CNF	CH_2CO_2H	Carboxymethylation and mechanical treatment[114, 131]	140 -520
Cationic CNF	$-N(CH_3)^+$ (from EPTMAC	EPTMAC treatment and mechanical treatment[115, 116]	1400-1600
P-CNF	Phosphate	Phosphorylation and mechanical disintegration[132]	1230-1740

After an initial determination of the type of the moieties decorating the surface of the CNMs (**see Section 4 and 6, and Table 3.1**), a measurement of the surface charge density by conductometric titration is recommended.[12, 27] Titration results for CNCs and CNFs are extensively reported in the literature and allow for the direct measurement of the volume of base required to titrate the negative acid groups on the surface of a given mass of CNM[133] (the converse is true for titrating cationic CNMs with acids[123]). This technique has clear advantages over elemental analysis such as the inexpensive equipment required, the rapid sample preparation, sensitivity of the measurement, and the relative ease of the technique and data analysis.

Conductometric titration results that align well with elemental analysis and/or alternatively, zeta potential is a straightforward indication (and a good relative measure) of surface charge density as described briefly in **Section 2**. Unfortunately, elemental analysis results are sometimes misinterpreted as if all detected groups are on the CNM surface. This assumption is incorrect if there are free charged groups in suspension (*e.g.*, residual acid), or if chemical modification has compromised the CNM crystal structure allowing for functionalization within the crystals or fibril, or significant peeling/defibrillation.[130] This remark is also valuable for TEMPO-oxidized CNCs, in this case, even more functionalization in the bulk of the crystal may occurs.[109]

For example, residual sulfuric acid after S-CNC production can lead to discrepancies between titration and elemental analysis results. As such, purification of CNMs by extensive centrifugation, dialysis, ultrafiltration and/or ion exchange resin (and most likely a combination of these) is recommended for accurate charge density measurements.

More specifically, the use of ion exchange resin to scavenge free acid groups and ensure all grafted surface groups are in the acid form (and are thus titratable) is discussed further in a number of publications.[44, 125, 133] Overall, after comparing elemental analysis and conductometric titration data for CNC samples purified either by dialysis, mixed-bed ion-exchange, or strong acid cation-exchange resins, it was concluded that thorough dialysis against purified water, alone or in combination with a strong acid cation-exchange *column* (not just adding the resin and allowing it to sit) was sufficient to give reproducible and comparable results

between techniques.[44, 125, 133] Importantly, while dialysis alone is sufficient following the extraction of CNCs (in other words, for "never dried" CNCs), dried CNC material is always in the sodium form (-OSO$_3$Na) and must be ion exchanged to acid form prior to titration.

3.2.   Determination of Surface Charge Density for CNCs

When determining the surface charge density of CNCs via conductometric titration it is critical to recognize whether the charged groups behave as strong acids (for example -OSO$_3$H) or weak acids (-COOH) as distinct titration procedures must be followed. For CNCs that behave as strong acids, such as S-CNCs, aqueous suspensions are titrated directly by NaOH yielding a titration curve with a sharp transition at the equivalence point (**Figure 3.2a**). In contrast, for CNCs with weak acid groups a known concentration of strong acid is added to the suspension in order to establish a measurable reduction in conductivity at the beginning of the titration. In this case, CNCs and free acid are titrated by NaOH, where the weak acid content is determined from the extended plateau between the acidic and basic regions (**Figure 3.2b**). In both procedures, the conductivity of the suspension decreases as protons are consumed by OH$^-$ groups until the equivalence point is reached. At the equivalence point, all CNC proton counterions have been replaced with Na$^+$ counterions. As NaOH is added in excess, the conductivity increases due to free OH$^-$ groups in suspension. Notably, the slope of the acidic region is steeper than the basic region since protons are more conductive than OH$^-$ groups.

As mentioned above, for conductometric titrations to be effective, charged groups on the CNC surface must be fully protonated. While, this can be achieved by dialysis following CNC production[125] many CNCs are commonly stored and commercially sold in sodium form,[32] and counterions must be exchanged to protons prior to titration. Beck *et al.* [44] recommend strong acid ion exchange resin (such as Dowex Marathon C hydrogen form strong acid cation exchange resin) as the most efficient method to treat freeze dried, spray dried and never dried CNCs from a variety of laboratory and commercial producers.
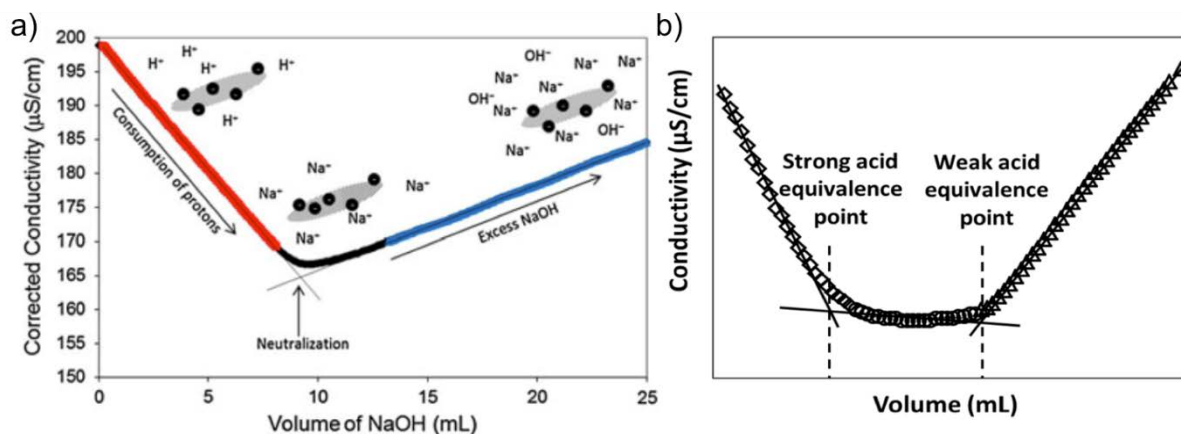
Figure 3.2. (a) Conductometric titration curve of S-CNCs from cotton (0.06 g cellulose) titrated against NaOH (1.31 mM) where the intersection of the two slopes (neutralization point) corresponds to the amount of strong acid (sulfate half ester groups) on the CNC surface. Figure reprinted with permission from reference.[125] (b) COOH-CNCs in acidic media titrated with NaOH. An initial step associated with the deprotonation of the free acid is followed by the deprotonation of the carboxyl groups and further with an increase of the conductivity associated with the excess NaOH. The linear fit (utilizing the highest coefficient of determination, "R^2" for all three lines) and two intersection points for determining the strong and weak acid equivalence points are annotated and the total carboxyl content is calculated from the volume difference of NaOH added between the equivalence points.

3.2.1. Data Analysis

The molar surface charge of CNCs is determined graphically by plotting the conductivity of the CNC suspension as a function of the volume of NaOH added. Critically, the conductivity is directly proportional to the amount of electrolytic solution and it is therefore essential that the measured conductivity be corrected for the volume of NaOH added at each data point by:

$$Conductivity_c = Conductivity_m \times \left(\frac{V_i + V_0}{V_i}\right) \qquad (3.1)$$

where, $Conductivity_c$ is the corrected conductivity in $\mu S \cdot cm^{-1}$, $Conductivity_m$ is the measured conductivity for each data point ($\mu S \cdot cm^{-1}$), V_i is the initial suspension volume in mL (i.e., the total volume of the diluted CNC suspension including and NaCl solution, prior to the first addition of NaOH) and V_0 is the added volume of NaOH at each point (mL). Determination of CNC molar surface charge for strong and weak acid CNCs, respectively, is discussed further below in **Section 3.2.2**.

3.2.2. Protocol for Conductometric Titration of CNCs

Small variations in titration protocols across different labs have been presented in the literature resulting in discrepancies in the overall charge densities reported and making a direct comparison difficult.[133] These discrepancies arise, probably, due to the lack of full protonation of the surface moieties and are a consequence of the sample pretreatment and/or the protocol employed for surface charge determination, as discussed above.[125] Although several protocols exist,[125, 133] the Canadian Standards Association (CSA) has recently published a suggested protocol for the determination of physical and chemical properties of CNMs entitled *Cellulosic nanomaterials — Test methods for characterization (CSA Z5100-14).*[15] Additionally, the ISO Standard, *ISO/WD TS 21400 -- Determination of Cellulose Nanocrystal Sulfur and Sulfate Half-Ester Content* describes conductometric titrations following a similar protocol.[41]

Before undertaking the conductometric titration of CNMs, a stock titrant solution of NaOH (5-10 mM) should be prepared in purified water.[15] The NaOH concentration should be precisely measured by pH titration with a standard acid of known concentration. The use of HCl as titrant is not recommended since the strength of the acid may change over time and with dilution of the acid, resulting in inaccurate measurements. It is therefore recommended to prepare a solution of potassium hydrogen phthalate (KHP) by first drying KHP in the oven at 105 °C for at least 4 h. Then dilute it in purified water to obtain a similar concentration to the NaOH solution. Titrate the KHP solution with NaOH using a calibrated pH meter and determine the equivalence point and the titre of the NaOH solution.

3.2.3. Titrating Strong Acid CNCs

As described in CSA Z5100-14 Standard in section 5.3.4[15]: 10 mL of 1 wt.% acid-form CNC suspension is diluted to 198 mL in deionized water. Stir until aggregates are no longer visible, and create a homogeneous suspension by sonicating (see **Section 2**). While the concentration and volume can vary, it is essential to know the exact mass of CNCs within the diluted suspension. To this, 2 mL of 100 mM NaCl (stock titrant) solution is added to increase conductivity to a measurable range. Under constant stirring, 10 mM NaOH is titrated in 100 µL intervals while continuously measuring the pH and conductivity. Prior to the first NaOH addition, pH typically ranges from 3 to 4 depending on charge density and CNC concentration. Following each NaOH addition, allow the conductivity to stabilize for 30 to 60 s before recording the value. Upon reaching the equivalence point, excess NaOH should be added such that sufficient data points are recorded for a statistically significant linear regression (typically equal to the number of points before the equivalence point). Measurements should be conducted in triplicate.

The equivalent molar charge is calculated via the molar volume of NaOH added, which is determined as the intersection point of the linear regressions of the regions before and after the equivalence point. This can be seen in **Figure 3.2a** as the red and blue regions respectively. The surface charge density is often reported as mmol/kg of CNC or weight percentage of sulfur but can be converted to surface charge density (e^-/nm^2) by knowing the average dimensions of the CNCs (see **Sections 7 and 9** for particle size analysis by TEM and atomic force microscopy (AFM), respectively).

3.2.4. Titrating Weak Acid CNCs

Similarly, a detailed procedure for determining the surface charge density for CNCs with weak acid groups can be found in CSA Z5100-14 Standard in section 5.3.5.[15] Importantly, when only weak acid surface groups are present, such as for COOH-CNCs, strong acid must be added to identify the two equivalence points;[32, 51, 70] the first equivalence point is where NaOH has titrated all the added strong acid and the second equivalence point is where NaOH has titrated all the weak acid groups (**Figure 3.2b**).

To 10 mL of 1 wt% acid form CNCs, add 1 mL of 100 mM HCl and dilute to 200 mL with deionized water. Although concentrations and volumes vary, 1 mL of 100 mM HCl should be added for every 0.1 g of CNC in suspension. Under constant stirring, titrate with 100 µL additions of 10 mM NaOH stock titrant solution while continuously measuring the pH and conductivity. Titration curves will exhibit two equivalence points that can be observed in both the conductivity and pH curves as a change in the slope or an inflexion point, respectively. Following the weak acid equivalence point, NaOH should be added such that sufficient data points are recorded for a statistically significant linear regression.

The molar surface charge is calculated as the molar volume of NaOH added between the strong acid and weak acid equivalence points. Because the equivalence points are not sharply defined as in the case of S-CNCs, the equivalence points are determined as the intersection points of linear regressions of the strong acid, plateau and excess NaOH regions (See **Figure 3.2b**). The molar volume of NaOH added between these intersection points is equivalent to the molar surface charge of the CNC. Similar to S-CNCs, the surface charge density is often reported as mmol/kg but can be converted to surface charge density (e^-/nm^2) by knowing the average dimensions of the CNCs (see **Sections 7 and 9** for particle size analysis by TEM and AFM, respectively).

3.3. Determination of Total and Surface Charge Density for CNFs

Charge determination of CNFs has been traditionally done via conductometric titration of the pulp, assuming that further mechanical disintegration will lead to fibrils with equal total charge density.[134] However, this is most likely to be only accurate when the delamination of the pulp into fibrils is done in a highly efficient manner. Moreover, the mechanical treatment (high pressures and temperature) has been shown to alter the chemistry of the produced nanofibrils, resulting in lower total charge densities.[135] Conductometric titration, in the case of CNFs and aggregated microfibrils, leads to the determination of the total charge density and it is not strictly limited to the surface charge, which can be substantially lower than the total charge density. Nevertheless, the determination of the total charge density brings valuable information to the characterization of CNFs and is a commonly used method and therefore standardization of the protocol is still imperative.

Surface charge determination of CNFs can be performed via direct or indirect polyelectrolyte (PE) titrations. The PE titration was introduced early in the development of the CNM field and consists of the adsorption of a known amount of PE on the surface of CNFs until the isoelectric point of the material is reached, assuming that the amount of charges present on the adsorbed PE corresponds to the amount of surface charges present on the CNF.[31, 136] This method is tedious and requires long adsorption times to ensure that the PE is not being adsorbed in an elongated conformation or bridging two or more CNFs. Dilution ratios are also critical, i.e., a too high PE concentration may create aggregates and a too low concentration may underestimate the charge content. The molecular weight of PE and its conformation at the surface of the CNFs (tail or loop) might also induced errors in calculation. For a more comprehensive discussion on PE titrations, the reader is referred to other studies on the topic.[31, 114, 136, 137]

3.3.1. Protocol for Conductometric Titration of CNFs

Conductometric titration of CNFs is challenging due to the high surface area of the nanofibrils and the tendency of the material to gel, especially at high concentration and pH values. This is due to the doprotinated anionic groups, which lead to strong electrostatic repulsion that results in a kinetically restricted attainment of equilibrium in the system. Thus, the conductometric titration technique of CNFs has been adapted to overcome these issues by performing an indirect version of the original protocol. That is,

CNF suspensions are initially deprotonated by the addition of excess NaOH and then back titrated with standardized (and freshly prepared) HCl solution. Following this strategy, the gelation of the sample is better controlled such that more accurate results can be obtained.[134, 137] Specifically, the suspension viscosity is at a maximum prior to titration and decreases with the HCl addition. Junka *et al.*[137] studied the effect of parameters such as the ionic strength and the amount of sample employed, on the reproducibility and accuracy of the total charge density measurements. The optimal conditions reported in this study are similar to the ones reported by the Scandinavian pulp, paper and board testing committee and are summarized as a protocol below.[134] Stock titrant solutions should be prepared following the procedure indicated in **Section 3.2.2** but adjusting to the concentrations specified below:

Prepare a 493 mL dilute suspension containing 300 – 500 mg of CNFs in deionized water. Prior to titration, CNF charged groups must be completely deprotonated such that the viscosity of the suspension can be controlled. This is achieved by the addition of 2 mL of 100 mM NaOH solution and stirring vigorously for a minimum of one hour. Following deprotonation, ca. 5 mL of 10 mM NaCl is added to adjust the conductivity to measurable range (total suspension ionic strength of ca. 1 mM). Because only the weak acid groups are present on the surface of CNFs, dissolved carbon dioxide can interfere with titration measurements. To limit the influence of carbon dioxide, N_2 should be gently bubbled through the suspension for a minimum of 30 min prior and continuously throughout titration. Under constant stirring, titrate with 100 μL of 100 mM HCl stock titrant solution while continuously measuring the pH and conductivity. Importantly, because HCl is being added instead of NaOH, as in the case of CNCs, titration curves will exhibit two equivalence points; the weak acid equivalence point followed by the strong acid equivalence point, which is opposite as displayed in **Figure 3.2b**. Data treatment should be performed following the steps indicated in **Section 3.2.2**, obtaining a plot in which strong and weak acid equivalence points should be clearly distinguished.

Concerning the PE titration strategy, poly(diallyldimethylammonium chloride) (PDADMAC) at 0.001 M is commonly used with CNF suspensions diluted to around 4×10^{-3} g L^{-1}.[138] Then 10 mL of NaCl solution is added in order to control the conductivity of the suspension (300 μS cm^{-1}), and the pH of the suspension is adjusted to be close to 9 with a sodium hydroxide solution to obtain the carboxylate form. Then, PDADMAC is added in known aliquots at different concentrations depending on the CNF type: i.e., 10^{-4} M and 10 g L^{-1} for enzymatically-treated CNFs and TEMPO-oxidized CNFs titrations, respectively. (The concentration of the PDADMAC solution added is higher for TEMPO-oxidized CNFs because they are expected to have a larger surface charge density.) At least 5 min of stirring is performed to ensure good mixing between the polymer and the CNFs after each addition. The adsorption of PDADMAC is performed during minimum 2 hours without stirring. Finally, the suspension is stirred quickly to have a better dispersion in water and the zeta potential of 100 μL of solution is measured to calculate the surface charge.[138]

3.4. Zeta Potential of CNCs and CNFs

As explained above, surface charge density is largely responsible for colloidal stability of CNMs in suspension. Zeta potential directly probes colloidal stability as discussed in **Section 2** and it is commonly used to characterize CNMs.[123, 139, 140] Due to the fact that the electrophoretic mobility of the nanoparticles is being measured and not the actual surface charge density, this technique is highly affected by pH, temperature and the presence/type of electrolytes in the suspension.[141, 142] Thus, to obtain reliable and comparable zeta potential measurements, consistent sample preparation (including precise dilution for CNFs or filtration with a 0.45 μm syringe filter for CNCs) should be carried out as suggested by the CSA.[15, 143] During the measurement, data should be recorded employing monomodal acquisition with fitting according to Smoluchowski theory. Analyses should be performed at least in triplicate and only samples recorded at the same temperature and pH can be compared.
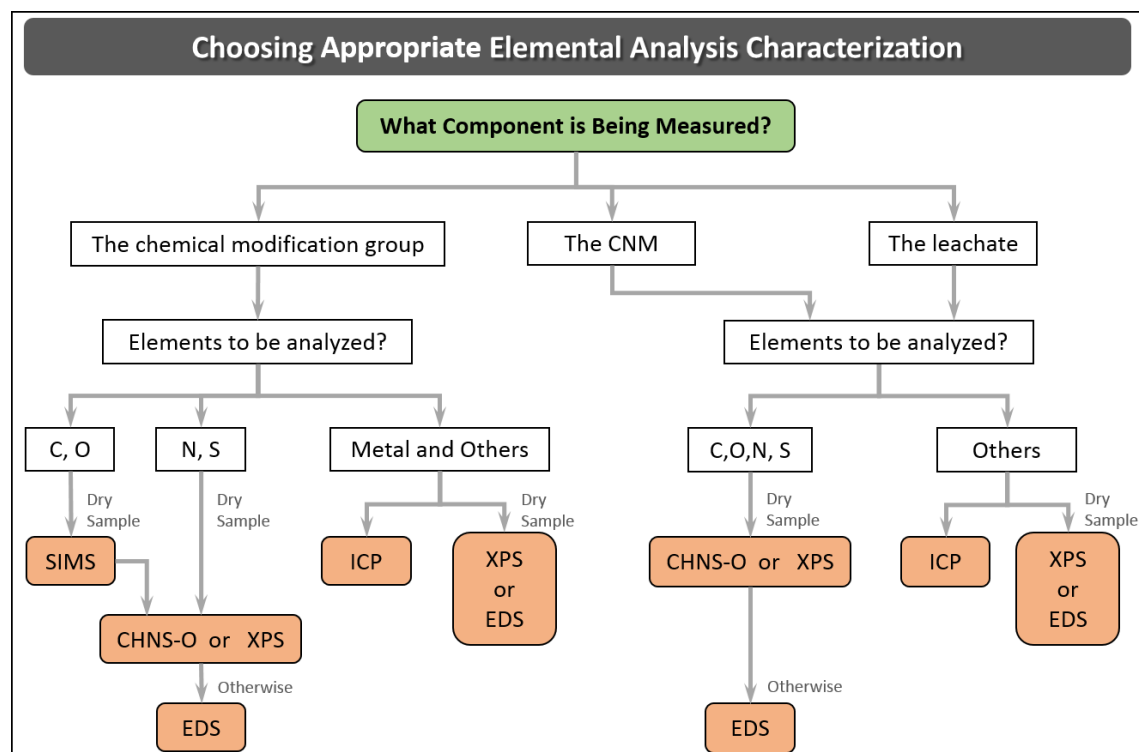
SECTION 4: Elemental Analysis of CNMs

Matthew Korey, Jeffrey Youngblood

4.1. Introduction

Elemental analysis (EA) is comprised of a variety of techniques that measure the elemental composition of a sample, as listed in **Table 4.1**. It is useful when trying to verify different elements within a sample to help ascertain the structure of, or for measuring the purity of, a known or unknown compound. EA techniques are often the fastest and most inexpensive methods to determine the purity of samples. These methods of chemical analysis are particularly useful in CNMs because they can provide validation and quantification of chemical modification, can help identify sulfur and other elements in a sample, can provide verification of acid hydrolysis of cellulose-containing compounds, and can assist in determining impurities in materials containing CNMs. While EA methods often cannot be used alone to determine the structure of a compound, they can be used to obtain useful complementary information for further verification.

It is important to choose the most applicable method of EA when characterizing CNMs. This review will focus on carbon hydrogen nitrogen sulfur elemental analysis (CHNS EA), secondary ion mass spectrometry (SIMS), x-ray photoelectron spectroscopy (XPS), auger electron spectroscopy (AES), energy dispersive x-ray spectroscopy (EDS or EDX), and atomic emission spectroscopy techniques including inductively coupled plasma (ICP). This is not to say these are the only techniques possible for such characterization, but these methods were determined the most valuable for characterizing CNMs. A decision tree is given in **Figure 4.1** to guide the reader how to choose which technique to use. A helpful summary of all of the EA methods is provided in **Table 4.1**.

Figure 4.1: A decision tree for elemental analysis characterization of the chemical modification group, the CNM or the leachate.

Table 4.1: A comparative guide to the elemental analysis methods discussed in this section: Advantages, disadvantages, and the type of elements capable of being measured.

Chemical Characterization Method	Acronym	Advantages	Disadvantages	Light Element	Sulfur	Medium to Heavy Element
Carbon Hydrogen Nitrogen Elemental Analysis	CHN CHNS CHNSO CHNSX	• Provides quantitative elemental data for C, H, N, O, S, and halogens	• Difficult to measure C, H, O chemical modification	√	√	
Secondary Ion Mass Spectrometry	SIMS	• Useful for C or H in modification procedure	• Difficult to quantify • Low detection limits and lateral space resolution	√	√	√
X-ray Photoelectron Spectroscopy and Auger Electron Spectroscopy	XPS and AES	• Quantitative analysis of specific atoms in sample • Good lateral space resolution • Best practice for elemental analysis when modified groups contain C, O, or H	• Sample must be solid • Lack sensitivity for trace chemical identification • Assumes bulk same as first few nanometers	√	√	√
Energy Dispersive X-ray Spectroscopy	EDS	• Useful for heavy atoms • Good lateral space resolution	• Difficult to characterize light elements • Lack sensitivity for trace chemical identification • Sample must be solid	√	√	√
Inductively Coupled Plasma: - mass spectrometry - atomic emission spectroscopy	ICP-MS ICP-AES	• Sample can be liquid • Useful for heavy atoms	• Cannot characterize light elements • Limited use with solid samples			√

4.2   CHN, CHNS, CHNS-O, and CHNS-X EA

CHN EA is used to characterize the major elements of an organic substance. The theory is based upon the Dumas method where in pure oxygen at high temperature (above 1000°C) all available carbon in a sample will react to form carbon dioxide, all available hydrogen will react to become water, all nitrogen will react to become nitrous oxides[144]. Advancements in this technology have allowed for additional chemicals to be characterized including sulfur using barium sulfate (CHNS),[145] oxygen using carbon and copper oxide (CHNS-O),[146] and even halogens using silver nitrates (CHNSX)[147] but in order to detect these elements an add-on to the device or a completely new detector is required.

After initial combustion, chemicals other than carbon (C), hydrogen (H), nitrogen (N), sulfur (S), and oxygen (O) in the sample, are converted to combustion products (such as chlorine into hydrogen chloride) which are absorbed by a variety of absorbents so they do not contaminate the output. The desirable combustion products are swept out of the combustion chamber by an inert gas, helium. The gas flows over high purity copper, which is used to remove any un-reacted oxygen not consumed in the initial combustion and to convert any nitrogen oxides into nitrogen gas.[148, 149] Absorbent traps are then used to remove any remaining contaminants. Detection of gasses is done in a variety of different ways, such as gas chromatography, infra-red thermal conductivity cells, and chemical traps, but these depend on the detector used and the manufacturer from which the device is purchased.

In the literature, there are three main cases in which CHNS analysis is used to characterize CNMs. The first such case is when proving acid hydrolysis using sulfuric acid. This method of characterization is particularly useful in this instance because residual sulfur groups from acid hydrolysis are easily identifiable

on the output spectra. This procedure has been done by researchers attempting to prove acid hydrolysis of cellulose I with sulfuric acid,[150] acid hydrolysis of cellulose into glucose,[151] and to prove extraction of CNFs from eucalyptus kraft pulp.[152]

The second such case is when functionalizing or incorporating a nanocellulose-based material with a functional group or molecule. If the functionalized groups contain N or S this procedure is particularly simple as these groups are easily identified in the output spectra. If the groups contain only elements also contained within nanocellulose itself (C, O, or H), CHNS analysis can be used for this as output CHNS spectra will show an increased peak for that element. However, although CHNS analysis can be used to prove C, O, and H bond modification, XPS is preferred for that particular situation as the modified C's in the sample can be identified more exclusively. Researchers have used CHNS to verify the degree of substitution of cetyl trimethylammonium bromide modified CNC,[153] degree of bisphosphonate modification of phosphonated nanocellulose,[154] verify aminosilane functionalization of CNCs,[155] peptide incorporation levels on CNCs from cotton,[156] glycidyl trimethyl ammonium chloride modified CNFs,[157] animation of a microfibrillated cellulose,[158] verification of poly(propylene carbonate)-coatings on nanofibrillated cellulose glycerol,[159] and azo dye adsorption onto the surface of microcrystalline cellulose.[160]

The third case is when attempting to measure the degree of chemical leeching in polymers containing CNMs when the leachate contains C, H, N, S, or O, such as when investigating organic chemical leaching outside of polymer solutions.[161] However, CHNS analysis cannot be run on a liquid sample, thus the sample must be dried beforehand.

While this method of analysis is highly quantitative in nature, it does have its limitations. The working range of CHNS analysis of C- or N- containing samples is generally accepted as above 0.05% by weight (500 ppm) among researchers, although some tools advertise values less than this[162-164]. Within the working range the uncertainty is 200-300ppm[162, 163, 165]; thus, one must be careful using CHNS analysis at low loading levels. Samples containing phosphorous can also suffer from systematic deviations in the determined carbon content exceeding the tolerance limits advertised on many tools[165]. It is difficult to characterize differences in C, O, or H content before and after chemical modification due to the large background signal from cellulose structure in CNMs. Due to chemical limitations of this EA technique, it is not useful for characterization of any element other than C, H, N, S, O and sometimes halogens in a CNM-containing sample.

4.3. Secondary Ion Mass Spectrometry and Time of Flight SIMS

SIMS chemical analysis is a method through which the surface of a material is characterized by being bombarded by a focused primary ion beam, typically argon ions (Ar^+), gallium ions (Ga^+) or alkali metal ions.[166] Primary ions sputter the surface and cause secondary ions from the surface of the material to be ejected into the atmosphere above the material. These secondary ions are then filtered into a mass spectrometer and are analyzed. SIMS detectors in this regard are limited in sampling depth to around 1-2 nm.[166] The most commonly used mass spectrometer detector used for organic molecules is time of flight (ToF) as one can obtain the full mass spectrum in one operation rather than having to scan through a full mass spectrum in one operation.[166]

There are three main modes of SIMS analysis: 1) static SIMS, 2) scanning SIMS, and 3) dynamic SIMS. In static SIMS, the surface is sputtered in the same location and the chemical composition of the material can be measured from the surface to a depth of around 1 nm.[166] Static SIMS is usually used to determine whether the composition of a material is changing with depth and can be used to determine the intermediate steps in a catalyzed reaction. Static SIMS is done to a depth of 1.5nm and a spatial resolution of 200nm.[167] However, with static SIMS quantification can be difficult. Scanning SIMS, in which the surface of a material is sputtered to a short depth but is scanned across a wide area, can also be performed to characterize if there are any chemical concentration differences along the surface of a material or to determine if there are any surface contamination and thin layer structures.[168] The spatial resolution is dependent upon the primary beam size, but can be anywhere in the range of 0.5-3µm.[169] The third method, dynamic SIMS, uses a very high beam intensity to cut the sample through a very fast sputtering technique. This allows you to measure the composition as a function of the depth of the material, but unlike in static SIMS this permanently damages the material.[166]

In literature, ToF-SIMS has been used to verify the presence of chemical modification and lateral amino acid distribution in amino acid modified cellulose surfaces and as confirmation of the presence of individual amino acids on the fibrous networks of cellulose after chemical coupling.[170] Other researchers have used this method for verification of fatty acyl chain modification in modified CNMs. This was done by looking for characteristic peaks associated with the acyl chain-derived ions, which was used to indicate that fatty acids had been attached by covalent bonds to the fiber matrix.[171] Other researchers have used ToF-SIMS to verify the surface modification of CNFs through acetylation in an ionic liquid.[172] In any case, the main application of SIMS in nanocellulose characterization is in verification of chemical modification.

From the literature, it is clear that time-of-flight secondary ion mass spectroscopy characterization has been used when characterizing CNMs for qualitative analysis of the presence of chemical functionalization on the surface of the CNMs. Because SIMS is a highly surface sensitive analysis technique (with sampling depths limited to the first atomic layers),[166] it is used in this application for the verification of surface chemical modification. However, ToF SIMS is limited due to the fact that its output is not easily quantifiable in nature, thus another EA method must be used to quantify results, such as XPS or CHNS.

4.4. X-ray Photoelectron Spectroscopy and Auger Electron Spectroscopy

XPS, also known as electron spectroscopy for chemical analysis (ESCA), is a chemical analysis method in which the surface of a material is irradiated with x-rays. Core shell electrons in the atoms on the surface are energized from these x-rays and escape from their atoms and become photoelectrons.[173] Core shell electrons in specific atoms in specific energy shells have specific, defined energies associated with them. The associated energy of emitted ions can therefore be used to characterize the composition of a material.[174] AES works very similar to XPS, but is based on the Auger theory in which the energy of a core shell electron entering a hole left by an escaping photoelectron is able to emit energetic electrons from the same atom known as Auger electrons.[175] These Auger electrons can be used to characterize the chemical composition of the material due to their characteristic energies. For the purposes of this analysis either method could be used for the characterization described in each source in this section, but as XPS has been used more in the context of cellulosic nanomaterials, the discussion will focus on that technique.

XPS has been used to characterize CNMs for two main reasons. First is to provide quantitative analysis of the carbon linkages to prove chemical modification on the surface of modified CNMs. This technique has proven chemical modification of PET fabrics with CNC particles,[175] bromine and sulfur in modified CNC samples,[176] carbon bond modification for esterification of CNCs,[177] and modification of CNCs for ATRP,[178] and to characterize oxygen and carbon content in CNFs.[179] XPS is also useful for characterization of heavier ions such as iron[180] and to characterize the oxidation state of metal nanoparticles in solutions containing CNMs.[181]

XPS and AES do have associated limitations. First, the sample must be solid. Second, they lack sensitivity for trace chemical identification. Third, the results one obtains for the material are only for the surface, not the bulk. Thus, in order to use XPS/AES to characterize a material one must assume the surface properties are indicative of the bulk material, which is not the case in every application. Another major consideration when performing these surface sensitive techniques is that of carbon contamination, which is present on nearly all surfaces exposed to the atmosphere. On cellulosic samples there is often a significant amount of C1 contamination (from 5-7% error) in output spectra.[182] The error is often even higher and less predictable in samples that have come in contact with other materials such as plastics, cellophane film, aluminum, and/or glass.[182] Thus, care in sample handling must be taken. It is also recommended that for reproducible data of cellulose that only low-power monochromatic irradiation be used.[182] Nevertheless, XPS is particularly useful when determining relative changes of non-carbon elements on the surface of a CNM.[32] While XPS and AES are quantitative by nature, the data are dependent upon sample handling/preparation to limit contamination, integrating all elements present, proper calibration of electron yield and work function, beam damage of the sample, and charge compensation. Thus it is advised to consider results relative to results obtained at the same time on the same instrument and not compare to results found in literature or on a different XPS analyzer, unless one is sure that proper methodologies were followed.[32]

4.5. Energy Dispersive X-ray Spectroscopy

EDS is an analytical technique where a high-energy beam of charged particles or an x-ray is used to characterize a sample. Atoms within the sample contain ground-state electrons in discrete energy levels bound to the nucleus which, when excited by an outside source, can be ejected from their shells creating an electron hole. An electron from an outer shell can then fill this hole, releasing an x-ray with energy equal to the energy difference between the outer-shell and inner-shell.[183] The number and energy of these x-rays is measured by an energy-dispersive spectrometer and is used to characterize the sample.

EDS is a particularly useful EA method for the characterization of CNMs because it is often attached to SEM devices. Because of this, one can easily obtain chemical composition of surfaces that are visually identified on the SEM. EDS has been used for quantitative measurement of chemical composition of metal nanoparticle-nanocellulose hybrid composites,[181] for characterizing CNF-containing copper nanoparticles,[184] characterizing S and N composition on S,N-doped graphene-modified nanocellulose,[185] for quantitative analysis of chemical composition on polypyrrole-nanocellulose composites,[186] for quantification of calcium and phosphorous content in bacterial nanocellulose scaffolds,[187] and for semi-quantitative EA of bacterial nanocellulose reinforced fiber-cement composites.[188] In every instance listed above, EDS was used in conjunction with SEM analysis.

EDS does have some limitations. It is difficult to characterize light elements with this characterization method, although researchers have used EDX to characterize C, O, and S content in sugarcane-sourced CNMs.[189] In this particular instance SIMS, XPS, and CHNS EA would be more applicable. Second, EDS lacks the sensitivity required to perform trace chemical identification and thus cannot be used for characterization of very small amounts of atoms.

4.6. Inductively Coupled Plasma -Mass Spectrometry and Atomic Emission Spectroscopy

Inductively coupled plasma (ICP) is a technique that uses a plasma to ionize atoms within the sample so they can be analyzed subsequently by mass spectrometry or atomic emission spectroscopy. Free electrons are introduced to an Argon gas stream inside a magnetic field. Electrons interact with the magnetic field and oscillate back and forth, colliding with gaseous atoms and releasing electrons which are then accelerated producing a fireball that consists mainly of argon atoms with a small fraction of free electrons and argon ions.[190] The sample to be studied enters the ICP, evaporates and causes constituent atoms to ionize. At high temperatures within the plasma, a significant proportion of the atoms become ionized, each atom losing its most loosely bound electron to form an ion with a single positive charge.[191] These ions are then extracted through a series of cones into a mass spectrometer and are separated on the basis of their mass-to-charge ratio. Alternatively, ICP-atomic emission spectroscopy (ICP-AES) can be used where the excited plasma photoemission is analyzed for characteristic frequencies and is similar to atomic adsorption and glow discharge spectroscopies. Both detection methods (MS or AES) are functionally equivalent in that the elemental composition is analyzed. Hence, we will refer to the technique as ICP-MS/AES

ICP-MS/AES is useful for characterization of CNMs when considering medium to heavy weight atoms in CNM-containing composites. The main application of this characterization method in the identification of metallic or salt compounds or impurities in a CNC sample. One group measured the amount of zirconia in their sample, as their milling process included the use of zirconia milling balls.[192] ICP-AES has been used to characterize palladium leaching in Pd nanoparticles supported onto bacterial CNFs[193] and for verification of Pd loading in CNC-catalyzed Heck coupling reactions.[194] ICP-AES analysis has also been used for characterization of Ca/P ratios for HA-CNC composite systems for biomimetic bone scaffolds.[195]

ICP-MS/AES is a powerful method of EA, but cannot be used for characterization of light elements. Further, due to hesitation of many scientists to inject solids or samples in which solids are dispersed into the instrument, ICP-MS/AES is often only performed on liquid samples. However, it is ideal for leachate analysis after ultrafiltration or centrifugation to remove the CNM.

SECTION 5: Solid-State Properties of CNMs

Wadood Y. Hamad, Laurent Heux, Umesh P. Agarwal

5.1. Introduction

The quantification of solid-state properties can help elucidate the molecular structure of CNMs. This would have a two-fold benefit. (1) To understand the basic structure of CNMs and hence be able to accurately and appropriately achieve efficient and effective surface functionalization and modification. (2) Improve CNM extraction methods so as to obtain appropriate structures for appropriate applications. For example, we would need to carefully ascertain the hydrolytic or homogenization processing conditions needed to produce CNCs or CNFs, respectively, which have the appropriate levels of surface and bulk crystallinity. This can then guide the manipulation of these CNMs for as diverse applications as flexible electronics or responsive materials in adaptive packaging. In this section we shall summarize best practices for measurement of solid-state properties via: (i) X-ray diffraction (XRD), (ii) solid-state nuclear magnetic resonance (ssNMR), and (iii) Raman spectroscopy. A decision tree to help guide decision-making is presented in **Figure 5.1**.
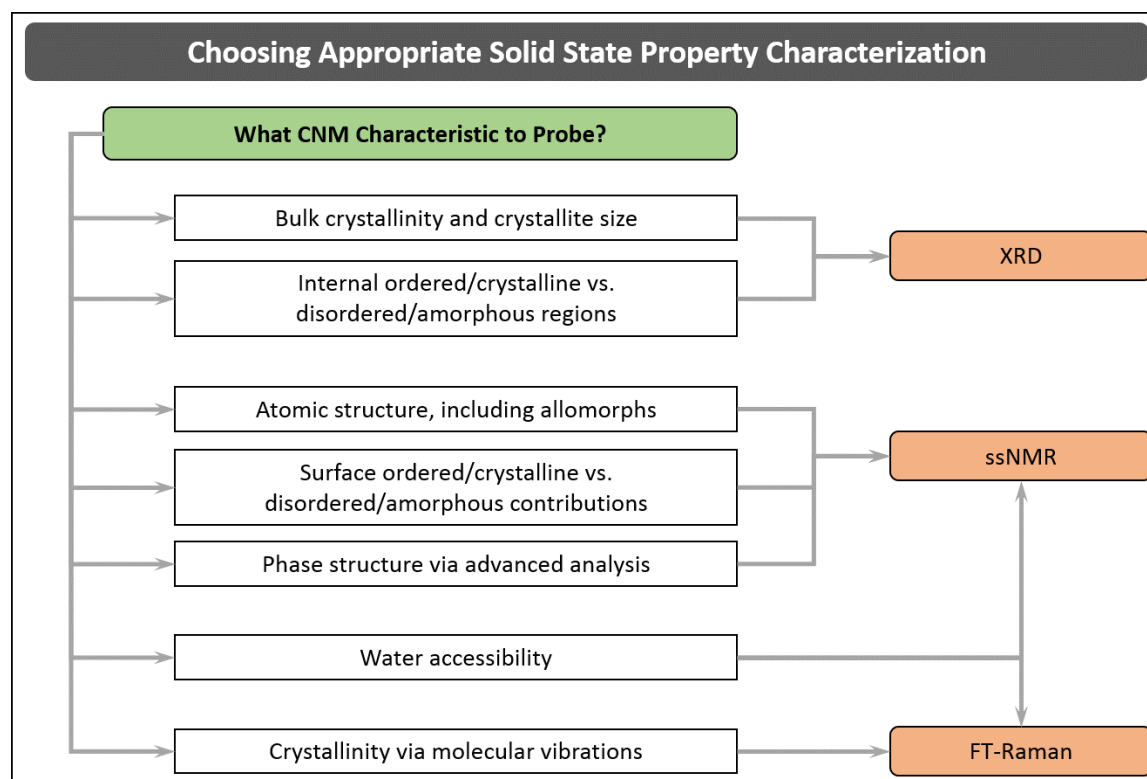
Figure 5.1: Decision tree for the three primary techniques used to analyze the solid-state structure of CNMs. These techniques are complementary to each other, and collectively will provide as comprehensive a picture as possible of the CNM solid-state structure. More detailed insights on the topic can be found in Hamad.[196]

5.2. X-Ray Diffractometric Analysis of CNMs

5.2.1   Relevance

X-ray diffractometric analysis can in principle be applied to all cellulosic materials, including CNCs and CNFs.[197-199] However, the significance of this approach is to use XRD analysis as a means not only to obtain a measure of crystallinity, which is a *bulk property* as determined by XRD, but also to systematically examine the factors influencing the transition and distribution of highly-ordered to least-ordered regions. The method, approach and analysis described in here are applicable to CNCs, CNFs, and other cellulosics.

5.2.2   Methodology & Analysis

The experimental protocol requires a powder X-ray diffractometer (PXRD) equipped with a CuX_α X-ray tube, a diffracted beam graphite monochromator and NaI scintillation detector used with the generator set to 40 kV and 40 mA (one example of commercially available systems is the Bruker D8 Advance family of instruments). Data should be collected at 2θ = 5-90° (or up to 60°, if there is little response beyond) using a step size of 0.02° and a counting time of 1 sec/step. 1.00 mm divergence and anti-scatter slits should be used with a 0.2 mm receiving slit, and the sample can be rotated during data collection. Specific care must be given to the form of CNM, whether spray-, freeze- or air-dried, since material handling, and morphology, can be different in each case. Ideally for PXRD, the sample will need to be packed in random orientation. Hence, spray-dried CNMs, for instance, can be packed in the appropriate XRD sample holder. For freeze-dried CNM a small amount, ideally 15 mg, should then be dispersed in water, which is poured onto a zero-background Si plate, and the sample is allowed to dry overnight to ensure complete water evaporation. (Heating the sample is not recommended.). In the case of pre-cast air-dried CNM films, squares (c.a., 2.5 cm by 2.5 cm) of the flattest part of the sample is cut out and taped as flat as possible onto the zero-background Si plate. In both of the latter two cases, the sample-on-zero-background-plate is then mounted flush in the sample holder of the X-ray diffractometer.

Diffraction patterns (**Figure 5.2**) of freeze dried CNCs and CNFs consist of well-defined peaks assigned to the (002) plane at $2\theta \approx 22.7°$ and the (101) and ($10\bar{1}$) planes at $2\theta \approx 14\text{-}17°$, as well as a contribution for the (040) plane at $2\theta \approx 34.3°$. The CNC diffraction patterns for hydrolysis at different temperatures vary in crystalline peak intensity and width, leading to different crystallinity and crystallite size, but are otherwise similar in overall response. The raw diffraction patterns of the extracted materials need to be resolved into their respective crystalline and amorphous regions based on known cellulose I peaks, and from which the solid-state properties can be determined. To do this, the Ruland-Rietveld approach is recommended, whose procedure is described below.
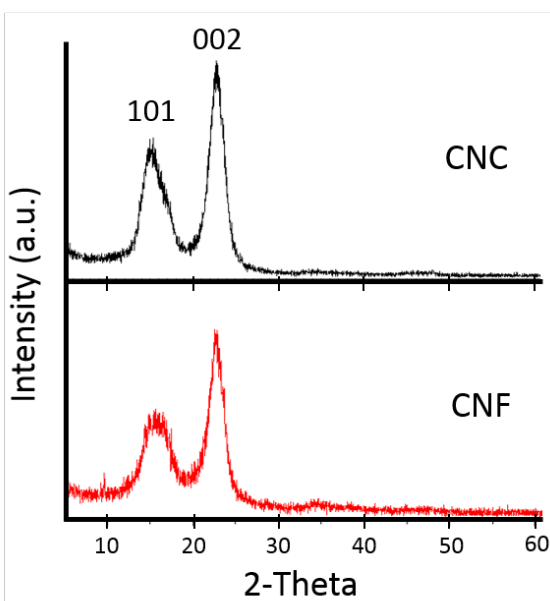
Figure 5.2: Diffraction pattern for freeze dried CNCs (hydrolyzed using 64 wt.% H_2SO_4, 45°C, 25 min) and CNFs (supplied by University of Maine) resolved into crystalline peaks and amorphous background

(following the Ruland-Rietveld analytical approach). It is worthy of note that both CNC and CNF samples have the same crystallite size of 5.9 nm but different crystallinities, $X_{c\text{-}CNC}$ = 86.2 % and $X_{c\text{-}CNF}$ = 68.6 %.

The peaks, along with the associated d-spacings and 2θ positions, should be assigned according to the monoclinic unit cell for cellulose I. DiffracPlus Topas software (Bruker-AXS), which uses the Rietveld method of refinement,[200] can be used to deconvolute the peaks of the diffraction patterns (**Figure. 5.2**). The degree of crystallinity, X_c, or more precisely crystallinity, defined as the fraction (or the percentage) in weight occupied by the crystallites, can be determined using Ruland's well-established theoretical approach.[201] The Topas (or other similar) software employs the Ruland method, which is based on rigorous physical considerations and on absolute corrected intensities expressed in electron units. This approach requires the separation of the scattering belonging to the crystalline peaks from the global background scattering. The software mathematically performs this separation,[202] using appropriate constants, to suitably scale and fit the scattering pattern of the amorphous phase, which has to be assumed to be available. The Ruland method and analyses reliant on this theoretical approach are based on the law of conservation of the total intensity scattered within the whole of the reciprocal space by a given set of atoms, independently of their state of structural order.

Assuming the total diffracted X-ray intensity to be made up of the diffracted X-ray intensity from both the crystalline and amorphous regions X_c, of extracted cellulose nanomaterials is determined using,

$$X_c(\%) = \frac{A_c}{A_c + A_a} \times 100 \tag{5.1}$$

where, A_c is the total crystalline area, and A_a, the total amorphous area of the deconvoluted XRD pattern after a subtraction of the background spectra. The deconvolution approach, based on Ruland's principles and Rietveld analysis, has successfully been used to study the supermolecular structure of various polymeric materials,[203] since it accurately permits the quantification of the solid-state properties. This approach is qualitatively different from the empirical method of Segal *et al.,*[204] widely used in lignocellulosic research,—where the crystallinity index relies on the arbitrary determination of the difference in the intensities of the (002) interference (representing crystalline peak) and amorphous scatter at 2θ ≈ 22.8 and 18°, respectively.

In powder X-ray diffractometric analysis we assume each crystal to consist of one or more crystallites, where the size of the crystallite is in general equal to or less than the crystal size. It is apposite to note that crystallite size is different from particle size, crystal size or domain size.[201, 205] Typically, particles consist of one or more crystals separated by large angle boundaries, amorphous or crystalline interfaces. Particle size is not accessible by powder diffraction, and is usually determined using TEM or AFM (see **section 7 and 9**). Similarly, for crystal size, agglomeration effects can hamper crystal size analysis (the size of a crystal is in general equal to or less than the particle size). A crystallite may consist of one or more coherently reflecting domains. If due to stacking fault twinning a two-domain crystallite gets broken into two domains, a correct association of domain(s) to crystallite(s) would depend on the reflection plane. Further, broadening due to domain size would be impossible to determine using powder diffraction. In conclusion, the domain size is generally equal to or less than the crystallite size. It should be noted that crystallite size can only be indirectly determined by means of powder diffraction. Actually, measurable quantities are the so-called column heights, and since the scattering power of a column is dependent on its volume, volume-weighted mean column heights, L_{vol}, are used. DiffracPlus Topas software was used to calculate (a measure of) the crystallite size based on the equation:

$$\beta_i = \frac{\lambda}{L_{vol} \cos \theta} \tag{5.2}$$

where β_i are integral breadths as proposed by Stokes and Wilson (Stokes and Wilson, 1944)[206] addressing domain-size broadening independent of crystallite shape, λ the radiation wavelength (1.542 Å), and θ the

Bragg diffraction angle, corresponding to the (002) plane in our case. Conceptually, **Eq. 5.2** is identical to the Scherrer equation (**Eq. 5.3**) with the constant K set to 1:

$$D = \frac{K\lambda}{\beta \cos\theta} \tag{5.3}$$

where D is the "apparent crystallite size," and β the full width of the diffraction peak measured at half maximum height (FWHM) of the instrument corrected line profile.

5.3. Crystallinity Estimation of CNMs by Solid-State Nuclear Magnetic Resonance

Solid-State NMR is a powerful technique for analyzing the atomic structure of CNMs.[207-209] The subject of NMR is vast and other specialized NMR techniques are available.[210] We shall focus in this section on ^{13}C CP-MAS NMR, the most commonly used NMR technique.

5.3.1. Relevance

^{13}C CP-MAS NMR spectroscopy is a high resolution technique (HR-ssNMR) that requires the combined use of cross-polarization (CP), magic angle spinning (MAS) and high dipolar decoupling devices. Compared to low resolution ssNMR spectroscopies (LR-ssNMR), it allows one to record spectra with a resolution comparable to classical liquid-state NMR spectra. Although the description of the physics underlying the technique is beyond the scope of this section, it suffices to note that this technique is fully quantitative when performed in tightly controlled conditions, in contrast with ^{13}C liquid-state NMR techniques. A ^{13}C CP-MAS NMR measurement is typically a prerequisite to sophisticated analysis using 2D-NMR techniques to study, for example, the phase structure of crystalline or semi-crystalline materials (see **Section 5.4**). It is worthwhile noting that the intrinsic anisotropy and/or disorder of common solids induce a dispersion of the chemical shifts resulting in wider spectral linewidths—which is characteristically different in the case of dissolved molecules that undergo rapid motions averaging out most NMR interactions. The dependence of the chemical shift on the local environment (conformation, packing, crystallinity, *etc.*) is indeed a strength for cellulosics that has allowed researchers to successfully detect the presence of two different allomorphs in native cellulose,[211] and ascertain the coexistence of crystalline and amorphous phases in cellulosic materials.[212]

5.3.2. Methodology

[13]C CP-MAS is usually performed on dry samples in order to remain fully quantitative, even if working with wet samples has proven to enhance the resolution of the spectra. In some cases, it may be informative to perform analyses in both the wet and dried states. Typically, 50 mg of material is required for routine experiments, although it may vary depending on equipment specifications and requirements.

5.3.3. Band Assignment and Spectrum Analysis: General Approach

Most of the chemical shifts of native cellulose have been assigned with the help of 2D-NMR experiments.[213, 214] However, due to signal overlap, only C1, C4 and C6 carbon signals have been well resolved, whereas the C2, C3 and C5 carbon signals are indistinguishable. C1 carbon displays a complex shape in relation with the different crystalline phases that can be found in cellulosic compounds; signals arising from C4 and C6 split into two main contributions, crystalline (around 89 and 65 ppm, respectively) and disordered (around 85 and 62 ppm, respectively) domains. **Table 5.1** summarizes the different chemical shifts and their assignments, and **Figure 5.3** shows the carbon associated with the chemical shifts.

It is worthwhile noting that, owing to the sensitivity of chemical shifts to conformational features, the same chemical entity (an anhydroglucose unit linked in β 1-4) can exhibit a large variety of chemical shifts depending on the crystalline phase (native Iα or Iβ, mercerized cellulose II) or degree of crystallinity (crystalline vs disordered chains), allowing for the estimation of allomorphic ratio and percent crystallinity to be calculated.

Table 5.1. Assignments of ssNMR chemical shifts corresponding to neat CNMs. Different CNMs exhibit similar features, apart from different ratios of crystalline/disordered regions.

Chemical shifts (ppm)	Carbon	Assignment
105.7 ; 103.9 105.0 107.0 ; 104.7	C1	• Cellulose Iα(Native cellulose) • Cellulose Iβ (Native cellulose) • Cellulose II (Mercerized cellulose)
89.4 ; 88.7 88.7 ; 87.9 84.2 ; 83.2 83.4 81.7	C4	• Cellulose Iα(Native crystalline cellulose) • Cellulose Iβ (Native crystalline cellulose) • Accessible disordered (amorphous) cellulose (Thin contribution) • Inaccessible disordered (amorphous) cellulose (Large contribution) • Hemicelluloses (Thin contribution)
78 – 70	C2, 3, 5	• Indistinguishable in 1D experiments. See Ref [213, 214]or detailed description of 2D NMR experiments
65.3 65.5 ; 64.8 62.9 ; 62.2 61.5		• Cellulose Iα(Native cellulose) • Cellulose Iβ (Native cellulose) • Cellulose II (Mercerized cellulose, thin contribution) • Disordered cellulose (Large contribution)
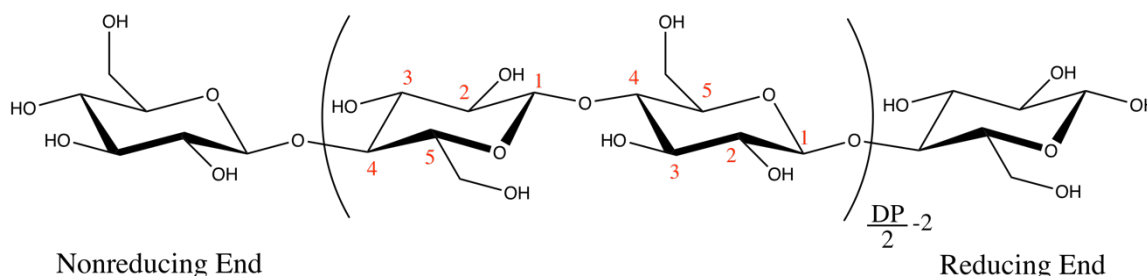
Figure 5.3: Chemical structure of cellulose and carbon atom numbering (C1-C5) of the glucose ring.

5.3.3.1 Allomorphic Ratio

Cellulose II can be easily and irreversibly obtained after swelling in NaOH,[215] and rinsing in water, which is a commonly used activation treatment for alkylation of cellulose. Cellulose II has a completely different set of chemical shifts, and its presence can be detected by an additional peak at 107 ppm for the C1 contribution, and a decrease of the 65 ppm contribution of the C6 peak. Examples of partial or complete transformation of CNC[216] or CNF[217] in cellulose II have already been described in the literature and is likely to happen during the soda treatment or acid hydrolysis. In the same vein, the ultrasonic treatment often used to disperse CNMs to enhance the reactivity of grafting moieties can cause allomorphic changes from Iα to Iβ and/or amorphization, i.e., a change in the crystallinity indices (*vide infra*).[218]

5.3.3.2 Crystallinity Indices

It has been known since the seminal work of Attala *et al.*[207] that cellulosic materials exhibit contributions that arise from the amorphous phase. It was not until the late 1990s, however, that the amount of crystalline vs. disordered phase was related to the size of the nanocrystalline elements in wood pulp[219, 220]or primary walls.[221] Briefly, the crystallinity indices can be calculated as the ratio of the areas of crystalline contribution for C4 carbons (*i.e.,* around 89 ppm, see **Table 5.1**) vs. the total C4 contribution (from **Table 5.1**), in a region where both signals are well separated. The percent crystallinity can be calculated with **Eq. 5.1**, where A_c and $A_α$, are the peak areas of the crystalline and amorphous peaks (listed in **Table 5.1**).The obtained values are usually comparable but lower than the crystallinity indices calculated from XRD experiments.

This simple measurement can also give an indication of the number of hydroxyls accessible to the reactants. Thus, considering the spindle-like shape of CNCs and the nanometric size of their physical

dimensions, one can estimate the number of chains that are exposed on the surface compared to the number of chains in the interior of the crystals (around one half for a crystal of 3 nm width). Utilizing the well-known inter-chain distance in the cellulose crystallite, and assuming the crystallites are a regular solid, a direct relation between the crystalline indices measured by ssNMR and the dimension of the crystal has been proposed.[219-221] Even if some subtleties have to be taken into account, like the presence of a relatively large amorphous phase in, for instance, CNF, the existence of possible inaccessible surfaces[220] or contamination with hemicelluloses,[221] this crystalline index value is, for a given system, a useful indicator of the morphology of the CNM, including preservation[222] or destruction[90] of crystallinity. An example is given in **section 6.3.5**

5.4.   Phase Structure of CNMs by ssNMR

Elaborate and specialized experiments can be carried out using ssNMR to probe the phase structure of CNM particles. Lemke *et al.*[223] were first to gain substantial insights into the structure of CNCs by subjecting these nanoparticles to ^{2}H/^{1}H exchange in order to label the regions accessible to water, and the reader is referred to their work for experimental details and analysis. Their approach, referred to as Rotational Echo Double Resonance (REDOR), is a high resolution ssNMR experiment employing magic angle spinning and cross polarization to measure the distance between two select labeled heteronuclei, such as C13-N15 or C13-O17 in the molecule. REDOR can provide relevant and precise information about the structure of biomaterials and polymers that are inaccessible with XRD or liquid-state NMR techniques. Based on this approach, Lemke *et al.* concluded that rather than well-defined crystalline and non-crystalline regions, CNCs contain a more finely varied distribution of environments.

5.5.   Crystallinity Estimation of CNMs by Raman Spectroscopy
5.5.1.   Relevance

Since the 1970s, Raman spectroscopy has been used in the analysis of cellulose materials. But it was not until 2005 that a method was developed to estimate crystallinity of cellulose.[224] This method (sometimes referred to as 1481-Raman) was based on CH_2 bending vibrations in cellulose molecules and is mostly suited to analyzing pure cellulose samples. This application of Raman spectroscopy was facilitated by the development of near-IR FT-Raman spectroscopy which allowed acquisition of good quality spectra from cellulose materials. In conventional Raman, such materials were difficult to investigate due to their intrinsic fluorescence. In 2010, Agarwal *et al.*[225] reported that, in the Raman spectra of cellulose materials, peak intensity ratio (I_{380}/I_{1096}) could be used to determine cellulose crystallinity. Unlike the 1481-Raman method, the 380 cm^{-1} band based method (referred to as 380-Raman) was applicable to both pure celluloses as well as materials that also contained non-cellulose components. However, for the 1481-Raman method, presence of hemicellulose and lignin is problematic because their CH_2 spectral contributions overlap with that of cellulose. In contrast, no such problem exists for most samples using the 380-Raman approach. The 380-Raman method is well suited to estimate crystallinities of CNMs and will be described here in detail. Moreover, because the method is able to study CNMs in both dry and hydrated states, it additionally provides information on how the supramolecular structure of cellulose in CNMs is altered upon drying.

5.5.2.   Method

The protocol for estimating crystallinity by the 380-Raman method calls for making a pellet from approximately 100 mg of CNM powder, size of granules does not matter. To make a pellet, one only needs to apply just enough compressive pressure so that the pellet holds its "shape", and can be handled (*e.g.,* ca. 280 x 10^6 dyn/cm^2). For never dried CNMs, small amount of ca. 5 wt.% or higher concentration suspension is typically added to a ca. 5 cm long NMR sampling tube. The pellet or the suspension is analyzed using a 1064 nm FT-Raman instrument and a spectrum with good signal-to-noise (S/N) ratio is recorded. Improvements in S/N can be achieved by increasing sampling time or laser power, which can vary from 330 to 990 mW and depends upon the nature and sampling mode of the CNM sample. Typically, for CNM pellets at 660 mW acquisition duration of ca. 30 mins (*e.g.,* 1024 scans) is used, while for 5 wt.% suspension of CNCs because it is so dilute, 990 mW (max power possible) for 8 h duration (*e.g.,* 16,000 scans) gives good S/N in the spectrum. The instrument manufacturer provided OPUS software program is used to find peak positions and process the spectral data. From the Raman spectra, amorphous contributions in the frequency region 250–700 cm^{-1} must be removed (for both pellet and suspension

cases), this can be completed by first normalizing (making band intensity equal) the spectra on 897 cm^{-1} band and then subtracting the corresponding spectrum of completely amorphous cellulose (*e.g.,* this can be from any pure cellulose source that is mechanically/chemically treated such that its crystallinity is completely destroyed, typically 120-min ball-milled sample of Whatman CC31 – cotton linters). This is necessary because Raman spectroscopy is a semi-quantitative technique. Typically, 897 cm^{-1} band is used because its peak height is minimally impacted by the process of ball milling. To calculate band intensity ratio (I_{380}/I_{1096}), using OPUS, peak heights of the 380 and 1096 cm^{-1} bands are calculated by a baseline method that involves choosing a minimum intensity wavenumber near the peak (*e.g.*, 358 and 944 cm^{-1} for 380 and 1096 cm^{-1} bands, respectively) and drawing a horizontal line (from that wavenumber) under the peak. Once the peak heights are measured a simple ratio of the two intensities can be calculated. The details have been reported in an earlier publication.[225] Cellulose crystallinity using 380-Raman ($X_{380\text{-Raman}}$) is estimated by **Eq. 5.4**,[225] which is a regression correlating crystallinities and the (I_{380}/I_{1096}) ratios of the calibration set samples.[225]

$$X_{380-Raman}(MultiRam) = \frac{\left(\frac{I_{380}}{I_{1096}} - 0.0286\right)}{0.0065} \tag{5.4}$$

In **Eq. 5.5** MultiRam indicates the FT-Raman instrument used for obtaining spectra. Subsequent investigations[226-229] indicated that this method is quite versatile and except for materials where significant fluorescence was generated upon 1064 nm laser excitation, estimation of crystallinity can be carried out quite reliably. Even in presence of water, 380-Raman method has been used to estimate crystallinity.[230]

Unless crystallinities are determined based on spectra obtained on the same FT-Raman instrument, absolute crystallinity values were found to vary.[226] To address this issue, so the absolute values of crystallinities obtained using different FT-Raman spectrometers can be compared, the crystallinity data needs to be corrected for instrument-dependence by analyzing the calibration set samples on the new instrument. For example, at the USDA-FPL Laboratory, the 380-Raman method (**Eq. 5.4**) was developed using Raman instrument RFS-100 (Bruker Inc.). If the band intensity ratio (I_{380}/I_{1096}) is obtained on a different FT-Raman instrument, *e.g.,* MultiRam (also from Bruker Inc.), the ratio will differ between the two instruments (RFS-100 vs. MultiRam). This instrument dependence of the ratio can be corrected for by using **Eq. 5.5**, which converts the crystallinities calculated using $X_{380\text{-Raman}}$ (Multi-Ram) to the data that would have been obtained on RFS-100 spectrometer - $X_{380\text{-Raman}}$ (RFS-100). This way, the absolute values of crystallinities obtained on these two different Raman instruments can be directly compared.

$$X_{380\text{-Raman}}(RFS\text{-}100) = \frac{(X_{380\text{-Raman}}(Multi\text{-}Ram) + 2.0212)}{0.8222} \tag{5.5}$$

A number of CNC and CNF samples have been analyzed using 380-Raman method, and the data are summarized in **Table 5.2**. While comparing the freeze dried vs. hydrated CNC data, it can be noted that the high to low crystallinity rankings in dry and hydrated states are different.

Table 5.2: Estimated crystallinities of CNCs and CNFs from $X_{380\text{-}Raman}$ method.

	Feedstocks	Freezedried	Hydrated	Reference
CNCs*	Bleached hard wood kraft pulp	55.5	53.3	[230]
	Heated poplar 200º C	62.0	58.0	[230]
	Whatman CC31	77.1	62.7**	[230]
	Bacterial cellulose	77.3	75.7	[230]
	Tunicin cellulose	69.9	74.7	[230]
	Cladophora cellulose	72.1	80.2	[230]
CNFs	Bleached softwood kraft pulp	40.4	ND***	[230]
	Refined pulp fiber	38	ND	[231]
	Refined and microfluidized fiber	39	ND	[231]
	Enzyme treated and refined fiber	44	ND	[231]
	Enzyme, refined, and microfluidized fiber	43	ND	[231]
	TEMPO treated, refined, and microfluidized fiber	25	ND	[230]

*All CNCs were produced using the 64% sulfuric acid method[229]
**Hydrated post freeze drying
***ND not done

5.6. Accessibility of CNMs to Water by Raman Spectroscopy

5.6.1. Relevance

Accessibility of CNMs to water is an important property to measure because a number of properties of the nanomaterials are influenced by CNM-water interactions.[232] Although NMR methods have been used by Lemke et al.[223] to evaluate CNMs' accessibility to water (see above), Raman spectroscopy provides yet another way to get this information. In 2016, Agarwal et al.[229] reported that in the Raman spectra of CNMs and other cellulose materials, peak intensity at 1380 cm^{-1} (CH$_2$ bending vibration in cellulose) increased upon OH-to-OD exchange. An example of this behavior for pulp-CNCs is shown in **Figure 5.4**. In Raman spectroscopy, accessibility to water is calculated based on the band intensity increase at 1380 cm^{-1}.
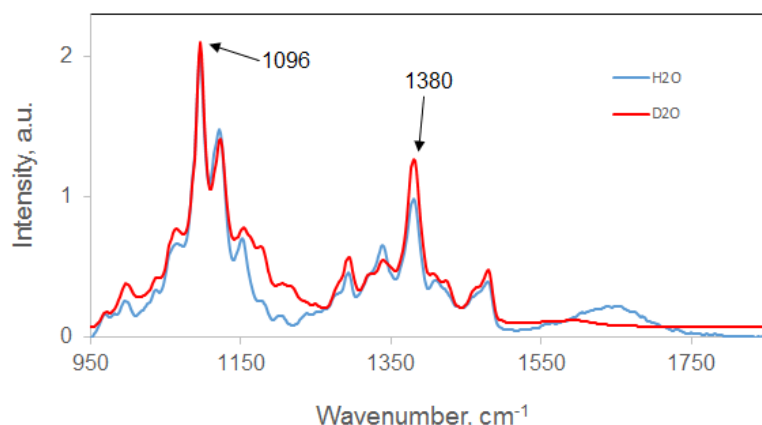
Figure 5.4. Raman spectra of CNCs in H$_2$O vs. D$_2$O (after fully exchanging replaceable OHs to ODs). In the spectrum obtained in D$_2$O, the increase in intensity at 1380 cm^{-1} can be noted.

5.6.2. Method

As described in Agarwal *et al.*,[229] the procedure for calculating accessibility to water (A) involves first obtaining a spectrum with good S/N ratio from ca. 20 mg of CNM in H_2O. The sample is analyzed in a shortened (ca. 5 cm length) NMR tube. To reduce time of acquisition to obtain good S/N ratio, the laser power can be as high as 990 mW. Subsequently, another 20 mg aliquot of the same sample is analyzed in D_2O after the sample has undergone a complete OH-to-OD exchange. The latter can be accomplished by removing excess H_2O (in case of never dried), putting the sample in D_2O (99.9 % deuterated), followed by centrifugation (4000xg) in a centrifugal filter (Amicon, Ultra-4, Ultracel-30K, Merck Millipore Ltd.) until excess D_2O is removed. Thereafter, this process should be repeated until the sample's 1380 cm^{-1} band intensity does not increase anymore, implying that most replaceable OHs are exchanged with ODs. Processing of spectra involves normalization of spectra in the region 950 to 1150 cm^{-1} and background correction using the ''rubber band option'' in OPUS. Using OPUS, intensities (peak heights) of the 1380 and 1096 cm^{-1} bands can be calculated by a baseline method that involves choosing a minimum intensity wavenumber near the peak (*e.g.*, 1440 and 950 cm^{-1} for 1380 and 1096 cm^{-1} bands, respectively) and drawing a horizontal line (from that wavenumber) under each peak. Subsequently, the peak heights are measured from this horizontal line. The intensity increase can be calculated as change in band intensity ratio (I_{1380}/I_{1096}) upon sampling in H_2O vs. D_2O and is designated as $\triangle I_{1380}$. For totally amorphous cellulose this increase is ca. 154%.[229] Further, assuming that in amorphous cellulose the C6 OH is completely accessible to D_2O, a reasonable supposition, the accessibility of CNMs to D_2O (or water) can be measured by simply ratioing the $\triangle I_{1380}$ for CNM to the $\triangle I_{1380}$ for amorphous cellulose. Thus, the percent accessibility to water, A, can be calculated by **Eq. 5.6**, where $\triangle I_{1380}$ is percent change in intensity at 1380 cm^{-1} upon deuteration.

$$A(\text{Raman}) = \frac{(\triangle I_{1380}(CN)*100)}{\triangle I_{1380}(\text{amorphous})} \tag{5.6}$$

For bleached Kraft pulp CNCs and CNFs the $\triangle I_{1380}$ have been reported to be 38.9 and 33.6%, respectively,[229] corresponding to an A of 25.3% and 21.8%. Strictly interpreting, the accessibility data based on Raman spectroscopy indicated that 25% and 22% of the cellulose CH_2OH groups, respectively for CNCs and CNFs, were accessible by water. How this translates to accessibility of CNM as a whole depends upon what model one uses to describe the nanomaterial. More specifically, the number of easily accessible surface CH_2OH needs to be known and that depends upon the number of cellulose chains contained in each CNC or CNF. For wood cellulose fibrils, some possible models were considered by Agarwal *et al.*[229] and may be useful in the present context.

Section 6. Surface Modification Characterization of CNMs

Laurent Heux, Bruno Jean, John Simonsen

6.1. Introduction

While the properties of CNMs have generated much interest both in the research area and commercially, the liabilities of CNMs have also generated much research in an attempt to overcome their limitations. Perhaps the most common surface modifications intend to overcome the hydrophilic nature of CNMs in order to disperse them in hydrophobic polymer matrices. A wide variety of modifications have been reported, *e.g.*, silanization,[233] transesterification,[234] vinyl esterification,[235] carbodiimide,[236] ATRP,[237] grafting from ring opening polymerization (ROP),[238] and many others, as summarized in recent reviews .[12, 13, 239]

There is an old saying that it takes 10 min to make a polymer (or graft to one), but 10 months to characterize it. Indeed, the task can be arduous and the tools limited, although sophisticated. Analysis and characterization of surface modified CNMs requires careful thought, meticulous work and is best begun with a thorough literature review. The characterization of as produced CNMs is covered in **Sections 3, 4 and 5**. Elemental analysis is a relatively straightforward method of determining the amount and type of atoms in a sample, but reveals no morphological or structural information, and limited information on bonding. Elemental analysis is covered in **Section 4**. The use of XRD for the characterization of surface modifications is typically limited to evaluating the preservation of crystallinity. XRD is covered in **Section 5.**

In this section a proposed approach to the characterization of chemically modified CNMs is presented and outlined in **Figure 6.1** in a decision tree format. Initially, the nature of the bonding of the modification (*e.g.*, adsorption, covalent bonding), and whether the grafted compound can be removed is discussed with respect to the types of characterization techniques available. This section then focuses on the application of and best practices for Fourier-Transform infrared spectroscopy (FTIR) and ssNMR, for the characterization of modifications on the CNM surface.

6.1.1. Adsorption vs. Covalent Bonding

The first consideration concerns the nature of the bond between the modifier and the CNM. If adsorption, accurate characterization can indeed be difficult, since most methods may dislodge the modifier from the surface. This includes zeta potential (**Section 3.4**), which can be useful, but only if the test conditions do not disturb the adsorption. Typically, the extent of adsorption is measured by determining the concentration of the modifier remaining in solution after adsorption. In this case, standard analytical methods for the adsorber from the literature should be used. CNMs with adsorbed modifiers may also be amenable to characterization by FTIR (**Section 6.2**), ssNMR (**Section 6.3**), and elemental analysis (**Section 4**).

6.1.2. Covalently Bonded Modifications

Two options are available: Characterize the modified CNM with the modifier attached, or remove the modifier and characterize it separately. Both methods present difficulties. The modifier, while covalently bound to the CNM, may have a too low grafting density for some methods to work. This can be the case with FTIR, which typically requires 5 wt.% minimum of the moiety of interest to be present in the sample in order to acquire a useful signal (and is rarely quantitative). ssNMR can have a lower detection limit depending upon the specific case.

6.1.3 Removal of the Modifier

At least two techniques for removal of the surface modifier have been reported in the literature: The first technique uses a clever synthesis strategy, in which a grafted polymer is removed by simple saponification using 2% NaOH. Centrifugation removes the CNM and careful workup provided the modifier for analysis using appropriate methods from the literature.[240] The second technique uses a more general method for isolating surface modifiers by removing the cellulose using cellulase enzyme. The surface modified CNM is digested in an aqueous buffered cellulase solution. Careful selection of the solvents used can typically separate the modifier from the digestion solution.[241] Note that this article did not use this technique on CNMs, but a submicron thick regenerated cellulose electrospun sheath. However, a number of studies have demonstrated the activity of cellulase on CNMs, although not surface modified CNMs.[242-244] Nevertheless,

the technique can be effective on surface modified CNMs. From the author's lab (unpublished data), a typical procedure follows: A 10 mL aliquot of solvent-rinsed and centrifuged grafted CNCs is mixed with 40 mL de-ionized H_2O and centrifuged for 30 min at 3500 rpm. The pellet is then resuspended in 20 mL of 0.05 M citrate buffer (pH 4.8) in a 30 mL vial with a cap. To the vial, 0.4 mL of *Trichoderma reesei* cellulase is added. The solution is incubated at 50 ^{o}C for 2 days. After the incubation period, the solution is boiled for 10 min to denature the enzyme. The solution is then centrifuged for 4 hours and the supernatant decanted. This procedure assumes the grafted moiety to be insoluble in water. Once the CNM has been removed, the modifier may be analyzed using appropriate techniques specific for the modifier.
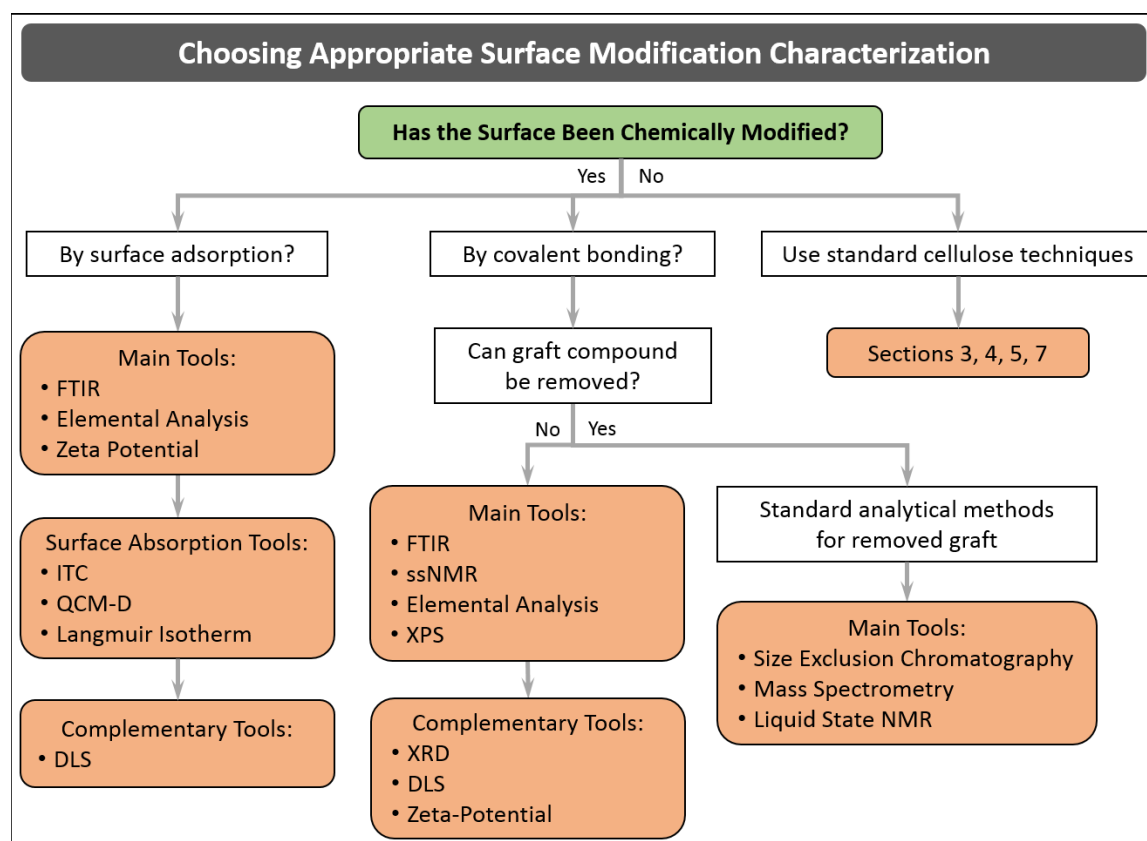
Figure 6.1. Decision tree showing a proposed approach for the characterization of chemical modification to CNM surfaces.

6.2. Fourier-Transform Infrared spectroscopy
6.2.1.   Principle and Relevance of the Technique
In FTIR spectroscopy, a sample is irradiated with infrared light. The device measures the amount of absorbed, transmitted, and/or reflected light after the light has interacted with the sample and reports the absorbance as a function of wavenumber. The resulting plot provides information on molecular vibrations, which can be used to identify the chemical and physical properties of functional groups within the sample. Basically, FTIR instruments collect interferograms using an interferometer and then perform a Fourier transform of the latter to yield the IR spectrum that can be analyzed. Previous FTIR instruments were dispersive, but are now obsolete. Present day FTIR spectrometers collect all wavelengths simultaneously, which is a major advantage of the technique along with high spectral resolution and high signal to noise ratio.[245]

As far as chemical modification of CNMs is concerned, FTIR stands as a key technique to establish the presence of specific groups and bonds on the surface of the nanoparticles and is therefore commonly used to validate the effectiveness of grafting to and grafting from chemical reactions targeting a specific

functionality. Though quantitative information can be obtained from the measured IR spectrum (see below), this technique is used in the vast majority of cases as a qualitative and comparative tool (quantitative data are then obtained by other techniques such as elemental analysis, titration or ssNMR).

6.2.2. Measurement Protocol
FTIR measurements described in the literature have usually been performed on dried solid CNMs either in transmission or in attenuated total reflectance (ATR) mode, which implies two different sample preparations.

In transmission mode, the freeze dried chemically modified CNMs are first finely dispersed in a dried KBr fine powder matrix by grinding in a mortar, prior to pellet formation using a pellet die and a press. Careful drying of both the CNM sample and KBr powder is a prerequisite to minimize water content. Typically, a concentration of 10 mg CNM per gram KBr (1 wt. %) is used and ca. 100 mg KBr is appropriate to obtain a thin transparent pellet, showing that the KBr pellet method only requires about 1 mg of CNM sample. The measurement is then performed in transmission in the typical wavenumber range 4000-400 cm^{-1} with a 4 cm^{-1} resolution using 16 to 64 sample scans. Background measurement using a neat KBr pellet helps to correct for light scattering losses in the pellet and for water adsorbed by KBr.

The ATR method involves pressing the sample against a high-refractive-index prism and measuring the infrared spectrum using infrared light that is totally reflected at the interface of the prism. ATR method therefore allows a direct measurement of a powder or film sample with minimal sample preparation compared with the transmission mode. With this technique, the effective pathlength varies with the wavelength of the radiation, resulting in ATR intensities decreasing at higher wavenumbers when compared to transmission spectra. Most FTIR software packages incorporate an ATR correction algorithm to account for this effect. Less than 10 mg sample is required to cover the ATR crystal surface.

In addition to these two methods, a simple and convenient procedure is to perform the measurements in transmission mode either directly on films obtained by evaporating suspensions on a PTFE surface or by forming a film by drying onto an IR transparent window.

6.2.3. Band Assignment and Spectrum Analysis General Approach
There are a number of literature reports on the IR data of native cellulose that provide a list of IR band assignments with special emphasis on the hydrogen bonding system.[246-251] This list, partially reproduced in **Table 6.1**, is the starting point of FTIR spectra analysis since it allows the researcher to assign bands corresponding to the reference non-modified CNMs.

After surface modification of CNMs, FTIR analysis can be carried out by investigating different regions of the spectrum. From variations of the OH and/or NH groups bands (frequency, intensity, contour) in the 3200-3700 cm^{-1} region, it is possible to get insights on the modification of these groups such as the degree of esterification of the hydroxyl groups. Absorption bands in the 2700-3200 cm^{-1} range are related to stretching vibrations of CH, CH$_2$ and CH$_3$ groups. Appearance of narrow bands in the 3000-3200 cm^{-1} region indicate the presence of CH groups linked to double bonds or in aromatic structures. Few vibration frequencies are expected in the 2000-2600 cm^{-1} region and investigation in this range therefore allows one to easily detect OD and SH groups as well as C≡N and C≡C triple bonds. Investigation of the 1600-1800 cm^{-1} range can detect the presence of C=O, C=C and N=O double bonds and the deformation vibrations of amino groups.

**Table 6.1**. Assignments of IR bands corresponding to neat CNMs.

Wave number (cm⁻¹)	Assignment
Between 3000 and 3700	Stretching vibration bands of the O-H bonds of the primary and secondary hydroxy groups
2900	Stretching vibration of the C-H bond
1650 (400 and 700)	Adsorbed water
1315, 1335, 1430 and 1470	In-plane bending vibration bands of the primary and secondary hydroxy groups
1160	Antisymmetric stretching vibration of the C-O-C glycosidic bond
1110, 1060 and 1035	Vibrations of the C-O bond of carbons 2, 3 and 6
665 and 705	out of plane torsional vibrations of the hydrogen bonded O-H groups (free OH: 240 cm⁻¹)

6.2.4. Examples of Characterization of Surface Modification of CNMs Using FTIR

FTIR can be considered a routine technique to characterize the surface modification of CNMs and FTIR data are thus widely reported in the literature. Reported results concern many aspects of surface modification of CNMs including esterification, oxidation, carbamation and amidation reactions used to impart covalently bonded functional groups or polymers, as well as characterization of the adsorption of molecules or polymers. An exhaustive survey is beyond the scope of this review but typical examples of the use of FTIR after chemical modification of CNMs are given below.

The two-step grafting of polystyrene (PS) chains from the surface of CNCs through surface-initiated atom transfer radical polymerization (SI-ARTRP) was successfully followed using FTIR.[178] First, the introduction of 2-bromoisobutyryl bromide (BiB) as surface initiator was proven by the appearance of the C=O vibration band at 1724 cm⁻¹. No significant change in the OH signal around 3350 cm⁻¹ was noticed despite esterification involving such groups. This is a common feature of reactions involving surface hydroxyl groups of CNMs as only surface groups are modified, while the internal hydroxyl groups remain untouched. Second, the presence of PS chains after surface-initiated polymerization is shown by the appearance of several signals related to the PS structure at 3025 cm⁻¹ (C-H stretching), 1494 cm⁻¹ (C=C stretching), and 700 cm⁻¹ (C-H bending) (**Figure 6.2**). Interestingly, the intensity of the latter band increases with the graft length and height relative to the 670 cm⁻¹ peak (corresponding to the cellulose structure) and was used to estimate the weight percentage of polystyrene in the final polymer-grafted nanoparticles using a calibration curve obtained from physical mixing of polystyrene and CNCs. The final PS content estimated by this method was consistent with elemental analysis.
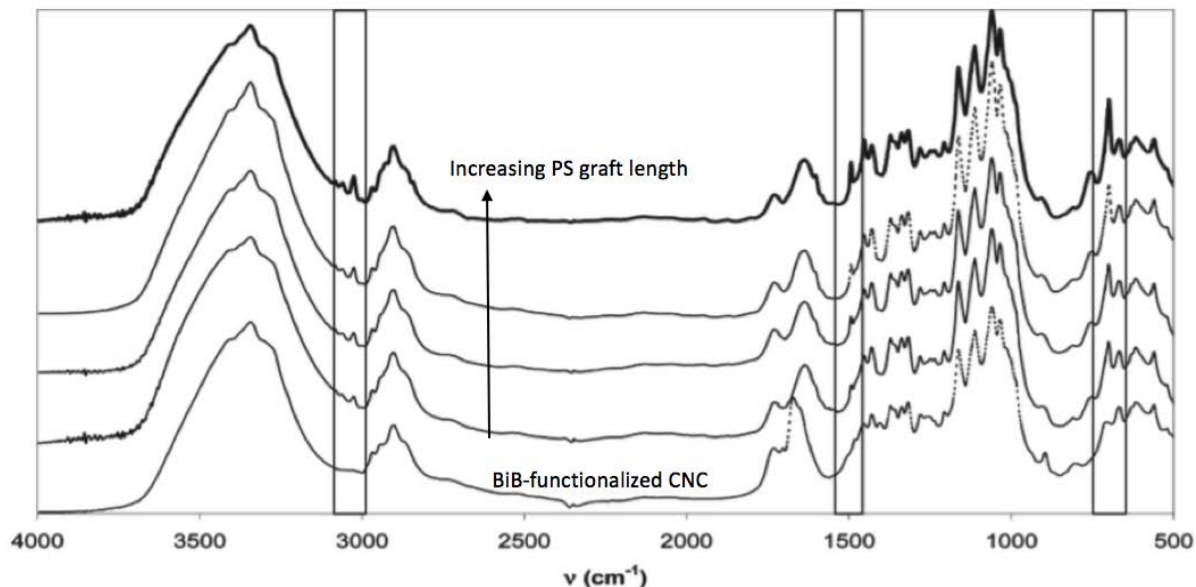
Figure 6.2. Full FTIR spectra of BiB-functionalized CNCs and PS-grafted CNCs. Reprinted with permission from reference.[178]

The carboxylation of CNMs through TEMPO-mediated oxidation of surface hydroxyl groups is a widespread functionalization pathway that can easily be investigated by FTIR from the appearance of the carbonyl band around 1730 cm^{-1}, whose intensity can be used to estimate the degree of oxidation.[252, 253] However, acidification of the medium with dilute HCl before analysis is a prerequisite for the observation of this band since the carboxylate form superimposes with the band of adsorbed water molecules at around 1650 cm^{-1}. The introduced carboxyl groups were further successfully used in several studies to perform amidation (peptidic coupling) reactions with amino-functionalized moieties in order to graft, *e.g.*, polyethylene glycol chains, DNA oligonucleotides or thermosensitive polymers onto CNMs.[254-258] In this case, the covalent amide linkage is unambiguously evidenced by the appearance of both amide I band at 1650 cm^{-1} and amide II band (N-H stretching) at 1550 cm^{-1}, which is accompanied by a decrease in the intensity of the carbonyl band due to consumption of carboxyl groups in the reaction with the amine-terminated grafts (**Figure 6.3**). Non-covalent functionalization of carboxylated CNCs can also be carried out by complexation with oppositely charged species like quaternary ammonium (QA) salts. In this case, FTIR was able to show the successful ionic exchange of Na$^+$ with QA salt by the presence of characteristic bands of QA.[259]
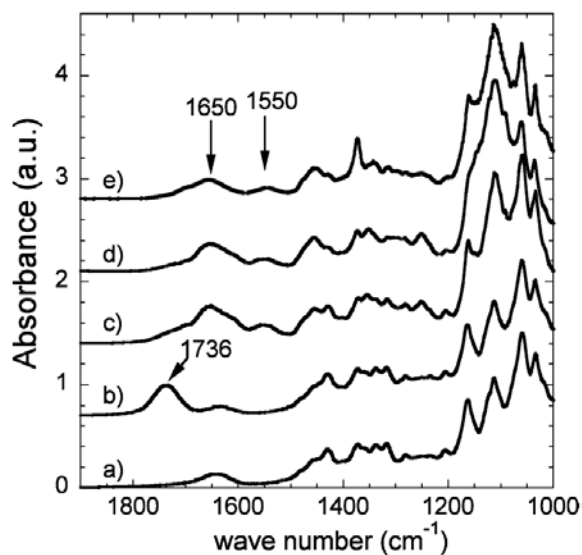
Figure 6.3. A snippit of an FTIR spectra of sulfated (a), oxidized (b), Jeffamine polyetheramine M1000-grafted (c), Jeffamine polyetheramine M2070-grafted (d), and Jeffamine polyetheramine M2005-grafted (e) CNCs. Reprinted with permission from reference.[260]

Introduction of azido-groups is also easily detected due the appearance of a characteristic band at 2120 cm^{-1} in a region free of cellulose signals, which disappears upon reaction with alkyne groups during Cu(I)-catalyzed Huisgen 1,3-dipolar cycloaddition.[261, 262] Conversely, ether linkages are not conveniently characterized by FTIR due to overlap with the characteristic bands of cellulose.[86]

A quantitative analysis of the FTIR spectra was conducted by Braun and Dorgan in the case of the functionalization of CNCs via a Fischer esterification reaction to obtain the total number of esters per cellulose repeat unit.[263] Their exact approach demonstrated that beyond the use of absorbance data (and not transmittance to ensure proportionality to concentration), knowledge of relative molar absorbance is required to complete the calculation.

6.3. Characterization of Surface Modification of CNMs Using ssNMR
ssNMR is a very powerful technique for analyzing surface modified CNMs. Here we cover ^{13}C CP-MAS NMR, the most commonly used NMR technique for analyzing surface modified CNMs.

6.3.1. Principle and Relevance of the Technique
As described in **section 5.3**, ^{13}C CP-MAS NMR spectroscopy is a high resolution technique that has been used in the characterization of CNM crystallinity, phase transition, physical transformation and chemical modification. The combining of information from both physical and chemical features offers the possibility to perform topochemical studies in a single experiment and hence to link the chemical modification to the physical transformation. NMR is an atom counting method, quantitative measurement can be easily performed, providing precautions concerning the dynamics of the studied samples are taken, especially that softer materials require specific calibration techniques. Combined with other structural characterization techniques like TEM or XRD, ^{13}C-CP MAS allows a quantitative evaluation of the chemical modification and a fine description of the morphological changes caused by the reaction. One weakness of ^{13}C-CP MAS is its low sensitivity (only 1% of the carbons are ^{13}C), which can be, in principle, overcome by isotopic labeling. However, the rise of interest in nanometric scaled cellulosics has reinforced interest in the technique, as high surface area materials exhibit a large number of modifiable sites, therefore enhancing the relative low response of ssNMR, compared to the sensitivity of FTIR or XPS. Even though less common in carbohydrate research compared to polymer research, dynamics can be probed by this technique to bring additional information on the nature of the chemical modification.

6.3.2. Measurement Protocol
^{13}C CP-MAS is usually performed on dry samples in order to remain fully quantitative, even if working with wet samples has proven to enhance the resolution of the spectra. In some cases, it may be informative to perform analyses in both the wet and dried states. For routine experiments, 50 mg of material is required due to equipment requirements, even if experiments could be conducted on samples weighing only a few milligrams.

The duration of the experiment strongly depends on the extent of the chemical modification and the level of noise acceptable for the spectrum (moderate for routine control or low for fine investigations) and ranges from 1 h in the most favorable cases to two or more days for loosely modified samples. As a rule of thumb, signal to noise increases as the square root of time, so that a twofold quality of the spectrum requires a fourfold duration of the experiment, making two days a reasonable upper limit for a single experiment acquisition time. Altogether, a detection limit of the degree of substitution lying between 0.001 and 0.01 seems reasonable, and strongly depends on the nature of the grafted chemical moieties. For example, complex structures will be harder to detect, as their signal will be scattered among a great number of sites, whereas simple chemical groups such as acetates will be very easy to detect at the lowest level. It has also to be noted that ^{13}C CP-MAS is a non-destructive experiment, the integrality of the sample being fully recovered, with the exception of small fragments attached to the filling tools.

### 6.3.3. Band Assignment and Spectrum Analysis: General Approach

As summarized in **section 5.3.3**., most of the chemical shifts of native cellulose have been assigned (**Table 5.1**). As a result of the high sensitivity of chemical shifts to conformational features, the same chemical entity (an anhydroglucose unit linked in β 1-4) can exhibit a large variety of chemical shifts allowing the researcher to follow morphological changes that can occur during chemical modification and give quantitative information on the topochemistry of the reaction.

Concerning grafted moieties on CNMs, determining the presence of the covalent bond attached to the cellulose is obviously dependent on the chemical shift of the newly formed bond. Conventionally, thanks to the relatively narrow spread of carbohydrate chemical shifts (ca.between 110 and 60 ppm), many chemical bonds can be easily detected in non-cellulose regions. This is especially the case for carboxylic moieties (ca. 175 ppm), *e.g.*, arising from the oxidation of the primary alcohol during TEMPO oxidation,[222, 264] the grafting of organic acids,[265] amide bonds (ca. 172 ppm) originating from the reaction of amines with TEMPO oxidized cellulose,[256] ester bonds (ca. 172 ppm) created by acyl chlorides,[266, 267] or vinyl esters[268] reacting with the hydroxyls of cellulose, or even thiol-ene chemistry. In most cases, the differences between grafted and ungrafted moieties allows the differentiation between covalently linked and adsorbed species, and is of great utility. However, some reactions lead to less detectable entities, like etherification, that creates new ether bonds that are sometimes barely detectable, or periodate oxidation, which produces carbonyls quickly recombining into hemiacetal bonds (between 80 and 100 ppm).[255, 270] In this last case, reductive amination in the presence of primary amine leads to the formation of a new secondary amine bond easily detected ca. 55 ppm.[270] Some other modifications lead to difficultly detectable or even not detectable effects on the spectra, *e.g.,* the formation of phosphoric or sulfate ester bonds with cellulose that is of primary importance in the production of CNCs. One solution can be the use of more exotic nuclei like ^{15}N or ^{31}P, but the absence of an internal reference as cellulose contains neither ^{15}N nor ^{31}P renders the experimental data difficult to interpret.

6.3.4. Examples of Characterization of CNMs using ssNMR
#### *6.3.4.1 Topochemistry*

One of the simplest and earliest examples of surface modification is the TEMPO oxidation of CNMs, for which the onset of the carboxylic acid at 178 ppm with increasing equivalents of NaClO has been used to monitor the progression of the reaction, together with the decrease of the C6 signal arising from the surface at 62 ppm, indicating a surface-limited reaction (**Figure 6.4.**).[222]
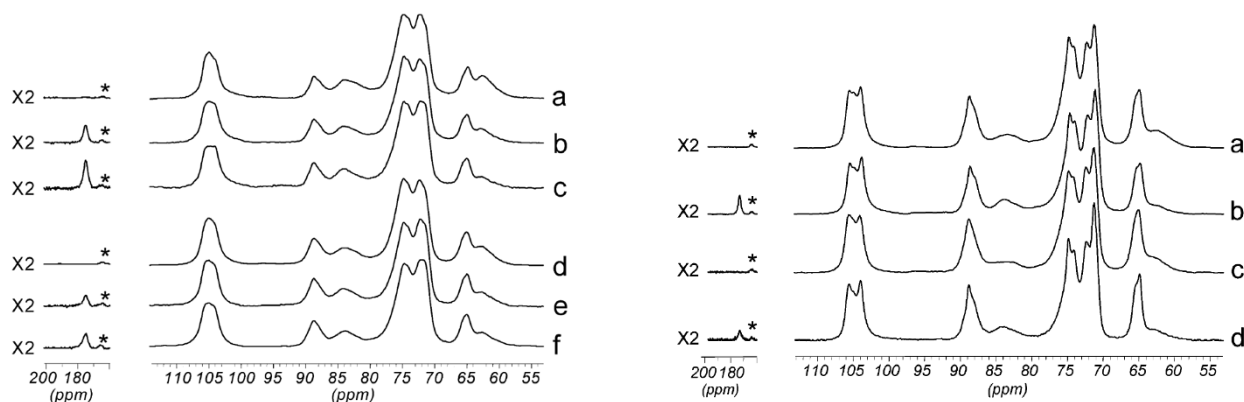
Figure 6.4. : *left:* CP-MAS Carbon-13 NMR spectra of microfibrillated sugar beet pulp (SBP) : (a) original sample; (b) oxidized SBP (0.75 mol NaClO/mol glycosyl unit); (c) oxidized SBP (2 mol NaClO/mol glycosyl unit); (d) HCl-hydrolyzed; (e) HCl-hydrolyzed and oxidized (0.75 molNaClO/mol glycosyl unit; (f) HCl-hydrolyzed and oxidized (2 mol NaClO/mol glycosyl unit). The spectral region corresponding to the CdO signals (175-200 ppm) has been multiplied by a factor 2. Asterisks (*) indicate residual spinning sidebands from the C1 signal. *Right:* CP-MAS Carbon-13 NMR spectra of cotton linters: (a) original sample; (b) oxidized (2molNaClO/molglycosyl unit); (c) HCl-hydrolyzed; and (d) HCl-hydrolyzed and oxidized (2 mol

NaClO/mol glycosyl unit). The spectral region corresponding to the C=O signals (175-200 ppm) has been multiplied by a factor 2. Asterisks (*) indicate residual spinning sidebands from the C1 signal. From reference [222].

ssNMR was similarly used to show that the reaction does not change the crystallinity, *e.g.*, in the aforementioned vinyl ester reaction,[268] and even to show that the grafting density depends on the specific surface area.[271] That was definitely not the case for gas-phase esterification, for which the reaction proceeds in three different steps as evidenced by the change in shape and intensity of the signals of both cellulosic and grafted moieties. Below a degree of substitution (DS) of 0.33, the signals arising from cellulose do not change, especially the crystalline (ca. 90 ppm) to disordered (around 85 ppm) ratio, indicating a global preservation of the crystalline core. From a DS of 0.66 to 1.83 the crystalline contribution strongly decreases, at the expense of the disordered contribution, and the onset of a triester contribution at 103 ppm further confirms this progressive modification of native cellulose into cellulose triester. Above a DS of 2.43, native cellulose has completely disappeared (**Figure 6.5.**).[267]
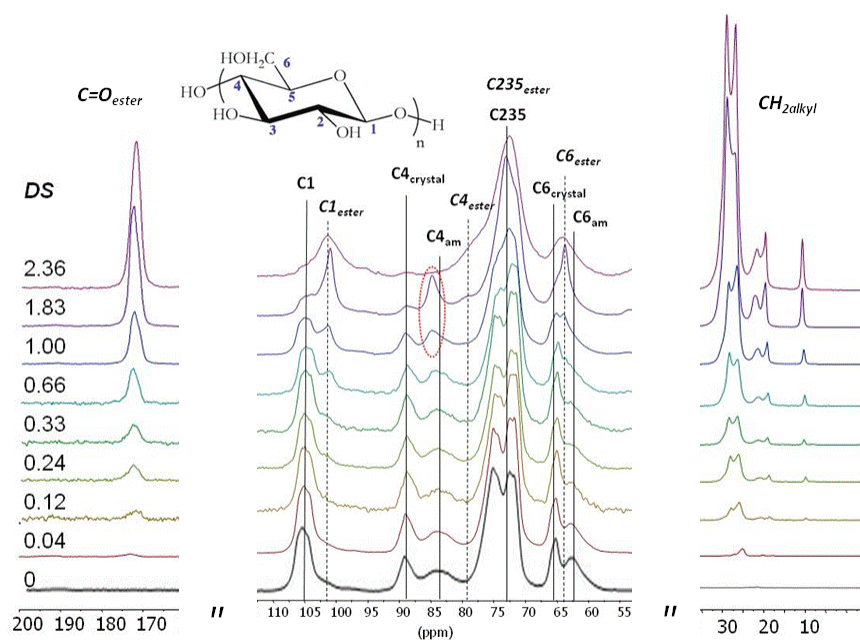
Figure 6.5. ssNMR spectra of CNF aerogels modified with palmitoyl acyl chloride vapours, with *DS* ranging from 0 to 2.36. From reference [267]

6.3.4.2 Grafting Onto
ssNMR has been used on many occasions to investigate grafting onto of polyetheramines,[256] poly (ε-caprolactone)[272] or poly (lactic acid) (PLA) chains.[273] In this last case, it was also used to quantify the surface coverage and the average chain length of lactic acid-modified CNCs. The ratio between the integrals of PLA, PLA chain ends and cellulose can be used to calculate both the average degree of polymerization of the grafted chains (DP$_{avg}$) and the surface coverage (ω) of the CNCs.

$$\omega = \frac{\text{Integral(C9')}}{\text{Integral(CNC)}/2} \times 100\% \qquad DP_{avg} = \frac{\sum \text{Integral(C9 + C9')}}{\text{Integral(C9')}} \times 100\%$$

(6.1)

C9' being the signal arising from chain ends and C9 from the central part of the grafted chains.

6.3.4.3 Limit of Detection

Pushing the limit of the technique, Navarro *et al.* have shown the co-grafting by click chemistry of two different types of flurophores by patiently accumulating the signal (here in **Figure 6.6.** the signal is multiplied by a factor of 40).[274] In the case of fluorescent probes, the very good response of the fluorescence to the excitation allows the detection of exceedingly low grafting frequencies.
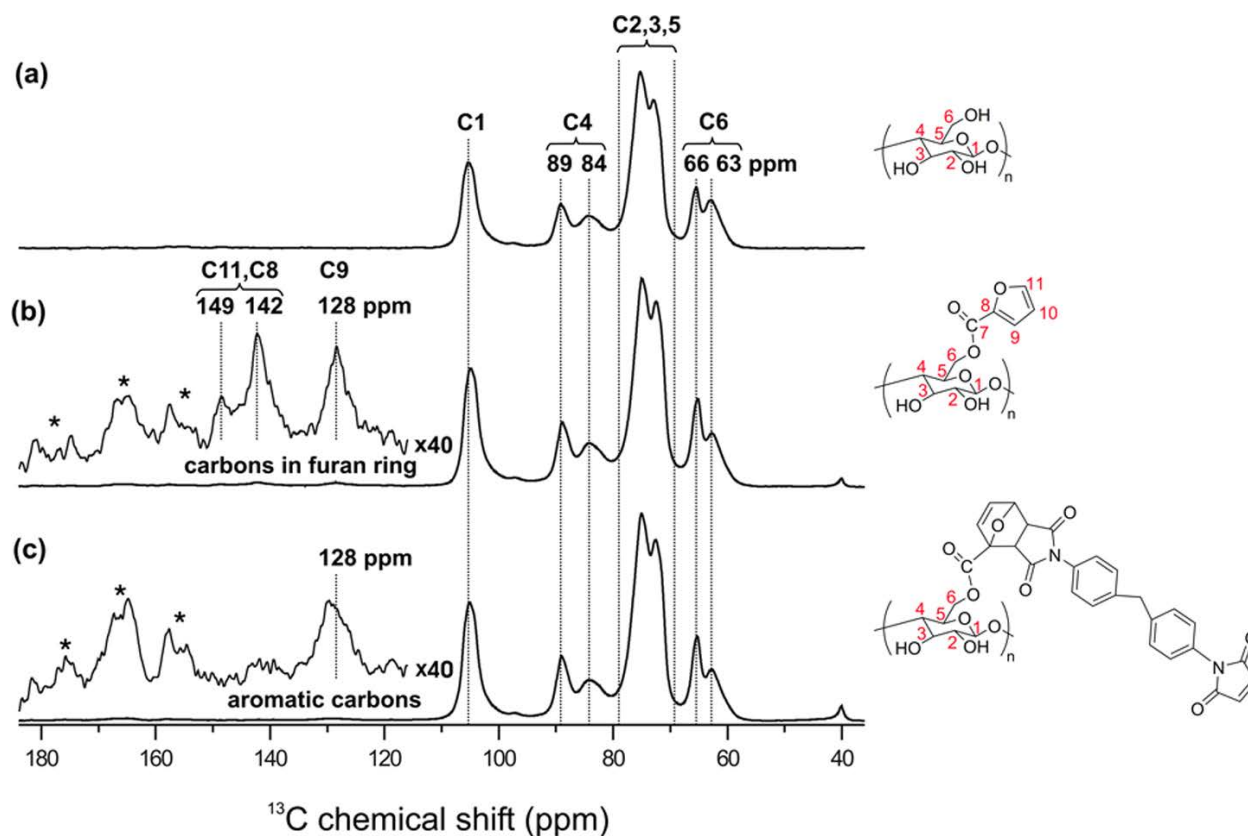
Figure 6.6. ssNMR characterization of surface-modified CNFs: CPMAS 13C NMR spectra of (a) unmodified CNF, (b) furoate CNF and (c) maleimide-modified CNF. The corresponding molecular structures of the CNF and the surface modified CNF are shown in the right panel. The insets in (b) and (c) display zooms over the spectral region 116−184 ppm, with some identified signals from the substituents indicated. Spinning sidebands are marked by asterisks. From reference [274]

SECTION 7: Electron Microscopy of CNMs

Rose Roberts, Kelly Stinson-Bagby, Johan Foster

7.1. Relevance of Electron Microscopy

Electron microscopy (EM) is extensively used in the characterization of CNMs (*e.g.*, morphology, aspect ratio, length, width), identifying CNM type, comparing changes to CNMs as a result of processing or chemical functionalization, determining the purity of the CNMs, determining the extent of CNM aggregation, and characterizing dispersion of CNMs within polymer composites.[256, 275, 53, 276, 277, 278, 279] However, obtaining relevant images for identification and statistical measurements can be challenging. This section reviews techniques used to mitigate the EM characterization challenges of CNMs. A decision tree is provided to be a starting point for EM imaging and sample preparation. Example images of CNMs will also guide the user on what to expect when using EM as a characterization technique.

7.2. Basics of Electron Microscopy

Electron microscopy uses a focused beam of accelerated electrons to generate magnified images of high resolution of several nanometers or less. The collision of the electrons with the sample generates an emission of various particles both reflected and transmitted. The interaction between sample and electron transforms the energy of the electron, and the differences in electron energy are detected and formed into an image. Scanning electron microscopy (SEM) is a surface imaging technique that takes advantage of the secondary electrons emitted from the sample. Alternatively, transmission electron microscopy (TEM) is a technique in which the electrons pass through the sample. Under ideal conditions SEM can resolve down to 1 nm and TEM can resolve down to 0.2 nm.[280, 281, 282] Hence, both SEM and TEM can be used to evaluate size and shape of nano-sized particles as well as the degree of dispersion and aggregation of the particles. Generally, TEM is the most used EM technique for the characterization of nanoparticles because of the high spatial resolution as compared with SEM.

There are several considerations to take into account when viewing CNMs using EM techniques. First, CNMs are made up of low electron density, non-conductive atoms that can be nearly invisible without enhancing contrast and resolution. Higher density atoms such as metals provide more contrast as a result of higher interaction potential with the electron beam, whether scattered or absorbed. Therefore, these atoms are more easily detected in both SEM and TEM than low-density atoms. Techniques to increase these interactions through sample preparation and modified beam control are discussed in later sections. Another consideration is the small height of the CNMs, which can be as small as 5 nm. SEM is a technique that depends on scattered electrons for topographical information and the smaller the height differences the less chance of imaging the particle. Likewise, the particles could be overpowered by debris or substrate surface roughness, which could hide the CNMs from direct sight of the detector. For TEM, the thinner the sample the less potential for the transmitted electron beam to interact with electrons within the CNM particles. This also means that contrast, which is dependent on higher or lower electron energy at the detector, for CNMs is more likely to be overpowered by competing signals from debris, substrate background, or other matrix materials present. With sample preparation and electron beam control there are methods to minimize the background signals and increase the contrast and resolution for better imaging.

7.3. Getting Started with EM Characterization of CNMs

The process of EM imaging of CNMs begins with the simple question of, "What do you want to measure?" The answer to this and several subsequent questions helps to narrow down the technique needed, SEM or TEM, and the approach on sample preparation.

A comparison of SEM to TEM at typical size scale found in literature for imaging CNMs (100 - 200 nm) is shown in **Figure 7.1**. The SEM images characteristically look like a blended mat of clustered CNMs (**Figure 7.1 b and d**). Imaging individual crystals is challenging if not impossible with many samples in part due to the resolution of the SEM. Hence, for these images, the contrast between the individual crystals is not clear though the morphology of the crystal interactions is apparent. Alternatively the transmitted electrons in the TEM reveal the individual crystals because of the high image contrast that is possible, approximately 5 times greater than with SEM.[281, 283, 284, 282] Hence, with TEM, morphology and dimensions of CNMs can be

studied. TEM images of CNCs usually consist of toothpick- or whisker-shaped structures that may or may not overlap, as illustrated in **Figure 7.1**. It should be noted that scanning transmission electron microscopy (STEM) is a technique that incorporates a transmission mode into the SEM technique. This has the potential to increase resolution though not to the extent of the TEM. For this discussion, SEM and TEM are the key techniques under evaluation.
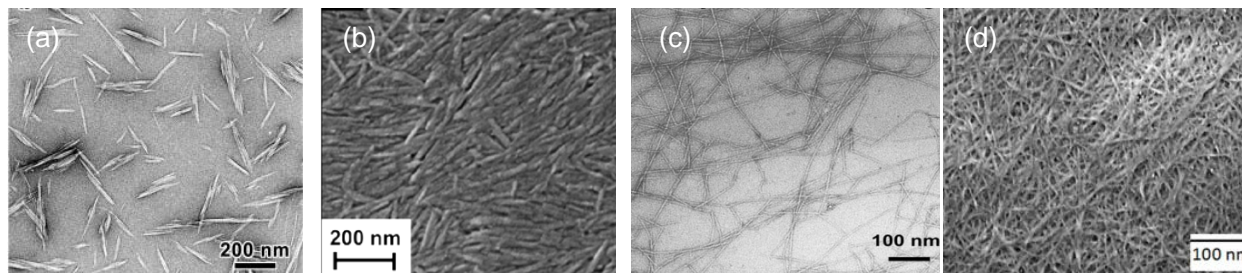
Figure 7.1. Images of what to expect from SEM and TEM of CNMs, (a) TEM of negatively stained CNCs,[256] (b) SEM of cast CNC film,[285] (c) TEM of negatively stained TEMPO-oxidized CNFs,[286] and (d) SEM of untreated CNFs.[287]

To best achieve the goal of what you want to measure, the decision tree given in **Figure 7.2** steps through the process of identifying the appropriate EM technique and sample preparation. As you work your way down the tree from the top, answers to the initial question, "What do you want to measure?" will be directed into one of two categories which can be summarized as qualitative and quantitative analysis or confirmation and dimensional analysis, respectively. The qualitative analysis is directed at confirming the existence of CNMs, verifying the purity of the CNMs and analyzing the dispersion of the CNMs. For low resolution needs or the analysis of a material matrix of some thickness, SEM is the technique of choice. For high resolution qualitative analysis, TEM is an option especially for imaging individual crystals. For quantitative analysis, such as dimensional measurements, higher magnification with high resolution is needed and TEM is the technique suggested. Generally, TEM sample preparation requires additional manipulation of the crystals such as diluting the CNMs in a suspension, incorporating additional surfactant dispersants and introducing a heavy metal stain.

Additional details on the techniques and sample preparation as well as challenges that may arise are in the following **Section 7.4**. Note that the decision tree is more specific to imaging CNCs, since their size makes imaging trickier; however, CNFs and other CNMs will have similar traits, so the decision tree can be used across all CNMs.
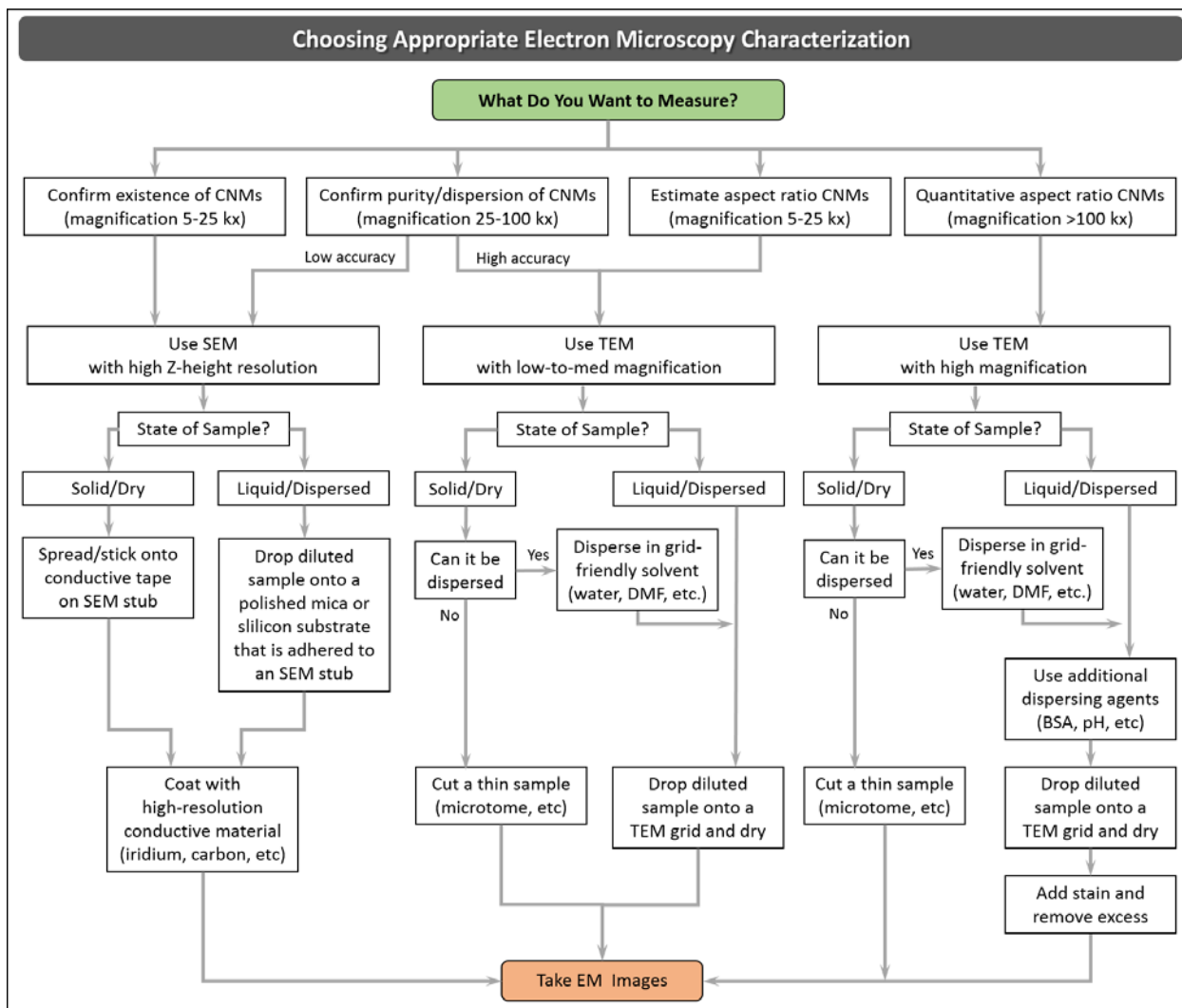
Figure 7.2. Decision tree for EM choice and sample preparation for imaging CNMs.

7.4. Challenges of EM Imaging of CNMs and How to Mitigate

Characterization of materials via SEM and TEM techniques provide valuable information to researchers and engineers; however, they do not come without challenges. Each CNM is unique and may require some experimentation to achieve the proper sample preparation protocols and imaging parameters. Below several challenges to CNM imaging via EM are identified and we offer suggested mitigations to these: Improved CNM dispersion on EM imaging substrate, improved CNM contrast, minimizing charging effects, imaging surface functionalization on CNMs, and imaging CNM-polymer composites.

7.4.1. Improved CNM Dispersion in EM Sample Preparation: Challenges

To characterize CNM morphology or to capture images for dimensional analysis, the CNM particles need to be well dispersed on the substrate. Ideally, nanomaterials should be individualized, free of clumping, bundling, and overlapping. This is addressed in two ways, in suspension prior to, and during the sample preparation process. This section discusses solution-based CNMs to be evaluated by EM.

7.4.1.1 Dispersion

When working with a dispersed suspension of CNMs in solvents such as water or DMF, characterization of individual CNMs can be challenging. CNMs, especially non-functionalized CNMs, are often strongly bonded together by hydrogen bonds (if they are not fully "unhinged" during production) that cause the CNCs to form bundles.[12, 288, 256] Even adding high-energy sonication may not fully separate the bundles.[275, 289,287, 290,291]

This can be detrimental if dimensional analysis is necessary for your sample. In addition to the surface chemistry of the CNMs, functionalized or not, the state of the materials has been found to be important. For example, dispersing CNMs from a dried state is generally more difficult than if the CNMs have never been dried. The dispersion of dried CNMs, most specifically CNCs, produces EM samples that are generally more clumped, usually aligning and sticking together along the longest dimension.[292]

7.4.1.2 Drying Effects
For CNMs in suspension deposited on an EM substrate, drying effects related to the liquid droplet must be taken into account. As the droplet dries the CNM particles may begin to agglomerate and/or follow flow characteristics of the liquid that will be seen in the EM images. Not all drying effects are apparent in the images and have the potential to affect the results. Carefully choosing the suspension medium and additional dispersing agents can help separate these bundles into individual crystals or fibers and keep them separated during drying.

7.4.2.   Improved CNM Dispersion in EM Sample Preparation: Mitigation Methods
To achieve an EM image of dispersed CNMs, take into consideration the CNM suspension prior to sample preparation and then during sample preparation. The starting suspension should be a dispersed suspension which can be manipulated with sonication, dilution levels, solvent choice, as well as the nature of the starting CNMs. During sample preparation when a droplet of the CNM suspension is placed on the substrate, methods can be used to ensure that dispersion is maintained or even enhanced while the particles are deposited on the substrate and the remaining solvent is removed and/or dried. Methods include using chemical dispersion agents, substrate surface preparation considerations, and excess solvent removal techniques.

7.4.2.1 Sample Dilution
A dilute CNM suspension for characterization of the nanoparticles is needed for EM imaging. Diluting samples can also help dispersion. Generally, the samples should be dispersed enough to get individual CNMs with little to no overlapping, but not so dilute that only one or two CNMs are visible in an image. Concentrations for TEM range around 0.01-0.5 mg/mL.[291, 53, 293]

7.4.2.2 State of CNM Starting Material
The starting material has an influence on the final dispersity, such as dried versus never dried material. Following extraction processes, such as acid hydrolysis, the CNM product can be further processed into a dried powder with freeze drying for example. Alternatively, the CNM product can be stored as a suspension such that they are never dried. For optimal and efficient dispersion the never dried CNMs have been found to work best.[294, 48, 295] **Figure 7.3** is an illustration of never dried versus dried CNCs redispersed and imaged with TEM under the same sample preparation and electron beam conditions. The never dried CNCs shown in **Figure 7.3a** have more well defined edges than those in **Figure 7.3b**. To aid in dispersing the CNMs into solution sonication methods are commonly used including bath or ultrasonication.[296, 76] Mechanical shearing has also been used, but is more common for the earlier step of isolation, or extraction, of the CNM rather than dispersing the CNM.[297, 290]
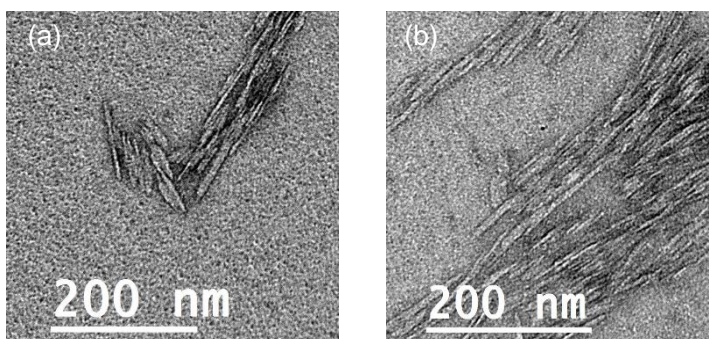
Figure 7.3. TEM images of unstained CNCs comparing (a) never-dried CNCs and (b) freeze dried and redispersed CNC.[298]

7.4.2.3 Dispersant and Additional Dispersing Agents

Solvent choice can also play a large role in dispersion of CNMs. Water and DMF are commonly used solvents for suspending CNMs. Further during sample preparation, drying effects may cause agglomeration of the particles so additional dispersants can be used. These dispersing agents can help with breaking up bundles and keeping individual CNMs separated during drying. An example is bovine serum albumin (BSA) which has been effective in avoiding drying effects. Another means of maintaining separation is charge differences by controlling pH.[299]

7.4.2.4 Substrate Choice and Preparation

For a substrate to be effective with CNMs, it must attract the particles, it must not compete with the sample signal, and it must support the particles for maximum exposure. The hydrophobicity and charge on the substrate surface has an effect on the deposition of the particles which also relates to how dispersed the particles will appear in the EM images. The substrate needs to be hydrophilic for most CNMs in aqueous solution to accept the deposition of the suspended CNM particles. This can be accomplished through cleaning with plasma glow-discharge or chemical methods prior to depositing the sample. Cleaning through these methods changes the surface of the substrate to attract the particles through charge or surface energy compatibility.

Another consideration is the substrate material and possible coatings. TEM grids best suited for CNM characterization have continuous carbon films rather than lacey grids; additionally, these carbon films can be enhanced with silicon monoxide coatings to increase the hydrophilic properties. Similarly, for SEM the substrates can be cleaned and/or coated to enhance the surface energy and attract the particles and solution to the surface. For SEM the flatness of the substrate surface must also be a consideration. Since the CNMs have such as small height, any roughness could interfere with the topographic imaging of the CNMs. Therefore, polished mica or silicon wafer pieces are commonly used. In addition to the low roughness, these substrates also have a low enough electron density to avoid overshadowing the CNMs of interest. More information on contrast is below. It is key that the particles deposit and remain on the substrate surface because the mechanical removal of excess solution (wicking with filter paper or the like) can potentially remove an excess of particles leaving behind too few for imaging or only the heavier agglomerated bundles.

7.4.3.   Contrast and Resolution: Challenges

Image quality is dependent on contrast and resolution, where contrast is related to the amount of useful signal across the dynamic range, or the minimum to maximum resolved brightness for the system, and resolution is the minimum spacing for which two features can be distinguished.[300] More simply stated, contrast is the difference between the light and dark parts of an image while resolution is the crispness in distinguishing between two close objects, or amount of resolved detail. CNMs are particularly tricky to image via SEM and TEM because of their low electron density and small thickness.

7.4.3.1 Electron Density

One reason that CNMs are difficult to image is related to the electron signal to the EM detector. The signal is the number of electrons that reach the detector above the noise. CNM particles are small, most specifically in thickness, and are composed of low atomic number elements such as carbon; both contribute to lower relative signal. Signals too close to the background noise in the system will not be seen in the image. This is apparent in both SEM and TEM where there is low contrast between the CNM against the substrate (pedestal and grid used in sample preparation, respectively). Hence, it is important to create contrast during sample preparation.

7.4.3.2 Sample Thickness

Sample thickness has a high impact on resolution of the EM image. TEM requires a sample thickness of 1 μm or less for the electron beam to travel to the sample.[301, 300] A sample layer that is one CNM thick will produce the best images. This is also generally true for SEM, however, since CNMs, especially CNCs, are usually around 5-10 nm in height (diameter), only high-resolution SEMs usually have the capability to visualize CNCs.[280, 302, 289]

Additionally, the CNM particle sizes can be overshadowed by contamination, or debris, that can inadvertently accompany the sample. Likewise, the sample preparation substrate surface roughness can affect visibility of the CNMs. To view the topographical morphology with SEM, it is suggested that a polished surface be used such as mica or silicon with a subsequent metal sputtered coating of several angstroms. For TEM the electrons need to penetrate the CNMs with minimal interference. Typically TEM substrates contain a porous surface, such as with a lacey grid, however, nanoparticles are not big enough to span the openings. Therefore, grids with various coatings are used to support the particles with minimal contribution to the output beam, typically carbon-based. For example, carbon-coated copper grids or silicon/Formvar-coated copper grids. Though we should note here because of the nature of CNMs being majority carbon, additional actions must be taken to distinguish the CNM carbon and the substrate carbon, as mentioned in the section on Electron Density.

7.4.4. Contrast and Resolution: Mitigation Methods

Several mitigation methods can be used individually or in combination to improve the quality of EM images of CNMs. The best method will be dependent on CNM source material, surface functionalization, size, and other variables, so some experimentation may be necessary to find the overall best method. Below are some tips regarding staining samples for improved contrast.

Staining with heavy metal elements is the main way to mitigate contrast issues.[303, 304, 305] Staining is typically most effective for TEM, whereas for SEM, sputter coating (*e.g.,* Au, Pt) onto the samples is used to intentionally produce coating defects which highlight the CNMs.[306] After CNMs materials are deposited onto an appropriate substrate, stains can be added. Positive stains chemically bond directly to the sample (making the sample material itself have more contrast) while negative stains, or shadowing, surround the outline of the sample, making the background around the sample have more contrast.[281] Negative staining is more common because of its relative ease of use. Common negative stains include uranyl acetate, ammonium molybdate and other heavy metal solutions including a vanadium-based product, Nanovan®.[305, 307] Uranyl acetate is most common, although access to and waste of uranyl acetate is restricted because it is radioactive. Some alternative stains have been developed with fewer restrictions on handling such as NanoVan and ammonium molybdate.

When applying the stain to the sample, a common method is to add a droplet of stain solution to the sample, which is allowed to sit for several seconds before removing excess. Several techniques to remove excess stain have been used, including wicking or dabbing off the solution droplet with a clean tissue, rinsing with droplets of water, or dunking in a bath of water before drying. **Figure 7.4** is an illustration of stained versus unstained CNCs. The unstained CNC in **Figure 7.4b** has a similar electron density to the carbon-based substrate film. During the TEM process, locating CNMs is made exceedingly more challenging when the nanoparticles cannot be located at lower magnification which is usually a function of contrast. In **Figure 7.4a**, the negatively stained CNCs are shadowed by the stain which sets them apart from the background. As you can imagine, at lower magnification within the TEM, around 30 kX magnification. It is easier to locate the CNMs in addition to the enhanced features that can be seen at the higher magnifications above 100 kX.
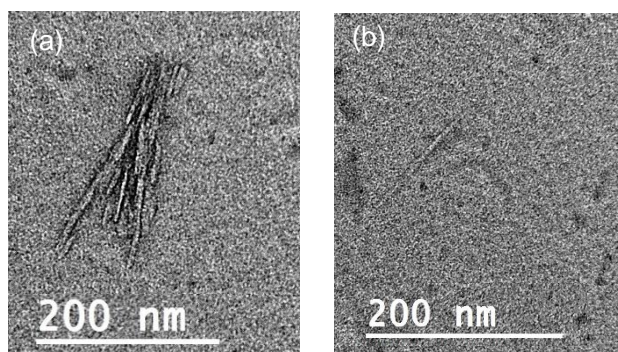
Figure 7.4. TEM images of CNCs prepared with (a) negative staining and (b) unstained (both images taken around 100 kX magnification).[298]

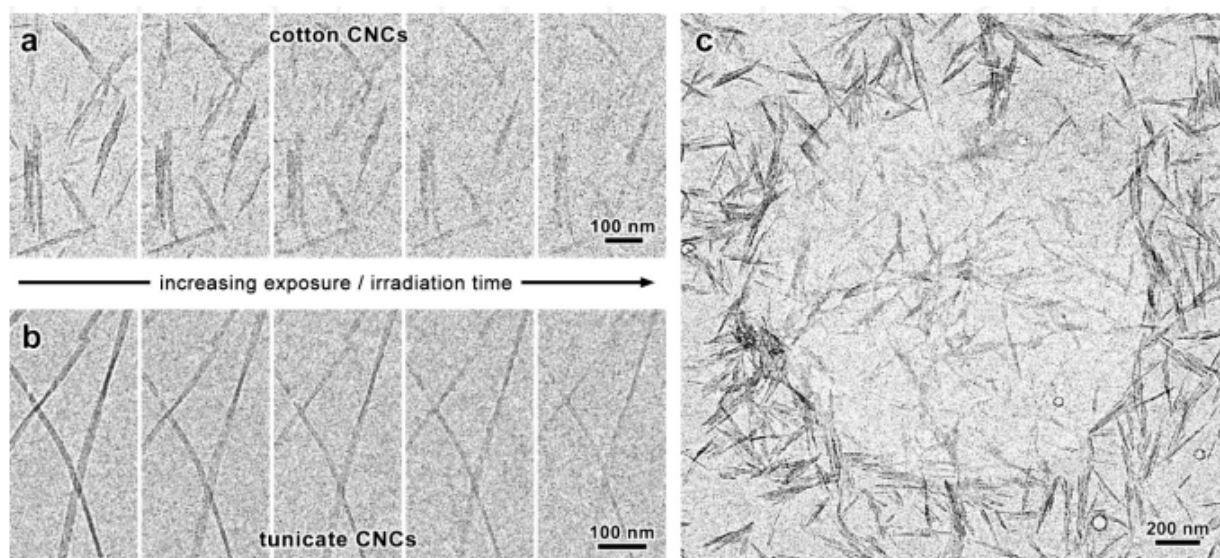### 7.4.5.   Charging and Sample Damage: Challenges

In electron microscopy, electrons are launched into the sample, an interaction happens, and electrons are ejected. Some materials, especially those with a high number of electrons or are conductive, can handle this exchange with minimal change to the bulk structure of the material. These materials are generally metals or something similar. CNMs are not similar to metals, do not have a lot of electrons, and do not conduct electricity. So, when electrons are pummeled into the sample, charging or damage to the sample can occur.

7.4.5.1 Surface Charging

Charging will occur in EM if the sample does not conduct electrons and allow them to disperse throughout the sample and into ground.[281, 291] Charging makes imaging difficult by causing streaking during imaging and causes the image to jump sporadically to a new position on the sample.[299, 305] Factors that affect charging include surface contamination on the samples, large samples not well connected to the sample holder (not well grounded), and samples with complex surface morphologies. These factors may also increase the likelihood of charging by conductively insulating the sample.

7.4.5.2 Sample Damage

Damage to CNMs under the electron beam in EM analysis is common and likely. The electron beam directed at the sample introduces a high voltage in a very small area and most organic materials show some type of degradation, especially if the beam remains in one location and extended period. **Figure 7.5** shows samples of beam damage to CNMs.

Figure 7.5. Illustrates damage of the CNMs under TEM as a result of radiation damage on unstained (a) cotton and (b) tunicate. In (c), the CNCs were damaged and shifted as the result of a condensed beam on one spot.[305]

7.4.6.   Charging and Sample Damage: Mitigation Methods
7.4.6.1 Conductive Coating

For SEM, sputter coating with a conductive material such as gold or platinum is commonly used for coating CNCs and making them conductive.[300] A major consideration here is the amount of material that is being layered onto the sample. Too much material will change the observed size of the CNCs or even completely mask the sample. Too little material will not prevent charging from occurring. TEM can also have issues with charging on CNC samples. Heavy metal stains can help with discharging the electrons.[308,304] Sputter coating is generally not used for TEM samples, although it can be used if other options are not possible.[281]

### 7.4.6.2 Electron Beam Manipulation

The electrons per area for EM techniques is akin to a needle through the skin with high forces focused in a small area. This can cause damage to the CNMs that can be seen in various ways such as reduction in contrast and/or size as well as the physical movement of the CNMs within the microscope.[309] The general approach is to minimize the probe diameter and maximize the probe current, which is a combination of optics adjustments, gun source output, electron brightness and accelerating voltage. Brightness increases, linearly with accelerating voltage, while the probe diameter decreases; however, this affects the overall resolution. Additionally, damage of CNMs under EM occurs within a short period of time, or exposure. Many times within a few seconds damage can begin; hence, adjusting beam settings, apertures, magnification and focus should be done on a sacrificial CNM to minimize damage to the nanoparticle of interest.

7.5. Applications of EM imaging

Below are some examples of how EM imaging has been used to characterize differences in CNM morphology, functionalized CNMs, and CNM-polymer composites.

7.5.1. CNM Morphology Comparisons

The morphology of CNMs is different when comparing material from different production sources. For example, a review paper by Jonoobi *et al.* [47] illustrates CNMs derived from a variety of sources as shown in **Figure 7.6**. The chemical and mechanical processing of these CNMs are also studied with respect to morphology. The size and level of smoothness were of interest and could be ascertained with EM techniques. It is reported that the EM analysis shows that the CNFs have a web-like network structure from all of the different sources studied. Measurements of the diameter and lengths were taken for all CNM samples and it was found that the diameters of the CNFs varied significantly depending on the source while the CNCs had similar diameters but varied in length, depending on source. The impact of chemical treatments on the CNMs was also reported and TEM images were used to observe the morphological differences. It was found that CNFs of certain treatments, including peroxide alkaline and potassium hydroxide, had a loose network. On the other hand, other CNF treatments, including peroxide alkaline-HCl, had reductions in size and short crystal-shaped particles were formed. These examples show the contribution that EM techniques provide to the characterization of CNMs.
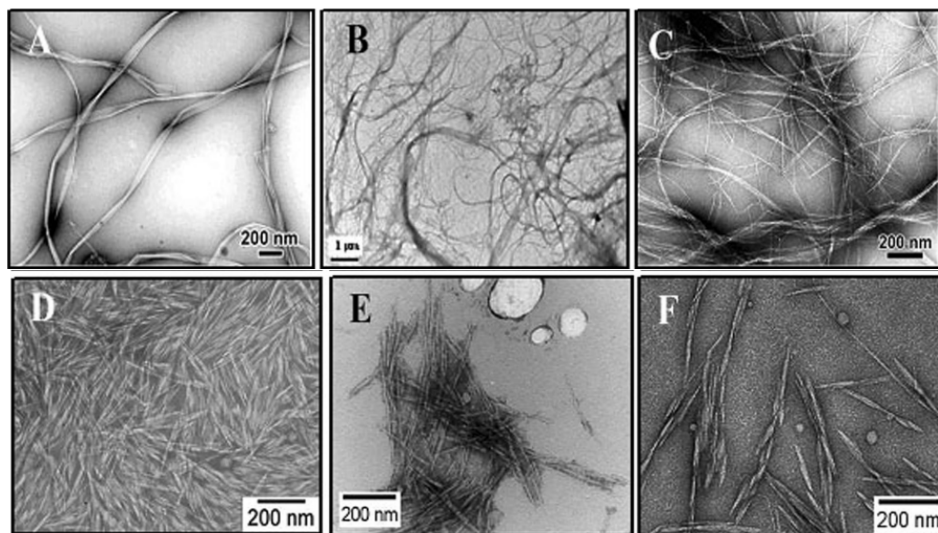
Figure 7.6. TEM images of CNMs:(a) bacterial cellulose CNFs, (b) bagasse CNFs, (c) banana rachis CNFs, (d) rice straw CNCs, (e) soy hulls CNCs, and (f) mengkuang leaf CNCs.**[47]**

7.5.2. Functionalized CNMs

Depending on the refining, post-production filtration and surface functionalization of CNMs, the morphology, degree of polymerization (DoP) and crystallinity will differ. EM imaging is one method to observe the differences, most specifically morphology and, in conjunction with other testing methods, for DoP and crystallinity. In one example, Qing *et al.* [231] found that for the EM images of the H_2SO_4 extracted CNCs, measurement of the larger particles were variable because of amorphous regions remaining with the

crystals. SEM and TEM images provided the researchers with a means to verify and visualize results (**Figure 7.7**). The researchers found through morphological observations that the conversion of cellulose to CNFs with enzymatic treatments reduced the length and networking of the fibers. Similarly the fiber bundles were non-uniform when refined with the SuperMassCollider and that the bundles converted to more uniform fibrils with the high-pressure microfluidizer. Hence, the observations made using SEM and TEM provided key insight into the behavior of the CNFs under chemical and mechanical refinement variations.
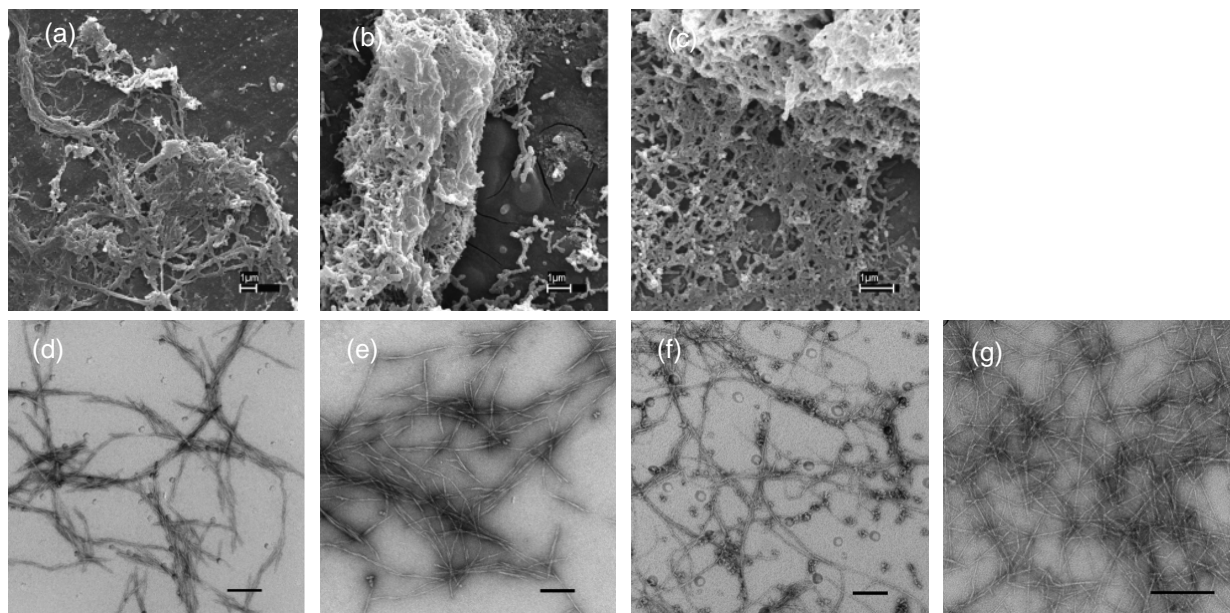
Figure 7.7. EM images of eucalyptus CNFs refined with different enzymatic and mechanical treatments; SEM images (a), (b), (c) have scale bars of 1 micron; TEM images (d), (e), (f), (g) have scale bars of 200 nm; (a) and (d) enzyme pretreated, refined with a SuperMassColloider; (b) and (e) enzyme pretreated, refined with a microfluidizer; (c) and (f) no pretreatment, refined with a microfluidizer; (g) pretreated with TEMPO oxidation, no refinement. [231]

7.5.3. CNM-Polymer Composites

Composite materials that contain CNMs generally use the CNMs as structural and/or actuating parts of the matrix or as templates for a dependent material.[310] A common method for sample preparation of the cross-section of a film is cryo-fracturing, or freezing the sample and then breaking it to get a brittle fracture edge unaffected by deformation that could be imposed by a cutting instrument. In one example, Mascheroni *et al.*[311] use EM assess how the CNM morphology effects the distribution of CNMs on the surface and within a composite film as seen in **Figure 7.8.** The film surfaces were homogeneous though the H_2SO_4/CNC films had a rougher surface than the ammonium persulfate (APS)/CNC films. The morphologies observed for the H_2SO_4/CNC film of higher roughness and more holes in the film as compared with the APS/CNC film confirmed the results of higher oxygen permeability and reduced transparency of the H_2SO_4 film. Furthermore the cross sections of the films verify the homogeneity and consistent distribution of the CNCs within the films. The study concluded that the APS/CNC films were viable materials for materials packaging.
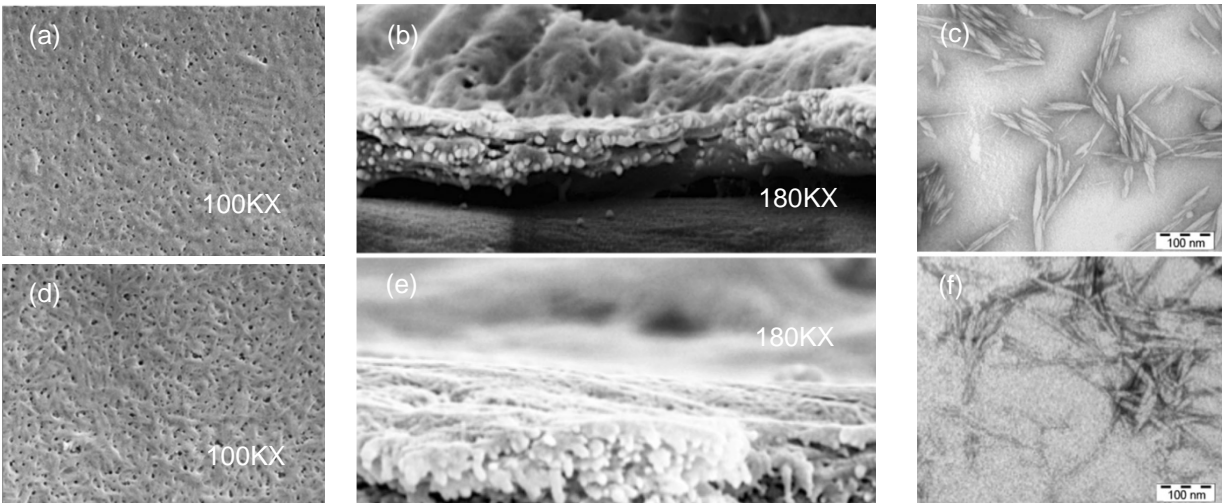
Figure 7.8. EM micrographs of the cross-section of CNC containing films where (a), (b), (c) (top images) contain sulfuric acid (H$_2$SO$_4$) treated CNCs, and (d), (e), (f) (bottom images) contain APS treated CNCs. Images (a) and (d) are surface topography SEM images of the two films. Images (b) and (e) are images showing cross sections of the films. Finally, images (c) and (f) are TEM images of the CNCs after treatments with H$_2$SO$_4$ and APS respectively.[311]

SECTION 8. Rheology of CNMs

*Michael J. Bortner, Jeff Youngblood, Kathleen J. Chan*

8.1. Relevance of CNM Rheology

Rheology, or the deformative response of a material to an applied force, is critical for understanding challenges in CNM composite processing.[9] CNM rheological response depends on the microstructure, degree of dispersion, and the interactions between the CNM and the solvent or matrix material in a composite system. Viscosity, or the resistance to flow, is very sensitive to changes in morphology and composition in a CNM system. Therefore, rheological analysis of the shear dependent viscoelastic response is effective for evaluating the contribution of CNM properties such as concentration, particle size, morphology and surface functionality on processability and quality of dispersion. [312-315]

Rheology is a tool that is commonly used for three primary purposes related to CNM analysis: 1) to determine the impact of CNM physical and chemical properties on processability, 2) to determine the impacts of processing on CNM dispersion/composite microstructure, and 3) as a quality control measure for comparison of different CNM suspensions and composites. Therefore, understanding the rheological response of CNM suspensions and composites is important to establish structure-process-property relationships.

The purpose of this section is to review the relevance of rheology on CNM characterization, with an emphasis on rheological measurement techniques for CNM measurements and practical techniques, limitations and challenges of using rheology for CNM analysis. A decision tree is provided in **Figure 8.1** to guide the reader through the steps to consider for evaluating rheology of CNMs.
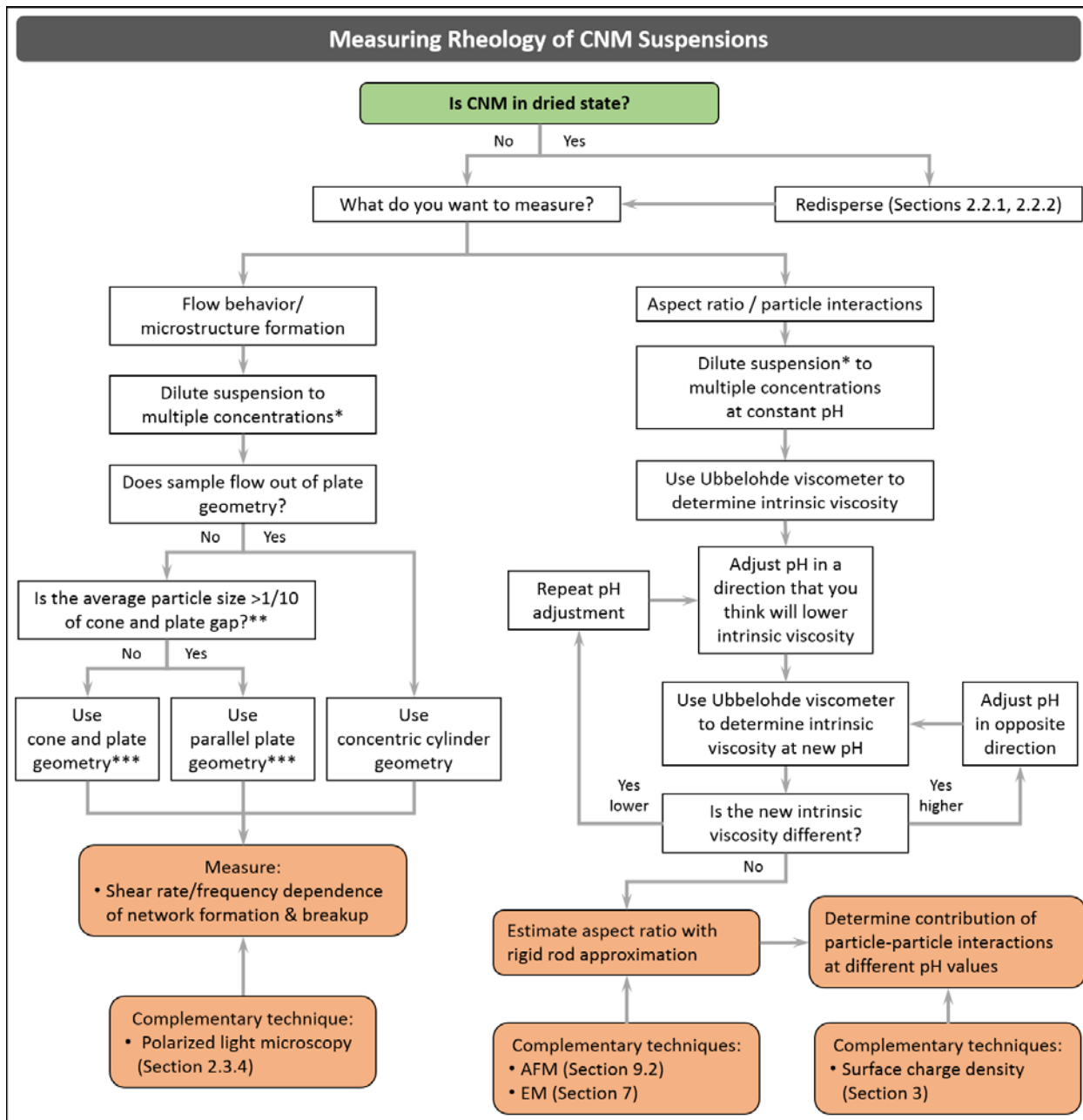
Figure 8.1. Decision tree to analyze rheology of CNM suspensions, *Suggested dispersion verification technique in **Figure 2.1**. **Use solvent trap to prevent sample evaporation. ***Use strain range within LVE region for subsequent test.

8.2.   Implementation of Rheology in CNM characterization

Here we will briefly discuss the common measurement types and mode, and geometry commonly used for CNM rheology characterization. Further general information on rheology measurements can be found in numerous reference texts. [316, 317]

8.2.1.   Measurement Type and Mode

The most common type of rheometers for CNM characterization are rotational (torsional) rheometers. While capillary rheology on CNMs has been done, data is sparse and, thus, we will not focus on it here. In a rotational rheometer, a sample is sheared between two plates. Plate geometries are selected based on

CNM format, depending on whether suspended in solvent or dispersed in a matrix. Rotational rheometers are commonly used to measure viscosity and viscoelastic properties of samples in relatively low shear rate ranges, typically from 0.001 – 100 s^{-1}. The two primary modes of testing in a rotational rheometer are steady shear and small amplitude oscillatory shear (SAOS). Steady shear mode is typically used to determine the bulk shear viscosity (η) and/or time dependent η of a sample, while SAOS is particularly useful in measuring the viscoelastic properties, *e.g.*, complex viscosity (η^*), shear storage modulus (G') and shear loss modulus (G"), of the sample.[316]

8.2.2. Measurement Fixtures and Geometry

Different fixture sizes and geometries are available for the rotational rheometer depending on the sample and experimental conditions. The three main geometries are: (1) cone and plate, (2) parallel plate, and (3) concentric cylinder. The cone and plate/ parallel plate geometries are typically used to test CNM samples with sufficient viscosity that the sample does not flow off of the plate during loading and/or analysis. These geometries only require a small sample volume (single mL) for analysis. Cone and plate fixtures should not be used if the particle size of the sample is greater than 1/10 the gap distance, which is typically 5 µm and may be a concern in systems where CNMs are agglomerated and not well dispersed. The concentric cylinder geometry is generally used for low viscosity (or dilute) samples that will not stay confined in the plate geometries, but requires substantially greater sample volume.[316] In general, plate geometries are more commonly used for CNM suspension and composite sample measurements. Viscosity measurements of very dilute CNM suspensions are commonly performed using an Ubbelohde viscometer.[98, 312, 318]

Sample slippage can also occur in high viscosity CNM suspensions or if the sample gets too viscous, *e.g.*, resulting from suspending medium evaporation. In CNM suspensions, slippage will generally occur due to localized depletion of CNMs and formation of a water layer at the smooth surface of the plate. Special cross-hatched geometries are available that can be used to prevent slippage.

8.3. Lab Protocol: Addressing Limitations and Practical Challenges

8.3.1. Suspending Medium Evaporation

When working with CNM suspensions in water or solvent, there is a strong effect of concentration on viscosity and potential flow alignment. Unless a controlled environment is maintained around the sample, suspending media evaporation can occur during the course of the test and substantially change the concentration. Sample evaporation can be reduced by implementing a solvent trap (sold by many instrument manufacturers) around the test fixture, or by saturating the environment with the suspending media within an environmental chamber. [312-315]

8.3.2. Quality of Dispersion

Dispersion of CNM is desired for nearly all applications to maximize the benefit afforded by CNMs and minimize the required quantity. As discussed in **Section 2**, quality of CNM dispersion is dependent on the CNM type, drying technique, surface charge, extent of sonication, *etc.* Extensive research have been conducted on the effects of various preparation techniques on dispersion on rheological properties of CNM suspensions. [295, 314, 315, 319]

For example, ultra-sonication is one of the most commonly used techniques to disperse CNMs in a suspension or polymer solution. Following ultrasonication, CNC suspensions exhibit the three-region viscosity profile similar to that reported for higher concentration CNC suspensions. The results indicate that the crystalline orientation is dependent on the degree of ultrasonication. The explanation for this behavior is that sonication breaks up the gel-like structure and disperses the CNCs throughout the suspension, facilitating liquid crystalline orientation.[314] Depending on the state of the CNM material being tested, redispersion and dilution techniques mentioned in section 2 should be followed to ensure reliable, and comparable results.

Once a baseline is established with a known well-dispersed sample, rheology is a powerful complimentary tool to analyze the quality of the dispersion. A poorly dispersed sample will appear as a sample with larger particles, generally resulting in a decrease in viscosity (particularly at low shear rates) resulting from a

decrease in number of particle-particle interactions. A shift of the shear rate associated with onset of shear thinning may also be observed. These comparisons are made assuming a fixed volume ratio/concentration and with similar CNM type, charge density, and at comparable pH. [320]

8.3.3. Uncharacterized CNM Sample Viscoelastic Analysis
When analyzing viscoelastic response to shear loading of a semi-dilute or concentrated, uncharacterized CNM suspension, it is important to determine the correct sample operating window before running other tests. The first step in characterizing the viscoelastic behavior of a CNM suspension is to determine the dependence of the strain amplitude of the G' and shear loss modulus (G'') and evaluate the region of strain within which linear viscoelastic response (LVE) of the sample is observed. To find the LVE strain region of the sample, an oscillatory strain sweep test should be performed at a constant frequency. G' and G'' should be plotted against strain. The LVE region is the region of strain within which G' remains constant, and below the critical strain at the onset of non-linear G' behavior. If G' is greater than G'', this indicates that the sample exhibits solid-like behavior in the LVE region. A maximum value of strain within the LVE region is typically desired to maximize torque readings, within the capabilities of the instrument, during oscillatory measurements.[316]

The time dependent rheological properties of the sample can be measured with an oscillatory time sweep test (with constant strain and frequency). In most cases, the viscosity of concentrated suspensions will have a stress induced transient response. To find the time dependence of the sample, G' should be plotted against time to determine the time before a constant G' is observed. If the sample exhibits time dependent behavior, a corresponding equilibration time should be implemented after the start of each loading (rate/frequency) to allow the sample to equilibrate before collecting data.[316]

8.4. Rheological Properties of CNMs
The rheological behavior of CNM suspensions has been studied to determine effects of concentration,[295] surface functional group density,[98, 295] aspect ratio,[98, 295, 318, 321] and extent of ultrasonication,[314] on phase behavior/microstructure. Polarized optical microscopy has also been coupled with a rheometer to confirm the microstructural changes of CNC samples under shear.[312-314]

8.4.1 Impact of CNM Aspect Ratio on Shear Rate Dependent Viscosity
A major consideration in measuring the rheological properties of CNM is that they are non-spherical particles- thus, the extent of interaction of the CNM with the suspending media (usually water) will be greater compared to spherical particles because non spherical shapes can rotate about an axis, resulting in larger effective volume compared to isotropic particles such as spheres. We think of CNM as rigid rods having an aspect ratio (r_p). In flow of particles with an aspect ratio, there is competition between Brownian motion randomizing the orientation of the particles in flow, and hydrodynamic forces causing the particles to orient in the flow field. For CNM we can consider a rotational Peclet number (Pe$_{rot}$, **Equation 8.1**) that captures the contributions of the hydrodynamic forces and Brownian motion on the flow behavior of the CNM.[320]

$$Pe_{rot} = \tau_{rot}\dot{\gamma} \qquad (8.1)$$

For rigid rods with an aspect ratio >>1, the rotational shear stress τ_{rot} can be represented by **equation 8.2**:

$$\tau_{rot}^{-1} = \frac{3k_BT(ln2r_p - 0.5)}{8\pi\eta_s a^3} \qquad (8.2)$$

Where k_BT is the thermal energy, a is the characteristic major axis length dimension of the CNM, and η_s is the suspending medium viscosity. As Pe$_{rot}$ approaches zero, Brownian motion dominates and one would expect largely randomized CNM suspensions representing the highest, zero shear viscosity (η_0) of the suspension. As Pe$_{rot}$>1, hydrodynamic forces become more significant and CNM will begin to align in the flow field, overcoming the effects of Brownian motion and exhibiting shear thinning behavior. [320]

8.4.2 Concentration Effects

The flow behavior of rigid rod particle suspensions is generally described by three regimes: dilute, semi-dilute, and concentrated, which are characterized by the following relationships in terms of the volume fraction of particles, Φ, and the aspect ratio of the particles[322]:

- Dilute: $\Phi \ll r_p^{-2}$
- Semi-dilute: $r_p^{-2} \ll \Phi < r_p^{-1}$
- Concentrated: $\Phi > r_p^{-1}$

Viscosity measurements of CNM suspensions in the dilute regime are typically made using an Ubbelohde viscometer and are useful to characterize CNM aspect ratio (with complimentary imaging techniques mentioned in **Section 7 and 9.2.3**) and to determine particle-particle interactions. [98, 312, 318] In the semi-dilute and concentrated CNM suspensions, SAOS and steady shear measurements in a rotational rheometer can probe viscoelastic properties and flow order transitions that result from network formation/percolation and subsequent break up as a function of shear rate.[98, 295, 312-315] The contributions elucidated from dilute suspension measurements can aid in understanding the nature of the response in the more concentrated suspensions. The following sections discuss the rheological characterization of CNM in these different concentration regimes.

8.4.3 Dilute Suspension CNM Characterization

Dilute CNM suspension viscosity measurements provide a powerful tool to analyze and decouple CNM aspect ratio and particle-particle interaction (electroviscous) effects.[98, 318] In the dilute regime, the relationship between particle concentration and resulting suspension viscosity can be described by the intrinsic viscosity in **equation 8.3**:[320]

$$[\eta] = \lim_{\Phi \to 0} \left(\frac{\eta - \eta_s}{\eta_s \Phi} \right) \tag{8.3}$$

Where $[\eta]$ is the intrinsic viscosity, η is the suspension viscosity (measured by an Ubbelohde viscometer), η_s is the viscosity of the suspending medium and Φ is the particle volume fraction. CNM suspension concentrations for these measurements are defined in **Section 8.4.2**, and have been reported to be on the order of, or less than, ~0.01 wt.% CNM.[318]

While Simha's equation can be used to estimate the aspect ratio of dilute CNMs suspensions with low aspect ratios, it is critical to ensure that interparticle interactions are not significant when using this approach. [98, 295] For example, Iwamoto *et al.* showed that the aspect ratio of CNFs estimated with the Simha Equation was significantly lower than the aspect ratio measured from AFM. [321] Studies have shown that deviations in the approximations are due to primary electroviscous effects. [98, 314, 318]

It has been well documented in colloidal literature that pH will substantially impact the particle-particle interactions.[320] In the case of CNM, and more specifically aqueous CNF suspensions, low pH on the order of ~1.5-2 will protonate the CNFs and significantly reduce the interactions. Therefore, multiple concentrations (volume fractions) can be measured at conditions where particle interactions are negligible to determine intrinsic viscosity and corresponding CNM aspect ratio, such as at low pH for many aqueous CNM suspensions.[318] The theoretically derived relationship in **Equation 8.4** has been used to relate intrinsic viscosity to aspect ratio for non-interacting, rigid rod suspensions with particle aspect ratio >> 1:[323]

$$[\eta] = \frac{8r_p^2}{45 \ln r_p} \tag{8.4}$$

The measurement of the electroviscous effect in aqueous CNM has been determined for CNF by further evaluating the intrinsic viscosity as a function of increasing pH and using **Equation 8.5**:

$$\frac{\eta}{\eta_s} = 1 + ([\eta]_0 + [\eta]_{ev})\phi \; as \; \phi \to 0 \tag{8.5}$$

Where $[\eta]_0$ is the intrinsic viscosity for uncharged particles and $[\eta]_{ev}$ is the primary electroviscous effect.[323] The electroviscous effect will be a strong function of pH in aqueous CNM suspensions, providing significant

insight into the impact of interparticle interactions as a function of level of protonation. For instance, Jowkarderis and van de Ven have measured instrinsic viscosities of CNF as low as 450 at a pH of 1.5, increasing to 2320 at a pH of 6.9 and highlighting the large impact of electroviscous effects on viscosity in dilute aqueous CNM suspensions.[318]

8.4.4. Rheology of non-dilute CNM Suspensions

As the concentration of CNM is increased into the semi-dilute and concentrated regions, rheology measurements provide insight into the shear rate dependent microstructural network of CNM suspensions by analyzing the complex non-Newtonian shear rate dependence of viscoelastic properties. [98, 295, 312-315] For instance, direct comparisions of CNC and CNF aqueous suspensions at concentrations ranging from 0.25-1.5 wt% are illustrated in **Figure 8.2**. SAOS results show that CNCs display viscous fluid-like behavior at low concentrations, and elastic gel-like behavior at the intermediate and high concentrations. The overall results indicate that CNC phase behavior is highly concentration dependent. CNC suspensions exhibit shear thinning behavior at low concentrations. At intermediate concentrations, CNC suspensions exhibit a three-phase transition, where shear thinning behavior is observed at low shear rates due to CNC orientation in the shear direction, after which a semi-plateau behavior is observed at an intermediate shear rate range resulting from interactions between oriented CNCs. A second shear thinning regime is then observed as shear rate is increased because the shear force is sufficient to disrupt the CNC interaction. At high concentrations, a single shear thinning profile (at a low viscosity) is observed, indicating a gel-like structure.[295] Understanding the shear rate dependent response is significant for flow of CNM suspensions and/or composites in a broad range of applications, including flow in confined geometries such as in pipes but also in open geometries such as open atmosphere flow channels.
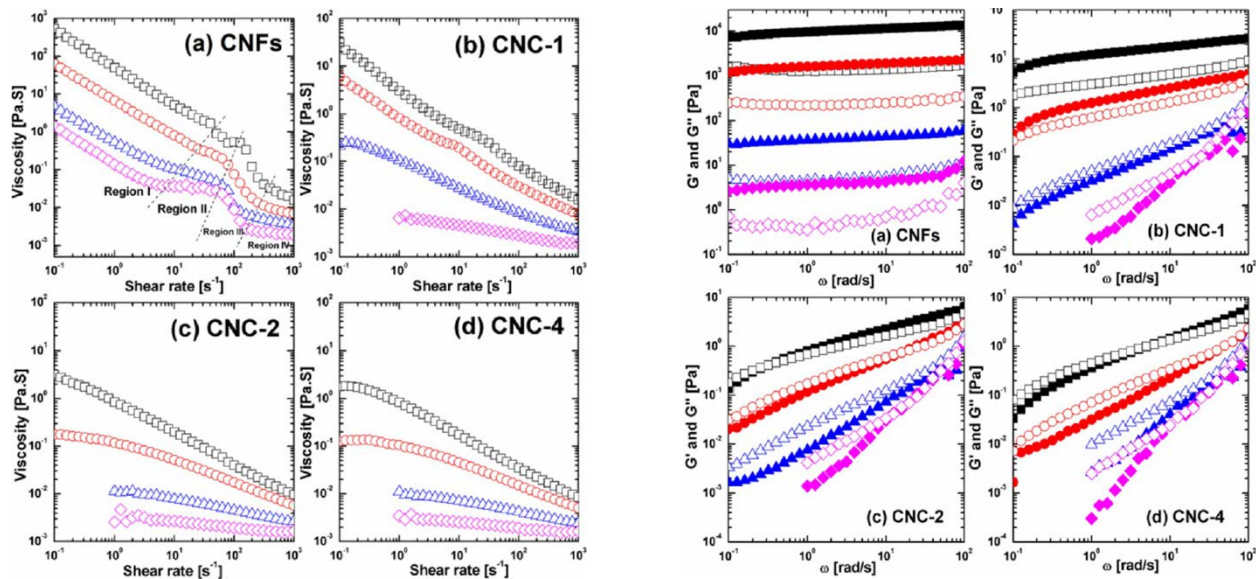
Figure 8.2. (left) Steady-state viscosity versus shear rate, (right) SAOS results illustrating shear storage modulus G' (solid symbols) and loss modulus G" (open symbols) as a function of angular frequency of (a) CNFs, (b) CNC-1, (2) CNC-2, (d) CNC-4 suspensions with concentrations of 1.5 wt% (black squares), 1.0 wt% (red circles), 0.5 wt% (blue triangles), and 0.25 wt% (magenta diamonds) at 25 C. The number after the CNC refers the hydrolysis time of 1 to 4 h. At a low concentration and low shear rate region, the viscosity could not be measured precisely because of the sensitivity of rheometer. [295]

Rheology measurements of CNF suspensions indicate a four-phase transition similar to the three-phase transitions seen in the CNC suspensions. Another viscosity plateau region is observed in the fourth region (**Figure 8.2 left, a**). At comparable concentration, CNF suspensions have a higher viscosity than CNC suspensions and have four phase regions at all concentrations, while CNCs only exhibit the same behavior at high concentrations. The difference in rheological response of CNCs and CNFs could be attributed to

difference in their structure and aspect ratio. The web-like structure of CNFs increases the likelihood of entanglement which contributes to its high viscosity and more solid-like behavior. These results indicate that phase behavior is also dependent on the aspect ratio (**Section 8.4.1**).[295] M. Lundahl *et al.* have reported an absence of plateau region even at high CNF concentrations when using a serrated plate.[324] The variations in data highlight the importance of sample and equipment consideration when running rheological tests.

Because CNMs are optically anisotropic, polarized optical microscopy can be used as a complimentary technique to confirm the microstructural changes of CNC samples under shear to determine the stability of suspension at various shear rates.[312-314] Likewise, comparisons to empirical relationships can be used as an indicator for microstructure formation. The Cox-Merz rule describes the correlation between dynamic and steady shear viscosity, and can be examined by plotting the complex and steady shear viscosity as a function of the angular frequency and shear rate, respectively. [325] It can be used to predict steady state viscosity at high shear rates with dynamic experiments, which are unattainable with steady oscillatory shear flow experiments. Deviations from Cox-Merz rule can be used to indicate microstructure formation of the sample.[313, 314]

SECTION 9: Preparation of CNM Thin Films for Particle Size Analysis by AFM and Optical, Surface Forces and Adsorption Studies

Michael S. Reid and Emily D. Cranston

9.1.   Types of CNM Thin Films: Submonolayer vs Full Coverage

This section is primarily focuses on the preparation of CNMs into film or film-like configurations that facilitates their characterization, and then secondary we provide some limited information on AFM measurement for CNM particle size characterization. CNM thin films have been used extensively as model cellulose surfaces to study polymer/small molecule adsorption and specific binding, swelling and solvent/vapor interactions, crystallinity, surface forces and adhesion. In contrast to traditional micron-thick films and coatings, we define CNM thin films as ranging from partial coverage films (*e.g.*, submonolayer) to complete, uniform films upwards of hundreds of nanometers in thickness.[9, 84, 326] In this section we outline the preparation of two types of CNM thin film configurations (*e.g.*, submonolayer, and complete surface coverage) that can be used to study individual particle properties, as well as fundamental adsorption, surface force and optical measurements. This section is not intended to describe how to make CNM or CNM composite coatings for application purposes, which is covered in most CNC/CNF nanocomposite reviews.

Common to the field of scanning probe microscopy, individual particle or molecule properties are studied as dispersed material on flat uniform surfaces. Often referred to as submonolayers films these surfaces consist of aggregated ("islands") or completely isolated particles through which particle-particle interactions are avoided when studying particle size and morphology, mechanical, electrical or thermal properties, amongst others.[327] While submonolayer films differ significantly from full coverage thin films, thick films and coatings, primarily because the underlying substrate is exposed, they have become an essential platform for studying individual particle/molecule properties. In contrast, full surface coverage CNM thin films, reflect more conventional films by consisting of several CNM layers that completely cover the underlying substrate. Full surface coverage CNM thin films however, are typically less than one micron thick (but most often in the 50-100 nm range) and are used for fundamental adsorption, swelling, surface forces and optical investigations. These CNM films offer advantages over regenerated cellulose surfaces in terms of surface roughness and reproducibility, and more closely mimic natural cellulose as they are primarily composed of cellulose I (the native crystal form of cellulose). The two types of CNM thin films described in this section can be produced or deposited onto substrates using various techniques such as spin coating, Langmuir-Blodgett/Schaeffer deposition or solvent casting.[328-334] A decision tree is given in **Figure 9.1** to guide the reader how to choose and prepare the appropriate CNM film for a given characterization study.)
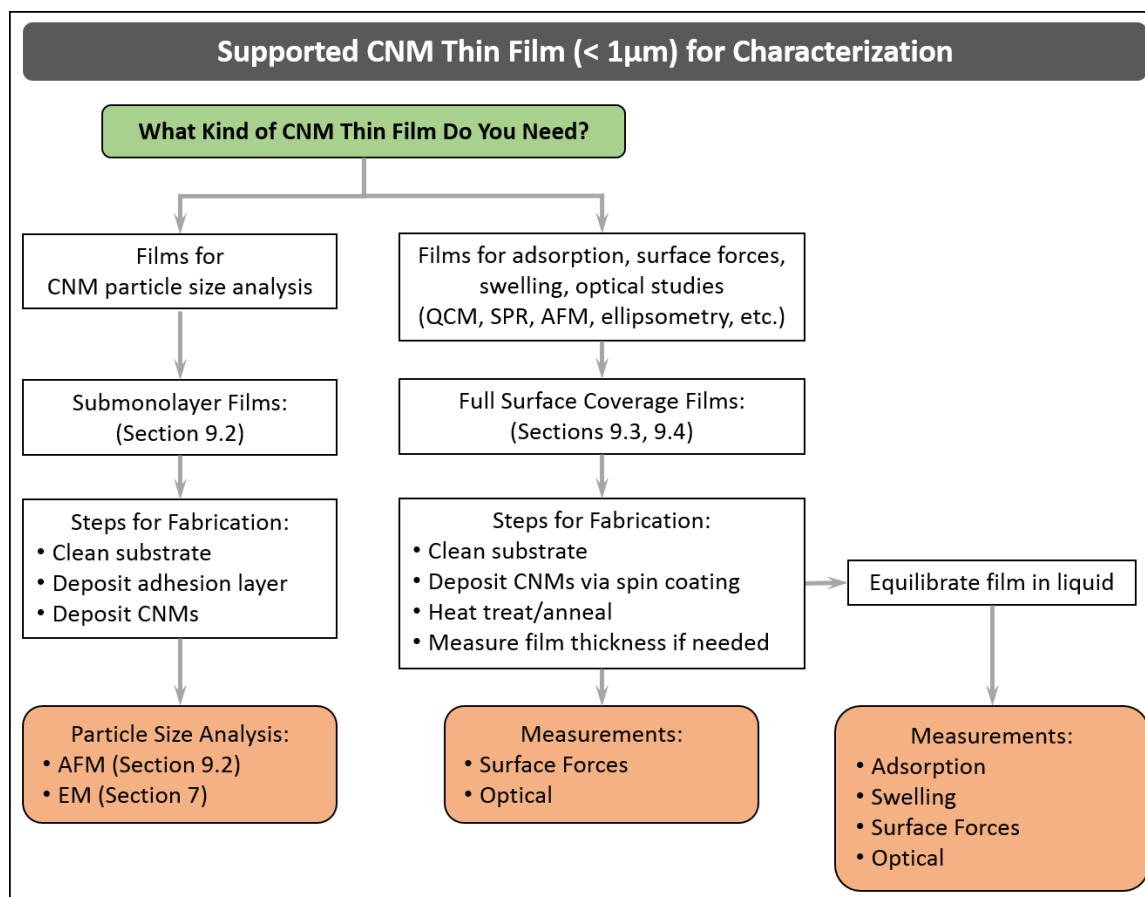
Figure 9.1: A decision tree pertaining to supported CNM thin films (<1 μm thick) used for various subsequent characterization techniques.

9.2. Submonolayer CNM Films for Particle Size Analysis

Particle size analysis, or surface force measurements (of isolated particles) by AFM require well-dispersed particles on a flat substrate such that individual particles can be measured. Aggregated or agglomerated material cannot be effectively measured as tip convolution makes particle edges indistinguishable. As such, films containing very high aspect ratio CNMs, such as tunicate CNCs or CNFs, must be carefully prepared or in some cases may not be suitable for particle size analysis (specifically length measurements) by AFM because fiber flexibility often yields overlapping or entangled material. To date, the majority of studies reporting particle size via AFM are of negatively charged CNCs extracted by sulfuric acid hydrolysis, and as such, is the focus of the discussion below. That being said, dispersed films of other CNMs have also been successfully prepared.[335, 336] An example of AFM height images of CNCs and CNFs that are suitable for size analysis is shown in **Figure 9.2**.

CNC submonolayer films for particle size analysis are deposited from dilute suspensions (<0.01 wt.%) onto atomically flat surfaces such as silicon wafers or mica.[32, 96, 337] Films can be prepared on other surfaces such as quartz crystal microbalance with dissipation (QCM-D) sensors or surface plasmon resonance spectroscopy (SPR) sensors, however, these surfaces are not recommended for particle size analysis, as the underlying semi crystalline gold surface is not smooth enough for reliable AFM measurements. Extensive substrate cleaning is crucial prior to film deposition as described below in **Section 9.3.1**. Preparation of submonolayer CNC films has been reported by solvent casting[96, 97, 335, 337, 338] and spin coating,[32, 334] with both procedures yielding films suitable for particle size analysis (**Figure 9.2**). Critically, both solvent casting and spin coating procedures require that, prior to CNC deposition, a cationic polymer adhesion or "anchor" layer be deposited.[97] While adhesion layers are not required and not recommended

for full surface coverage films (discussed further in **Section 9.3.1**), they aid in particle adsorption by electrostatically immobilizing negatively charged CNCs, thus limiting aggregation upon drying. Without cationic adhesion layers, capillary action during both spin coating and solvent casting drive dispersed CNCs to aggregate on the substrate. Analysis of these films requires the user to search for isolated particles away from bulk aggregates.[339] Importantly, when measuring adhesion or elastic properties of isolated CNCs, polymer adhesion layers should be avoided as they can influence or convolute measurements.[97, 339] Poly(allylamine hydrochloride) and poly-L-lysine (0.01 – 0.1 wt.%), or amine-terminated monolayers, are commonly used cationic adhesion layers and can be deposited by incubating substrates or by spin coating followed by thorough rinsing.[32, 96, 340] Note that poly(ethyleneimine) is also sometimes used as an adhesion layer, however, due to its highly branched nature and thicker film forming ability we recommend against using this polymer.

9.2.1 Solvent Casting Submonolayer Films
A detailed description of the solvent casting procedure for anionic CNCs can be found in section 9.2.4 in the Canadian Standard, *Cellulosic Nanomaterials - Test Methods for Characterization* (CSA Z5100-14).[15] Briefly, freshly cleaved mica (ca. 1 cm × 1 cm) is incubated in poly-L-lysine solution (0.01 wt.%) for 30 min followed by thorough rinsing. A 100 – 200 μL dilute suspension of CNCs (<0.01 wt.%) is deposited onto the substrate and incubated for 1 – 2 min. Surfaces are then rinsed thoroughly in water and blown dry. Notably, CNC suspension concentrations may need to be altered to optimize particle dispersion on the surface.

9.2.2 Spin Coating Submonolayer Films
Spin coating is commonly used to prepare complete surface coverage CNM films but is readily adaptable for submonolayer films by including a cationic adhesion layer and working from dilute CNM suspensions. Coating speeds, drying times and sample volumes may vary with laboratory conditions (humidity, temperature, *etc.*) and substrate dimensions but generally films are prepared by coating static substrates with 200 – 500 μL of material and spinning (>3000 rpm) until Newtonian rings are no longer visible and the film is completely dry (>30 s).[32, 334] Specifically, submonolayer films are prepared by first covering a clean static substrate with cationic polymer solution (0.01 – 0.1 wt.%) and spinning the substrate dry. Without removing the substrate from the spin coating chuck, the substrate is covered with water and spun dry to remove excess polymer. Finally, dilute CNM suspensions (< 0.01 wt.%) are deposited and spun dry.
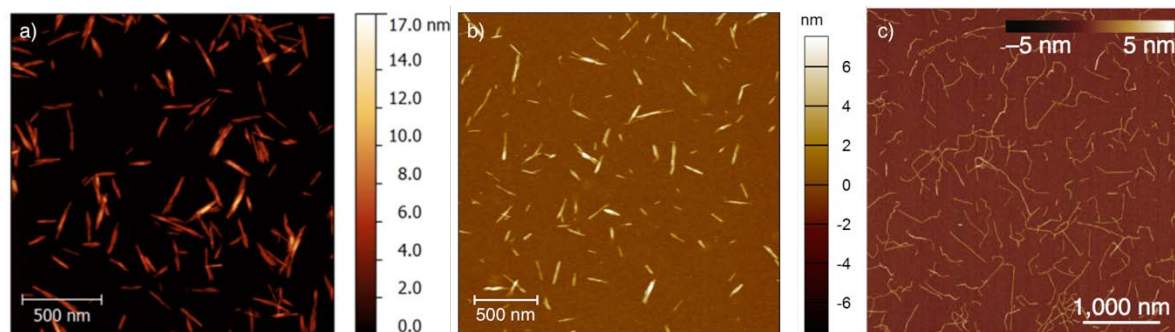
Figure 9.2. AFM images for particle size analysis of CNMs. (a) Sulfuric acid hydrolyzed CNCs from bleached softwood kraft pulp[341] deposited by solvent casting on poly-L-lysine coated mica, reprinted from reference [96] with permission from L. Johnston and the American Chemical Society. (b) CNCs produced by CelluForce deposited via spin coating on a poly(allylamine hydrochloride) coated silicon wafer. (c) TEMPO-oxidized CNFs solvent cast onto (3-aminopropyl)triethoxysilane coated mica, adapted from reference [335].

9.2.3. Particle Size Analysis by AFM
As discussed in **Section 2**, due to the high aspect ratio of CNMs, particle size/size distribution cannot be effectively measured by DLS. As a result, particle analysis by microscopy such as AFM or TEM (see

Section 7) is recommended to fully assess both particle width (height) and length. Notably, AFM and TEM suffer from tip convolution/broadening and staining effects, respectively, and particle sizes between techniques may differ.[96] Moreover image analysis can be somewhat subjective, varying between analysts and laboratories, yet AFM and TEM serve as the most effective methods to determine particle size and size distribution.[96]

AFM size measurements can only be performed on *height* images of well-dispersed particles (hence the need for submonolayer films as discussed above) and we emphasize that size measurements on AFM images from amplitude, phase, deflection, modulus, *etc.* channels will not give accurate readings and should be avoided. Importantly because of tip broadening effects, particle widths measured by AFM are erroneously large and should not be reported unless probe dimensions have been thoroughly characterized. Instead, particle height (from the cross sectional height analysis) measured across the center of the particle, should be reported in particle size distributions. Similarly, the average height across the length of the nanocrystal yields an accurate cross section. Differences between CNC particle width and height have been reported earlier in a study which co-deposited well-defined gold nanoparticles during film preparation to accurately measure probe size.[97] Height and width of CNCs in this report differed by 1.4 nm suggesting that CNCs cannot be specifically treated as cylindrical rods. AFM images should be collected in intermittent contact (also called tapping or alternating current) mode to minimize particle movement and probe damage and a minimum of 100 isolated particles should be measured. For further information regarding AFM parameters and image processing the reader is directed to Section 8.2.4 of the Canadian Standard, *Cellulosic Nanomaterials - Test Methods for Characterization* (CSA Z5100-14).[15]

9.3.   Full Surface Coverage CNM Thin Films for Adsorption, Surface Forces, and Optical Studies

Complete surface coverage CNM films have been used extensively in swelling,[57, 330, 331, 342, 343] adsorption,[344, 345] forces/adhesion,[346-350] and enzymatic[351-353] studies of cellulose surfaces. Although, specific experimental requirements may differ between techniques, generally cellulose films must be flat, uniform, and complete (i.e., no open substrate). While numerous methods have been reported for the deposition of these films not all techniques are amenable to produce thin films suitable for QCM-D, SPR, AFM or ellipsometry studies. Many of these techniques were developed for the preparation of regenerated cellulose surfaces, from dissolved cellulose, and cannot be directly adapted to CNM films.[328] For example, Langmuir-Blodgett and Langmuir-Schaeffer are commonly used techniques for the preparation of trimethylsilylcellulose (TMSC) films, however deposition of CNMs is significantly more challenging because of the limited surface activity of native CNMs.[354] Deposition of CNM thin films by Langmuir Blodgett/Schaeffer techniques require careful preparation of the air-water interface and the use of cationic surfactants, such as dioctadecyldimethylammonium (DODA), to adsorb anionic CNMs.[332, 333] The resulting films can be further processed to remove DODA, yielding flat uniform cellulose films, however only monolayers can be achieved and may not be suitable for swelling or adsorption studies as substrate effects cannot be ignored.

Solvent casting is also commonly used to produce thick (> 1 μm) or freestanding films to study the chiral nematic behavior of CNCs.[105] However, the slow drying of CNM films by solvent casting results in non-uniform rough surfaces due capillary forces and the coffee-ring-effect.[355] Recently, Gençer *et al.* reported that ethanol can increase Marangoni flow, and reduce the coffee-ring-effect during drying to create more uniform films however, these films remain too rough for highly surface sensitive techniques like QCM-D, SPR and AFM.[356]

A number of recent studies have prepared CNM films for QCM-D *in situ* by flowing CNC or CNF suspensions over cationically functionalized sensor surfaces within the instrument. Although CNCs clearly adsorb only a submonolayer (or monolayer at best) can be effectively deposited as CNCs saturate the cationic surface layer. Moreover, by preparing films *in situ*, film quality (uniformity, thickness and density) cannot be effectively measured prior to adsorption studies, which potentially leads to erroneous measurements due to interactions with the substrate or the undying cationic polymer layer. As a result, it is recommended that CNM films be prepared prior to optical, surface force or adsorption studies such that films can be thoroughly characterized (and full surface coverage ensured) prior to measurements.

9.4. Spin Coating Full Surface Coverage CNM Films

Spin coating is the most common method used to produce full surface coverage films for optical, surface force or adsorption studies. Uniform, flat, thin films can be readily prepared from CNM suspensions on a variety of substrates including, mica, silicon wafers, regenerated cellulose and Au, SiO_2 or TiO_2 coated QCM-D and SPR sensors. **Figure 9.3** shows AFM height images of spin coated CNF and CNC films on QCM-D and SPR sensors, respectively. Notably, CNF films are more porous than CNC films due the high aspect ratio of the particles and the lower suspension concentrations required for spin coating. While in some cases film preparation by spin coating can be considered trivial, it is critical to recognize the key parameters that affect film quality and deposition procedures.
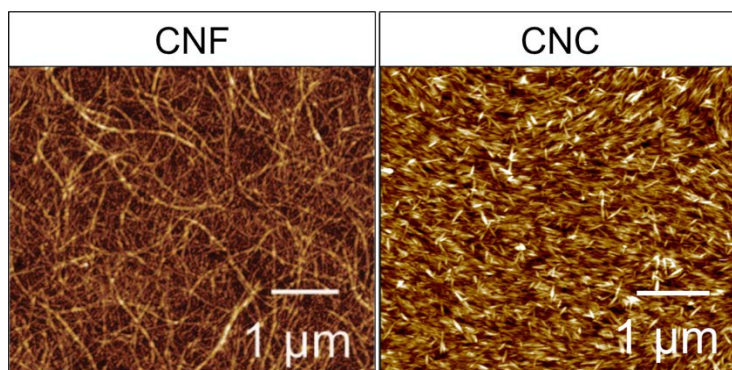
Figure 9.3. AFM height images of spin coated CNF (left) and CNC (right) films showing different film topography and porosity. CNF films were prepared from 0.4 g L^{-1} suspension on 3-aminopropyl-trimethoxysilane coated SiO_2 QCM-D sensors, adapted from reference [351] with permission from the American Chemical Society. CNC films were prepared from 3 wt.% suspension spin coated on SiO_2 coated SPR sensors.

9.4.1. Substrate Preparation

Prior to spin coating, substrates must be thoroughly cleaned. Cleaning procedures vary by substrate but can include, UV/ozone, plasma/corona discharge, chromerge/BIC, or piranha (3:1 $H_2SO_4:H_2O_2$) amongst others. Particular care is recommended for QCM-D and SPR substrates as sensors are expensive and coatings can be subject to etching depending on the cleaning procedure selected. When spin coating, surfaces should be activated such that aqueous CNM suspensions wet the substrate. Spin coating onto low surface energy materials (contact angle θ>90˚) can be challenging as non-uniform wetting occurs resulting, in incomplete films not suitable for analysis.

9.4.2. Adhesion Layers

Numerous studies report the use of cationic adhesion layers prior to CNM film deposition. These layers electrostatically bind anionic CNMs creating dense uniform films. Amine terminated self-assembled monolayers,[357] 3-aminopropyltrimethoxysilane,[330] and cationic polyelectrolytes such as poly(ethyleneimine),[331] poly(allylamine hydrochloride),[358] poly-L-lysine[125] and poly(vinylamine)[330] have been successfully used for film preparation. Adhesion layers are particularly useful when preparing dense films of very high aspect ratio CNMs, such as CNFs and tunicate CNCs, as suspension concentrations required for uniform film formation can result in gelation. The use of adhesion layers promotes adsorption to the surface and thus CNM suspension concentration can be lowered.

Recently, some reports question if adhesion layers affect film behavior during swelling/adsorption studies (particularly when CNM monolayers and sub 50 nm thick films are investigated) as underlying polymer layers in multilayer films have been shown to have non-negligible effects.[349] This has led to the development of "cellulose-only" films whereby CNMs are spin coated directly onto the substrate for swelling and adsorption studies.[57, 342] CNC films without adhesion layers are typically prepared from spin coating concentrated suspensions, *e.g.*, 1-5 wt.% (where viscosity remains suitable for the spin coating process). It is thus recommended that complete surface coverage CNM films be prepared without adhesion layers

whenever possible, as to avoid unwanted effects from underlying polymer layers. In studies where adhesion layers are required, CNM films should be thick enough (>10 nm) to limit the impact of the underlying polymer on film behavior.

9.4.3.   Spin Coating Parameters

Specific spin coating parameters, such as acceleration, rotations per minute (rpm) and drying time are dependent on laboratory conditions (humidity, temperature, *etc.*) and substrate dimensions. Generally full surface coverage cellulose-only films can be prepared by covering clean substrates with 100 – 500 µL of CNM suspension (1-3 wt.%) and spinning at >3000 rpm (with <10 s acceleration ramp) until the film is dry (>30s).[57] Spin coating under N_2 is also recommended, or at a minimum the humidity inside the spin coater should be kept low as residual moisture can significantly affect film thickness. Silicon wafers and SiO_2 coated QCM-D and SPR sensors are suggested over gold substrates and tend to lead to the most reproducible films. Film thickness can be controlled from submonolayer to >100 nm by increasing CNM suspension concentration however, spin coating on top of an already deposited film is not recommended as rehydration of the CNM film can delaminate material from the surface resulting in non-uniform films.

Generally, film quality can be assessed by eye whereby surfaces should be free of defects and of uniform color. Film thickness can be approximated (to tens of nanometers) by color that arises from thin film interference,[353, 359] (not to be confused with chiral nematic structural color) however, color is substrate specific and accurate measurements require advanced methodology (see **Section 9.5**). Importantly, film structure near substrate edges is typically non-uniform due to capillary and drying effects and measurement of properties or interactions near film edges should be avoided.

9.4.4.   Heat Treatment of CNM Films

The stability of CNM films in liquid (i.e., throughout swelling, adsorption, surface force measurements, and other investigations) is essential for gathering reproducible results. Thermal or heat treatment following spin coating has proven to be an effective method to stabilize CNM films in aqueous environments. Without thermal treatment, films delaminate and redisperse in aqueous media.[360] Temperatures from 80-120°C and drying times of 15 min to 12 h have been reported to produce stable films.[57, 342, 343] To date, the specific mechanism of thermal treatment "annealing" has not been explicitly studied, however, the removal of residual and surface bound water, likely promotes cellulose-cellulose hydrogen bonding and stronger van der Waals interactions improving the stability of the film. To obtain reproducible data from thin film experiments with CNCs, we generally heat treat overnight at 80°C, rinse with water to remove any loosely bound nanoparticles and heat treat again for 8 hours at 80°C.[57]

9.4.5.   Equilibration of CNM Films

While some reports have monitored film swelling from the dry to wet state,[57, 331, 342] many investigations study CNM film behavior in varying aqueous environments and require stabilized films. Failure to fully stabilize CNM films can lead to measurement drift and potentially misleading results due to solvent uptake and film swelling. Equilibration is often achieved by incubating CNM films in water or buffer solution for several hours or overnight.[344, 357]

9.5.   Measuring CNM Film Thickness

Measuring the thickness of thin (< 1 µm) CNM films can be challenging. Optical techniques employing single wavelength light sources such as standard ellipsometry and SPR require well-defined slab geometries and known optical properties in order to effectively model film dimensions using the Fresnel equations. The birefringence of CNMs, especially in oriented films, can also induce complications for some optical techniques.[361] CNM films are porous, resulting in an unknown effective refractive index, which can range from ca. n =1.55 for bulk CNMs to near n = 1.0 for highly porous films in air. The unknown porosity and orientation of CNMs generally forces users to assume optical parameters. Scratch height analysis whereby a razor is used to cut through the film to measure the cross sectional height, by profilometry or AFM, is a destructive process and cannot be used for QCM-D or SPR sensors. Other film thickness measurements can be employed such as freeze fracturing and edge profiling in SEM or film masking for profilometry, however, these techniques are similarly destructive and cannot be used prior to measurement

(forces, adsorption or swelling) and produce non-uniform films. As a result, more advanced techniques have been employed to measure CNM film thicknesses as described below.

Multiple wavelength optical techniques such as spectroscopic ellipsometry (SE) and multi-parameter surface plasmon resonance spectroscopy (MP-SPR) can deconvolute film thickness and effective refractive index based on optical modeling (Fresnel equations), and can account for interface roughness and nanoparticle orientation as well.[57, 342, 343, 357, 362] An example with a CNC film is shown in **Figure 9.4**, demonstrating how using two lasers in MP-SPR allows independent thickness (*d*) and refractive index (*n*) values to be determined from the crossover point of an *n vs. d* plot.[57]

Although the theory behind these techniques is beyond the scope of this review, the effective refractive index is a measure of film density/porosity and can vary significantly between CNM films (**Figure 9.3**). For example, films produced from CNFs are highly porous and can have *n* <1.3 indicating that more than 50% of the film is open space or air.[343] In contrast, CNC films, which can be deposited to form dense/packed films have been reported to have refractive indices from $n = 1.4 - 1.52$ suggesting films contain 70 – 95% cellulose (or are 5 – 30% porous).[57, 342, 357] These techniques have been correlated to, *in situ* scratch height analysis whereby an AFM probe is pushed through the CNM film and scanned in contact mode to remove a small (1 μm × 1 μm) region of the film. The same region is then re-imaged in intermittent contact mode to measure the cross section of the scratched area (as shown in **Figures 9.4 a – c**).[57] Agreement between physical and optical measurements is evident in **Figures 9.4c and 9.4f** where both techniques yield a thickness of ca. 40 nm for a CNC film spin coated onto a SiO_2 coated SPR sensor. While physical measurements such as scratch height analysis are not always possible (*i.e.,* it is a destructive process), they are useful for the development of accurate layer models for optical techniques.
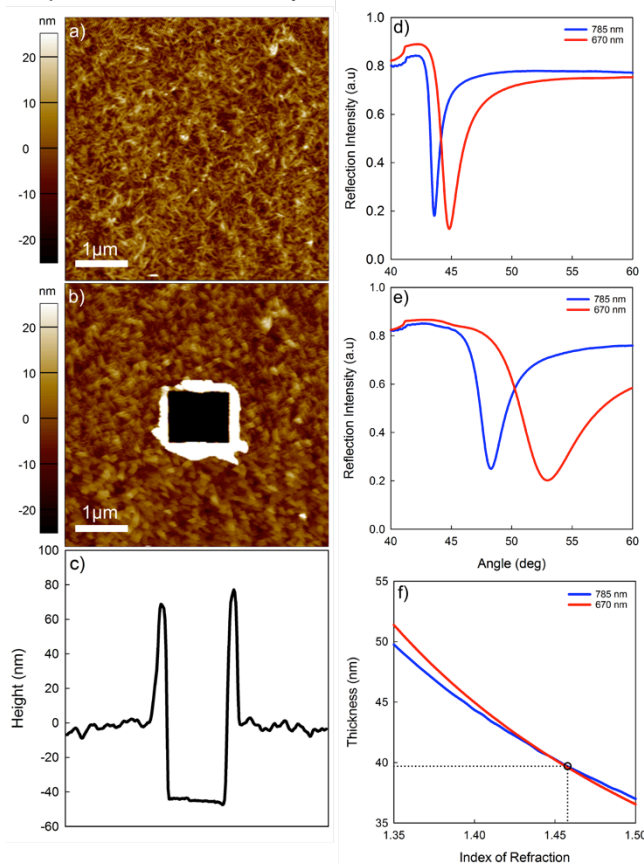
Figure 9.4. AFM height image of (a) a dry CNC film, (b) scratched CNC film, and (c) cross section height analysis of scratched image used to determine film thickness. MP-SPR spectrum of (d) bare SiO_2 substrate and (e) dry CNC film. Wavelength crossover (f) displays an index of refraction of 1.4578 and a thickness of 39.7 nm. Reprinted from reference [57] with permission from the Royal Society of Chemistry.

SECTION 10: Fluorescence Labeling of CNMs for Structure and Dynamics Characterization

Douglas Fox, Julien Bras

10.1. Interest in Fluorescence Labelling

Monitoring the distribution and degree of dispersion of CNMs in polymer composites and biological media is challenging. The traditional method of using electron microscopy is tedious and not always representative of the bulk. The dimensions of cellulose aggregates are often larger than the dimensions of TEM specimens, further complicating image interpretation. And, as hydrocarbons themselves, cellulosic materials have densities similar to polymers, making TEM contrast difficult without staining. Polymer nanocomposites containing CNMs are most often stained with uranyl acetate as a contrast.

Similar issues happen when CNCs or CNFs are introduced into fiber-based materials like paper or mat for thermoset composites. In the first case, it is obvious that cellulose fibers are chemically and morphologically similar to CNMs and distinction is almost impossible. The key issue is also when looking for distribution of CNFs in paper at microscale and only fluorescence labelling will give an idea using appropriate fluorescent microscope. CNCs might also be used as anti-counterfeiting particles by becoming a template of fluorescent molecule and allowing printing patterns by inkjet or iridescent fluorescent structure.[363]

Fluorescent imaging techniques can provide alternative methods for obtaining structural information in composites and biological media. In polymer systems, fluorescence imaging has been used to quantify the quality of dispersion and size of aggregates in clay – epoxy[364] and carbon nanotube – polystyrene systems.[365] Maupin, *et al.* [366] used fluorescence and optical spectroscopy to monitor the exfoliation of clay during melt extrusion of clay in nylon. Fluorescence imaging has also been used to identify the distribution and orientation of probe molecules along a clay fiber,[367] and the distribution of co-polymers in a composite.[368] Fluorescence imaging techniques have been used even more extensively in biological media. Fluorescence has been used for decades to identify and locate structures within a cell,[369, 370] and recent instrument and technique advances has expanded the use of fluorescence imaging to include dynamic and quantitative processes, such as real time physiological function.[369, 371, 372]

Using fluorescent lifetime imaging microscopy (FLIM) can add flexibility and a range of applications, such as dynamic processes,[373, 374] changes to the local environment,[372] location of interfacial regions,[375-377] dye aggregation,[375] confinement,[366, 373] or motion restriction.[376] Plus, fluorescence lifetime is an intrinsic property of the fluorophore and is independent of the concentration, exact excitation wavelength, or excitation power.[373] Specific pairs of fluorophores can form a couple resulting in Forster resonance energy transfer (FRET). This is a phenomenon that can only occur at short length scales (< 10 nm) and can provide information on the interface and interphase regions of the matrix.[377-380] Although FRET can be observed using several fluorescent techniques, the use of FLIM is most often employed. Many of these imaging techniques have been used for cellulose, including migration of microspheres in blood,[381] migration of nanocrystals in tissue,[382] the binding of cellulose to carbohydrate domain modules,[383-386] the network structure of mixed cellulose fibers,[387] and the interface of nanofibrillated cellulose fibers in polymers.[388, 389]

There are relatively few studies on the use of fluorescent techniques to examine the structure of the CNMs and their composites, but there have been quite a few fluorescent tagging procedures developed for CNMs. They fall into three main categories: physisorbed, ion exchanged, and covalently bonded. A decision tree for choosing an appropriate labeling chemistry is shown in **Figure 10.1**. It should be noted that this is used only as a general guide and that different choices may be better suited for specific applications or systems. The following subsections provide a more detailed discussion of the different labeling methods and their most useful applications.
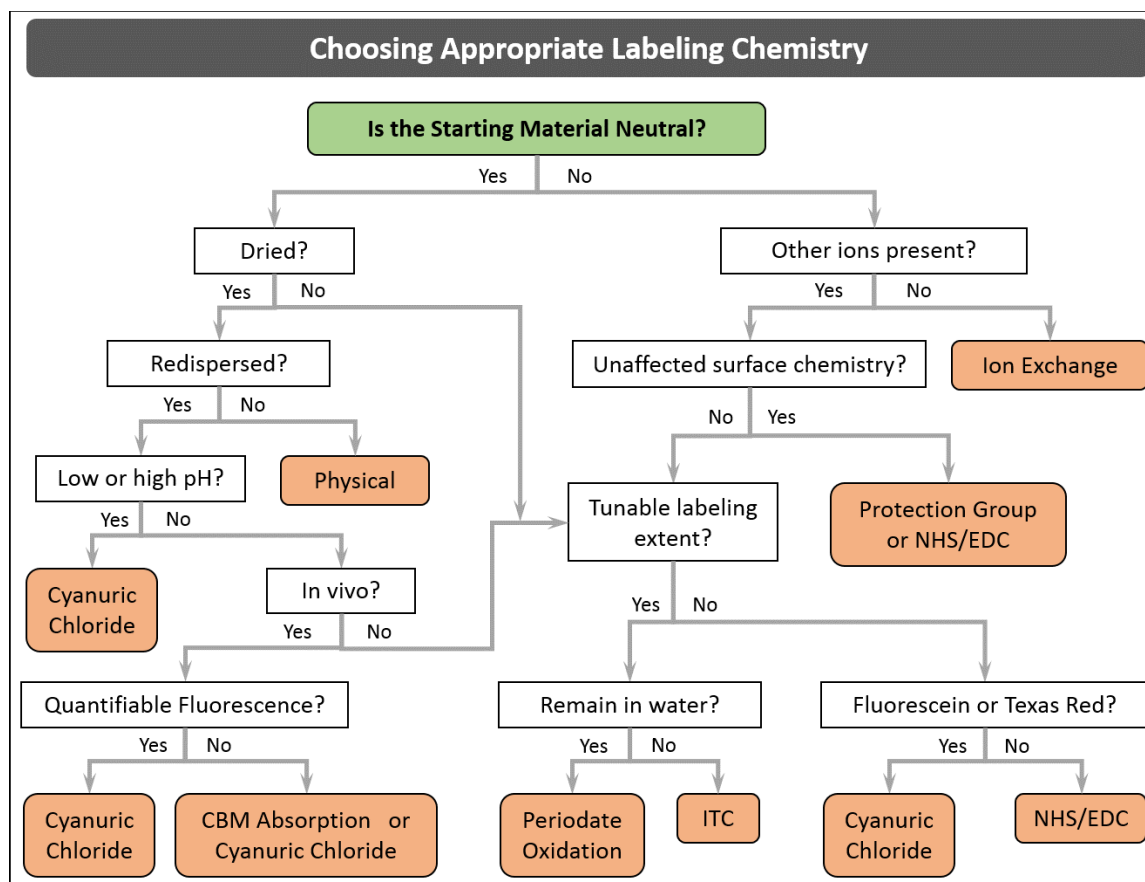
Figure 10.1. Decision tree for choosing an appropriate labeling chemistry.

10.2. Physisorbed Labeling

Physisorbed labeling offers very simple processes with a wide range of fluorophores. In fact, there is often residual lignin adsorbed to CNM after their manufacture, leading to auto-fluorescence.[278, 390, 391] Physisorbed fluorophores can be used to produce fluorescent cellulose films that preserve the nematic structure of cellulose. A wide variety of fluorophores have been used, including quantum dots,[392, 393] latex nanoparticles,[394, 395] noble metal nanoparticles,[396, 397] and optical brighteners.[363, 398]

The key point is to check if the physisorption is not reversible and monitor the quantity of fluorophores used. For example, by exploiting papermaking science, a fluorescent molecule may be labeled onto CNC. Indeed, distyrylbiphenyl sulfonate (DSBP) derivatives are widely used as efficient optical brightening agents (OBAs) to improve the brightness of paper, and these derivatives exhibit excellent affinity toward cellulose fibers.[399] The combination of a CNC suspension with an OBA agent (Tinopal® HW) has recently been proposed by Zhang and coworkers,[398] who reported a simple and efficient method to manufacture an iridescent film with fluorescent properties.

Bardet *et al.* [363] have studied the self-assembly of cellulose using DSBP. They found a strong affinity between DSBP and the CNCs, with a loading (adsorbed amount) of about 50 µmol/g$_{CNC}$. The amount of dye that adhered to the cellulose after dialysis was equivalent to fluorescein isothiocyanate (FTIC) with values ranging from 3 to 30 µmol/g and several times higher (5–50 nmol/g) than that of grafted aminofluroescein (DTAF). This method produces CNCs with strong fluorescence (**Figure 10.2**) and is significantly more efficient for CNCs than for cellulosic fibers. The amount of DSBP labeled onto CNC is estimated to be 38±3 µM, i.e., 19 µmol/gCNC, whereas a value twenty times lower (1 µmol/g) was reported for DSPB adsorbed on cellulosic fibers. Such a difference may be related to the difference between the

surface area of the cellulosic fibers and CNCs of 1–3 m²/g and 150 m²/g, respectively, and shows the value of this method for CNMs over larger cellulosic fibers or crystals. Another point of interest for using DSBP instead of other fluorescent molecules is that the labeling could be carried out without chemical modification and did not require the use of a multistep reaction.
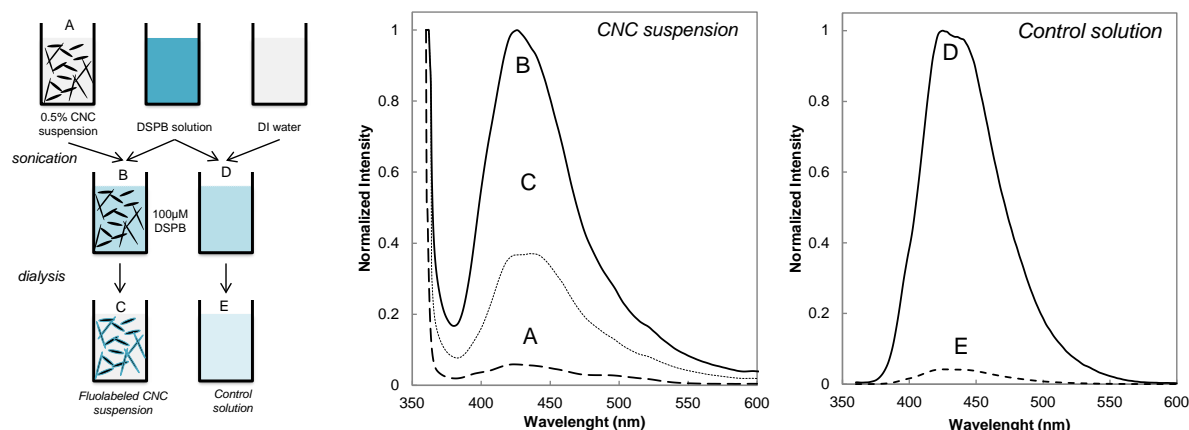
Figure 10.2. Fluorescence spectra of 0.5 wt % neat CNC suspension (A), with 100 µM DSBP solution before (B) and after dialysis (C). Control spectra corresponding to the 100 µM DSBP solution before (D) and after dialysis (E). Intensities are standardized with respect to the absorbance of a 100 µM DSBP solution. λ_{ex} = 351 nm.[363]

These methods suffer from transient binding and their usefulness is probably limited to pure cellulose films under dry conditions. Catchmark, *et al.* [400] mixed CNCs, biotin, and cellulose binding domain to improve the adhesion between the cellulose and the fluorophore. The biotinylated CNCs were shown to be adhere strongly to biotinylated microtubules. Vogel and co-workers[382] developed a similar tagging procedure using an expressed tinylated protein containing a carbohydrate binding domain. The protein did exhibit strong binding to cellulose and survived in vivo long enough to image lung tissue after pharyngeal aspiration. However, the physisorption is still an equilibrium process (K_D = 6 nM), the presence of other carbohydrates can reduce the amount of cellulose bound to the fluorophore as all carbohydrates may compete for the binding domain, the required proteins containing cellulose binding domains are typically expressed in E. coli (a time consuming process that is not readily conducted in every lab), and the quantities that can be prepared are typically very small (micro-scale).

10.3. Ion Exchange Labeling
Ion exchange offers a simple modification process for tracking and quantifying dried CNMs. Unlike physisorbed cellulose, the ion exchanged fluorophore is electrostatically bound to the cellulose and will not be transient in nonionic media. Ion-exchange requires cellulose materials that are charged, such as sulfated CNCs and carboxylated CNFs prepared using TEMPO oxidation. The dye can be attached by simply adding a small amount of cationic dye to a CNM colloidal suspension, then dialyzing against pure water or by using a co-exchanged column of ion exchange resin.[389] It is important to use degassed, type I water for dialysis to prevent exchange with residual ions in the water. Once dried, these materials can be incorporated into non-ionic polymers using standard thermosetting, solvent casting, in-situ polymerization, or melt-blending procedures. The dye can migrate away from the cellulose only if a charged polymer, such as polyacrylic acid or ionic salts, such as LiCl, are used in the process. Tam *et al.*[401] and Tang *et al.*[402] used carboxylated CNFs to immobilize Cd^{2+} prior to forming quantum dots using a Na_2S solution. By controlling the concentrations and Cd : CNF ratios, they were able to produce well dispersed quantum dots with improved colloidal stability and tunable emission wavelengths.

10.4. Covalent Labelling
To provide the largest range of applications, the fluorophore needs to be covalently attached to the CNMs. One of the most common methods employed is the grafting of fluoresceine isothiocyanate or rhodamine B isothiocyanate in alkaline media.[403-405] The CNMs are modified with either epichlorohydrin followed by

ammonium hydroxide to form a thiourea bond with the isocyanate,[406, 407] are modified with sodium hydroxide to form a thiocarbamate bond with the isocyanate,[408] or is reacted directly with the isothiocyanate using dibutyltindilaurate as a catalyst.[403-405] Although this chemistry has been extensively used for biochemical applications and is relatively easy to control, the thiourea and thiocarbamate bonds are unstable in more extreme conditions and may be unsuitable for some biochemical applications.[409-411] Further, the use of sodium hydroxide in some of the processes used can desulfate CNCs.[123, 412] The fluorescence intensity variations with pH changes in both acidic and alkaline conditions for Rhodamine B isothiocynate labeled CNCs was shown in the work by Ding et al.[413] As an alternative, a cyanuric chloride derivative can be used to form ether bonds between the dye and cellulose. Flourescein and Texas Red (Rhodamine 101) derivatives are available commercially and have been used to in 1-pot reactions to label CNMs.[84, 388, 414] The same chemistry has been used to attach an Alexa Fluor® dye to CNCs in acetonitrile, but the solvent exchange may not be necessary.[415] Although not discussed in literature, these reactions can affect the sulfate half ester surface groups on CNCs. Using NaOH can desulfate the crystals, so the use of Na_2CO_3 to form the alkaline solution is a better choice, as the cellulose will be less prone to desulfation. It should be noted that the dichlorotriazine group can react with the sulfates, reducing the overall charge of the CNCs.

Other labeling methods can be used with more selective reactivities. N-hydroxysuccinimide (NHS)-ester linkages are very selective towards primary amines. Combined with N-(3-dimethylaminopropyl)-N-ethylcarbodiimide hydrochloride (EDC), amines and carboxylic acids can be linked to form stable amide bonds.[416, 417] These reactions require an additional amination or carboxylation step, which can alter the surface chemistry of the CNMs. In addition, many of the NHS-ester fluorophores are water insoluble, requiring the use of DMSO or DMF to solubilize the dye. Nevertheless, a wide range of fluorescently labeled CNMs have been prepared in this manner. Carboxylation of CNF or CNC prepared from HCl hydrolysis can be readily achieved by activation with TEMPO, followed by oxidation with $NaClO_2$ or by hydrolysis in ammonium persulfate solution. These methods has been used to prepare CNMs labeled with amino acids,[418] a dihexyl-fluorene compound,[419] a quinolone compound,[420] rhodamine B amine,[421] carbon dots,[131] and CdSe/ZnS quantum dots.[422] Alternatively, the CNMs can be aminated and reacted with a carboxyl containing fluorophore. Pyrene,[423] rhodamine B,[274] and fluorescein[424] have been attached to CNMs in this manner. Amines and hydrazines react with ketone and aldehyde moieties. They can be reacted at the reducing ends of the cellulose chains without any intermediate steps.[425, 426] This, however, limits the extent of labeling. The number of available reaction sites can be increased through the use of periodate oxidation.[415] This method quantitatively and selectively creates dialdehydes at the C-2 and C-3 position of the cellulose.[427, 428] The imine bond can then be reduced using $NaBH_4$ to form the more stable secondary amine. The periodate oxidation must be kept to a minimum to prevent the cellulose chains from kinking or peeling the outerlayer.[429]

There are a few other methods for fluorescently labeling CNMs available in literature. Many of these methods are more complex designed to fulfill a specific purpose and are not recommended for routine labeling. For example, Bergström et al.[274] used 2-furoyl chloride and 1,1-(methylenedi-4,1-phenylene) bismaleimide in DMSO to produce CNFs that fluoresced different colors at two different excitations and Edwards et al. [430] used diisopropylcarbodiimide and 4-dimethylaminopyridine to graft a peptide chain onto CNCs. One method that may be of interest is the procedure performed by Zhou et al., in which pyrene was grafted onto CNC using bromo-pyrene.[431] Whereas they used epichlorohydrin and ammonium hydroxide as a linker to create an amine – hydroxyl bidentate for metal coordination, performing the reaction using NaOH without epichlorohydrin may generate the more stable ether bond.

For CNFs, the best method for most applications is the one based on dichloro-cyanuric acid chemistry, because the reaction can be performed in water in one step and the ether bond is very stable. For CNCs, covalently bound dyes tend to be more stable. Ding et al.[413] investigated the labeling efficiency, bond stability, photobleaching, and pH stability of rhodamine B iosthiocyanate labeled CNCs, comparing physisorbed to covalently bound dye. They found that the number of CNCs with bound dye was around 95% for both labeling methods, but that the covalently bound dye was more stable toward an anionic quencher, photobleaching, and continuous dialysis against water. There does not appear to be a best covalent bond chemistry for labeling CNCs, though a growing number of limitations to using the isothiocyanate chemistries have recently emerged. DTAF reacts with sulfate groups, periodate weakens chain and may cause delamination of the outer layer, FITC and RITC form less stable thiourea or

thiocarbamate bonds, and EDC/NHS reactions require amination or carboxylation of the cellulose first. Leng *et al.* [432] have recently compared the photophysics of rhodamine labeled CNCs using isothiocyanate and NHS/EDC chemistries. They found that the isothiocyanate chemistry leads to physisorbed J-dimers as the dye concentration increases in the reaction mixture, whereas few dimers are observed for the NHS/EDC chemistry. The periodate and EDC/NHS methods provide the greatest flexibility in terms of fluorophore choice. Regardless of the choice, it is important that any excess free dye is removed CNMs prior to further use. For CNCs, dialysis over 1 week or tangential flow filtration (TFF) over 2 – 3 days can typically remove excess free dye. For CNFs, the fibrils will likely create too high a pressure for TFF and dialysis is inefficient against the entangled fibrils. Instead, centrifugal filtration or soxhlet extraction can be employed. Although fluorescence intensities can be used to predict the removal of free dye, lifetime measurements are more precise. As illustrated in **Figure 10.3**, dye that has been covalently attached will have a single narrow lifetime distribution, while excess physisorbed dye will produce a broader lifetime distribution, shifted towards lower lifetimes.
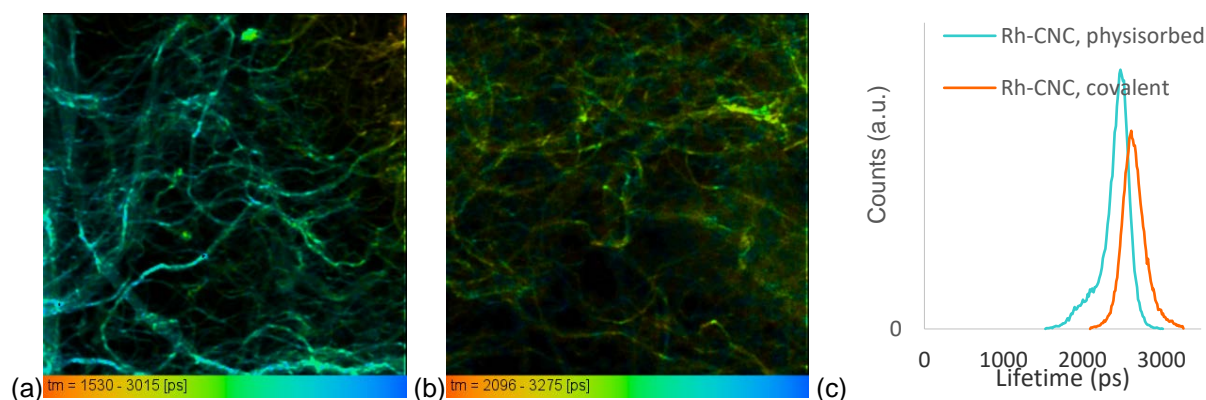
Figure 10.3. Fluorescence lifetime image of Rhodamine 110 labeled CNCs (a) physisorbed and (b) covalently bound with free dye removed using tangential flow filtration. (c) The lifetime distributions narrow to a single peak and shift towards higher lifetimes when the dye is bound.
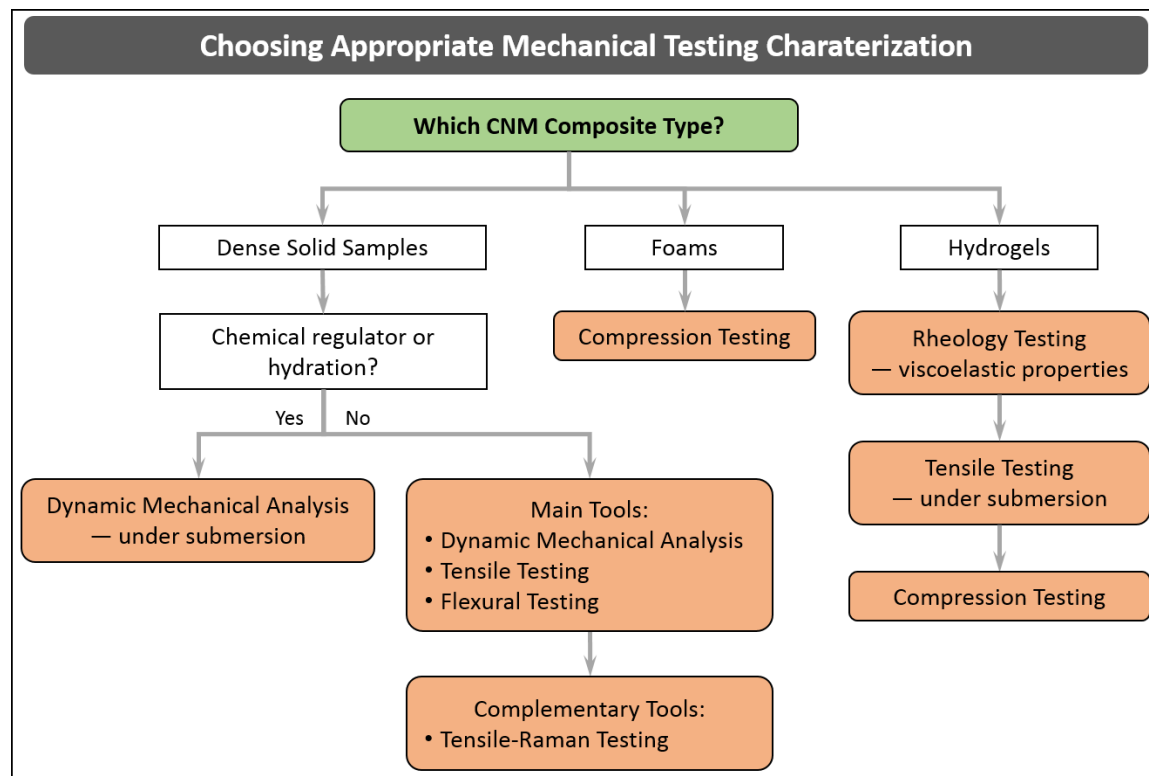
SECTION 11: Mechanical Properties of CNM Composites and Interfaces

Steve Eichhorn, Nandula Wanasekara

CNM composites have attracted significant interest in a wide range of fields owing in part to their excellent mechanical properties. These mechanical properties are obtained by exploiting the inherent high strength and stiffness (modulus) of the cellulose molecular chains, their dispersibility and interfacial properties. Critical to composite design and optimum mechanical performance are the ability to correctly and reproducibly measure the mechanical properties, their relationship to the mechanical models and the role of CNM-polymer matrix interface properties. In this section, we summarize best practices for: i) mechanical property measurement of CNM-composites, ii) inferring these mechanical properties from models, and iii) measuring CNM-polymer matrix-interface properties via Raman spectroscopy.

11.1. Measurement of CNM-Composite Properties

The best approaches to measure the mechanical properties of CNM composites are dependent on the type of structure; whether CNM-polymer composites, CNM foams or CNM hydrogels. A decision tree shown in **Figure 11.1** summarizes the best practices for mechanical characterization of CNM composites.

Figure 11. 1. Decision tree showing the best options for characterization of the mechanical properties of CNM composites.

11.1.1. Static Tensile Testing of CNM-Polymer Composites

Mechanical property measurement techniques have been widely reported for an array of CNM-polymer composites. Young's modulus, tensile strength, strain-at-break are the most widely measured mechanical properties. It is important to apply standard test methods for the measurement of mechanical properties of CNM-composites since data can then be compared to other filler types across a very broad family of materials. ASTM D 638-01, ASTM D3039/D3039M-14 and ISO 527-1 provide standard test methods to

measure the tensile properties of plastics and composites. These standards can also be applied to CNM-polymer composites. More specifically the ASTM D3039 test method has been used for determining the in-plane tensile properties of polymer matrix composite materials reinforced by high-modulus fibers such as CNCs and CNFs. Typically these tensile tests are carried out on a number of samples and the results reported with standard errors/deviations. Tensile tests on CNM-polymer composites involve exerting tensile forces until the samples until fracture occurs. Several factors have been shown to play critical roles in mechanical properties of CNM-polymer composites such as moisture content[288, 433, 434] and the degree of CNM orientation.[435, 436] The hydroxyl groups of CNMs attract water and thus decrease the mechanical properties. To safeguard against the property loss from water sorption, CNM-polymer composite samples can be pre-conditioned in a desiccator prior to testing and furthermore, testing could also be carried out in an environmental chamber with controlled humidity. Preferential alignment of CNMs in the matrix material could give rise the mechanical property anisotropy in the composite when testing parallel or perpendicular to the direction of CNM alignment. Therefore it is important to test, analyze and report the results providing the test direction relative to the CNM alignment. Gindl and Keckes[436] showed the significance of CNM alignment on mechanical properties on their study of stretched solvent cast all-cellulose composites. The degree of mechanical stretching had a strong influence on the properties along the stretching direction: random, 0% strained CNC/Cellulose films had an elastic modulus of 9.9 GPa while the highly oriented, 50% strained CNC/Cellulose films showed an even higher modulus of 33.5 GPa along the stretching direction. Static tensile testing is mostly employed for composite films and fibres, but this does not capture fully the often viscoelastic nature of CNM-polymer composites. For these properties to be fully explored one has to employ dynamic methods.

11.1.2. Dynamic Mechanical Testing of CNM Composites

Dynamic mechanical analysis (DMA) is a useful experimental tool to determine viscoelastic mechanical properties such as tensile storage modulus (E'), tensile loss modulus (E'') and tan δ (the ratio E''/E') of CNM-polymer composites. DMA has been particularly used to measure the mechanical response of composites in which it should be possible to dynamically alter the modulus of the composites through the addition or removal of a chemical regulator that could interfere with the extent of hydrogen bonding of the CNMs. In pioneering of Weder and Rowan,[110] responsive CNC-reinforced composites were developed where the formation and disruption of a percolating CNC network was selectively and reversibly modulated via a response to an array of triggers such as hydration or pH. The mechanical response was measured by DMA experiments performed in ambient air and water submerged conditions. They found that the DMA approach to mechanical measurement enabled the use of wet samples in the testing chamber, thus allowing environmental triggers on mechanical stiffness to be investigated. Care should be taken however in using these measurements to report mechanical data at an appropriate operating temperature for the *in situ* performance of the composite. Reporting data above the glass transition temperature of the polymer can be misleading to the operational performance of the material.

11.1.3. Mechanical Characterization of CNM Composite Foams

Mechanical property measurement of cellulose-based composite foams involves compression testing to determine the mechanical integrity of foams. Compression tests are carried out by applying compressive force to foams and elastic modulus is obtained from the initial gradient of the stress-strain curve. Compression properties of foams are especially important from their application in products, typically where they might be used for cushioning and in the case of CNM-based materials as a replacement for polyurethane. In this respect Berglund *et al.*[437] performed compression tests on an array of new cellulose-based foam materials.[438, 439] They fabricated bio-foams from amylopectin-rich potato starch and CNF by freezing the mixtures and removing the water by sublimation. Cylindrically shaped foams were cut into cube specimens and used to carry out compression testing of their samples. In this case, the cubes were compressed in the direction parallel to the cylinder axis of the original foam and compressive stress−strain curves were plotted. DMA can also be used to determine the dynamic compressive properties of foams. Ikkala *et al.*[440] studied mechanically robust aerogels which were fabricated by freeze drying of cellulose nanofiber water suspensions.[440] They utilized DMA in a compression mode to determine strength using parallel plate clamps.

11.1.4. Interaction Between CNM-Matrix

Critical to the mechanical reinforcement of polymer matrices are the interfacial interactions between CNM-

matrix and the dispersibility of CNCs in the matrix. Various methods such as the addition of silanes, maleic anhydride and other coupling agents have been investigated to increase these interfacial interactions.[441] The best practices to analyze the interfacial interaction and stress-transfer between the nanofibres and matrix materials include Dynamic Mechanical Thermal Analysis (DMTA)[110, 442] and Raman spectroscopy.[443] DMTA has been utilized to infer the interactions of the polymer matrix with the reinforcing phase.[442, 444] Raman spectroscopy has been applied to nanocomposite materials, including carbon nanotube reinforced polymers, whereby the interfacial stress-transfer has been determined from the rate of shift of a particular Raman band, with respect to strain or stress.[443] This approach is especially important since it allows a non-contact approach, with spatial resolution, to analyse the interface between the CNM and the matrix. In recent times it has also been possible to quantify the level of mixing of two phases within clustered CNMs in a thermoplastic matrix,[445] something which has hitherto only been inferred from mechanical measurements. Little has also been published on assessing the breakdown of interfaces in CNM composites. This is where molecular deformation analysis using Raman spectroscopy is particularly useful. A strong correlation between the plateauing of the Raman shifts with a breakdown of the interfaces between the resin matrix and the CNCs and within the network of CNCs themselves has been established,[446] Further, using this technique it is possible to quantify a 'work of adhesion' between the CNCs and the matrix, something which has not been possible to do previously.[446]

11.1.5. Mechanical Characterization of CNM Hydrogels

Mechanical property measurement of cellulose-based hydrogels includes viscoelastic measurements such as shear stress and modulus, tensile testing under hydration and single or cyclic compression tests. These time-dependent measurements are needed since hydrogels have viscoelastic properties. These measurements are typically performed on a rheometer and samples are prepared in the form of disks. Usually, specimens are incubated in distilled water for at least 24 h to achieve equilibrium-swelling conditions. Chang and coworkers measured the viscoelastic mechanical properties of a series of hydrogels prepared from cellulose and PVA aqueous solutions using both physical and chemical crosslinking methods.[447] No evidence of distortion under high loading suggested high strength of the physically cross-linked gel. In addition, strain (shear) sweep tests can also be carried out to determine the shear moduli in the linear viscoelastic zone. Tensile testing could also be carried out for high strength gels in a controlled aqueous environment. In a study on bacterial cellulose and PVA hydrogels, tensile testing was carried out inside a tank with distilled water.[448] Another common mechanical testing method for cellulose-based hydrogels is compression testing in an unconfined environment (**Figure 11.2**). This test involves unconfined compression of the hydrogel between two impermeable platens. For example, anisotropic swelling and mechanical behavior of composite hydrogels of bacterial cellulose–poly(acrylamide or acrylamide–sodium acrylate) were investigated by long-term cycling compression tests of the gel samples in water medium.[449] Elastic moduli and ultimate compressive stress of hydrogels were determined using the initial cross-sections of uncompressed specimens.
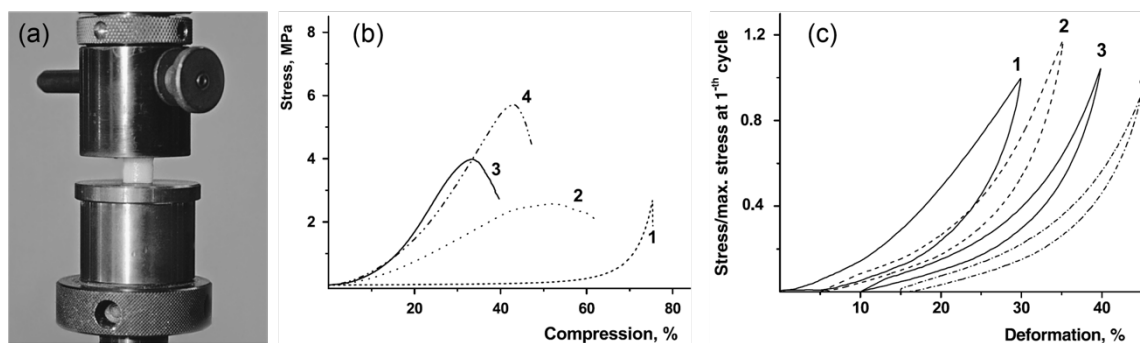

Figure 11.2. (a) Photograph of a typical unconfined compression test of BC–PAAm hydrogel (b) stress–strain curves in compression of a series of hydrogels with different BC concentrations: 0 (1), 4.0 (2), 8.0 (3) and 14 (4) wt%, and (c) cyclic compression–unloading curves of BC–PAAm hydrogel samples 1: 1-st cycle; 2: 2000-th cycle; 3: 4000-th cycle; 4: 6000-th.[449]

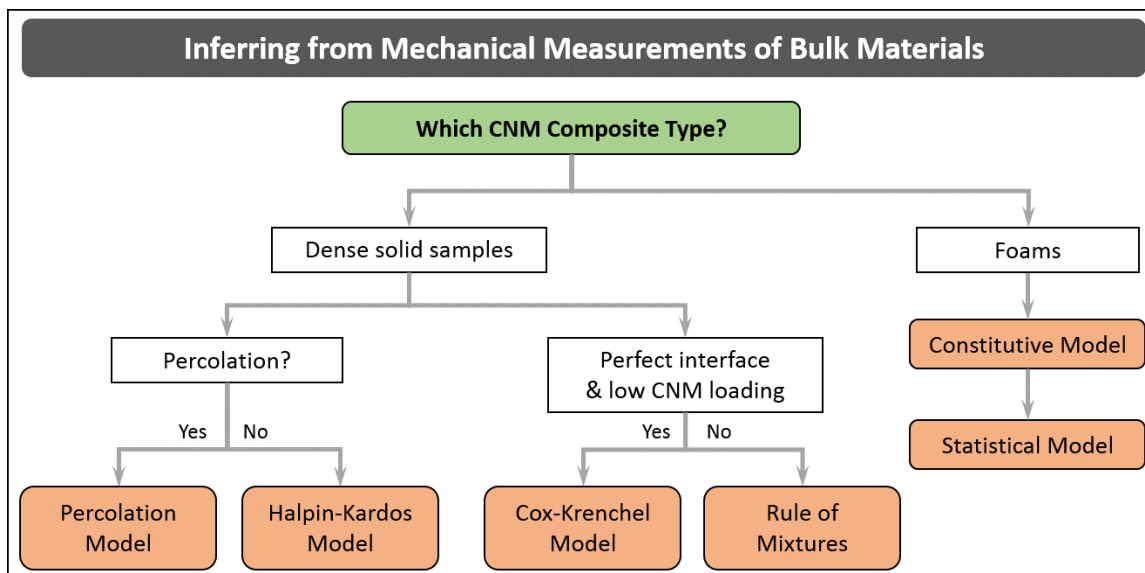## 11.2. Inferring from Mechanical Measurements of Bulk Materials

The mechanical properties of composites can be both experimentally and theoretically determined based on a number of models available in the literature, where many have been applied to CNM composites[9]. It is important to understand the best practices to apply each of these models when solving a particular question. See decision tree in **Figure 11.4**. The models for CNM-polymer composites are widely used and applied to solve problems whereas models for foams are very limited and complex. For CNM-polymer composites, CNMs can be dispersed in the matrix at weight fractions above or below the percolation threshold where CNMs can form a network. The percolation model can be used to predict the mechanical properties of such networks of CNCs within a composite.[450] Weder and co-workers developed responsive CNC-reinforced composites where the storage modulus of the composite was successfully predicted using the percolation model.[110] It should be emphasized that this model utilized the elastic modulus of a CNC film instead of individual nanocrystals. This suggests that one can utilize the experimental bulk measurement of elastic modulus of a composite (having CNC percolation) to back-calculate the elastic modulus of a CNC sheet. Similarly, when the CNCs are homogenously dispersed in a polymer matrix without pronounced CNC-CNC interactions, the Halpin-Kardos model can be used to back-calculate the elastic modulus of individual CNCs using the experimentally determined modulus values of CNC-reinforced composites.[451]

All-cellulose composites have attracted much attention due to the near perfect fiber-matrix interface as similar cellulose components are used as for both the matrix and filler. Conventional impregnation methods of cellulose matrix into cellulose fibers has been utilized to fabricate all-cellulose composites based on CNCs,[452] bacterial cellulose[453] and ligno-cellulose fibers such as ramie[454] and rice husk.[455] The Cox–Krenchel[456, 457] model provides a good estimation of modulus for these kinds of composites with the assumptions of a perfect fiber-matrix interface, elastic deformation of fibers and matrix and no axial loads on fiber ends.[458] As shown in **Figure 11.3a** it is evident that the Cox-Krenchel model predictions of composite modulus are only accurate for low CNF loadings. It is important to note that the rule-of-mixtures model utilizes the stiffness of cellulose nanopaper instead of individual nanofibers and therefore, this model cannot be used to back-calculate the modulus of individual CNFs. In another study, the value of a single filament of bacterial cellulose (BC) cellulose was back-calculated from the molecular deformation of nanocellulose in the nanocomposite using Raman spectroscopy.[459] This technique involved calculating the Raman band shift rate with respect to strain and a calibration of Raman band shift against modulus, using previously published data, and using Cox-Krenchel analysis to back-calculate the modulus of a single fibril. More importantly this work showed[459] that orthogonal strains could be measured in the samples. These measurements demonstrate a small but negative in-plane Poisson's ratio – a so called auxetic effect – in the networks, much the same as seen in other carbon nanotube networks.[460]

Fiber-reinforced foams/aerogels can exhibit complex mechanical behavior under compressive loading such as a strong nonlinearity, cyclic stress softening and permanent set. There have been very few approaches reported to model the mechanical properties of composite foams. A constitutive model of fiber-reinforced aerogels developed by Rege and Itskov[461] was found to show good agreement with experimental data (**Figure 11.3b**). This model could potentially be applied to CNF-reinforced foams where the prime source of elasticity could be the effect of bending of fibers (**Figure 11.3c**). Rege *et al.*[462] have also developed a micromechanical model for cellulose aerogels to describe the mechanical behavior. In another approach,[463] analysis of variance (ANOVA) has been applied to describe the mechanical behavior of fiber-reinforced phenolic foam. This model is developed to describe the compression properties of phenolic foam reinforced with glass fibers, but could equally work for CNF-reinforced foams as well. A decision tree shown in **Figure 11.4** summarizes the best models available for inferring CNF properties from the mechanical measurement of bulk materials.
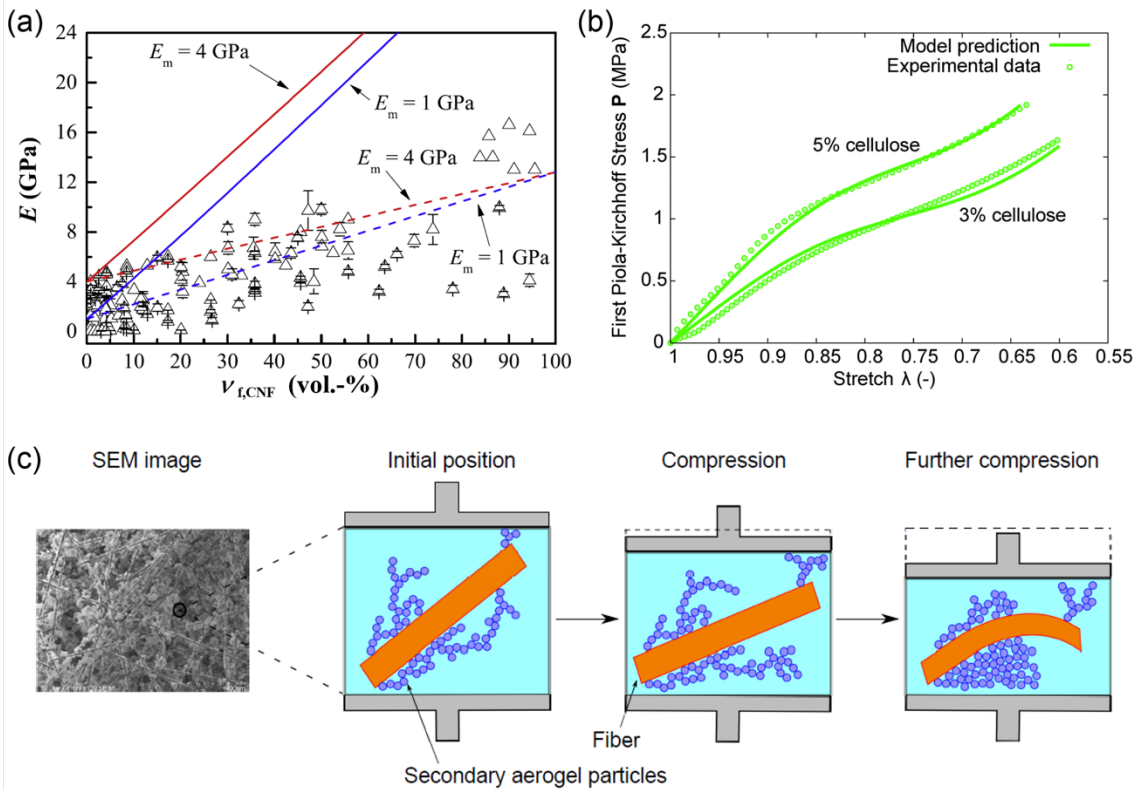
Figure 11.3. (a) Theoretical and experimental tensile moduli values of CNF reinforced composites. The hollow icons represent the experimental data and the solid line and dashed line denote the theoretical values obtained using Cox–Krenchel model and theoretical values obtained using rule-of-mixtures, respectively. This figure is obtained from Lee *et al.*[458] reproduced under the terms of Creative Commons Attribution License; (b) Model predictions of the constitutive response of cellulose aerogels compared with experimental data[462] (Reproduced from Ref. [462] with permission from The Royal Society of Chemistry) (c) An illustration of the damage behavior in the fiber-aerogel composite foam[461] (Reproduced from Ref. [461] with permission from John Wiley and Sons)

Figure 11.4. Decision tree showing the models available for inferring the mechanical measurement of bulk materials

11.3. Raman Spectroscopic Characterization of CNM Mechanical Properties and Interfaces

Raman spectroscopy is an excellent tool for characterizing the stiffness of CNM within composite matrix materials and for better understanding the CNM-matrix interface region. The Raman spectroscopic technique to evaluate molecular deformation relies on an effect discovered by Mitra *et al.,*[464] for stressed polydiacetylene single crystals, where a shift in the peak position of a characteristic Raman band of the polymer was followed, towards a lower wavenumber, upon tensile deformation. This type of shift in the position of a Raman peak is thought to be as a result of direct deformation of the molecular backbone of the polymer. The best practices for using Raman spectroscopy to measure the CNM mechanical properties involve following the shift of the characteristic Raman band for cellulose initially located at ~1095 cm^{-1}. Sturcova *et al.*[465] reported an elastic modulus of 143 GPa for tunicate cellulose using a Raman spectroscopic technique where a shift in the position of the Raman band was followed (**Figure 11.5**). This technique involved using epoxy beams containing a cellulose-epoxy composite film which were deformed using a 4-point bending mode test under the microscope of a Raman spectrometer (**Figure 11.5a**). This experimental value of the elastic modulus compared well to theoretical determination of 145 GPa using a molecular mechanics approach and an empirical force field.[465] Raman spectroscopy has also been proposed as an effective and best approach for studying the interfaces in all-cellulose composites. Pullawan *et al.*[466] carried out an extensive study on the interfaces of all-cellulose nanocomposites that were produced using dissolved microcrystalline cellulose as the matrix and CNCs as the reinforcement. A shift in the Raman band initially located at 1095 cm^{-1} for the CNCs and matrix, and another at 895 cm^{-1} related only to the matrix have been followed to obtain the local micromechanics of the interface. Another study[467] has utilized these Raman shifts to investigate the orientation and stress-transfer between the matrix and the filler in all-cellulose composites. They obtained a value of 1.9 cm^{-1} %$^{-1}$ for the Raman shift rate with respect to strain which was different from other values reported for PVAc/CNCs[468] (−0.5 cm^{-1} %$^{-1}$) and for epoxy resin/CNCs[465] (−2.4 cm^{-1} %$^{-1}$). These differences are representative of the nature of the interface between the different resins and the CNCs and the cellulose–cellulose interactions were found to be stronger than PVAc–cellulose, but weaker than epoxy–cellulose. An observed shift in the position of peaks arising from the PLA[469] for PLA/nanocellulose composites was attributed to the stress transfer to the stiffer matrix phase. Furthermore, the broadening[466] of the Raman band located at 1095 cm^{-1} with tensile deformation was attributed to the non-uniform stress distribution over the structure. This was indicative of the stress-transfer from the matrix to the reinforcing CNCs. Raman spectroscopy could also be used to investigate the breakdown of interfaces between the filler and the matrix upon deformation. Studies on cyclic tensile and compressive deformation on CNC/epoxy resin composites and molecular deformation analysis using Raman spectroscopy showed a strong correlation between the plateauing of the Raman shifts to a breakdown of the interfaces between the resin matrix and the CNCs and within the network of CNCs themselves.[446]
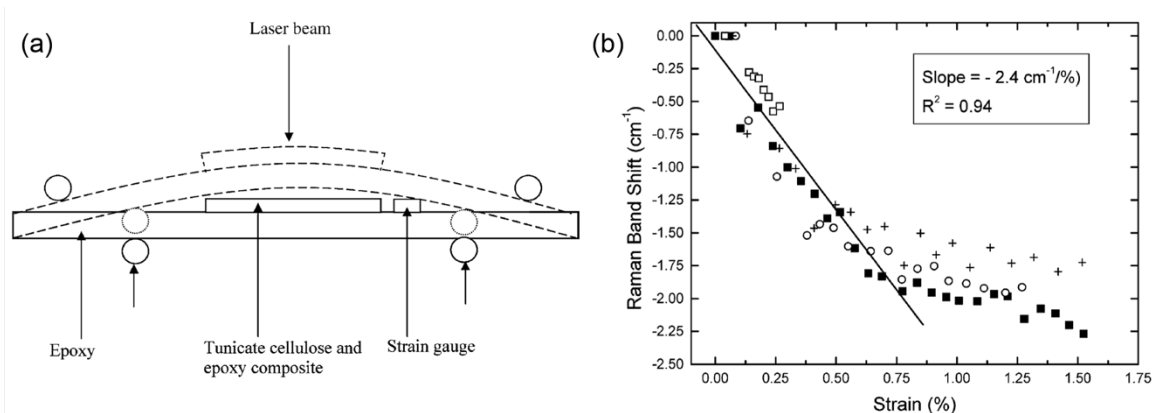
Figure 11.5. (a) Schematic of the 4-point bending test used to deform epoxy/tunicate composite samples under the Raman microscope;[465] (b) Shifts in the position of the Raman band initially located at ~1095 cm^{-1} from tunicate CNCs embedded in epoxy resin and deformed under 4-point bending in tension (Figures are reproduced with permission from Ref [465] Copyright (2005) American Chemical Society).

**SECTION 12: Health/Safety Characterization Methods, in Vitro, in Vivo:**
Jo Anne Shatkin, Kimberly J. Ong, Martin J. D. Clift

12.1. Introduction

There is a need to characterize CNMs from a human and environmental health and safety perspective, where the exposure, fate, and biological effects of a CNM are considered. For full characterization of these biological aspects, analysis of the life cycle of the CNM reveals the release points and exposure conditions; measurement of the nanomaterial (NM) physico-chemical properties is needed to evaluate the fate and interaction with biological organisms, and determining the effects of NMs on organisms and the environment helps to more accurately assess potential hazard. **Figure 12.1** is a decision tree to prioritize the types of nanoscale specific physico-chemical and biological testing (**Table 12.1**) that could aid in determining the safety characteristics of a CNM product intended for one-time use food packaging. In this scenario, different life stages are considered; first the manufacturing of the CNM source, then its use phase as part of food packaging, and then its post-use or end of life. Scenarios of higher priority in terms of assessing exposure and biological impacts of a CNM are highlighted in red, and the corresponding physico-chemical and biological characterizations are in **Table 12.1**. Scenarios with no exposure potential to nanomaterial forms are not a priority in terms of nanoscale specific testing, however conventional testing for risk assessment may still be necessary. Conventional testing can include standard tests, such as *in vitro* genotoxicity,[470-472] and *in vivo* acute, subchronic, and chronic testing.[473-477]

A diversity of biological models and systems have been used for the health and environmental safety characterization of several forms of CNMs.[38] A fairly low ecological toxicity profile for CNC was initially demonstrated in 2010.[478] This, along with increased commercialization interests, prompted progress towards characterizing the human and environmental safety of CNMs. Research has focused upon the inhalation toxicology of CNMs in terms of occupational exposure routes, with comparisons being made to historically known hazardous fibers and particles (*e.g.,* asbestos and crystalline quartz).[479, 480] As yet though, knowledge regarding the inhalation texology of CNMs remains limited. The implications of CNM exposure to skin and the gastro-intestinal tract remain unexplored in the literature. Due to the number of different biological systems, concentrations/doses, CNM types and toxico-dynamic approaches, a definitive characterization of CNMs from a human and environmental health perspective is currently missing from the field.

This scenario is not uncommon within the field of nanoparticle toxicology. In fact, this issue has faced the field since the term 'Nanotoxicology' was first coined in 2004.[481] With the influx of more and more NM types,[482] the ability for hazard assessment to keep up-to-date has been almost impossible. Thus, there has been a focus upon what components of NMs drive their toxicity. In this regard, it was reported over a decade ago that the physico-chemical characteristics of NMs predominantly drive their (adverse) biological impact.[483] In this section, we highlight considerations for characterizing CNMs for human and environmental safety testing, and how specific methods can be adopted to provide developers, stakeholders and regulators with information relative to their specific needs.
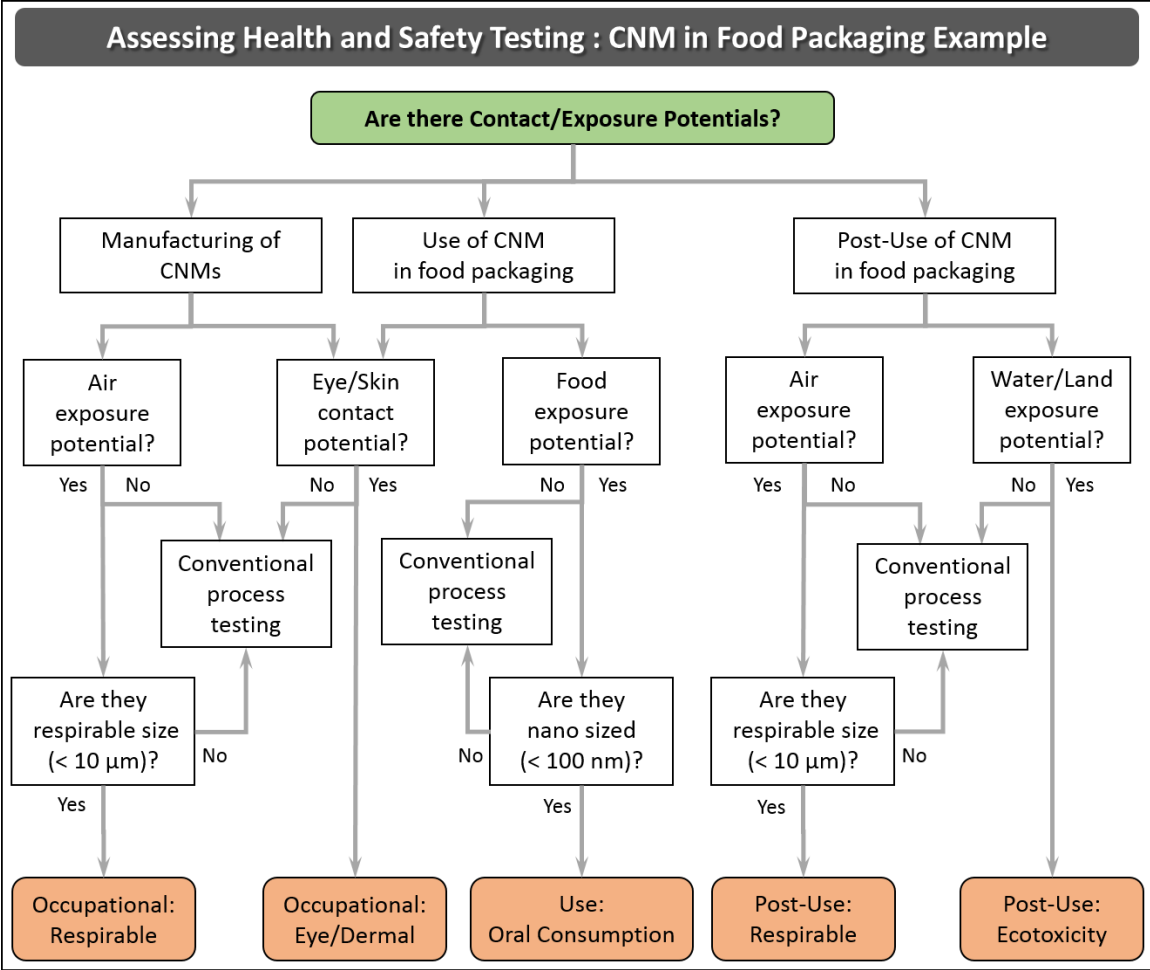
Figure 12.1. Decision tree to prioritize the types of NM-specific physico-chemical and biological testing for the manufacture of CNMs, use of CNM in food packaging, and post-use in food packaging that could aid in exposure and hazard characterization of CNMs in food packaging products.

Table 12.1. Types of physico-chemical and biological testing that could aid in hazard characterization of a food packaging product containing CNMs.

| | | OCCUPATIONAL: | | USE: | POST-USE: | |
		Respirable	Eye/Dermal	Oral consumption	Respirable	Ecotoxicity
Physico-Chemical Properties	Explosive properties	X				
	Purity	X	X	X	X	X
	Biodegradation				X	X
	Stability					X
	Size and size distribution	X	X	X	X	X
	Agglomeration/aggregation	X	X	X	X	X
	Shape and aspect ratio	X	X	X	X	X
	Surface Composition	X	X	X	X	X
	Specific Surface Area	X	X	X	X	X
	Surface Charge	X	X	X	X	X
	Hydrophobicity					X
	Dustiness	X	X			
Biological Tests	Eye irritation	X	X			
	Skin irritation & corrosion	X	X			
	Genotoxicity	X		X		
	Toxicokinetic testing	X		X		
	Systemic testing	X*		X**	X*	
	Ecotoxicity				X	X

* Inhalation toxicity
** Oral toxicity

12.2. Characterizing the Life Cycle of CNMs

The life cycle risk assessment (LCRA) of a substance starts at the raw material stage, then considers potential exposures at the processing and manufacturing stages, then during the use and application phase, through to the end-of-life, where the product may be reused, recycled, or disposed. At each stage of the assessment, all potential environmental health and safety exposure scenarios are considered. For example, during the production phase, are the materials an aerosolized powder that may be inhaled by workers, or are they in solution, where they may come in contact with bare skin or eyes. A NANO LCRA has been developed for CNMs that characterizes the CNM by evaluating potential hazard, exposure, and toxicity for five CNM product applications.[15, 484] The LCRA helps prioritize the exposure conditions where additional data may be needed, which in turn influences the types of physico-chemical measurements and safety tests.

## 12.3.	Characterizing the Physico-Chemical Properties of CNMs

The physico-chemical characteristics of NMs can drive their release, exposure, and fate characteristics, which can affect their hazard and health/environmental risk. Until it is understood how nanoscale characteristics relate to toxicity profiles, it is practical to measure parameters other than the typically measured physico-chemical parameters. Recording and reporting physico-chemical data, along with the information outlined in the sample checklist in **Section 2.1.4**, will aid in consistency and comparability amongst studies.

NMs are colloids and their surfaces interact with various ligands (*e.g.*, natural organic matter, other nanoparticles, proteins, *etc.*) that can affect their movement in media, their stability, their uptake into biological organisms, *etc.* Therefore, measuring properties that are related to size and surface properties can help characterize their potential effects. **Table 12.2** provides examples of traditional properties that are applicable to CNM physico-chemical characterization, and some 'nanoscale' properties that can be measured for risk characterization. The physico-chemical properties of a NM are dependent on the surrounding environment, and the properties will change over the life cycle of the material, therefore characterization of a NM in media that is representative of its surroundings is necessary. For measurement methods, see earlier sections of this review for protocols.

Table 12.2. Examples of both traditional and nanoscale-specific physico-chemical properties used to characterize potential effects

Traditional property	Nanoscale property
Flammability	Size and size distribution
Flash point	Agglomeration/aggregate state
Explosive properties	Shape and aspect ratio
Relative density	Surface composition
Viscosity	Specific surface area
Spectral data	Surface charge
Purity	Crystallinity
Biodegradation	Hydrophobicity
Stability	Dustiness
	Dispersibility

For CNMs, a key physical parameter that has been postulated to affect their potential hazard has been their length and width (*i.e.,* aspect ratio). Yet, in a recent study, there was no indication in the difference of CNM length in relation to their mammalian cell interaction *in vitro*.[480] Additional variables merit attention in this regard; for example, in fiber toxicology, the characteristic of stiffness is considered an additional key variable of any fibers' pathogenicity [485]. Yet, based upon current knowledge, most CNM, at least within any form of biological matrix (*i.e.,* cell culture media) elicit limited stiffness, and can be described as 'supple'. Coupled to this, a specific length range has been shown, historically, for a fiber to be pathogenic.[486] For glass-wool fibers and asbestos this was reported as a length threshold >8µm,[487, 488] whilst recently for Ag nanowires it was shown that a length threshold of >5µm is necessary.[489] Since the longest CNM, sourced from tunicates, can reach only a maximum length of ca. 6 µm, it is debatable as to the ability of CNM to be considered in the same light as carbon, silicon and glass-wool fibers, despite their enhanced mechanical strength compared to these classical fiber types.

Irrespective of the toxicological characterization of interest, an understanding of the physico-chemical characteristics of CNM is essential. Discussion surrounds 'which' physico-chemical properties must be measured prior to any toxicological testing.[490] Size, shape, chemical composition, surface composition, and charge are key parameters in driving the toxicology of NMs. In some studies, the surface chemistry can show limited influence in terms of the toxicology seen due to the adherence of proteins to the NM surface.[491, 492] Yet, on the contrary, the specific NP-protein complex interaction with mammalian cells has been highlighted as promoting a pathophysiological response,[493] and so both (surface composition/charge and

protein interactions) should be strongly considered for any NM, including CNM. Other factors such as density, crystallinity, agglomeration/aggregation status, and dustiness of the sample, as well as the properties of the suspension media (*e.g.,* pH, salinity), can impact NM interaction with the biological system.[490,494] When developing a study to characterize the toxicity of CNM, the biological system, exposure method, toxico-kinetic approach and regulatory regime influences which additional physical and chemical parameters are relevant.

12.4.   Characterizing the Biological Impact of CNMs

Generally, current standardized toxicity testing approaches are recommended for CNM testing, though some will require modifications to ensure accurate results. Here we discuss toxicity methodologies and strategic approaches for efficient testing of CNMs, based on the reviews and guidelines that specifically address NM testing[495, 496]ISO/TR 16197:2014. Nanotechnologies – Compilation and description of toxicological screening methods for manufactured nanomaterials, 2014. https://www.iso.org/standard/55827.html with consideration of CNM properties.

Classical toxicity testing methods are often required to meet regulatory requirements. Some regulatory agencies accept the use of non-animal, or 'alternative testing' approaches, where live vertebrate animal testing is reduced or avoided,[497, 498] and at a minimum these tests can provide valuable supporting information. These include biochemical, *in vitro*, *ex vivo*, and *in silico* methods, and the use of grouping materials by properties, as well as read-across of data from related materials to reduce the number of animal tests needed.[499] A strategic combination of these methods can be used as a weight-of-evidence approach to support a safety conclusion. Since these tests represent simplified biological processes, they are often used in combination with *in vivo* results or other alternative methods. They are also used as a starting point in determining the concentrations to use for *in vivo* tests.[500]

Stepwise strategies for grouping have been developed, but advanced predictive methods such as quantitative structure-activity relationships (QSARs) and adverse outcome pathways (AOPs) are still in development for broad use in NM-safety testing.[497, 501] Data from conventional counterparts (*e.g.*, microcrystalline cellulose and bulk cellulose) may be used for read-across purposes, and under different grouping schemes, may be considered "poorly soluble/low toxicity particles/dust" or, in the case of CNF, "fibrous particles",[502] though universal acceptance of a NM grouping scheme does not yet exist.

Biochemical, *in vitro* and *ex vivo* methods are regularly used for NM testing, and researchers have established some NM-specific recommendations. Most of these tests are applicable to CNM testing. However, NMs can interfere with commonly used assays, resulting in false negative/positive results.[503, 504] NMs can absorb light, or be fluorescent, and interfere with the assay detection methods, and they can also bind, inhibit, or catalyze assay components.[38, 503, 504] Assays can be run with only the NM to see if they are interfering with the assay components. To limit interference, NMs can be used at dilutions that do not cause interference, or NMs can be removed from the sample (for example, through washing of excess particles, or by transfer of supernatant to another well or cuvette) before measurement. More than one type of assay is often run to confirm the result for the same endpoints.[495] In addition, CNMs may contain endotoxins or cytotoxic chemicals as a result of the manufacturing process. These unwanted additions to the NM sample may contribute to an altered pH of the cell culture medium, and aggregation may lead to settling or heterogeneous distribution in the test system.[38] Thus, physico-chemical property measurements of CNMs in relevant biological media are critical for proper interpretation of toxicity results. It is important to highlight that many test methods employ biochemical or cellular assays as part of the overall analysis; therefore, these limitations should be considered initially in any study design.

The use of *in vivo* methods may be necessary for certain types of materials and applications, and usually represent the most likely routes of exposure.[484] For example, the production of CNMs can expose workers to respiratory hazards, so experiments addressing inhalation are performed, similarly, the use of CNM in food may warrant oral exposure testing. Both toxicokinetic evaluation (following the movement and distribution of the substance throughout the body), and systemic studies (assessing the overall impact on the organism as a result of intake) help determine *in vivo* effects. For context-relevant results, the principle concern for NM testing is to ensure that the exposure regime (*i.e.,* timing, dose, method of introducing the substance into the body) is representative of a realistic situation.

A further important methodological aspect to consider when characterizing the potential biological hazards of CNMs is their interaction with the biological system. A lack of internalization by a cell may indicate a low intrinsic hazard of a NM, yet this is relative to the specific physico-chemical characteristics of the NM itself (*e.g.,* solubility, shape).[490] Therefore, the measurement of CNM uptake by appropriate methods is highly advised, keeping in mind that several parameters can influence cell uptake,[505] *e.g.*, agglomeration, protein coating..[506]

12.5.   Cytotoxicity

Single-parameter *in vitro* tests can provide an indication of the relative concentrations at which a substance is toxic, as well as the mechanisms of the effects. Celluloar toxicity tests such as tetrazolium-based assays (*e.g.*, MTT (3-(4,5-dimethylthiazol-2-yl)-2,5-diphenyltetrazolium bromide), MTS (3-(4,5-dimethylthiazol-2-yl)-5-(3-carboxymethoxyphenyl)-2-(4-sulfophenyl)-2H-tetrazolium), XTT (2,3-bis-(2-methoxy-4-nitro-5-sulfophenyl)-2H-tetrazolium-5-carboxanilide)), trypan blue, alamar blue, lactate dehydrogenase assay, and neutral red uptake are regularly used to determine NM cytotoxicity.[507] Sub-lethal oxidative stress has been identified as one of drivers in regard to NM hazard[508] and methods such as DCF fluorescence, lipid peroxidation, and assays measuring oxidative stress-associated biomarkers (*e.g.*, glutathione, superoxide dismutase) are commonly employed.[507] Many cytotoxicity assays are affected by NM-interference, and hence result in false negatives or false positives. The ISO is currently developing a standard for the "*in vitro* MTS assay for measuring cytotoxic effects of nanoparticles"[509] that details performance requirements and control experiments that identify interference and improve the reliability of results.

Of particular relevance to testing design is choosing a biological system that represents realistic exposure pathways. For example, in foods, CNMs will most likely come in contact with gastrointestinal cells, rather than lung or dermal cells.

12.6.   Eye Irritation and Corrosion

In situations where CNM may contact eyes, evaluating whether serious eye damage might occur can be achieved by using strategic combinations of alternative tests. Tests that use isolated eyes *in situ*, such as the Bovine Corneal Opacity and Permeability[510] and the Isolated Chicken Eye[511] the Hen's Egg Test on the Chorio-Allantoic Membrane[495], as well as more complex *in vitro* tests, such as those using reconstructed human cornea-like epitheliums[512], are validated as acceptable alternatives to the traditional *in vivo* rabbit eye test. While these have not been specifically validated for NMs, there is no clear scientific basis against using their use for NMs.[513] For the *in situ* tests, solid test materials are generally diluted in deionized water prior to application; CNMs will likely agglomerate, resulting in sedimentation and increased concentration directly on the eye.[514] Therefore, applying the dry powdered CNMs directly to the eye might better mimic a realistic situation. Validated tests based on cytotoxicity or cell-function (*e.g.,* the Cytosensor Microphysiometer Test Method and the Fluorescein Leakage Method) are not well-suited to CNMs, as they are recommended for water-soluble substances.

12.7.   Skin Irritation and Corrosion

Several applications of CNMs involve dermal contact, such as cosmetics and wound dressings. For skin irritation and corrosion, *in vitro* tests that represent three-dimensional (3D) reconstructed human epidermis[470, 471] and the rat skin transcutaneous electrical resistance assay[472] are acceptable in determining whether a substance can cause skin damage, and replace traditional methods that involve applying the substance to the skin of a live animal. The 3D epidermis tests are dependent on cytotoxicity assays, so limitations regarding NM-assay interference apply. Several alternative test methods have been validated for the assessment of skin irritation and corrosion.[515, 516] For example, the Corrositex test[473] for skin corrosion uses a synthetic macromolecular bio-barrier; however, it is limited to substances that cause changes in the Chemical Detection System, and no published studies have confirmed its validity for CNMs. The OECD has developed a guidance document that lays out an integrated approach to testing and assessment (IATA) to help develop a sound approaches to skin irritation and corrosivity testing [474]

12.8.   Dermal Sensitizers

Substances intended for use in cosmetics, household cleaners, and other products that can cause dermal allergic reactions should be tested for their ability to cause skin sensitization. Traditionally, these are tested with guinea pigs (via OECD), but efforts to reduce animal testing have resulted in validation of the *in vivo*

Local Lymph Node Assay (LLNA),[475-477] which uses fewer animals and avoids animal pain and distress associated with an allergic reaction. Studies using these tests for CNC testing have not reported any CN-specific test modifications.[517] Skin sensitization is caused by a series of key molecular events, and each stage can be tested with different tests that contribute to the assessment of skin sensitization potential.[518] Commonly used tests include the Direct Peptide Reactivity Assay (DPRA),[519] the ARE-Nrf2 Luciferase Test Method,[520] the human Cell Line Activation test (h-CLAT). Due to the mechanistic complexity of skin sensitization, these *in vitro* and *in chemico* methods should be used in strategic combinations; the OECD has developed a guidance document that lays out an IATA to help develop a sound approaches to skin sensitization testing.[518]

12.9. Genotoxicity

Genotoxicity testing determines whether a substance can induce gene mutation, structural and/or numerical chromosomal alterations. Most studies of CNM indicate a lack of genotoxic activity,[484] however there is some uncertainty, and new production methods and surface modifications may need evaluation.[521] For all substances, including NMs, no single assay can detect all genotoxic effects, and therefore a battery of assays must be performed. Substances can first be tested using a series of *in vitro* tests, and if there are positive results, *in vivo* testing may be necessary.

To study gene mutations, the *in vitro* Bacterial Reverse Mutation (Ames) assay[522] and the Mammalian Cell Gene Mutation Tests[523, 524] be employed. If these indicate genotoxic potential, then *in vivo* tests such as the Transgenic Rodent Gene Mutation,[525] Comet Assay,[526] and Unscheduled DNA Synthesis with Mammalian Cells[527] tests can be considered. Of the *in vitro* tests, the Ames assay is more commonly used, but this method may produce false-negative results with NM testing. NMs may not be able to cross the bacterial cell wall, rendering the test unusable to determine direct gene effects.[495, 528, 529] A negative test should only be considered valid if there is proof of bacterial wall penetration and absence of bactericidal activity. Anti-bacterial experiments suggest that CNMs do not disturb the cell wall[530] and therefore this test can be considered inappropriate for CNMs, as it is for all NMs.[531]

For structural and numerical chromosomal effects, the *in vitro* Mammalian Chromosome Aberration Test[532] or the Mammalian Cell Micronucleus Test[533] can be used. For these tests, the OECD suggests NM-specific modifications including a post-treatment or delayed co-treatment protocol, where the cell culture system is first exposed to the NM in the absence of cytochalasin B to avoid decreased cellular uptake of the NM.[529, 534] *In vivo* tests such as the Mammalian Erythrocyte Micronucleus Test[535] the Mammalian Bone Marrow Chromosomal Aberration Test,[536] or the Comet Assay[526] can be used to follow up on any positive *in vitro* results.

12.10. Immunotoxicity, Neurotoxicity, Reproductive and Carcinogenic Effects

While immunotoxic, neurotoxic, reproductive and carcinogenic studies are often not part of the basic standard set of requirements for regulatory approvals, more research is still needed to assess CNM safety in terms of these endpoints. Few data for conventional equivalents are available. *In vivo* tests such as standard 28-day or 90-day, or one-generation toxicity studies can incorporate endpoints capable of detecting potential effects (such as motor activity assessment, changes in hematological parameters, changes in organ weights, the appearance of lesions, histopathological analysis, *etc.*).[495] To date, no CN-specific modifications appear to be needed for these tests.

If developmental effects are of concern, *in vivo* developmental neurotoxicity[537] or immunotoxicity[495] tests may be performed. However, these tests are not yet internationally accepted and there is little guidance, as there is not much experience in interpreting the results of these tests.[495] Measurements of inflammatory cells such as alveolar macrophages, neutrophils, eosinophils, and lymphocytes, histology of tissues, and the use of the enzyme-linked immunosorbent assay (ELISA) to measure cytokines and antibodies are more commonly used to detect inflammatory response.[507] Much like other cytotoxicity assays, ELISA is susceptible to interference; though, of twenty-four NMs, only nano-TiO_2 affected the ELISA test by binding to the cytokine.[503] CNM were not tested,[503] but have been reported not to interfere with this method.[538]

12.11. Toxicokinetic Testing

Especially for biomedical applications, full toxicokinetic testing is performed *in vivo*.[539] The absorption, distribution, metabolism, and excretion (ADME) of NMs after oral, inhalation, or dermal exposure are dependent on physico-chemical parameters.[495] Until more is understood about CNM ADME, generation of data on transformation in biological fluids, potential for translocation across biological barriers, presence in tissues and organs over different time periods, and, for oral studies, measurement of CNM in the urine and feces, and any potential irritation to gut can be informative. Some studies have looked at discrete stages of ADME, such as uptake of CNC over the lung,[480] or biodistribution and clearance after intravenous injection of CNC,[426] but no full toxicokinetic studies are available for other exposure routes. Quantifying and detecting NMs in general is analytically and technically challenging,[495] especially for CNM, as they cannot be detected as easily as metal NMs. They need to be tagged with fluorescent or radioactive tags for detection (**Section 10**), which can affect their intrinsic physico-chemical properties,[426, 540] or employ advanced methods such as multiplexed imaging by laser desorption/ionization mass spectrometry or Time-of-Flight Secondary Ion Mass Spectrometry.[495] Due to the low predicted toxicity of CNM, in combination with detection challenges, ADME testing may not be as important in situations where human exposure to CNM would be low.

12.12. Systemic Testing

Systemic *in vivo* toxicity testing in mammals requires focus on the most relevant exposure pathways. Standard tests exist for acute oral toxicity,[541, 542] inhalation toxicity,[543, 544] and dermal toxicity[545] and repeated dose subchronic or chronic oral,[546, 547] dermal,[548, 549] and inhalation[550-552]. In theory, all these tests are appropriate for CNM testing, with some additional factors considered, including consideration of the toxicokinetic movement of the CNMs, and sample preparation and the physico-chemical properties of the CNM in the delivery media.

Inhalation testing of NMs is important for occupational safety. Poorly soluble particles (PSPs) of predicted low toxicity, like CNMs, may cause artificially elevated adverse pulmonary effects if inhaled over short periods of time at high concentrations, since the natural lung clearance mechanisms cannot remove the materials properly.[495] Inhalation of PSPs at low concentrations may be cleared via normal mechanisms at a constant clearance rate, usually generating minor or reversible responses.[553] Therefore, care must be taken in designing *in vivo* inhalation studies, and interpretation of such studies should take the dose, timing, and delivery method into account. To help compare CNMs to other PSPs, collection of data on lung burden and clearance, samples of organs at different time points, and testing of the bronchoalveolar lavage (BAL) will aid in determining the long-term immunological and systemic effects.[495]

12.13. Ecotoxicity

The potential effects of nanomaterials on organisms in the environment can be considered in the context of accidental spills, discharge from point sources like manufacturing sites, and the release from products (either intentional or not). Two investigations suggest a low ecological toxicity profile for CNMs, however gaps exist.[554, 555] Aquatic ecotoxicity is likely of the highest environmental concern, and CNMs can affect some aquatic tests. The Fish Embryo Acute Toxicity Test[556] is often used to determine acute toxicity; the addition of organic matter (OM) and removal of the chorion can affect the behavior of certain NMs.[557] For CNMs, the addition of OM does not appear to have an effect, but the chorion does appear to provide some protection.[558] ISO is in the process of developing a standard method using dechorionated zebrafish embryos.[41] CNMs have been shown to interfere with the invertebrate *Daphnia magna* test [559]; a test where organisms get mechanically trapped in the test solution due to an uneven distribution of CNM.[555]

12.14. Beyond Standardized Methods

Many of the conventional toxicity testing methods are *in vitro* or *in situ* simplified models of biological systems, or, conversely, require the use of live animals. Tests that more closely represent *in vivo* situations, but are less costly and more time efficient, are of particular interest for researchers who may need to characterize several forms of one NM, due to changes in their physico-chemical properties. As the database grows for all forms of CNMs, there will be a greater ability to use alternative testing methods to read across from well-studied forms to new derivations or surface modifications. The development of increasingly sophisticated *in vitro* models present the ability to better mimic conditions *in vivo*, and are more cost-effective and higher throughput. Three-dimensional co-cultures (*i.e.,* combining multiple cell types), such as those used in standardized dermal irritation studies are emerging techniques used to create more realistic exposure conditions by reflecting the morphology and physiology of natural tissue, and co-cultures

that represent the lung are being developed.[560] Organs-on-chips are being developed where the physiological responses of entire organs and systems are captured on a small chip demonstrate advancement towards alternative models that better simulate human complexity.[561] There is ongoing development of dynamic models that incorporate physiologically-relevant parameters such as mechanical strain that mimics lung expansion and compression during breathing and muscular contractions such as peristalsis in the gut, and represent realistic fluid compositions and incubation times.[561, 562] Eventually, relationships between physico-chemical properties and safety will allow models such as QSARs to be used to characterize biological behavior, but this is a long-term target for integrating the alternative testing methods towards testing the potential NM hazard towards human health.[499]

SECTION 13: Summary and Outlook
World Nieh, Robert Moon, Johan Foster

Within recent years there has been exponential growth in cellulose nanomaterials research and development greater than 10-fold increase in journal articles found in database searches between 2005 and 2015. This field of study is still evolving, with new types of CNMs developed, new scientific understanding of how to manipulate CNMs published, and new application areas for CNMs emerging. Potential high-value market areas include biomedical, inks, and beauty products in development, along with high-volume applications such as drilling fluids, and concrete. However, despite the great potential of CNMs, we should be aware that "Life has a malicious way of dealing with great potential". [563] With this in mind, there is heighten importance for improving the quality of CNM characterization. As creative researchers and companies progress in their CNM endeavors, it has become essential to be able to describe CNM consistently without confusion, whether it is for scientific curiosity, quality control, product development or selling to different markets. This review outlines a foundation in the chemical, morphological, and property characterization guidelines and protocols tailored for CNMs, enabling better consistency, reliability and accuracy in measurement and analysis, which benefits both academic and industrial pursuits.

By highlighting two contrasting forms of CNMs (CNCs and CNFs), the characterization approaches presented in this review will have applicability to the many different types of existing CNMs and new varieties to be developed in the future. For some techniques, characterization approaches for CNC and CNF are very similar, whereas in others they can be very different. While CNC may be easier to characterize, characterizing CNFs is more challenging because they do not have a well-defined size and shape. Moreover, different CNF producers may employ different manufacturing technologies to produce CNF resulting in different properties. Other types of CNMs may be favored in different geographic regions and products containing these CNMs are already commercially available.

While efforts in standards development for CNM characterization are accelerating, gaps still remain. In the interume, , this review seeks to refine and suggest CNM characterization techniques that will help researchers, developers and end users adopt the same language, and have a common frame of reference, for the materials. This review will also provide scientists with a common knowledge base if they wish to refine protocols for improved measurement and analysis of CNMs. With more consistent protocols and measurements used throughout the community, this will help to reduce systematic uncertainty in data measurements, allowing higher confidence when comparing results between research groups. Thus, besides maintaining good scientific process, this also facilitates progress in the CNM field of study.

Besides the guidelines for measurements, the sample checklist in **Section 2.1.4** is an attempt to layout a few basic characteristics that are important in the application of CNMs. The properties in the checklist are by no means complete, but are properties important to the production and application of CNMs. By following and referencing this checklist, researchers and developers can hopefully understand the similarities and differences of CNMs with some confidence and providing a way to facilitate communication and future developments of CNMs. For example, besides product development, commercial applications require characterization of CNMs for monitoring production batches, adequately describing the material produced, providing essential information for downstream product formulation and providing a total quality assurance to customers. Being able to characterize CNMs as they flow through the production line and become sellable products is essential to their success. In a business transaction, it is not unusual for the supplier and customer to mutually agree on the properties a supplier reports to the customer. Sometimes a certificate of analysis accompanies the delivery of a batch of material and the receiving party can conduct their own quality control (QC) tests on the material. Customers can reject and return a batch if it fails their own QC tests. Conflicts follow if the delivering party and the receiving party used different tests or test methods to characterize the agreed upon properties. For a material such as CNM where its markets and consensus on test methods are still emerging, it is of the utmost importance to develop characterization standards based on best available technologies. At a minimum, the standards should include the agreed upon characteristics and the most appropriate test methods for them. Consensus standards based on best

available technologies can provide confidence, eliminate confusions, provide a system to manage errors and when used properly, will allow scientists to utilize them as a platform for future developments.

This review attempts to summarize lessons learned by experts from the development of CNMs. The goal of this review paper is to provide a state-of-the-art common knowledge base in the characterization of CNMs for material identification, property description, and understanding their health and safety profiles. It is the authors' intent for this common knowledge base to not only facilitate communication between research groups and remove barriers for product development, but also provide scientists with a foundation for future discoveries in this fast-developing area of CNMs.

References

1. R. J. Moon, G. T. Schueneman and J. Simonsen, *JOM*, 2016, **68**, 2383-2394.
2. J. Zhou, N. Butchosa, H. S. Jayawardena, J. Park, Q. Zhou, M. Yan and O. Ramstrom, *Biomacromolecules*, 2015, **16**, 1426-1432.
3. K. A. Potter, M. Jorfi, K. T. Householder, E. J. Foster, C. Weder and J. R. Capadona, *Acta Biomater*, 2014, **10**, 2209-2222.
4. H. Yagoub, S. Ma, S. Yang and J. Xu, *Materials Research Innovations*, 2014, **18**, S4-821-S824-824.
5. E. D. Cranston and D. G. Gray, *Biomacromolecules*, 2006, **7**, 9.
6. C. A. de Assis, M. C. Iglesias, M. Bilodeau, D. Johnson, R. Phillips, M. S. Peresin, E. M. Bilek, O. J. Rojas, R. Venditti and R. Gonzalez, *Biofuels, Bioproducts and Biorefining*, DOI: 10.1002/bbb.1835, n/a-n/a.
7. M.-C. Li, Q. Wu, K. Song, Y. Qing and Y. Wu, *ACS applied materials & interfaces*, 2015, **7**, 5006-5016.
8. C. A. de Assis, C. Houtman, R. Phillips, E. M. Bilek, O. J. Rojas, L. Pal, M. S. Peresin, H. Jameel and R. Gonzalez, *Biofuels, Bioproducts and Biorefining*, 2017, **11**, 682-700.
9. R. J. Moon, A. Martini, J. Nairn, J. Simonsen and J. Youngblood, *Chemical Society Reviews*, 2011, **40**, 3941-3994.
10. L. Brinchi, F. Cotana, E. Fortunati and J. M. Kenny, *Carbohydrate Polymers*, 2013, **94**, 154-169.
11. O. Nechyporchuk, M. N. Belgacem and J. Bras, *Industrial Crops and Products*, 2016, **93**, 2-25.
12. Y. Habibi, *Chemical Society Reviews*, 2014, **43**, 1519-1542.
13. S. Eyley and W. Thielemans, *Nanoscale*, 2014, **6**, 7764-7779.
14. ISO, *ISO/TS 20477:2017 Preview Nanotechnologies -- Standard terms and their definition for cellulose nanomaterial*, ISO, Geneva, Switzerland, 2017.
15. A. Canadian Standards, *Cellulosic nanomaterials — Test methods for characterization (CSA Z5100-14)*, Report 9781771395380, 2014.
16. R. Reiner and A. Rudie, in *Production and Applications of Cellulose Nanomaterials*, eds. M. Postek, R. Moon, A. Rudie and M. Bilodeau, TAPPI Press, 2013, pp. 21-24.
17. R. Reiner and A. Rudie, in *Production and Applications of Cellulose Nanomaterials*, eds. M. Postek, Robert, A. Rudie and M. Bilodeau, TAPPI Press, 2013, pp. 177-178.
18. A. Dufresne, J. Y. Cavaille and M. R. Vignon, *Journal of Applied Polymer Science*, 1997, **64**, 1185-1194.
19. S. J. Hanley, J. F. Revol, L. Godbout and D. G. Gray, *Cellulose*, 1997, **4**, 209-220.
20. S. Ifuku, M. Nogi, K. Abe, K. Handa, F. Nakatsubo and H. Yano, *Biomacromolecules*, 2007, **8**, 1973-1978.
21. O. Nechyporchuk, M. N. Belgacem and J. Bras, *Industrial Crops and Products*, 2016, **In Press**.
22. S. Camarero Espinosa, T. Kuhnt, E. J. Foster and C. Weder, *Biomacromolecules*, 2013, **14**, 1223-1230.

23. S. Camarero Espinosa, T. Kuhnt, C. Weder and E. J. Foster, in *Production and Applications of Cellulose Nanomaterials*, eds. M. T. Postek, R. Moon, M. Bilodeau and A. Rudie, TAPPI Press, 2013.

24. L. Chen, Q. Wang, K. Hirth, C. Baez, U. P. Agarwal and J. Y. Zhu, *Cellulose*, 2015, **22**, 1753-1762.

25. J.-F. Revol, H. Bradford, J. Giasson, R. H. Marchessault and D. G. Gray, *International Journal of Biological Macromolecules*, 1992, **14**, 170-172.

26. M. Pääkkö, M. Ankerfors, H. Kosonen, A. Nykänen, S. Ahola, M. Österberg, J. Ruokolainen, J. Laine, P. T. Larsson, O. Ikkala and T. Lindström, *Biomacromolecules*, 2007, **8**, 1934-1941.

27. T. Saito and A. Isogai, *Biomacromolecules*, 2004, **5**, 1983-1989.

28. L. Wågberg, G. Decher, M. Norgren, T. Lindström, M. Ankerfors, K. Axnas and K. Axnäs, *Langmuir*, 2008, **24**, 784-795.

29. M. Henriksson, G. Henriksson, L. A. Berglund and T. Lindstrom, *T. Eur. Polym. J.*, 2007, **43**, 3434-3441.

30. K. J. De France, T. Hoare and E. D. Cranston, *Chemistry of Materials*, 2017, **29**, 4609-4631.

31. D. Klemm, F. Kramer, S. Moritz, T. Lindstrom, M. Ankerfors, D. Gray and A. Dorris, *Angewandte Chemie-International Edition*, 2011, **50**, 5438-5466.

32. M. S. Reid, M. Villalobos and E. D. Cranston, *Langmuir*, 2017, **33**, 1583–1598.

33. Y. Peng, D. J. Gardner, Y. Han, A. Kiziltas, Z. Cai and M. a. Tshabalala, *Cellulose*, 2013, **20**, 2379-2392.

34. A. G. Assaf, R. H. Haas and C. B. Purves, *Journal of the American Chemical Society*, 1944, **66**, 66-73.

35. S. Shrestha, J. A. Diaz, S. Ghanbari and J. P. Youngblood, *Biomacromolecules*, 2017, **18**, 1482-1490.

36. S. Beck and J. Bouchard, *Nordic Pulp & Paper Research Journal*, 2014, **29**, 6-14.

37. B. O'Connor, R. Berry and R. Goguen, ed. B. D. M. Hull Ms, Oxford: William Andrew Publishing, 2014, pp. 225-246.

38. M. Roman, *Industrial Biotechnology*, 2015, **11**, 25-33.

39. S. Camarero-Espinosa, C. Endes, S. Mueller, A. Petri-Fink, B. Rothen-Rutishauser, C. Weder, M. Clift and E. Foster, *Fibers*, 2016, **4**, 21.

40. J. A. Shatkin and B. Kimb, *Environ. Sci.: Nano*, 2015, **2**, 477-499.

41. *Journal*, 2017, DOI: https://www.iso.org/standard/70861.html.

42. M. Chau, S. E. Sriskandha, D. Pichugin, H. Thérien-Aubin, D. Nykypanchuk, G. Chauve, M. Methot, J. Bouchard, O. Gang and E. Kumacheva, *Biomacromolecules*, 2015, **16** 2455–2462.

43. X. M. Dong and D. G. Gray, *Langmuir*, 1997, **13**, 2404-2409.

44. S. Beck, J. Bouchard and R. Berry, *Biomacromolecules*, 2012, **13**, 1486-1494.

45. D. Cheng, Y. Wen, L. Wang, X. An, X. Zhu and Y. Ni, *Carbohydrate polymers*, 2015, **123**, 157-163.

46. M. Labet and W. Thielemans, *Cellulose*, 2011, **18**, 607-617.

47. M. Jonoobi, R. Oladi, Y. Davoudpour, K. Oksman, A. Dufresne, Y. Hamzeh and R. Davoodi, *Cellulose*, 2015, **22**, 935-969.

48. Y. Habibi, L. A. Lucia and O. J. Rojas, *Chemical Reviews*, 2010, **110**, 3479-3500.

49. B. L. Peng, N. Dhar, H. L. Liu and K. C. Tam, *Can. J. Chem. Eng.*, 2011, **89**, 1191-1206.
50. S. Beck-Candanedo, M. Roman and D. G. Gray, *Biomacromolecules*, 2005, **6**, 1048-1054.
51. A. B. Fall, A. Burman and L. Wågberg, *Nordic Pulp & Paper Research Journal*, 2014, **29**, 176-184.
52. Y. Peng, D. J. Gardner and Y. Han, *Cellulose*, 2012, **19**, 91-102.
53. J. Han, C. Zhou, Y. Wu, F. Liu and Q. Wu, *Biomacromolecules*, 2013, **14**, 1529-1540.
54. V. Khoshkava and M. R. Kamal, *Biomacromolecules*, 2013, **14**, 3155-3163.
55. V. Khoshkava and M. R. Kamal, *Powder Technology*, 2014, **261**, 288-298.
56. K. Missoum, J. Bras and M. N. Belgacem, *Biomacromolecules*, 2012, **13**, 4118-4125.
57. M. S. Reid, M. Villalobos and E. D. Cranston, *Nanoscale*, 2016, **8**, 12247-12257.
58. M. Shimizu, T. Saito and A. Isogai, *Biomacromolecules*, 2014, **15**, 1904-1909.
59. M. S. Reid, M. Villalobos and E. D. Cranston, *Current Opinion in Colloid & Interface Science*, 2017, **29**, 76-82.
60. F. Jiang and Y.-L. Hsieh, *ACS applied materials & interfaces*, 2014, **6**, 20075-20084.
61. R. Vehring, *Pharmaceutical Research*, 2008, **25**, 999-1022.
62. M. Mumenthaler and H. Leuenberger, *International Journal of Pharmaceutics*, 1991, **72**, 97-110.
63. 2011.
64. J. P. Amorij, A. Huckriede, J. Wilschut, H. W. Frijlink and W. L. J. Hinrichs, *Pharmaceutical Research*, 2008, **25**, 1256-1273.
65. C. Eyholzer, N. Bordeanu, F. Lopez-Suevos, D. Rentsch, T. Zimmermann and K. Oksman, *Cellulose*, 2010, **17**, 19-30.
66. N. Butchosa and Q. Zhou, *Cellulose*, 2014, **21**, 4349-4358.
67. S. Takaichi, T. Saito, R. Tanaka and A. Isogai, *Cellulose*, 2014, **21**, 4093-4103.
68. J. Jancar, J. F. Douglas, F. W. Starr, S. K. Kumar, P. Cassagnau, A. J. Lesser, S. S. Sternstein and M. J. Buehler, *Polymer*, 2010, **51**, 3321-3343.
69. C. B. Tan, B. M. Fung, J. K. Newman and C. Vu, *Advanced Materials*, 2001, **13**, 644-646.
70. F. Cherhal, F. Cousin and I. Capron, *Langmuir*, 2015, **31**, 5596-5602.
71. S. Beck, J. Bouchard and R. Berry, *Biomacromolecules*, 2011, **12**, 167-172.
72. J. Bouchard, M. Méthot, C. Fraschini and S. Beck, *Cellulose*, 2016, **23**, 3555.
73. M. Henriksson, L. A. Berglund, P. Isaksson, T. Lindstrom and T. Nishino, *Biomacromolecules*, 2008, **9**, 1579-1585.
74. S. Iwamoto, A. Isogai and T. Iwata, *Biomacromolecules*, 2011, **12**, 831-836.
75. S. Hooshmand, Y. Aitomäki, N. Norberg, A. P. Mathew and K. Oksman, *ACS applied materials & interfaces*, 2015, **7**, 13022-13028.
76. F. Jiang and Y.-L. Hsieh, *Carbohydrate Polymers*, 2013, **95**, 32-40.
77. C. Miao and W. Y. Hamad, *Cellulose*, 2013, **20**, 2221-2262.
78. S. J. Eichhorn, C. A. Baillie, N. Zafeiropoulos, L. Y. Mwaikambo, M. P. Ansell, A. Dufresne, K. M. Entwistle, P. J. Herrera-Franco, G. C. Escamilla, L. Groom, M.

Hughes, C. Hill, T. G. Rials and P. M. Wild, *Journal of Materials Science*, 2001, **36**, 2107-2131.

79. A. Dufresne, *Nanocellulose from Nature to High Performance Tailored Materials*, Walter de Gruyter GmbH, Berlin, 2012.

80. G. Siqueira, J. Bras and A. Dufresne, *Polymers*, 2010, **2**, 728-765.

81. D. Viet, S. Beck-Candanedo and D. G. Gray, *Cellulose*, 2006, **14**, 109-113.

82. L. Heux, G. Chauve and C. Bonini, *Langmuir*, 2000, **16**, 8210-8212.

83. M. Salajkova, L. a. Berglund, Q. Zhou, M. Salajková and M. Salajkov, *Journal of Materials Chemistry*, 2012, **22**, 19798-19805.

84. T. Abitbol, H. Marway and E. D. Cranston, *Nordic Pulp & Paper Research Journal*, 2014, **29**, 46-57.

85. J. Araki, M. Wada and S. Kuga, *Langmuir*, 2000, **17**, 21-27.

86. E. Kloser and D. G. Gray, *Langmuir*, 2010, **26**, 13450-13456.

87. Y. Yoo and J. P. Youngblood, *ACS Sustainable Chemistry & Engineering*, 2016, **4**, 3927-3938.

88. W. Shang, J. Huang, H. Luo, P. R. Chang, J. Feng and G. Xie, *Cellulose*, 2012, **20**, 179-190.

89. Z. Hu, R. M. Berry, R. Pelton and E. D. Cranston, *ACS Sustainable Chemistry & Engineering*, 2017, **5**, 5018-5026.

90. M. Fumagalli, F. Sanchez, S. M. Boisseau and L. Heux, *Soft Matter*, 2013, **9**, 11309-11317.

91. R. K. Johnson, A. Zink-Sharp and W. G. Glasser, *Cellulose*, 2011, **18**, 1599-1609.

92. S. Bhattacharjee, *Journal of Controlled Release*, 2016, **235**, 337-351.

93. C. Fraschini, G. Chauve, J.-F. L. B. S. Ellis, M. Méthot, B. O'Connor and J. Bouchard, *Nordic Pulp & Paper Research Journal*, 2014, **29**, 31-40.

94. E. E. Urena-Benavides and C. L. Kitchens, *RSC Advances*, 2012, **2**, 1096-1105.

95. Y. Boluk and C. Danumah, *J Nanopart Res*, 2013, **16**, 2174.

96. A. Brinkmann, M. Chen, M. Couillard, Z. J. Jakubek, T. Leng and L. J. Johnston, *Langmuir*, 2016, **32**, 6105–6114.

97. M. T. Postek, A. Vladar, J. Dagata, N. Farkas, B. Ming, R. Wagner, A. Raman, R. J. Moon, R. Sabo, T. H. Wagner and J. Beecher, *Measurement Science & Technology*, 2011, **22**, 24005-24015.

98. Y. Boluk, R. Lahiji, L. Zhao and M. T. McDermott, *Colloids and Surfaces A: Physicochemical and Engineering Aspects*, 2011, **377**, 297-303.

99. H. Yang, M. N. Alam and T. G. M. van de Ven, *Cellulose*, 2013, **20**, 1865-1875.

100. A. B. Fall, S. B. Lindström, O. Sundman, L. Ödberg and L. Wågberg, *Langmuir*, 2011, **27**, 11332-11338.

101. J. Israelachvili, *Intermolecular & Surface Forces*, Academic Press Inc., London, 2 edn., 1992.

102. M. Shimizu, T. Saito, Y. Nishiyama, S. Iwamoto, H. Yano, A. Isogai and T. Endo, *Macromolecular Rapid Communications*, 2016, **37**, 1581-1586.

103. J. Pan, W. Hamad and S. K. Straus, *Macromolecules*, 2010, **43**, 3851-3858.

104. X. M. Dong, J. F. Revol and D. G. Gray, *Cellulose*, 1998, **5**, 19-32.

105. J. P. F. Lagerwall, C. Schütz, M. Salajkova, J. Noh, J. Hyun Park, G. Scalia and L. Bergström, *NPG Asia Materials*, 2014, **6**, e80-e80.

106. M. A. S. A. Samir, F. Alloin, J. Y. Sanchez, N. El Kissi and A. Dufresne, *Macromolecules*, 2004, **37**, 1386-1393.
107. J. Araki, M. Wada, S. Kuga and T. Okano, *Colloids and Surfaces A: Physicochemical and Engineering Aspects*, 1998, **142**, 75-82.
108. I. Kalashnikova, H. Bizot, B. Cathala and I. Capron, *Biomacromolecules*, 2012, **13**, 267-275.
109. F. Hoeng, A. Denneulin, C. Neuman and J. Bras, *Journal of Nanoparticle Research*, 2015, **17**, 1-14.
110. J. R. Capadona, K. Shanmuganathan, D. J. Tyler, S. J. Rowan and C. Weder, *Science*, 2008, **319**, 1370-1374.
111. M. Roman and W. T. Winter, *Biomacromolecules*, 2004, **5**, 1671-1677.
112. A. C. W. Leung, S. Hrapovic, E. Lam, Y. Liu, K. B. Male, K. A. Mahmoud and J. H. T. Luong, *Small*, 2011, **7**, 302-305.
113. B. Sun, Q. Hou, Z. Liu and Y. Ni, *Cellulose*, 2015, DOI: 10.1007/s10570-015-0575-5.
114. L. Wagberg, G. Decher, M. Norgren, T. Lindstrom, M. Ankerfors and K. Axnas, *Langmuir*, 2008, **24**, 784-795.
115. S. Saini, C. Yucel Falco, M. N. Belgacem and J. Bras, *Carbohydrate Polymers*, 2016, **135**, 239-247.
116. A. Pei, N. Butchosa, L. A. Berglund and Q. Zhou, *Soft Matter*, 2013, **9**, 2047.
117. H. Liimatainen, T. Suopajärvi, J. Sirviö, O. Hormi and J. Niinimäki, *Carbohydrate Polymers*, 2014, **103**.
118. L. Bhattacharyya and J. S. Rohrer, *Applications of Ion Chromatography for Pharmaceutical and Biological Products*, John Wiley & Sons, Inc., Hoboken, NJ, USA, 2012.
119. C. F. Castro-Guerrero and D. G. Gray, *Cellulose*, 2014, **21**, 2567-2577.
120. S. Dong, M. J. Bortner and M. Roman, *Industrial Crops and Products*, 2016, DOI: 10.1016/j.indcrop.2016.01.048, 1-12.
121. Q. Wang, X. Zhao and J. Y. Zhu, *Industrial & Engineering Chemistry Research*, 2014, **53**, 11007-11014.
122. N. Lavoine, I. Desloges, A. Dufresne and J. Bras, *Carbohydrate polymers*, 2012, **90**, 735-764.
123. M. Hasani, E. D. Cranston, G. Westman and D. G. Gray, *Soft Matter*, 2008, **4**, 2238-2244.
124. F. Jiang, A. R. Esker and M. Roman, *Langmuir*, 2010, **26**, 17919-17925.
125. T. Abitbol, E. Kloser and D. G. Gray, *Cellulose*, 2013, **20**, 785-794.
126. A. Nicharat, J. Sapkota, C. Weder and E. J. Foster, *Journal of Applied Polymer Science: Applied Polymer Symposium*, 2015, **132**, 42752-42762.
127. Y. Habibi, H. Chanzy and M. R. Vignon, *Cellulose*, 2006, **13**, 679-687.
128. L. Chen, J. Y. Zhu, C. Baez, P. Kitin and T. Elder, *Green Chem.*, 2016, DOI: 10.1039/c6gc00687f.
129. F. Azzam, M. Galliot, J.-L. Putaux, L. Heux and B. Jean, *Cellulose*, 2015, DOI: 10.1007/s10570-015-0785-x.
130. H. Yang, A. Tejado, N. Alam, M. Antal and T. G. M. van de Ven, *Langmuir : the ACS journal of surfaces and colloids*, 2012, **28**, 7834-7842.

131. K. Junka, J. Guo, I. Filpponen, J. Laine and O. J. Rojas, *Biomacromolecules*, 2014, **15**, 876-881.
132. Y. Noguchi, I. Homma and Y. Matsubara, *Cellulose*, 2017, **24**, 1295.
133. S. Beck, M. Methot and J. Bouchard, *Cellulose*, 2015, **22**, 101-116.
134. p. a. b. t. c. Scandinavian paper, *Journal*, 2002, **SCAN-CM 65:02**.
135. I. Solala, A. Volperts, A. Andersone, T. Dizhbite, N. Mironova-Ulmane, A. Vehniainen, J. Pere and T. Vuorinen, *Holzforschung*, 2012, **66**, 477-483.
136. L. Wågberg, L. Winter, L. Ödberg and T. Lindström, *Colloids and Surfaces*, 1987, **27**, 163-173.
137. K. Junka, I. Filpponen, T. Lindström and J. Laine, *Cellulose*, 2013, **20**, 2887-2895.
138. K. Missoum, Doctor of Philosophy Grenoble INP, 2012.
139. A. C. Corrêa, E. de Morais Teixeira, L. A. Pessan and L. H. C. Mattoso, *Cellulose*, 2010, **17**, 1183-1192.
140. K.-Y. Lee, F. Quero, J. J. Blaker, C. A. S. Hill, S. J. Eichhorn and A. Bismarck, *Cellulose*, 2011, **18**, 595-605.
141. R. Prathapan, R. Thapa, G. Garnier and R. F. Tabor, *Colloids and Surfaces A: Physicochemical and Engineering Aspects*, 2016, **509**, 11-18.
142. A. Romdhane, M. Aurousseau, A. Guillet and E. Mauret, *Starch - Stärke*, 2015, **67**, 319-327.
143. B. G. Compton and J. A. Lewis, *Advanced Materials*, 2014, **26**, 5930-5935.
144. M. Thompson, *AMC Technical Briefs*, 2008, **29**, 1-2.
145. A. Steyermark, in *Quantitative Organic Microanalysis*, Academic Press Inc., New York, NY, 2 edn., 1961, ch. 10, pp. 276-315.
146. A. Steyermark, in *Quantitative Organic Microanalysis*, Academic Press Inc., New York, NY, 2 edn., 1961, ch. 14, pp. 377-409.
147. A. Steyermark, in *Quantitative Organic Microanalysis*, Academic Press Inc., New York, NY, 2 edn., 1961, ch. 11, pp. 316-353.
148. A. Steyermark, in *Quantitative Organic Microanalysis*, Academic Press Inc., New York, NY, 2 edn., 1961, ch. 7, pp. 151-187.
149. M. Thompson, *The Royal Society of Chemistry*, 2008, 1-2.
150. W. Neto, J. Putaux, M. Mariano, Y. Ogawa, H. Otaguro, D. Pasquini and A. Dufresne, *Rsc Advances*, 2016, **6**, 76017-76027.
151. J. Pang, A. Wang, M. Zheng and T. Zhang, *Chemical Communications*, 2010, **46**, 6935-6937.
152. G. Tonoli, E. Teixeira, A. Correa, J. Marconcini, L. Caixeta, M. Pereira-da-Silva and L. Mattoso, *Carbohydrate Polymers*, 2012, **89**, 80-88.
153. N. Zainuddin, I. Ahmad, H. Kargarzadeh and S. Ramli, *Carbohydrate Polymers*, 2017, **163**, 261-269.
154. J. Sirvio, T. Hasa, J. Ahola, H. Liimatainen, J. Niinimaki and O. Hormi, *Carbohydrate Polymers*, 2015, **133**, 524-532.
155. N. Mohd, N. Ismail, J. Zahari, W. Fathilah, H. Kargarzadeh, S. Ramli, I. Ahmad, M. Yarmo and R. Othaman, *Journal of Nanomaterials*, 2016, DOI: 10.1155/2016/4804271.
156. J. Edwards, N. Prevost, K. Sethumadhavan, A. Ullah and B. Condon, *Cellulose*, 2013, **20**, 1223-1235.

157. N. Pahimanolis, A. Salminen, P. Penttila, J. Korhonen, L. Johansson, J. Ruokolainen, R. Serimaa and J. Seppala, *Cellulose*, 2013, **20**, 1459-1468.
158. Y. Meng, T. Young, P. Liu, C. Contescu, B. Huang and S. Wang, *Cellulose*, 2015, **22**, 435-447.
159. S. Spoljaric, A. Salminen, N. Luong and J. Seppala, *European Polymer Journal*, 2015, **69**, 328-340.
160. J. Garcia-Amoros, A. Bucinskas, M. Reig, S. Nonell and D. Velasco, *Journal of Materials Chemistry C*, 2014, **2**, 474-480.
161. A. Takegawa, M. Murakami, Y. Kaneko and J. Kadokawa, *Polymer Composites*, 2009, **30**, 1837-1841.
162. *Journal*, 2011, 1-12.
163. *Journal*, 2011.
164. S. Bance, *Michrochemical Journal*, 1980, **15**, 590-597.
165. Elemental CHNS Analysis, https://www.univie.ac.at/Mikrolabor/CHNS_eng.htm, (accessed September 27, 2017).
166. J. Griffiths, *Analytical Chemistry*, 2008, **80**, 7194-7197.
167. Time-of-Flight Secondary Ion Mass Spectrometry (TOF-SIMS), (accessed September 26, 2017).
168. M. Gritsch, C. Brunner, K. Piplits, H. Hutter, P. Wilhartitz, A. Schintlmeister and H. Martinz, *Fresenius Journal of Analytical Chemistry*, 1999, **365**, 188-194.
169. N. Kota, University of Wisconsin- Madison, 2017.
170. D. Kalaskar, R. Ulijn, J. Gough, M. Alexander, D. Scurr, W. Sampson and S. Eichhorn, *Cellulose*, 2010, **17**, 747-756.
171. C. Freire, A. Silvestre, C. Neto, A. Gandini, P. Fardim and B. Holmbom, *Journal of Colloid and Interface Science*, 2006, **301**, 205-209.
172. K. Missoum, M. Belgacem, J. Barnes, M. Brochier-Salon and J. Bras, *Soft Matter*, 2012, **8**, 8338-8349.
173. D. Briggs, *Handbook of X-Ray and Ultraviolet Photoelectron Spectroscopy*, Heyden & Son, London, 1977.
174. K. SIEGBAHN, *Uspekhi Fizicheskikh Nauk*, 1982, **138**, 223-248.
175. W. Li and E. Ding, *Surface Review and Letters*, 2006, **13**, 819-823.
176. A. Boujemaoui, S. Mongkhontreerat, E. Malmstrom and A. Carlmark, *Carbohydrate Polymers*, 2015, **115**, 457-464.
177. C. Tian, S. Fu, Y. Habibi and L. Lucia, *Langmuir*, 2014, **30**, 14670-14679.
178. G. Morandi, L. Heath and W. Thielemans, *Langmuir*, 2009, **25**, 8280-8286.
179. S. Huan, L. Bai, G. Liu, W. Cheng and G. Han, *Rsc Advances*, 2015, **5**, 50756-50766.
180. S. Liu, Y. Liu, F. Deng, M. Ma and J. Bian, *Rsc Advances*, 2015, **5**, 74198-74205.
181. M. Kaushik and A. Moores, *Green Chemistry*, 2016, **18**, 622-637.
182. L.-S. Johansson and J. M. Campbell, *Surface and Interface Science*, 2004, **36**, 1018-1022.
183. D. E. Newbury, in *Characterization of Materials*, John Wiley & Sons, Inc., 2002, DOI: 10.1002/0471266965.com087.
184. T. Zhong, G. Oporto, Y. Peng, X. Xie and D. Gardner, *Cellulose*, 2015, **22**, 2665-2681.

185. C. Ruiz-Palomero, M. Soriano, S. Benitez-Martinez and M. Valcarcel, *Sensors and Actuators B-Chemical*, 2017, **245**, 946-953.
186. A. Hebeish, S. Farag, S. Sharaf and T. Shaheen, *Carbohydrate Polymers*, 2016, **151**, 96-102.
187. J. Sundberg, C. Gotherstrom and P. Gatenholm, *Bio-Medical Materials and Engineering*, 2015, **25**, 39-52.
188. F. Mohammadkazemi, K. Doosthoseini, E. Ganjian and M. Azin, *Construction and Building Materials*, 2015, **101**, 958-964.
189. A. Kumar, Y. S. Negi, V. Choudhary and N. K. Bhardwaj, *Journal of Materials Physics and Chemistry*, 2014, **2**, 1-8.
190. M. HUANG and G. HIEFTJE, *Spectrochimica Acta Part B-Atomic Spectroscopy*, 1989, **44**, 739-749.
191. M. Jean-Michel, in *Inductively Coupled Plasma Spectrometry and its Applications*, ed. S. J. Hill, Blackwell Publishing Ltd, Plymouth, UK, 2007, ch. 2, pp. 27-60.
192. K. Amin, P. Annamalai, I. Morrow and D. Martin, *Rsc Advances*, 2015, **5**, 57133-57140.
193. C. Cirtiu, A. Dunlop-Briere and A. Moores, *Green Chemistry*, 2011, **13**, 288-291.
194. S. Shi, S. Chen, X. Zhang, W. Shen, X. Li, W. Hu and H. Wang, *Journal of Chemical Technology and Biotechnology*, 2009, **84**, 285-290.
195. N. Yin, S. Chen, Y. Ouyang, L. Tang, J. Yang and H. Wang, *Progress in Natural Science-Materials International*, 2011, **21**, 472-477.
196. W. Y. Hamad, *Cellulose Nanocrystals: Properties, Production and Applications*, Wiley & Sons Ltd., Oxford & New York, 2017.
197. A. D. French and M. S. Cintrón, *Cellulose*, 2013, **20**, 583-588.
198. S. Park, J. O. Baker, M. E. Himmel, P. A. Parilla and D. K. Johnson, *Biotechnology for biofuels*, 2010, **3**, 10.
199. C. Driemeier and G. A. Calligaris, *Journal of Applied Crystallography*, 2011, **44**, 184-192.
200. H. Rietveld, *Journal of Applied Crystallography*, 1969, **2**, 65-71.
201. W. Ruland, *Acta Crystallographica*, 1961, **14**, 1180-1185.
202. C. Vonk, *Journal of Applied Crystallography*, 1973, **6**, 148-152.
203. S. Rabiej, *European Polymer Journal*, 1991, **27**, 947-954.
204. L. Segal, J. J. Creely, A.E. Martin, Jr. and C. M. Conrad, *Textile Research*, 1959, **29**, 786-794.
205. S. Chandrasekhar, *Liquid Crystals*, Cambridge University Press, 2nd edn., 1992.
206. A. R. Stokes and A. J. C. Wilson, *Proceedings of the Physical Society*, 1944, **56**, 174.
207. R. H. Atalla and D. L. VanderHart, *Solid State Nuclear Magnetic Resonance*, 1999, **15**, 1-19.
208. S. Park, D. K. Johnson, C. I. Ishizawa, P. A. Parilla and M. F. Davis, *Cellulose*, 2009, **16**, 641-647.
209. S. H. Kim, C. M. Lee and K. Kafle, *Korean Journal of Chemical Engineering*, 2013, **30**, 2127-2141.
210. A. E. Derome, *Modern NMR techniques for chemistry research*, Elsevier, 2013.
211. R. H. Atalla and D. L. VanderHart, *Science* 1984, **223**, 283-285.

212. R. H. Atalla, J. C. Gast, D. W. Sindorf, V. J. Bartuska and G. E. Maciel, *Journal of the American Chemical Society*, 1980, **102**, 3249-3251.
213. T. Erata, T. Shikano, S. Yunoki and M. Takai, *Cellul Commun*, 1997, **4**, 128-131.
214. H. Kono, S. Yunoki, T. Shikano, M. Fujiwara, T. Erata and M. Takai, *Journal of the American Chemical Society*, 2002, **124**, 7506-7511.
215. F. Porro, O. Bédué, H. Chanzy and L. Heux, *Biomacromolecules*, 2007, **8**, 2586-2593.
216. G. Sèbe, F. d. r. Ham-Pichavant, E. Ibarboure, A. L. C. Koffi and P. Tingaut, *Biomacromolecules*, 2012, **13**, 570-578.
217. E. Dinand, M. Vignon, H. Chanzy and L. Heux, *Cellulose*, 2002, **9**, 7-18.
218. B. Briois, T. Saito, C. Pétrier, J.-L. Putaux, Y. Nishiyama, L. Heux and S. Molina-Boisseau, *Cellulose*, 2013, **20**, 597-603.
219. R. H. Newman, *Solid state nuclear magnetic resonance*, 1999, **15**, 21-29.
220. K. Wickholm, P. T. Larsson and T. Iversen, *Carbohydrate Research*, 1998, **312**, 123-129.
221. L. Heux, E. Dinand and M. Vignon, *Carbohydrate Polymers*, 1999, **40**, 115-124.
222. S. Montanari, M. Roumani, L. Heux and M. R. Vignon, *Macromolecules*, 2005, **38**, 1665-1671.
223. C. H. Lemke, R. Y. Dong, C. A. Michal and W. Y. Hamad, *Cellulose*, 2012, **19**, 1619-1629.
224. K. Schenzel, S. Fischer and E. Brendler, *Cellulose*, 2005, **12**, 223-231.
225. U. P. Agarwal, R. S. Reiner and S. A. Ralph, *Cellulose*, 2010, **17**, 721-733.
226. U. P. Agarwal, R. R. Reiner and S. A. Ralph, *Journal of Agricultural and Food Chemistry*, 2013, **61**, 103-113.
227. A. L. Barnette, C. Lee, L. C. Bradley, E. P. Schreiner, Y. B. Park, H. Shin, D. J. Cosgrove, S. Park and S. H. Kim, *Carbohydrate Polymers*, 2012, **89**, 802-809.
228. U. P. Agarwal, S. A. Ralph, R. S. Reiner, R. K. Moore and C. Baez, *Wood Science and Technology*, 2014, **48**, 1213-1227.
229. U. P. Agarwal, S. A. Ralph, R. S. Reiner and C. Baez, *Cellulose*, 2016, **23**, 125-144.
230. U. P. Agarwal, presented in part at the ACS Symposium Series, Washington DC, 2017.
231. Y. Qing, R. Sabo, J. Y. Zhu, U. Agarwal, Z. Cai and Y. Wu, *Carbohydr Polym*, 2013, **97**, 226-234.
232. H. Fukuzumi, T. Saito and A. Isogai, *Carbohydrate Polymers*, 2013, **93**, 172-177.
233. S. Saini, M. N. Belgacem and J. Bras, *Materials Science and Engineering C* 2017, **75**, 760–768.
234. L. Wei, U. P. Agarwal, K. C. Hirtha, L. M. Matuana, R. C. Saboa and N. M. Stark, *Carbohydrate Polymers*, 2017, **169**, 108–116.
235. J. Brand, G. Pecastaings and G. Sèbea, *Carbohydrate Polymers*, 2017, **169**, 189–197.
236. I. Filpponen and D. S. Argyropoulos, *Biomacromolecules FIELD Full Journal Title:Biomacromolecules*, 2010, **11**, 1060–1066.
237. C.-F. Huang, J.-K. Chen, T.-Y. Tsai, Y.-A. Hsieh and K.-Y. A. Lin, *Polymer*, 2015, **72**, 395-405.

238. J. K. Muiruri, S. Liu, W. S. Teo, J. Kong and C. He, *ACS Sustainable Chem. Eng.*, 2017, **5**, 3929−3937.
239. A. Gandini and M. N. Belgacem, in *Advances in Polymer Science: Cellulose Chemistry and Properties: Fibers, Nanocelluloses and Advanced Materials*, ed. O. J. Rojas, American Chemical Society, Washington, DC, 2015, DOI: 10.1007/12_2015_305, pp. 169-206
.
240. J. O. Zoppe, Y. Habibi, O. J. Rojas, R. A. Venditti, L.-S. Johansson, K. Efimenko, M. O. sterberg and J. Laine, *Biomacromolecules*, 2010, **11**, 2683–2691.
241. M. Miyauchi, J. Miao, T. J. Simmons, J.-W. Lee, T. V. Doherty, J. S. Dordick and R. J. Linhardt, *Biomacromolecules*, 2010, **11**, 2440–2445.
242. S. Ahola, X. Turon, M. Osterberg, J. Laine and O. J. Rojas, *Langmuir*, 2008, **24**, 11592-11599.
243. D. J. Dagel, Y. S. Liu, L. Zhong, Y. Luo, Y. Zeng, M. Himmel, S. Y. Ding and S. Smith, *Proc. SPIE*, 2011, **7905**, 79050P/79051-79050P/79056.
244. A. Villares, H. Bizot, C. Moreau, A. Rolland-Sabate and B. Cathala, *Carbohydrate Polymers*, 2017, **157**, 1105-1112.
245. *Infrared and Raman Spectroscopy: Methods and Applications*, VCH Publishers, Inc, New York 1995.
246. Y. Maréchal and H. Chanzy, *Journal of Molecular Structure*, 2000, **523**, 183-196.
247. C. Y. Liang and R. H. Marchessault, *Journal of Polymer Science*, 1959, **37**, 385-395.
248. T. Kondo, *Cellulose*, 1997, **4**, 281.
249. A. J. Michell, *Carbohydrate Research*, 1993, **241**, 47-54.
250. A. J. Michell, *Carbohydrate Research*, 1990, **197**, 53-60.
251. J. Sugiyama, J. Persson and H. Chanzy, *Macromolecules*, 1991, **24**, 2461-2466.
252. T. Saito, Y. Nishiyama, J.-L. Putaux, M. Vignon and A. Isogai, *Biomacromolecules*, 2006, **7**, 1687-1691.
253. I. Filpponen, H. Sadeghifar and D. S. Argyropoulos, *Nanomaterials and Nanotechnology*, 2011, **1**, 7.
254. J. Araki, M. Wada and S. Kuga, *Langmuir*, 2001, **17**, 21-27.
255. F. Azzam, M. Galliot, J.-L. Putaux, L. Heux and B. Jean, *Cellulose*, 2015, **22**, 3701-3714.
256. F. Azzam, L. Heux, J.-L. Putaux and B. Jean, *Biomacromolecules*, 2010, **11**, 3652-3659.
257. A. P. Mangalam, J. Simonsen and A. S. Benight, *Biomacromolecules*, 2009, **10**, 497-504.
258. E. Lasseuguette, *Cellulose*, 2008, **15**, 571-580.
259. M. Salajkova, L. A. Berglund and Q. Zhou, *Journal of Materials Chemistry*, 2012, **22**, 19798-19805.
260. F. Azzam, L. Heux, J. L. Putaux and B. Jean, *Biomacromolecules*, 2010, **11**, 3652-3659.
261. I. Filpponen and D. S. Argyropoulos, *Biomacromolecules*, 2010, **11**, 1060-1066.
262. H. Sadeghifar, I. Filpponen, S. P. Clarke, D. F. Brougham and D. S. Argyropoulos, *Journal of Materials Science*, 2011, **46**, 7344-7355.
263. B. Braun and J. R. Dorgan, *Biomacromolecules*, 2008, **10**, 334-341.

264. T. Saito, M. Hirota, N. Tamura, S. Kimura, H. Fukuzumi, L. Heux and A. Isogai, *Biomacromolecules*, 2009, **10**, 1992-1996.
265. S. Spinella, A. Maiorana, Q. Qian, N. J. Dawson, V. Hepworth, S. A. McCallum, M. Ganesh, K. D. Singer and R. A. Gross, *ACS Sustainable Chemistry & Engineering*, 2016, **4**, 1538-1550.
266. S. Berlioz, S. Molina-Boisseau, Y. Nishiyama and L. Heux, *Biomacromolecules*, 2009, **10**, 2144-2151.
267. M. Fumagalli, D. Ouhab, S. M. Boisseau and L. Heux, *Biomacromolecules*, 2013, **14**, 3246-3255.
268. N. S. Çetin, P. Tingaut, N. Özmen, N. Henry, D. Harper, M. Dadmun and G. Sèbe, *Macromolecular Bioscience*, 2009, **9**, 997-1003.
269. J.-L. Huang, C.-J. Li and D. G. Gray, *RSC Advances*, 2014, **4**, 6965-6969.
270. N. Guigo, K. Mazeau, J.-L. Putaux and L. Heux, *Cellulose*, 2014, **21**, 4119-4133.
271. A. G. Cunha, Q. Zhou, P. T. Larsson and L. A. Berglund, *Cellulose*, 2014, **21**, 2773-2787.
272. K. Li, J. Song, M. Xu, S. Kuga, L. Zhang and J. Cai, *ACS applied materials & interfaces*, 2014, **6**, 7204-7213.
273. S. Gårdebjer, A. Bergstrand, A. Idström, C. Börstell, S. Naana, L. Nordstierna and A. Larsson, *Composites Science and Technology*, 2015, **107**, 1-9.
274. J. R. Navarro, G. Conzatti, Y. Yu, A. B. Fall, R. Mathew, M. Edén and L. Bergström, *Biomacromolecules*, 2015, **16**, 1293-1300.
275. S. Elazzouzi-Hafraoui, Y. Nishiyama, J.-L. Putaux, L. Heux, F. Dubreuil and C. Rochas, *Biomacromolecules*, 2007, **9**, 57-65.
276. P. Lu and Y.-L. Hsieh, *Carbohydrate Polymers*, 2012, **87**, 564-573.
277. A. Mandal and D. Chakrabarty, *Carbohydrate Polymers*, 2011, **86**, 1291-1299.
278. I. A. Sacui, R. C. Nieuwendaal, D. J. Burnett, S. J. Stranick, M. Jorfi, C. Weder, E. J. Foster, R. T. Olsson and J. W. Gilman, *ACS Applied Materials & Interfaces*, 2014, **6**, 6127-6138.
279. R. Shinoda, T. Saito, Y. Okita and A. Isogai, *Biomacromolecules*, 2012, **13**, 842-849.
280. M. Kaushik, W. C. Chen, T. G. Van de Ven and A. Moores, *Nanocellulose*, 2014, **29**, 23.
281. J. Ayache, L. Beaunier, J. Boumendil, G. Ehret and D. Laub, *Sample preparation handbook for transmission electron microscopy: techniques*, Springer Science & Business Media, 2010.
282. P. Bubner, H. Plank and B. Nidetzky, *Biotechnology and Bioengineering*, 2013, **110**, 1529-1549.
283. R. Amini, S. K. Brar, M. Cledon and R. Y. Surampalli, *Journal of Hazardous, Toxic, and Radioactive Waste*, 2015, **20**, B4015004.
284. P. Krishnamachari, R. Hashaikeh and M. Tiner, *Micron*, 2011, **42**, 751-761.
285. D. Gaspar, S. Fernandes, A. De Oliveira, J. Fernandes, P. Grey, R. Pontes, L. Pereira, R. Martins, M. Godinho and E. Fortunato, *Nanotechnology*, 2014, **25**, 094008.
286. T. Saito, S. Kimura, Y. Nishiyama and A. Isogai, *Biomacromolecules*, 2007, **8**, 2485-2491.
287. B. Soni and B. Mahmoud, *Carbohydrate polymers*, 2015, **134**, 581-589.

288. S. J. Eichhorn, A. Dufresne, M. Aranguren, N. E. Marcovich, J. R. Capadona, S. J. Rowan, C. Weder, W. Thielemans, M. Roman, S. Renneckar, W. Gindl, S. Veigel, J. Keckes, H. Yano, K. Abe, M. Nogi, A. N. Nakagaito, A. Mangalam, J. Simonsen, A. S. Benight, A. Bismarck, L. A. Berglund and T. Peijs, *Journal of Materials Science*, 2009, **45**, 1.

289. J. Guo, X. Guo, S. Wang and Y. Yin, *Carbohydrate Polymers*, 2016, **135**, 248-255.

290. M.-C. Li, C. Mei, X. Xu, S. Lee and Q. Wu, *Polymer*, 2016, **107**, 200-210.

291. B. Michen, C. Geers, D. Vanhecke, C. Endes, B. Rothen-Rutishauser, S. Balog and A. Petri-Fink, *Scientific Reports*, 2015, **5**, 9793.

292. M. Uhlig, A. Fall, S. Wellert, M. Lehmann, S. Prévost, L. Wågberg, R. von Klitzing and G. Nyström, *Langmuir*, 2016, **32**, 442-450.

293. X. Xu, F. Liu, L. Jiang, J. Zhu, D. Haagenson and D. P. Wiesenborn, *ACS applied materials & interfaces*, 2013, **5**, 2999-3009.

294. A. Brinkmann, M. Chen, M. Couillard, Z. J. Jakubek, T. Leng and L. J. Johnston, *Langmuir*, 2016, **32**, 6105-6114.

295. M.-C. Li, Q. Wu, K. Song, S. Lee, Y. Qing and Y. Wu, *ACS Sustainable Chemistry & Engineering*, 2015, **3**, 821-832.

296. W. Chen, H. Yu, Y. Liu, P. Chen, M. Zhang and Y. Hai, *Carbohydrate Polymers*, 2011, **83**, 1804-1811.

297. W. Chen, Q. Li, J. Cao, Y. Liu, J. Li, J. Zhang, S. Luo and H. Yu, *Carbohydrate Polymers*, 2015, **117**, 950-956.

298. K. R. Stinson-Bagby, Rose; Foster, Johan, 2017.

299. P.-C. Lin, S. Lin, P. C. Wang and R. Sridhar, *Biotechnology advances*, 2014, **32**, 711-726.

300. J. Goldstein, D. E. Newbury, P. Echlin, D. C. Joy, A. D. Romig Jr, C. E. Lyman, C. Fiori and E. Lifshin, *Scanning electron microscopy and X-ray microanalysis: a text for biologists, materials scientists, and geologists*, Springer Science & Business Media, 2012.

301. V. B. Özdöl, V. Srot and P. A. van Aken, in *Handbook of Nanoscopy*, Wiley-VCH Verlag GmbH & Co. KGaA, 2012, DOI: 10.1002/9783527641864.ch14, pp. 473-498.

302. M. Ioelovich, in *Handbook of Nanocellulose and Cellulose Nanocomposites*, Wiley-VCH Verlag GmbH & Co. KGaA, 2017, DOI: 10.1002/9783527689972.ch2, pp. 51-100.

303. D. F. Barreto-Vieira and O. M. Barth, *Negative and Positive Staining in Transmission Electron Microscopy for Virus Diagnosis*, 2015.

304. R. Harris, D. Bhella and M. Adrian, *Microscopy and Analysis*, 2006, **113**, 17.

305. M. Kaushik, C. Fraschini, G. Chauve, J.-L. Putaux and A. Moores, *Transmission Electron Microscopy for the Characterization of Cellulose Nanocrystals*, 2015.

306. B. O'Connor, R. Berry and R. Goguen, in *Nanotechnology Environmental Health and Safety (Second Edition)*, William Andrew Publishing, Oxford, 2014, DOI: http://doi.org/10.1016/B978-1-4557-3188-6.00010-4, pp. 225-246.

307. J. F. Hainfeld, D. Safer, J. S. Wall, M. Simon, B. Lin and R. D. Powell, 1994.

308. S. Brenner and R. Horne, *Biochimica et biophysica acta*, 1959, **34**, 103-110.

309. S. Amelinckx, 1997.

310. A. d. A. C., I. M.C., B. M., J. D., P. R., P. M.S., B. T., R. O.J., V. R. and G. R., *Biomacromolecules*, 2010, **11**, 674-681.

311. E. Mascheroni, R. Rampazzo, M. A. Ortenzi, G. Piva, S. Bonetti and L. Piergiovanni, *Cellulose*, 2016, **23**, 779-793.

312. M. Bercea and P. Navard, *Macromolecules*, 2000, **33**, 6011-6016.

313. E. E. Ureña-Benavides, G. Ao, V. A. Davis and C. L. Kitchens, *Macromolecules*, 2011, **44**, 8990-8998.

314. S. Shafiei-Sabet, W. Y. Hamad and S. G. Hatzikiriakos, *Langmuir*, 2012, **28**, 17124-17133.

315. G. Agoda-Tandjawa, S. Durand, S. Berot, C. Blassel, C. Gaillard, C. Garnier and J. L. Doublier, *Carbohydrate Polymers*, 2010, **80**, 677-686.

316. C. W. Macosko, *Rheology: Principles, Measurements, and Applications*, Wiley-VCH, Inc. , 1994.

317. T. A. Osswald and N. Rudolph, *Polymer Rheology: Fundamentals and Applications*, Hanser, 2015.

318. L. Jowkarderis and T. G. M. van de Ven, *Cellulose*, 2014, **21**, 2511-2517.

319. C. Goussé, H. Chanzy, M. L. Cerrada and E. Fleury, *Polymer*, 2004, **45**, 1569-1575.

320. N. Willenbacher and K. Georgieva, in *Product Design and Engineering: Formulation of Gels and Pastes*, eds. U. Brockel, W. Meier and G. Wagner, Wiley-VCH Verlag GmbH & Co. KGaA, 1 edn., 2013, ch. 1, pp. 7-49.

321. S. Iwamoto, S.-H. Lee and T. Endo, *Polymer Journal*, 2013, **46**, 73-76.

322. S. Mueller, E. W. Llewellin and H. M. Mader, *Proceedings of the Royal Society A: Mathematical, Physical and Engineering Sciences*, 2009, **466**, 1201-1228.

323. M. L. Mansfield and J. F. Douglas, *Macromolecules*, 2008, **41**, 5422-5432.

324. M. J. Lundahl, A. G. Cunha, E. Rojo, A. C. Papageorgiou, L. Rautkari, J. C. Arboleda and O. J. Rojas, *Sci Rep*, 2016, **6**, 30695.

325. W. P. Cox and M. E.H., in *International Symposium on Plastics Testing and Standardization*, American Society for Testing & Materials, 1959, DOI: 10.1520/STP44206S, pp. 178-188.

326. I. Hoeger, O. J. Rojas, K. Efimenko, O. D. Velev and S. S. Kelley, *Soft Matter*, 2011, **7**, 1957-1967.

327. E. Kontturi, T. Tammelin and M. Osterberg, *Chem. Soc. Rev.*, 2006, **35**, 1287-1304.

328. E. Kontturi, T. Tammelin and M. Österberg, *Chemical Society Reviews*, 2006, **35**, 1287-1304.

329. E. D. Cranston and D. G. Gray, *Model Cellulose I Surfaces; A Review*, ACS Publishing, Washington, DC, 2009.

330. S. Ahola, J. Salmi, L. S. Johansson, J. Laine and M. Österberg, *Biomacromolecules*, 2008, **9**, 1273-1282.

331. C. Aulin, S. Ahola, P. Josefsson, T. Nishino, Y. Hirose, M. Österberg and L. Wågberg, *Langmuir*, 2009, **25**, 7675-7685.

332. Y. Habibi, L. Foulon, V. Aguié-Béghin, M. Molinari and R. Douillard, *Journal of Colloid and Interface Science*, 2007, **316**, 388-397.

333. Y. Habibi, I. Hoeger, S. S. Kelley and O. J. Rojas, *Langmuir*, 2010, **26**, 990-1001.

334. E. Kontturi, L. S. Johansson and K. S. Kontturi, *Langmuir*, 2007, 9674-9680.

335. I. Usov, G. Nyström, J. Adamcik, S. Handschin, C. Schütz, A. Fall, L. Bergström and R. Mezzenga, *Nature Communications*, 2015, **6**, 7564-7564.
336. I. A. Sacui, R. C. Nieuwendaal, D. J. Burnett, S. J. Stranick, M. Jorfi, C. Weder, E. J. Foster, R. T. Olsson and J. W. Gilman, *ACS Applied Materials and Interfaces*, 2014, **6**, 6127-6138.
337. CSA, *Journal*, 2014, **Z5100-14**, 52-56.
338. S. Elazzouzi-Hafraoui, Y. Nishiyama, J.-L. L. Putaux, L. Heux, F. F. Dubreuil and C. Rochas, *Biomacromolecules*, 2008, **9**, 57-65.
339. R. R. Lahiji, Y. Boluk and M. McDermott, *Journal of Materials Science*, 2012, **47**, 3961-3970.
340. T. Abitbol, A. Palermo, J. M. Moran-Mirabal and E. D. Cranston, *Biomacromolecules*, 2013, **14**, 3278-3284.
341. D. Dubief, E. Samain and A. Dufresne, *Macromolecules*, 1999, **32**, 5765-5771.
342. E. Niinivaara, M. Faustini, T. Tammelin and E. Kontturi, *Langmuir*, 2015, **31**, 12170-12176.
343. K. S. Kontturi, E. Kontturi and J. Laine, *Journal of Materials Chemistry A*, 2013, **1**, 13655-13655.
344. Z. Hu, E. D. Cranston, R. Ng and R. Pelton, *Langmuir*, 2014, **30**, 2684-2692.
345. P. Eronen, K. Junka, J. Laine and M. Österberg, *BioResources*, 2011, **6**, 4200-4217.
346. J. O. Zoppe, M. Österberg, R. a. Venditti, J. Laine and O. J. Rojas, *Biomacromolecules*, 2011, **12**, 2788-2796.
347. S. M. Notley, M. Eriksson, L. Wågberg, S. Beck-Candanedo and D. G. Gray, *Langmuir*, 2006, **22**, 3154-3160.
348. J. Lefebvre and D. G. Gray, *Cellulose*, 2005, **12**, 127-134.
349. E. D. Cranston, D. G. Gray and M. W. Rutland, *Langmuir*, 2010, **26**, 17190-17197.
350. J. Stiernstedt, N. Nordgren, L. Wågberg, H. I. I. I. Brummer, D. G. Gray and M. W. Rutland, *Journal of Colloid and Interface Science*, 2006, **303**, 117-123.
351. S. Ahola, X. Turon, M. Österberg, J. Laine and O. J. Rojas, *Langmuir*, 2008, **24**, 11592-11599.
352. G. Cheng, Z. Liu, J. K. Murton, M. Jablin, M. Dubey, J. Majewski, C. Halbert, J. Browning, J. Ankner, B. Akgun, C. Wang, A. R. Esker, K. L. Sale, B. a. Simmons and M. S. Kent, *Biomacromolecules*, 2011, **12**, 2216-2224.
353. C. Cerclier, A. Guyomard-Lack, C. Moreau, F. Cousin, N. Beury, E. Bonnin, B. Jean and B. Cathala, *Advanced Materials*, 2011, **23**, 3791-3795.
354. Z. Hu, T. Patten, R. Pelton and E. D. Cranston, *ACS Sustainable Chemistry & Engineering*, 2015, **3**, 1023-1031.
355. D. G. Gray and X. Mu, *Materials*, 2015, **8**, 7873-7888.
356. A. Gencer, C. Schütz and W. Thielemans, *Langmuir*, 2017, **33**, 228-234.
357. J. D. Kittle, X. Du, F. Jiang, C. Qian, T. Heinze, M. Roman and A. R. Esker, *Biomacromolecules*, 2011, **12**, 2881-2887.
358. A. Villares, C. Moreau, A. Dammak, I. Capron and B. Cathala, *Soft Matter*, 2015, **11**, 6472-6481.
359. E. D. Cranston and D. G. Gray, *Biomacromolecules*, 2006, **7**, 2522-2530.
360. C. D. Edgar and D. G. Gray, *Cellulose*, 2003, **10**, 299-306.

361. E. D. Cranston and D. G. Gray, *Colloids and Surfaces, A: Physicochemical and Engineering Aspects*, 2008, **325**, 44-51.

362. E. D. Cranston, M. Eita, E. Johansson, J. Netrval, M. Salajková, H. Arwin and L. Wågberg, *Biomacromolecules*, 2011, **12**, 961-969.

363. R. Bardet, C. Sillard, N. Belgacem and J. Bras, *Cellulose Chemistry and Technology*, 2015, **49**, 587-595.

364. J. Langat, S. Bellayer, P. Hudrlik, A. Hudrlik, P. H. Maupin, J. W. Gilman and D. Raghavan, *Polymer*, 2006, **47**, 6698-6709.

365. S. Bellayer, J. W. Gilman, N. Eidelman, S. Bourbigot, X. Flambard, D. M. Fox, H. C. D. Long and P. C. Trulove, *Advanced Functional Materials*, 2005, **15**, 910-916.

366. P. H. Maupin, J. W. Gilman, R. H. Harris, S. Bellayer, A. J. Bur, S. C. Roth, M. Murariu, A. B. Morgan and J. D. Harris, *Macromolecular Rapid Communications*, 2004, **25**, 788-792.

367. V. Martinez-Martinez, C. Corcostegui, J. B. Prieto, L. Gartzia, S. Salleres and I. L. Arbeloa, *Journal of Materials Chemistry*, 2011, **21**, 269-276.

368. J. H. Huang, F. C. Chien, P. L. Chen, K. C. Ho and C. W. Chu, *Analytical Chemistry*, 2010, **82**, 1669-1673.

369. V. E. Centonze, A. Takahashi, E. Casanova and B. Herman, *Journal of Histotechnology*, 2000, **23**, 229-234.

370. I. V. Turchin, *Physics-Uspekhi*, 2016, **59**, 487-501.

371. P. Timpson, E. J. McGhee and K. I. Anderson, *Journal of Cell Science*, 2011, **124**, 2877-2890.

372. C. De Los Santos, C. W. Chang, M. A. Mycek and R. A. Cardullo, *Molecular Reproduction and Development*, 2015, **82**, 587-604.

373. M. Y. Berezin and S. Achilefu, *Chemical Reviews*, 2010, **110**, 2641-2684.

374. O. Pekcan and M. Erdogan, *Journal of Physical Chemistry B*, 2002, **106**, 5351-5357.

375. A. Shundo, Y. Okada, F. Ito and K. Tanaka, *Macromolecules*, 2012, **45**, 329-335.

376. A. Shundo, *Polymer Journal*, 2015, **47**, 719-726.

377. P. I. H. Bastiaens and A. Squire, *Trends in Cell Biology*, 1999, **9**, 48-52.

378. E. B. van Munster and T. W. J. Gadella, in *Microscopy Techniques*, ed. J. Rietdorf, 2005, vol. 95, pp. 143-175.

379. J. P. S. Farinha and J. M. G. Martinho, *Journal of Physical Chemistry C*, 2008, **112**, 10591-10601.

380. C. E. Rowland, C. W. Brown, I. L. Medintz and J. B. Delehanty, *Methods and Applications in Fluorescence*, 2015, **3**.

381. M. Brandl, J. Hartmann, T. Posnicek, F. R. Ausenegg, A. Leitner and D. Falkenhagen, *Blood Purification*, 2005, **23**, 181-189.

382. K. B. Knudsen, C. Kofoed, R. Espersen, C. Hojgaard, J. R. Winther, M. Willemoes, I. Wedin, M. Nuopponen, S. Vilske, K. Aimonen, I. E. K. Weydahl, H. Alenius, H. Norppa, H. Wolff, H. Wallin and U. Vogel, *Chemical Research in Toxicology*, 2015, **28**, 1627-1635.

383. W. Helbert, H. Chanzy, T. L. Husum, M. Schulein and S. Ernst, *Biomacromolecules*, 2003, **4**, 481-487.

384. D. J. Dagel, Y. S. Liu, L. Zhong, Y. Luo, Y. Zeng, M. Himmel, S. Y. Ding and S. Smith, in *Single Molecule Spectroscopy and Imaging Iv*, eds. J. Enderlein, Z. K. Gryczynski and R. Erdmann, 2011, vol. 7905.

385. L. Q. Wang, Y. Q. Wang and A. J. Ragauskas, *Analytical and Bioanalytical Chemistry*, 2010, **398**, 1257-1262.

386. J. M. Moran-Mirabal, *Cellulose*, 2013, **20**, 2291-2309.

387. C. I. Thomson, R. M. Lowe and A. J. Ragauskas, *Carbohydrate Polymers*, 2007, **69**, 799-804.

388. M. Zammarano, P. H. Maupin, L.-P. Sung, J. W. Gilman, E. D. McCarthy, Y. S. Kim and D. M. Fox, *ACS Nano*, 2011, **5**, 3391-3399.

389. D. M. Fox, N. Kaufman, J. Woodcock, C. S. Davis, J. W. Gilman, J. R. Shields, R. D. Davis, S. Matko and M. Zammarano, in *Composites from Renewable and Sustainable Materials*, InTech, 2016.

390. J. A. Olmstead and D. G. Gray, *Journal of Photochemistry and Photobiology a-Chemistry*, 1993, **73**, 59-65.

391. E. Kalita, B. K. Nath, F. Agan, V. More and P. Deb, *Industrial Crops and Products*, 2015, **65**, 550-555.

392. T. Niu, Y. Q. Gu and J. G. Huang, *Journal of Materials Chemistry*, 2011, **21**, 651-656.

393. M. Zhu, X. Q. Peng, Z. W. Wang, Z. L. Bai, B. K. Chen, Y. T. Wang, H. Y. Hao, Z. Q. Shao and H. Z. Zhong, *Journal of Materials Chemistry C*, 2014, **2**, 10031-10036.

394. H. Therien-Aubin, A. Lukach, N. Pitch and E. Kumacheva, *Angewandte Chemie-International Edition*, 2015, **54**, 5618-5622.

395. H. Therien-Aubin, A. Lukach, N. Pitch and E. Kumacheva, *Nanoscale*, 2015, **7**, 6612-6618.

396. I. Diez, P. Eronen, M. Osterberg, M. B. Linder, O. Ikkala and R. H. A. Ras, *Macromolecular Bioscience*, 2011, **11**, 1185-1191.

397. D. Qu, J. N. Zhang, G. Chu, H. J. Jiang, C. F. Wu and Y. Xu, *Journal of Materials Chemistry C*, 2016, **4**, 1764-1768.

398. Y. P. Zhang, V. P. Chodavarapu, A. G. Kirk and M. P. Andrews, *Journal of Nanophotonics*, 2012, **6**.

399. S. B. Yamaki, D. S. Barros, C. M. Garcia, P. Socoloski, O. N. Oliveira and T. D. Z. Atvars, *Langmuir*, 2005, **21**, 5414-5420.

400. V. Verma, J. M. Catchmark, N. R. Brown and W. O. Hancock, *Journal of Biological Engineering*, 2012, **6**.

401. L. Chen, Y. Liu, C. Lai, R. M. Berry and K. C. Tam, *Materials Research Express*, 2015, **2**.

402. Q. W. Wang, A. M. Tang, Y. Liu, Z. Q. Fang and S. Y. Fu, *Nanomaterials*, 2016, **6**.

403. J. S. Haghpanah, R. Tu, S. Da Silva, D. Yan, S. Mueller, C. Weder, E. J. Foster, I. Sacui, J. W. Gilman and J. K. Montclare, *Biomacromolecules*, 2013, **14**, 4360-4367.

404. C. Endes, S. Mueller, C. Kinnear, D. Vanhecke, E. J. Foster, A. Petri-Fink, C. Weder, M. J. D. Clift and B. Rothen-Rutishauser, *Biomacromolecules*, 2015, **16**, 1267-1275.

405. S. Camarero-Espinosa, B. Rothen-Rutishauser, C. Weder and E. J. Foster, *Biomaterials*, 2016, **74**, 42-52.

406. S. P. Dong and M. Roman, *Journal of the American Chemical Society*, 2007, **129**, 13810-+.
407. K. A. Mahmoud, J. A. Mena, K. B. Male, S. Hrapovic, A. Kamen and J. H. T. Luong, *Acs Applied Materials & Interfaces*, 2010, **2**, 2924-2932.
408. L. J. Nielsen, S. Eyley, W. Thielemans and J. W. Aylott, *Chemical Communications*, 2010, **46**, 8929-8931.
409. P. R. Banks and D. M. Paquette, *Bioconjugate Chemistry*, 1995, **6**, 447-458.
410. I. Dubey, G. Pratviel and B. Meunier, *Bioconjugate Chemistry*, 1998, **9**, 627-632.
411. R. Sunasee and R. Narain, in *Chemistry of Bioconjugates*, John Wiley & Sons, Inc., 2014, DOI: 10.1002/9781118775882.ch1, pp. 1-75.
412. F. Jiang, A. R. Esker and M. Roman, *Langmuir*, 2010, **26**, 17919-17925.
413. Q. Ding, J. Zeng, B. Wang, W. Gao, K. Chen, Z. Yuan and J. Xu, *Carbohydrate Polymers*, 2017, **175**, 105-112.
414. D. M. Fox and J. Woodcock, unpublished results.
415. J. W. Grate, K. F. Mo, Y. Shin, A. Vasdekis, M. G. Warner, R. T. Kelly, G. Orr, D. H. Hu, K. J. Dehoff, F. J. Brockman and M. J. Wilkins, *Bioconjugate Chemistry*, 2015, **26**, 593-601.
416. H. Sahoo, *Rsc Advances*, 2012, **2**, 7017-7029.
417. O. Koniev and A. Wagner, *Chemical Society Reviews*, 2015, **44**, 5495-5551.
418. S. Barazzouk and C. Daneault, *Cellulose*, 2011, **18**, 643-653.
419. Q. Y. Niu, K. Z. Gao and W. H. Wu, *Carbohydrate Polymers*, 2014, **110**, 47-52.
420. J. Zhou, N. Butchosa, H. S. N. Jayawardena, J. Park, Q. Zhou, M. D. Yan and O. Ramstrom, *Biomacromolecules*, 2015, **16**, 1426-1432.
421. B. J. Harper, A. Clendaniel, F. Sinche, D. Way, M. Hughes, J. Schardt, J. Simonsen, A. B. Stefaniak and S. L. Harper, *Cellulose*, 2016, **23**, 1763-1775.
422. T. Abitbol, H. S. Marway, S. A. Kedzior, X. Yang, A. Franey, D. G. Gray and E. D. Cranston, *Cellulose*, 2017, **24**, 1287-1293.
423. Q. A. Yang and X. J. Pan, *Journal of Applied Polymer Science*, 2010, **117**, 3639-3644.
424. L. R. Tang, T. Li, S. Y. Zhuang, Q. L. Lu, P. F. Li and B. Huang, *Acs Sustainable Chemistry & Engineering*, 2016, **4**, 4842-4849.
425. J. L. Huang, C. J. Li and D. G. Gray, *Acs Sustainable Chemistry & Engineering*, 2013, **1**, 1160-1164.
426. L. Colombo, L. Zoia, M. B. Violatto, S. Previdi, L. Talamini, L. Sitia, F. Nicotra, M. Orlandi, M. Salmona, C. Recordati, P. Bigini and B. La Ferla, *Biomacromolecules*, 2015, **16**, 2862-2871.
427. B. T. Hofreiter, B. H. Alexander and I. A. Wolff, *Analytical Chemistry*, 1955, **27**, 1930-1931.
428. A. J. Varma and M. P. Kulkarni, *Polymer Degradation and Stability*, 2002, **77**, 25-27.
429. K. Conley, M. A. Whitehead and T. G. M. van de Ven, *Cellulose*, 2016, **23**, 1553-1563.
430. J. V. Edwards, K. R. Fontenot, D. Haldane, N. T. Prevost, B. D. Condon and C. Grimm, *Cellulose*, 2016, **23**, 1283-1295.
431. L. Z. Zhang, Q. Li, J. P. Zhou and L. N. Zhang, *Macromolecular Chemistry and Physics*, 2012, **213**, 1612-1617.

432. T. Leng, Z. J. Jakubek, M. Mazloumi, A. C. W. Leung and L. J. Johnston, *Langmuir*, 2017, **33**, 8002-8011.
433. A. Dufresne, J.-Y. Cavaillé and M. R. Vignon, *Journal of Applied Polymer Science*, 1997, **64**, 1185-1194.
434. M. Henriksson, L. A. Berglund, P. Isaksson, T. Lindström and T. Nishino, *Biomacromolecules*, 2008, **9**, 1579-1585.
435. I. Kvien and K. Oksman, *Applied Physics A*, 2007, **87**, 641-643.
436. W. Gindl and J. Keckes, *Journal of Applied Polymer Science*, 2007, **103**, 2703-2708.
437. L. A. Berglund and T. Peijs, *MRS Bulletin*, 2010, **35**, 201-207.
438. A. J. Svagan, M. A. S. Azizi Samir and L. A. Berglund, *Biomacromolecules*, 2007, **8**, 2556-2563.
439. A. J. Svagan, L. A. Berglund and P. Jensen, *ACS Applied Materials & Interfaces*, 2011, **3**, 1411-1417.
440. M. Pääkkö, J. Vapaavuori, R. Silvennoinen, H. Kosonen, M. Ankerfors, T. Lindström, L. A. Berglund and O. Ikkala, *Soft Matter*, 2008, **4**, 2492-2499.
441. S. J. Eichhorn, C. A. Baillie, N. Zafeiropoulos, L. Y. Mwaikambo, M. P. Ansell, A. Dufresne, K. M. Entwistle, P. J. Herrera-Franco, G. C. Escamilla, L. Groom, M. Hughes, C. Hill, T. G. Rials and P. M. Wild, *Journal of Materials Science*, 2001, **36**, 2107-2131.
442. W. Helbert, J. Y. Cavaillé and A. Dufresne, *Polymer Composites*, 1996, **17**, 604-611.
443. C. A. Cooper, R. J. Young and M. Halsall, *Composites Part A: Applied Science and Manufacturing*, 2001, **32**, 401-411.
444. N. D. Wanasekara, D. A. Stone, G. E. Wnek and L. T. J. Korley, *Macromolecules*, 2012, **45**, 9092-9099.
445. A. E. Lewandowska and S. J. Eichhorn, *Journal of Raman Spectroscopy*, 2016, **47**, 1337-1342.
446. R. Rusli and S. J. Eichhorn, *Nanotechnology*, 2011, **22**, 325706.
447. C. Chang, A. Lue and L. Zhang, *Macromolecular Chemistry and Physics*, 2008, **209**, 1266-1273.
448. L. E. Millon and W. K. Wan, *Journal of Biomedical Materials Research Part B: Applied Biomaterials*, 2006, **79B**, 245-253.
449. A. L. Buyanov, I. V. Gofman, L. G. Revel'skaya, A. K. Khripunov and A. A. Tkachenko, *Journal of the Mechanical Behavior of Biomedical Materials*, 2010, **3**, 102-111.
450. J. R. Capadona, O. Van Den Berg, L. A. Capadona, M. Schroeter, S. J. Rowan, D. J. Tyler and C. Weder, *Nat Nano*, 2007, **2**, 765-769.
451. J. C. H. Affdl and J. L. Kardos, *Polymer Engineering & Science*, 1976, **16**, 344-352.
452. M. Grunert and W. T. Winter, *Journal of Polymers and the Environment*, 2002, **10**, 27-30.
453. W. Gindl and J. Keckes, *Composites Science and Technology*, 2004, **64**, 2407-2413.
454. T. Nishino, I. Matsuda and K. Hirao, *Macromolecules*, 2004, **37**, 7683-7687.

455. Q. Zhao, R. C. M. Yam, B. Zhang, Y. Yang, X. Cheng and R. K. Y. Li, *Cellulose*, 2009, **16**, 217-226.
456. H. L. Cox, *British Journal of Applied Physics*, 1952, **3**, 72.
457. H. Krenchel, PhD Thesis, Technical University of Denmark 1964.
458. K. Y. Lee, Y. Aitomaki, L. A. Berglund, K. Oksman and A. Bismarck, *Composites Science and Technology*, 2014, **105**, 15-27.
459. Y. C. Hsieh, H. Yano, M. Nogi and S. J. Eichhorn, *Cellulose*, 2008, **15**, 507-513.
460. Y. J. Ma, X. F. Yao, Q. S. Zheng, Y. J. Yin, D. J. Jiang, G. H. Xu, F. Wei and Q. Zhang, *Applied Physics Letters*, 2010, **97**.
461. A. Rege and M. Itskov, *Proceedings in Applied Mathematics and Mechanics*, 2015, **15**, 347-348.
462. A. Rege, M. Schestakow, I. Karadagli, L. Ratke and M. Itskov, *Soft Matter*, 2016, **12**, 7079-7088.
463. A. Desai, S. R. Nutt and M. V. Alonso, *Journal of Cellular Plastics*, 2008, **44**, 391-413.
464. V. K. Mitra, W. M. Risen and R. H. Baughman, *Journal of Chemical Physics*, 1977, **66**, 2731-2736.
465. A. Sturcova, G. R. Davies and S. J. Eichhorn, *Biomacromolecules*, 2005, **6**, 1055-1061.
466. T. Pullawan, A. N. Wilkinson and S. J. Eichhorn, *Composites Science and Technology*, 2010, **70**, 2325-2330.
467. T. Pullawan, A. N. Wilkinson and S. J. Eichhorn, *Journal of Materials Science*, 2013, **48**, 7847-7855.
468. R. Rusli, K. Shanmuganathan, S. J. Rowan, C. Weder and S. J. Eichhorn, *Biomacromolecules*, 2010, **11**, 762-768.
469. S. Tanpichai, W. W. Sampson and S. J. Eichhorn, *Compos. Pt. A-Appl. Sci. Manuf.*, 2012, **43**, 1145-1152.
470. OECD, *Test No. 431: In Vitro Skin Corrosion: Human Skin Model Test*, OECD Publishing, 2004.
471. OECD, *Test No. 439: In Vitro Skin Irritation: Reconstructed Human Epidermis Test Method*, OECD Publishing, 2015.
472. OECD, *Test No. 430: In Vitro Skin Corrosion: Transcutaneous Electrical Resistance Test (TER)*, OECD Publishing, 2004.
473. OECD, *Test No. 435: In Vitro Membrane Barrier Test Method for Skin Corrosion*, OECD Publishing, 2006.
474. OECD, *Test No. 203: Fish, Acute Toxicity Test*, OECD Publishing, 1992.
475. OECD, *Test No. 429: Skin Sensitisation*, OECD Publishing, 2010.
476. OECD, *Test No. 442A: Skin Sensitization*, OECD Publishing, 2010.
477. OECD, *Test No. 442B: Skin Sensitization*, OECD Publishing, 2010.
478. C. Endes, S. Camarero-Espinosa, S. Mueller, E. J. Foster, A. Petri-Fink, B. Rothen-Rutishauser, C. Weder and M. J. Clift, *J Nanobiotechnology*, 2016, **14**, 78.
479. A. A. Shvedova, E. R. Kisin, N. Yanamala, M. T. Farcas, A. L. Menas, A. Williams, P. M. Fournier, J. S. Reynolds, D. W. Gutkin, A. Star, R. S. Reiner, S. Halappanavar and V. E. Kagan, *Part Fibre Toxicol*, 2016, **13**, 28.

480. C. Endes, O. Schmid, C. Kinnear, S. Mueller, S. Camarero-Espinosa, D. Vanhecke, E. J. Foster, A. Petri-Fink, B. Rothen-Rutishauser, C. Weder and M. J. Clift, *Part Fibre Toxicol*, 2014, **11**, 40.

481. K. Donaldson, V. Stone, C. L. Tran, W. Kreyling and P. J. Borm, *Occup Environ Med*, 2004, **61**, 727-728.

482. R. P. Kulkarni, *J Biomed Discov Collab*, 2007, **2**, 3.

483. R. Duffin, L. Tran, D. Brown, V. Stone and K. Donaldson, *Inhal Toxicol*, 2007, **19**, 849-856.

484. J. A. Shatkin and B. Kim, *Environ. Sci.: Nano*, 2015, **2**, 477-499.

485. K. Donaldson, F. A. Murphy, R. Duffin and C. A. Poland, *Particle and Fibre Toxicology*, 2010, **7**.

486. K. Donaldson, F. A. Murphy, R. Duffin and C. A. Poland, *Part Fibre Toxicol*, 2010, **7**, 5.

487. H. Greim, M. J. Utell, L. D. Maxim and R. Niebo, *Inhal Toxicol*, 2014, **26**, 789-810.

488. J. M. Davis, J. Addison, R. E. Bolton, K. Donaldson, A. D. Jones and T. Smith, *Br J Exp Pathol*, 1986, **67**, 415-430.

489. A. Schinwald, T. Chernova and K. Donaldson, *Part Fibre Toxicol*, 2012, **9**, 47.

490. H. Bouwmeester, I. Lynch, H. J. Marvin, K. A. Dawson, M. Berges, D. Braguer, H. J. Byrne, A. Casey, G. Chambers, M. J. Clift, G. Elia, T. F. Fernandes, L. B. Fjellsbo, P. Hatto, L. Juillerat, C. Klein, W. G. Kreyling, C. Nickel, M. Riediker and V. Stone, *Nanotoxicology*, 2011, **5**, 1-11.

491. T. Cedervall, I. Lynch, S. Lindman, T. Berggard, E. Thulin, H. Nilsson, K. A. Dawson and S. Linse, *Proc Natl Acad Sci U S A*, 2007, **104**, 2050-2055.

492. V. Hirsch, C. Kinnear, M. Moniatte, B. Rothen-Rutishauser, M. J. Clift and A. Fink, *Nanoscale*, 2013, **5**, 3723-3732.

493. S. Tenzer, D. Docter, J. Kuharev, A. Musyanovych, V. Fetz, R. Hecht, F. Schlenk, D. Fischer, K. Kiouptsi, C. Reinhardt, K. Landfester, H. Schild, M. Maskos, S. K. Knauer and R. H. Stauber, *Nat Nanotechnol*, 2013, **8**, 772-781.

494. H. M. Braakhuis, M. V. Park, I. Gosens, W. H. De Jong and F. R. Cassee, *Part Fibre Toxicol*, 2014, **11**, 18.

495. E. C. Agency, *Guidance on Information Requirements and Chemical Safety Assessment*, 2016.

496. ISO, *Journal*, 2014.

497. E. C. Agency, *ECHA's Approach on Avoiding Unnecessary Animal Testing: 40th Meeting of the Management Board*, 2015.

498. E. P. Agency, Pesticide Registration: Bridging or Waiving Data Requirements, https://www.epa.gov/pesticide-registration/bridging-or-waiving-data-requirements).

499. N. Burden, K. Aschberger, Q. Chaudhry, M. J. D. Clift, S. H. Doak, P. Fowler, H. Johnston, R. Landsiedel, J. Rowland and V. Stone, *Nano Today*, 2017, **12**, 10-13.

500. OECD, *Test No. 129: Guidance document on using cytotoxicity tests to estimate starting doses for acute oral systematic toxicity tests*, OECD Publishing, 2010.

501. J. H. Arts, M. Hadi, M. A. Irfan, A. M. Keene, R. Kreiling, D. Lyon, M. Maier, K. Michel, T. Petry, U. G. Sauer, D. Warheit, K. Wiench, W. Wohlleben and R. Landsiedel, *Regul Toxicol Pharmacol*, 2015, **71**, S1-27.

502. H. Godwin, C. Nameth, D. Avery, L. L. Bergeson, D. Bernard, E. Beryt, W. Boyes, S. Brown, A. J. Clippinger, Y. Cohen, M. Doa, C. O. Hendren, P. Holden, K. Houck,

A. B. Kane, F. Klaessig, T. Kodas, R. Landsiedel, I. Lynch, T. Malloy, M. B. Miller, J. Muller, G. Oberdorster, E. J. Petersen, R. C. Pleus, P. Sayre, V. Stone, K. M. Sullivan, J. Tentschert, P. Wallis and A. E. Nel, *ACS Nano*, 2015, **9**, 3409-3417.

503. A. Kroll, M. H. Pillukat, D. Hahn and J. Schnekenburger, *Arch Toxicol*, 2012, **86**, 1123-1136.

504. K. J. Ong, T. J. MacCormack, R. J. Clark, J. D. Ede, V. A. Ortega, L. C. Felix, M. K. Dang, G. Ma, H. Fenniri, J. G. Veinot and G. G. Goss, *PLoS One*, 2014, **9**, e90650.

505. C. Brandenberger, M. J. Clift, D. Vanhecke, C. Muhlfeld, V. Stone, P. Gehr and B. Rothen-Rutishauser, *Part Fibre Toxicol*, 2010, **7**, 15.

506. K. A. Mahmoud, J. A. Mena, K. B. Male, S. Hrapovic, A. Kamen and J. H. Luong, *ACS Appl Mater Interfaces*, 2010, **2**, 2924-2932.

507. D. R. Nogueira, M. Mitjans, C. M. Rolim and M. P. Vinardell, *Nanomaterials (Basel)*, 2014, **4**, 454-484.

508. V. Stone, M. R. Miller, M. J. Clift, A. Elder, N. L. Mills, P. Moller, R. P. Schins, U. Vogel, W. G. Kreyling, K. A. Jensen, T. A. Kuhlbusch, P. E. Schwarze, P. Hoet, A. Pietroiusti, A. De Vizcaya-Ruiz, A. Baeza-Squiban, C. L. Tran and F. R. Cassee, *Environ Health Perspect*, 2016, DOI: 10.1289/EHP424.

509. ISO, unpublished work.

510. OECD, *Test No. 437: Bovine Corneal Opacity and Permeability Test Method for Identifying Ocular Corrosives and Severe Irritants*, OECD Publishing, 2009.

511. OECD, *Test No. 438: Isolated Chicken Eye Test Method for Identifying Ocular Corrosives and Severe Irritants*, OECD Publishing, 2009.

512. OECD, *Test No. 492: Reconstructed human Cornea-like Epithelium (RhCE) test method for identifying chemicals not requiring classification and labelling for eye irritation or serious eye damage*, 2015.

513. SCCS, *Journal*, 2012.

514. S. N. Kolle, U. G. Sauer, M. C. Moreno, W. Teubner, W. Wohlleben and R. Landsiedel, *Part Fibre Toxicol*, 2016, **13**, 18.

515. J. R. C. E. ECVAM, Validation and regulatory acceptance, https://eurl-ecvam.jrc.ec.europa.eu/validation-regulatory-acceptance).

516. U. S. N. T. Program, Alternative Methods Accepted by U.S. Agencies, https://ntp.niehs.nih.gov/pubhealth/evalatm/iccvam/acceptance-of-alternative-methods/index.html).

517. B. O'Connor, R. Berry and R. Goguen, in *Nanotechnology Environmental Health and Safety: RIsks, Regulation, Management, Second edition.*, eds. M. Hull and D. Bowman, Elsevier, Waltham, MA, 2014, ch. 10.

518. OECD, *Test No. 256: Guidance Document on the Reporting of Defined Approaches and Individual Information Sources to be Used Within Integrated Approaches to Testing and Assessment (IATA) for Skin Sensitisation*, OECD Publishing, 2016.

519. OECD, *Test No. 442C: In Chemico Skin Sensitisation*, OECD Publishing, 2015.

520. OECD, *Test No. 442D: In Vitro Skin Sensitisation*, OECD Publishing, 2015.

521. J. Catalan, E. Rydman, K. Aimonen, K. S. Hannukainen, S. Suhonen, E. Vanhala, C. Moreno, V. Meyer, D. D. Perez, A. Sneck, U. Forsstrom, C. Hojgaard, M. Willemoes, J. R. Winther, U. Vogel, H. Wolff, H. Alenius, K. M. Savolainen and H. Norppa, *Mutagenesis*, 2017, **32**, 23-31.

522. OECD, *Test No. 471: Bacterial Reverse Mutation Test*, OECD Publishing, 1997.

523. OECD, *Test No. 476: In vitro Mammalian Cell Gene Mutation Test*, OECD Publishing, 1997.

524. OECD, *Test No. 490: In Vitro Mammalian Cell Gene Mutation Tests Using the Thymidine Kinase Gene*, OECD Publishing, 2015.

525. OECD, *Test No. 488: Transgenic Rodent Somatic and Germ Cell Gene Mutation Assays*, OECD Publishing, 2011.

526. OECD, *Test No. 489: In Vivo Mammalian Alkaline Comet Assay*, OECD Publishing, 2014.

527. OECD, *Test No. 486: Unscheduled DNA Synthesis (UDS) Test with Mammalian Liver Cells in vivo*, OECD Publishing, 1997.

528. R. Landsiedel, M. D. Kapp, M. Schulz, K. Wiench and F. Oesch, *Mutat Res*, 2009, **681**, 241-258.

529. OECD, *Test No. 43: Genotoxicity of Manufactured Nanomaterials : Report of the OECD Expert Meeting*, OECD Publishing, 2014.

530. A. Jebali, S. Hekmatimoghaddam, A. Behzadi, I. Rezapor, B. H. Mohammadi, T. Jasemizad, S. A. Yasini, M. Javadzadeh, A. Amiri, M. Soltani, Z. Rezaei, N. Sedighi, M. Seyfi, M. Rezaei and M. Sayadi, *Cellulose*, 2013, **20**, 2897-2907.

531. M. J. Clift, D. O. Raemy, C. Endes, Z. Ali, A. D. Lehmann, C. Brandenberger, A. Petri-Fink, P. Wick, W. J. Parak, P. Gehr, R. P. Schins and B. Rothen-Rutishauser, *Nanotoxicology*, 2013, **7**, 1373-1385.

532. OECD, *Test No. 473: In vitro Mammalian Chromosome Aberration Test*, OECD Publishing, 1997.

533. OECD, *Test No. 487: In Vitro Mammalian Cell Micronucleus Test*, OECD Publishing, 2010.

534. L. Gonzalez, B. J. Sanderson and M. Kirsch-Volders, *Mutagenesis*, 2011, **26**, 185-191.

535. OECD, *Test No. 474: Mammalian Erythrocyte Micronucleus Test*, OECD Publishing, 1997.

536. OECD, *Test No. 475: Mammalian Bone Marrow Chromosome Aberration Test*, OECD Publishing, 1997.

537. OECD, *Test No. 426: Developmental Neurotoxicity Study*, OECD Publishing, 2007.

538. M. J. Clift, E. J. Foster, D. Vanhecke, D. Studer, P. Wick, P. Gehr, B. Rothen-Rutishauser and C. Weder, *Biomacromolecules*, 2011, **12**, 3666-3673.

539. OECD, *Test No. 417: Toxicokinetics*, OECD Publishing, 2010.

540. B. J. Harper, A. Clendaniel, F. Sinche, D. Way, M. Hughes, J. Schardt, J. Simonsen, A. B. Stefaniak and S. L. Harper, *Cellulose (Lond)*, 2016, **23**, 1763-1775.

541. OECD, *Test No. 425: Acute Oral Toxicity: Up-and-Down Procedure*, OECD Publishing, 2008.

542. OECD, *Test No. 420: Acute Oral Toxicity - Fixed Dose Procedure*, OECD Publishing, 2002.

543. OECD, *Test No. 436: Acute Inhalation Toxicity – Acute Toxic Class Method*, OECD Publishing, 2009.

544. OECD, *Test No. 403: Acute Inhalation Toxicity*, OECD Publishing, 2009.

545. OECD, *Test No. 402: Acute Dermal Toxicity*, OECD Publishing, 1987.
546. OECD, *Test No. 407: Repeated Dose 28-day Oral Toxicity Study in Rodents*, OECD Publishing, 2008.
547. OECD, *Test No. 408: Repeated Dose 90-Day Oral Toxicity Study in Rodents*, OECD Publishing, 1998.
548. OECD, *Test No. 410: Repeated Dose Dermal Toxicity: 21/28-day Study*, OECD Publishing, 1981.
549. OECD, *Test No. 411: Subchronic Dermal Toxicity: 90-day Study*, OECD Publishing, 1981.
550. OECD, *Test No. 412: Subacute Inhalation Toxicity: 28-Day Study*, OECD Publishing, 2009.
551. OECD, *Test No. 413: Subchronic Inhalation Toxicity: 90-day Study*, OECD Publishing, 2009.
552. OECD, *Test No. 452: Chronic Toxicity Studies*, OECD Publishing, 2009.
553. ECETOC, *Poorly soluble particles/lung overload. Technical Report No. 122*, 2013.
554. T. Kovacs, V. Naish, B. O'Connor, C. Blaise, F. Gagné, L. Hall, V. Trudeau and P. Martel, *Nanotoxicology*, 2010, **4**, 255-270.
555. J. Vartiainen, T. Pöhler, K. Sirola, L. Pylkkänen, H. Alenius, J. Hokkinen, U. Tapper, P. Lahtinen, A. Kapanen, K. Putkisto, P. Hiekkataipale, P. Eronen, J. Ruokolainen and A. Laukkanen, *Cellulose*, 2011, **18**, 775-786.
556. OECD, *Test No. 236: Fish Embryo Acute Toxicity (FET) Test*, OECD Publishing, 2013.
557. K. J. Ong, X. Zhao, M. E. Thistle, T. J. Maccormack, R. J. Clark, G. Ma, Y. Martinez-Rubi, B. Simard, J. S. Loo, J. G. Veinot and G. G. Goss, *Nanotoxicology*, 2014, **8**, 295-304.
558. K. J. Ong, J. A. Shatkin, K. Nelson, J. D. Ede and T. Retsina, *NanoImpact*, 2017, **6**, 19-29.
559. OECD, *Test No. 202: Daphnia sp. Acute Immobilisation Test*, OECD Publishing, 2004.
560. S. G. Klein, J. Hennen, T. Serchi, B. Blomeke and A. C. Gutleb, *Toxicol In Vitro*, 2011, **25**, 1516-1534.
561. S. N. Bhatia and D. E. Ingber, *Nat Biotechnol*, 2014, **32**, 760-772.
562. D. J. McClements, G. DeLoid, G. Pyrgiotakis, J. A. Shatkin, H. Xiao and P. Demokritou, *NanoImpact*, 2016, **3-4**, 47-57.
563. W. Allen, *Journal*, 2004.